AUS DEM LEHRSTUHL FÜR NEUROCHIRURGIE
PROF. DR. NILS OLE SCHMIDT
DER FAKULTÄT FÜR MEDIZIN
DER UNIVERSITÄT REGENSBURG

THE ROLE OF CARBONIC ANHYDRASE IX IN THE HYPOXIA INDUCED INVASION OF MALIGNANT GLIOMA CELLS

Inaugural – Dissertation
zur Erlangung des Doktorgrades
der Medizin

der
Fakultät für Medizin
der Universität Regensburg

vorgelegt von
Zhenwei Qiu

2021

AUS DEM LEHRSTUHL FÜR NEUROCHIRURGIE
PROF. DR. NILS OLE SCHMIDT
DER FAKULTÄT FÜR MEDIZIN
DER UNIVERSITÄT REGENSBURG

THE ROLE OF CARBONIC ANHYDRASE IX IN THE HYPOXIA INDUCED INVASION OF MALIGNANT GLIOMA CELLS

Inaugural – Dissertation
zur Erlangung des Doktorgrades
der Medizin

der
Fakultät für Medizin
der Universität Regensburg

vorgelegt von
Zhenwei Qiu

2021

Dekan:	Prof. Dr. Dirk Hellwig
1. Berichterstatter:	Prof. Dr. Martin Proescholdt
2. Berichterstatter:	Prof. Dr. Peter Hau
Tag der mündlichen Prüfung:	19.07.2021

Contents

Zusammenfassung

Einführung: Das Glioblastoma (GBM) ist der häufigste und bösartigste Primärtumor im zentralen Nervensystem. Patienten mit einem GBM haben eine außergewöhnlich schlechte Prognose. Die heterogene und invasive Natur des GBM macht eine Heilung durch die derzeitige Behandlung unmöglich. GBM ist außerdem durch eine Reprogrammierung des zellulären Stoffwechsels, einer Ansäuerung des Tumor Microenvironments (TME) sowie einer intratumoralen Hypoxie gekennzeichnet. Die Carboanhydrase IX (CAIX) ist in GBM überexprimiert, nicht aber in normalem Hirngewebe. Es wird angenommen, dass die spezifischen Eigenschaften der CAIX, nämlich der tumor-spezifischen Expression, der hohen katalytischen Aktivität sowie der extrazellulären Membranlokalisation dieses Enzym zu einem wichtigen Faktor machen, der die Extrusion von intrazellulären Wasserstoffionen in den extrazellulären Raum für die TME-Azidifizierung vermittelt, was zu einer verstärkten Invasion von GBM-Zellen führen könnte. Die Expression von CAIX und die Invasion von GBM-Zellen sind unter Hypoxie nachweislich erhöht. Daher wird hypothetisiert, dass CAIX ein spezifisches Ziel für die Invasion von GBM-Zellen insbesondere unter Hypoxie darstellen kann. Das Ziel dieser Studie ist es, die Rolle von CAIX auf die GBM-Zellinvasion unter Hypoxie zu untersuchen.

Methoden: Die Rolle von CAIX wurde in vitro untersucht, indem zwei etablierte GBM-Zelllinien, zwei mesenchymale und zwei proneurale BTICs (brain tumour initiating cells), verwendet wurden. Sie wurden in DMEM bzw. RHB-A Stammzellmedium kultiviert. Das DMEM mit 4,5g/L Glukose wurde verwendet, weil dies die identische Glukosekonzentration im Vergleich zu RHB-A darstellt. Zur Optimierung des Versuchsablaufs wurden zunächst verschiedene Hypoxie-Induktionsmethoden und zwei Methoden zur Zellernte untersucht. Experimente mit niedriger Konfluenz und Wortmannin-Inhibition wurden durchgeführt, um den Einfluss der CAIX-Expression durch die Zellkulturdichte und den PI3K (Phosphoinositid-3-Kinasen)-Signalweg unter Normoxie zu testen. Anschliessend wurde die Expression von CAIX in allen sechs Zelllinien sowohl unter Normoxie als auch unter Hypoxie untersucht, als Vergleich wurden zwei Isoformen von VEGF (Vascular Endothelial Growth Factor) ebenfalls getestet, um die experimentelle Bedingung der Hypoxie zu validieren. Zell-Immunfluoreszenzfärbung wurde durchgeführt, um die Expression des membranständigen Proteins CAIX unter Normoxie und Hypoxie spezifisch zu testen. Das Zellviabilitätsexperiment

wurde durchgeführt, indem die Zellen mit verschiedenen Konzentrationen eines spezifischen Inhibitors der extrazellulären Carboanhydrasen (U104) behandelt wurden, um die optimale Konzentration und die Einwirkungstage für den Invasionstest zu finden, bevor der Zelltod eintritt. Schließlich wurde die Zellinvasion in einer mit Matrigel beschichteten Transwell-Kammer und mit oder ohne CAIX-Inhibitor unter Normoxie und Hypoxie untersucht.

Ergebnisse: Die direkte Zugabe von reinem Stickstoff in das Medium in T75-Flaschen war die beste Methode zur Hypoxie-Induktion. Die Accutase/Trypsin-Methode war der Scraper-Methode zur Zellernte in dieser Studie überlegen. Alle Zelllinien exprimierten sehr geringe mRNA und Basisprotein von CAIX unter verschiedenen Konfluenzzuständen und Normoxie, mit Ausnahme der hohen Expression von CAIX mRNA in U87 unter Hochkonfluenzkultur. CAIX konnte durch den PI3K-Inhibitor Wortmannin in den meisten Zelllinien unter Normoxie herunterreguliert werden. Die Ergebnisse der Normoxie- und Hypoxie-Experimente zeigten eine erhöhte mRNA-Expression von CAIX/VEGF165/VEGF121 in allen 6 Zelllinien nach 24 Stunden anhaltender Hypoxie. Die experimentellen Ergebnisse zeigten auch eine signifikant erhöhte Proteinexpression von CAIX in zwei etablierten Zelllinien, eine leicht erhöhte Expression in BTIC13/17/18 und keine signifikante Veränderung in BTIC12 unter 24-stündiger anhaltender Hypoxie. Die Zell-Immunfluoreszenz-Färbung zeigte, dass alle GBM-Zelllinien eine Grundexpression des CAIX-Proteins unter Normoxie hatten, sowie eine erhöhte Proteinexpression in etablierten Zelllinien bzw. BTICs in unterschiedlichem Ausmaß unter Hypoxie. Das Zellviabilitätsexperiment zeigte eine dosis- und expositionszeitabhängige toxische Wirkung von U104 in allen Zelllinien. Hypoxie erhöhte die Zellviabilität nur bei bestimmten Zelllinien (U87 und BTIC13) und experimentellen Bedingungen. U87 und BTIC18 waren im Vergleich zu den anderen Zelllinien weniger empfindlich gegenüber U104. Der Matrigel-beschichtete Transwell-Assay für die Zellinvasion zeigte eine hohe Heterogenität zwischen den Zelllinien und bei identischen experimentellen Bedingungen derselben Zelllinie. Alle Zelllinien zeigten eine reduzierte Invasionsfähigkeit nach seriellen Passagen. Hypoxie erhöhte die Zellinvasion nur bei bestimmten Zelllinien (U87 und BTIC12) und experimentellen Bedingungen. Unter dem Lichtmikroskop konnten keine offensichtlichen morphologischen Veränderungen der invadierten Zellen zwischen verschiedenen Behandlungsgruppen sowie Normoxie und Hypoxie in derselben Zelllinie beobachtet werden. Mesenchymale BTICs zeigten eine viel höhere Invasionsfähigkeit als andere Zelllinien. Der CAIX-Inhibitor U104 reduzierte die

Invasion nur bei mesenchymalen BTICs.

Schlussfolgerungen: Die meisten GBM-Zelllinien werden durch den PI3K-Signalweg reguliert und nicht durch die Zellkonfluenz für die Grundexpression von CAIX unter Normoxie auf Transkriptions- und Translationsebene. Die Expression von CAIX mRNA wird durch Hypoxie in allen Zelllinien stark induziert. Während die Proteinexpression von CAIX nur in etablierten Zelllinien durch Hypoxie signifikant induziert wird, könnte dies auf die posttranslationale Stabilisierung des Proteins hinweisen. U104 könnte als gezielte Substanz zur Behandlung des GBM eingesetzt werden, da die Inhibition von CAIX ein metabolisches Ziel bei der Inhibition von GBM Invasion darstellen könnte, jedoch primär bei mesenchymal differenzierten Tumoren.

Abstract

Objective: GBM (glioblastoma multiforme) is the most common and devastating primary tumor in central nervous system. The patient with GBM has an exceptionally poor prognosis. Heterogeneous and invasive nature of GBM makes it impossible to be cured by current treatment. GBM is also characterized by cellular metabolism reprogramming and TME (tumour microenvironment) acidification as well as intratumoral hypoxia. CAIX (carbonic anhydrase IX) is overexpressed in GBM but not in normal brain tissue. The characteristics of specific expression, hypoxia inducible, high catalytic activity and extracellular membrane location of CAIX are hypothesized to make it an important factor to mediate the extrusion of intracellular hydrogen ions into the extracellular space for TME acidification followed by the enhanced invasion of GBM cells. The expression of CAIX and invasion of GBM cells are also demonstrated to be enhanced under hypoxia. Therefore, CAIX is supposed to be a specific target for GBM cell invasion especially under hypoxia. The purpose of this study is to investigate the role of CAIX on GBM cell invasion under hypoxia.

Methods: The role of CAIX was investigated *in vitro* by using two established GBM cell lines, two mesenchymal and two proneural BTICs (brain tumour initiating cells). They were cultured in DMEM and RHB-A stem cell medium, respectively. The DMEM of 4.5g/L glucose was used because it had the same glucose concentration as RHB-A. Various hypoxia induction methods and two cell harvesting methods were examined first to optimize the experimental procedure. Low confluence and Wortmannin inhibition experiments were performed to test the influence of CAIX expression by cell culture density and PI3K (phosphoinositide 3-kinases) pathway under normoxia. Later, the expression of CAIX was examined in all six cell lines under both normoxia and hypoxia, and two single-isoform VEGFs (vascular endothelial growth factors) were also tested to validate the experimental condition of hypoxia. Cell immunofluorescence staining was performed to specifically test the expression of membrane protein CAIX under normoxia and hypoxia. Cell viability experiment was conducted by treating cells with different concentration of a specific inhibitor of extracellular carbonic anhydrases (termed U104) to find the optimized concentration and action days for invasion assay before cell death occurs. At last, cell invasion was investigated by Matrigel coated Transwell chamber and with or without CAIX inhibitor under normoxia and hypoxia.

Results: Gassing nitrogen up to the medium in T75 flask directly was the best way for hypoxia

induction. Accutase/Trypsin method was superior to scraper method for cell harvest in this study. All cell lines expressed very low mRNA and baseline protein of CAIX under various confluence states and normoxia apart from the high expression of *CAIX* mRNA in U87 under high confluence culture. CAIX could be downregulated by PI3K inhibitor Wortmannin in most cell lines under normoxia. Results of normoxia and hypoxia experiment showed increased mRNA expression of *CAIX/VEGF165/VEGF121* in all 6 cell lines after 24-hour sustained hypoxia. Experimental results also showed significantly increased protein expression of CAIX in two established cell lines, mildly increased expression in BTIC13/17/18 and no significant change in BTIC12 under 24-hour sustained hypoxia. Cell immunofluorescence staining illustrated that all GBM cell lines had a baseline expression of CAIX protein under normoxia, as well as increased protein expression in established cell lines and BTICs respectively to various degrees under hypoxia. Cell viability experiment revealed a dose and exposure time dependent toxic effect of U104 in all cell lines. Hypoxia increased cell viability only in specific cell lines (U87 and BTIC13) and experimental conditions. U87 and BTIC18 were less sensitive to U104 in comparing with other cell lines. Matrigel coated Transwell assay for cell invasion presented high heterogeneity between cell lines and in identical experimental condition of same cell line. All cell lines showed reduced invasion ability after serial passages. Hypoxia increased cell invasion only in specific cell lines (U87 and BTIC12) and experimental conditions. No obvious morphological changes of invaded cells could be observed between different treatment groups as well as normoxia and hypoxia in same cell line under optical microscope. Mesenchymal BTICs showed much higher invasion ability than other cell lines. CAIX inhibitor U104 reduced invasion only in mesenchymal BTICs.

Conclusions: Most GBM cell lines are regulated by PI3K pathway rather than cell confluence for the baseline expression of CAIX under normoxia on transcription and translation levels. The expression of *CAIX* mRNA is strongly induced by hypoxia in all cell lines. While the protein expression of CAIX is significantly induced by hypoxia only in established cell lines, this may attribute to the protein stability post-transcriptionally. U104 may be used as a targeted drug for treatment of GBM cells. The inhibition of CAIX is also a potential metabolic target for the invasion repression of GBM cells but only in mesenchymal BTICs.

1 Introduction

1.1 GBM

1.1.1 Overview

Gliomas are neuro-epithelial tumors and may arise from neuro-glial cells or their precursor cells, originating in the CNS (central nervous system).[1] WHO (World Health Organization) grade III and IV gliomas are known as malignant gliomas traditionally.[2] Malignant gliomas account for 95.8% of all gliomas, and GBMs account for 59% of all malignant gliomas. GBM has an exceptionally poor prognosis measured by months rather than by years.[3]

Despite research progress in the understanding of the molecular pathogenesis, associated cell signaling pathways,[4-6] and application of new therapeutic methods in recent years,[7, 8] there are no curable treatment approaches because of the heterogeneous and invasive nature of GBM.[9, 10] Thence, it is very important to search for new approaches or optimize currently available treatment options to improve patient survival.

1.1.2 Classification and grading

Percival Bailey and Harvey Cushing were the first to establish a brain tumor classification under the presumption of different cells of origin linked to patient's outcome data.[11] For the last century, brain tumor classification was largely based on histogenesis according to the histological microscopic similarities of putative original cells and differentiation levels by hematoxylin-eosin staining, immunohistochemical staining and ultrastructural analysis dependent on light microscope.[12] 2016 World Health Organization Classification of Tumors of the Central Nervous System, the latest version, is the first time to define entities, variants and patterns according to integrated phenotypic and genotypic parameters.[12]

CBTRUS (The Central Brain Tumor Registry of the United States) defines tumors of ICD-O-3 (3^{rd} edition international classification of diseases for oncology) histology codes 9440, 9441, 9442 as GBMs. [3, 13] Four-tiered WHO histological grading scheme (grade I, II, III, IV) is widely used and is based on tumour's malignant biological behavior and the patient's prognosis. The malignancy increases with the increased grade.[14] GBMs can be classified into primary and secondary GBMs on the basis of both history of disease and biogenetic characteristics, despite

that they are morphologically indistinguishable.[2] Primary GBMs which account for the vast majority (>90%), occur in older patients (>50 years) and arise without a known precursor. They are characterized by *EGFR* (epidermal growth factor receptor) amplification, LOH (loss of heterozygosity) of chromosome 10, *PTEN* (phosphatase and tensin homolog) tumor suppressor gene mutation, *TERT* (telomerase reverse transcriptase) promoter mutation, $p16^{INK4a}$ deletion. Secondary GBMs which account for the minority (<10%), occur in younger patients (<45 years) and progress from low-grade or anaplastic astrocytoma precursors. They are characterized by mutations of *IDH1/2* (isocitrate dehydrogenase 1/2), *TP53* (tumor protein P53), as well as *ATRX* (alpha thalassemia/mental retardation syndrome X-linked) and chromosome 19q loss. [2, 15, 16] The molecular classification of GBMs, based on the abnormal gene expression of genome, includes classical, mesenchymal, proneural, and neural types. (More details please refer to 1.1.6.3)

1.1.3 Epidemiology

The incidence of GBMs varies significantly in different countries.[17] According to the statistical report of CBTRUS (2011-2015), GBM is the most common (47.7%) primary malignant brain tumor. The average annual incidence rate is 3.21 per 100,000. The incidence increases from 2000 to 2005 and no significant change from 2005 to 2015. GBM is more common in older adults and less in children. The median age at diagnosis is 65 years old. The incidence rate increases with age, and the highest is in 75-84 years old. Males are 1.58 times more common than females. Whites are 1.93 times higher compared to Blacks, and are also higher than American Indian/Alaskan Natives and Asian/Pacific Islanders. The incidence in urban areas (3.13 per 100,000) is slightly higher than in rural areas (3.03 per 100,000). Incidence of Hispanic ethnicity (2.4 per 100,000) is lower than non-Hispanic ethnicity (3.30 per 100,000). The relative survival rates of GBM post-diagnosis in all age are 1-year 40.2%, 2-year 17.4%, 5-year 5.6%, 10-year 2.8%, respectively. The average annual age-adjusted mortality rate for primary malignant brain and other CNS tumors is 4.37 per 100,000. 61.2% gliomas occur in the supra-tentorium of brain, and the incidences of the frontal, temporal, parietal, and occipital lobes decrease gradually.[3]

1.1.4 Etiology

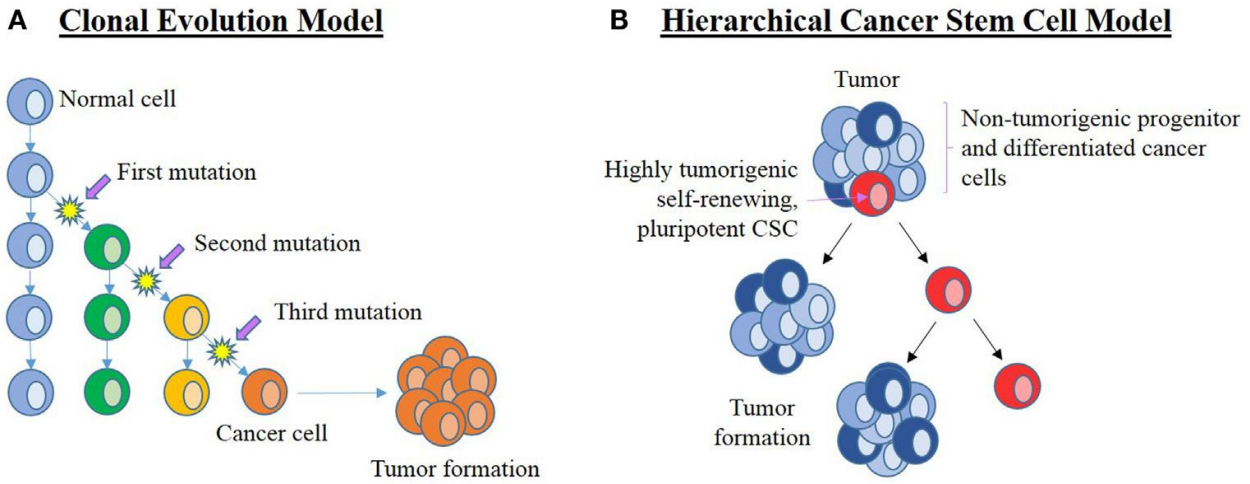

Figure 1.1 Schematic representation of two hypotheses about cellular origin of GBMs. [18, 19]

The origin of glioma cells is not fully understood and may arise from NSCs (neural stem cells), glial progenitor cells, or the dedifferentiation of mature cells.[20] There are at least two hypotheses. Stochastic or clonal evolution hypothesis is featured as random acquisition of mutational events followed by creating clonally derived subpopulations in the tumor. Hierarchies or cancer stem cells (CSCs) hypothesis is defined as a subset of cells represent stem-like properties which include the ability of self-renew and proliferation as well as the creation of complex cell types in the tumor.[18]

Many environmental and genetic risk factors have been investigated for glioma, while most of them are inconclusive and underpowered.[17] Medium to high dose of ionizing radiation (e.g., radiotherapy, atomic bomb) is the only established environmental risk factor for CNS tumors. While the low dose ionizing radiation (e.g., medical exposures of X rays and CT) is controversial.[21] Numerous large studies report a strong inverse association between glioma risk and allergy history.[17] The association between usage of antihistamine and glioma risk shows inconsistent results.[22-24] There is no indication of an increased risk of glioma in relation to the use of mobile phone [25, 26] as well as the occupational exposure to extremely low frequency magnetic fields.[17] While the Monograph Program of IARC (the International Agency for Research on Cancer) in 2011 and a meta-analysis in 2017 reported an increased risk of glioma in long-term heavy mobile phone users.[27, 28] Other research that focus on jobs and occupational exposures with glioma risk show inconsistent results because of small samples.[17]

Although familial heritable genes in monogenic Mendelian cancer syndromes are associated with increased glioma risk, they account for a small part of glioma incidence rate on the population level.[17] These include Neurofibromatosis 1 (*NF1*), Neurofibromatosis 2 (*NF2*), Tuberous sclerosis (*TSC1,TSC2*), Lynch syndrome [*MSH2/6* (mutS homolog 2/6)*, MLH1* (mutL homolog 1)*, PMS2* (postmeiotic segregation increased 2)], Li-Fraumeni syndrome (*TP53*), Melanoma-neural system tumor syndrome [*p16/CDKN2A* (cyclin-dependent kinase inhibitor 2A)], Ollier disease/Maffucci syndrome (*IDH1/IDH2*).[29, 30] Segregation analysis of polygenic model by GWASs (genome-wide association studies) identified 8 independently germline DNA SNPs (single nucleotide polymorphisms) located in 7 genes, which increase the risk of gliomas. These include *TERT* (rs2736100-C); *EGFR* (rs2252586-A, rs11979158-A); *CCDC26* (coiled-coil domain containing 26) (rs55705857-G); *CDKN2B* (cyclin-dependent kinase 4 inhibitor B) (rs1412829-G); *PHLDB1* (pleckstrin homology-like domain family B member 1) (rs498872-A); *TP53* (rs78378222-C); *RTEL1* (regulator of telomere elongation helicase 1) (rs6010620-A). [17, 29]

1.1.5 Clinic

1.1.5.1 Early screening and prevention

Screening is only limited to persons with genetic risks and relatives of patients whose tumors carry germline mutations associated with gliomagenesis.[31] Although there are some reports about blood-based biomarkers for the diagnosis and screening of gliomas,[32] there are no relevant recommendations in the guidelines.[7, 8] MRI (magnetic resonance imaging) is more sensitive to detect small tumors. Prevention strategies are not available.[7]

1.1.5.2 Clinical manifestations

Neurological symptoms and signs of GBM patients depend on the tumor size, tissue characteristics and the involved brain anatomic structures.[2, 33] Characteristic clinical presentations are indicators of increased intracranial pressure (e.g., headache, nausea, vomit, altered consciousness), focal neurological function deficits (e.g., hemiplegia, hemidysesthesia, aphasia), neurocognitive impairments (e.g., personality changes, memory loss, depression and anxiety), new onset epilepsy, and non-specific systemic symptoms (e.g., fatigue).[7, 34]

1.1.5.3 Imaging diagnostics

Conventional MRI such as native and gadolinium-DTPA (diethylenetriaminepentaacetic acid) contrast-enhanced T1-weighted, T2-weighted and FLAIR (fluid-attenuated inversion recovery) sequences are the gold standard of minimum recommended sequences to detect gliomas.[35] Conventional MRI of GBM classically presents hypointense to isointense on T1 imaging, hyperintense on T2-weighted and FLAIR imaging, and thick irregularly shaped dense ring-enhancing lesion with hypointense central areas of necrosis on T1 enhancing imaging.[36] There is usually more extensive peritumoral edema than anaplastic gliomas. Involvement of the deep white matter and the corpus callosum are common. Hemorrhage, ventricular distortion or displacement may also be present. The extent and distribution of contrast enhancement reflect the extent of blood brain barrier disruption more than strictly delineation of tumor.[37, 38] Radiographic patterns such as local, distant, multifocal, and diffuse are present in both initial and recurrent GBMs. However, when comparing the presentation of growth pattern of newly diagnosed to recurrent GBMs, there appear to be a decrease of local pattern and an increase of diffuse pattern in the recurrent settings.[39]

Advanced MRI protocols are getting more widely used in the diagnosis and treatment of GBMs. DWI (diffusion-weighted imaging) reflects the diffusion impedance of water thermal motion in tissue and cellularity, which can be used as differential diagnosis, preoperative grading, surgical planning and therapeutic response monitoring. DTI (diffusion tensor imaging) traces white matter tracts based on diffusion anisotropy, because white matter myelin sheaths are important barriers to extracellular water diffusion. DTI is mainly used as preoperative guidance. T1P (dynamic contrast-enhanced T1-weighted imaging) measures vessel permeability of neocapillaries based on the destruction of the BBB (blood brain barrier). T1P is usually used as preoperative tumor grade estimation and postoperative therapeutic monitoring. PWI (perfusion-weighted imaging) measures rCBV (relative cerebral blood volume) in neovascular capillary bed. GBM shows increased blood volume because of the histological hallmark of neovascularity. SWI (susceptibility-weighted imaging) identifies microhemorrhages. MRS (magnetic resonance spectroscopy) detects the metabolites levels and differentiates tumor from necrosis or benign lesions. MRS of patient with GBM shows typically a high choline peak and a low or absent N-acetylaspartate peak with lipid and lactate peaks, as compared with the unaffected brain areas. Although the specificity of this finding for malignant gliomas is comparably low.[37, 40]

CT (computed tomography) can be done faster and displays acute hemorrhages more accentuated compared to MRI. However, it displays a lower soft tissue resolution than MRI especially in posterior fossa. Therefore, for the diagnosis of GBM, CT is usually used only when MRI is not available.[7] CT imaging of GBM classically presents an iso to high density signal mass lesion with surrounding low density signal of vasogenic edema. Contrast-enhanced CT reveals a centrally necrotic ring-enhancing mass. Intratumoral hemorrhage is common. Calcification can be seen occasionally.[37]

PET (positron emission tomography) technique uses various radio tracers to visualize biological and molecular processes (e.g., glucose metabolism, amino acid analogs uptake, cell proliferation, cell membrane biosynthesis and hypoxia). PET can be used for glioma grading, differential diagnosis, pretreatment planning, posttreatment assessment, recurrence monitoring and prognostication. Radio tracers of PET can be divided into glucose metabolism tracers [e.g., 18F-FDG (18F-2-fluoro-2-deoxy-D-glucose)] and amino acid transport tracers [e.g., 11C-MET ([11C-methyl]-methionine), 18F-FET (O-(2-[18F]-fluoroethyl)-L-tyrosine), 18F-FDOPA (3,4-dihydroxy-6-[18F]-fluoro-L-phenylalanine)].[41, 42]

CSF (cerebrospinal fluid) studies do not play an important role in diagnosis of gliomas. Lumbar puncture carries a high risk of brain hernia especially in patient with a large space-occupying effect. Electroencephalography helps to monitor tumor-associated epilepsy and determine the causes of altered consciousness.[7]

Imaging genomics (radiogenomics) is an emerging clinical science that explores relations between radiophenotypes (certain radiologic features) and genotypes (genomic and molecular profiles). Associated noninvasive imaging techniques quantitatively and qualitatively analyze biomarkers that surrogate genomic and molecular profiles of GBMs with conventional invasive surgical procedures.[43]

1.1.5.4 Pathology

The assessment of cytological or frozen specimen in operation room is to ensure that it is sufficient for diagnosis and also used for the decision-making by neurosurgeons. After surgery or biopsy, fresh tumor specimen is formalin-fixed and paraffin-embedded for hematoxylin-eosin, immunohistochemical staining and molecular analyses, as well as the diagnosis by neuropathologist. If it's possible, the remaining specimen should be cryopreserved for molecular

marker studies in the future.[7]

GBM is characterized by infiltrating GFAP (glial fibrillary acidic protein) immunopositive with marked pleomorphism, cellular and nuclear anaplasia, high cellularity, brisk mitotic activity, microvascular proliferation, invasiveness, and intratumoral pseudopalisading necrosis.[2, 9, 20, 44, 45] Pseudopalisades are severely hypoxic GBM cells that actively migrate away from necrotic center. Pseudopalisading cells accumulate hypoxia-inducible factors and secrete proangiogenic factors.[46] The formation of pseudopalisades necrotic center is hypothesised as high cell confluence by intense replication and vaso-occlusion by intravascular thrombosis. Pseudopalisading cells develop an invasive phenotype and migrate to better oxygen and nutrients irrigated areas.[47] GBM cells tend to invade along existing structures for the formation of distant satellite tumours even to the contralateral brain.[48] The invasive single GBM cell is undetectable by the most sophisticated imaging techniques and contributes to tumor recurrence.[49] The molecular pathology of GBM please refers to 1.1.6.

1.1.5.5 Differential diagnosis

The differential diagnosis of GBM includes brain metastasis, CNS lymphoma, non-neoplastic conditions such as abscess or intraaxial parasites. GBM presents more irregular shapes than metastasis because of the predilection invasive nature along white matter tracts. Primary CNS lymphoma normally presents homogeneous in signal intensity and enhancement in immunocompetent patients, while imaging performances of central necrosis and heterogeneity are more common in immunocompromised patients.[37]

1.1.5.6 Therapy overview

MDT (multidisciplinary discussion) should be performed for the management plan of GBM and throughout the whole disease course. These include dedicated neurosurgeons, neuroradiologists, neuropathologists, radiation oncologists, neurooncologists, psychologist, therapists, specialist nurses and research staff. [7, 8]

Stupp protocol is the standard multimodal treatment for newly diagnosed GBM patients between 18 and 70 years. The latest recommendations from NCCN (National Comprehensive Cancer Network) and EANO (European Association of Neuro-Oncology) guidelines include maximal

well-tolerated safe microsurgical resection, concomitant radiochemotherapy plus six cycles of adjuvant temozolomide chemotherapy.[7, 8] After the application of Tumour Treatment Fields in recent years, the overall survival of the patients has increased from 14.6-16.7 months to 20.9 months.[50]

1.1.5.7 Supportive care

Regular hematology, blood glucose, blood concentration of anti-epileptic drugs, hepatic and renal laboratory examinations, exclusion of major heart or lung diseases and infection are required for GBM patients.[7]

Corticosteroids (e.g., dexamethasone) can be prescribed to control tumor-associated vasogenic edema and alleviate accompanying symptoms and signs. This should be carried out without contraindications such as suspicion of primary cerebral lymphoma or inflammatory lesions.[7, 51] Prophylactic corticosteroids are not necessary in patients without edema-associated neurological function deficits or increased intracranial pressure. There is no necessity for prolonged application after surgery or prophylaxis during radiotherapy in asymptomatic patients. Rapid reduction and discontinuation of corticosteroids are recommended to avoid long-term complications which include osteoporosis and compression fractures, corticosteroid myopathy, lymphopenia and risk of infection, Cushing syndrome. Calcium, vitamin D, bisphosphonates and antibiotics should be considered for the treatment of complications.[2, 44] NSAIDS (non-steroidal anti-inflammatory drugs), analgesics and co-analgesics can also be considered in the relief of headache.[51] Osmotic agents (e.g mannitol) are rarely necessary preoperatively.[7] Patients with epileptic seizures should be controlled by AEDs (antiepileptic drugs). Prophylaxis of tranditional AEDs is not indicated in patients without seizures.[7, 8] While a short-term prophylaxis prescription of newer generation AEDs can be considered for patients who undergo a craniotomy approximately 1 week postoperatively.[52] Phenobarbital, phenytoin, carbamazepine and primidone significantly induce hepatic cytochrome P-450 enzymes which increase the metabolism of many chemotherapy drugs. Levetiracetam, topiramate, lamotrigine, pregabalin are preferred.[8, 52] Malignant glioma patients are at a high risk of VTE (venous thromboembolism), especially PE (pulmonary emboli) and DVT (deep venous thromboembolism) from leg and pelvic veins. This risk is throughout the disease course and caused by many reasons which include neurological deficits, corticosteroids usage, chemoradiation, and so on.[44, 53, 54]

Duplex venous ultrasonography and laboratory testing are recommended for initial diagnosis of VTE, especially in patients with extremity edema, pain, and erythema. In cases of negative or indeterminate ultrasound results, CTA (CT angiography), MRV (magnetic resonance venography) and standard invasive venography are recommended for confirmed diagnosis. Anticoagulants and mechanical devices can be used for prophylaxis or treatment of VTE patients.[55]

1.1.5.8 Microsurgical resection or biopsy

The choice of surgical method depends on the condition of the patient, the number, size and location of the tumor, etc.[56] While it is more important to preserve neurological functions and avoid new permanent neurological deficits than extent of surgical resection, because glioma can not be curatively treated by surgery. This is precluded by the infiltrative growth nature and often in eloquent areas.[57, 58]

Microsurgery is recommended to perform in high-volume specialist centers. It is aimed at removing as much of the tumor as safely for improving neurological functions and establishing a histological and molecular diagnosis or studies.[7, 59] Some studies have reported that only gross total resection (≥98%), not influenced by *MGMT* (O^6-methylguanine DNA methyltransferase) promoter methylation, is associated with improved OS (overall survival) and PFS (progression-free survival).[60-62] Others have also reported that subtotal resection (≥70-78%) and residual volume (≤5 cm^3) are associated with better survival and reduced recurrence.[63, 64] Low-quality evidence support the supra total resection, beyond all T1-enhanced and T2/FLAIR abnormalities, improves OS and PFS in both LGG (low-grade glioma) and HGG (high-grade glioma) patients.[65, 66] It also reduces malignant transformation in LGG glioma patients.[67] Gross total resection is defined as the radiographic absence of contrast-enhancing regions in HGG, and T2/FLAIR hyperintensity regions in non-enhancing lesions postoperatively. In order to achieve the maximum safe resection, a large technical portfolio can be used for surgical assistance.[68] These include functional MRI-guided neuronavigation, navigable intraoperative ultrasound, intraoperative MRI, fluorescence (e.g., 5-aminolevulinic acid or sodium fluorescein) guided resection, as well as awake craniotomy with cortical and subcortical stimulation mapping. All these techniques improve the surgical safety and increase the extent of resection attainable.[68] Postoperative assessment by MRI without and with contrast-enhanced is recommended within 24-48h and no more than 72h. This can be used as a baseline to assess

therapeutic efficacy and tumor progression.[69]

Stereotactic needle biopsy is often performed along the trajectory under local anesthesia. This can be done only in patients who have inoperable tumors which are located in critical or deep areas of the brain.[7, 8] Biopsy results may be misleading, especially from small samples. This is because gliomas often have altered degrees of mitoses, cellularity, microvascular proliferation and necrosis from one area to another.[8]

After surgery, patients wait around 2 weeks for the surgical incision healing before radiochemotherapy.[33]

1.1.5.9 Radiotherapy

The purpose of RT (radiotherapy) is to improve local control for increasing survival and preserve function at a reasonable benefit risk ratio.[7]

RT has been the cornerstone of care in GBM patients for more than 4 decades. This is because BTSG (Brain Tumor Study Group) 6601-6901-7201 RCT (randomized controlled trail) studies reported in the 1970s the survival benefit in GBM patients by comparing WBRT (whole-brain RT) with supportive care alone postoperatively.[70] Base on the local recurrence (90 % within 2 cm margin of the primary area) nature of gliomas[71] and brain damage by high-dose WBRT, some investigators reduced radiation portals.[70] BTCG (Brain Tumor Cooperative Group) 8001 RCT study reported similar effect between WBRT and focal irradiation in 1989.[72]

IFRT (involved field RT) is the standard method and defined as radiotherapy encompasses the tumor and surrounding brain tissue whthin 3 cm.[70] The standard dose for patient with newly diagnosed GBM is 59.4-60 Gy (Gray) in 1.8-2 Gy fractions between 18 and 70 years.[7, 8, 73] Dose-escalation shows increased toxicity (normal brain tissue necrosis at the tumor periphery) without additional survival benefit.[74] 50 Gy in 1.8 Gy fractions is used in patients ≥70 years with good KPS (Karnofsky Performance Status).[75] Hypofractionated RT dose 40 Gy in 2.67 Gy fractions alone is the appropriate mode for elderly patients with worse prognostic factors.[7, 8] Novel imaging techniques can be used as assistant for RT field design.[70] While neither accelerated hyperfractionated or hypofractionated methods nor brachytherapy, stereotactic RT boost or radiosurgery are better than the standard method for survival of patients.[7]

1.1.5.10 Chemotherapy

The earliest began in the 1970s, a large number of clinical trials of chemotherapy reagents (e.g., nitrosoureas, cisplatin) had been examined and with disappointing results, because of both chemo-responsiveness or intrinsic chemoresistance and blood-brain or blood-tumour barriers in preventing sufficient drug concentration. Only nitrosourea concomitant with or after radiotherapy appeared modest survival benefit in younger (< 60 years) patients with GBMs in some research and in patients with anaplastic astrocytomas.[76]

Nitrosoureas are DNA alkylating agents easy to penetrate blood-brain barrier because of high lipophilicity.[77] Nitrosoureas [such as procarbazine, CCNU (lomustine), BCNU (carmustine), ACNU (nimustine) or fotemustine] are the second choice for anaplastic glioma in most European countries.[7] Relatively serious and persisting complications limit the usage of nitrosoureas. These include significant leukopenia, thrombocytopenia with bone marrow suppression, liver and renal toxicity, pulmonary fibrosis.[7]

TMZ (temozolomide, brand name Temodal® or Temodar®) is extensively used in GBM treatment. It is an oral DNA alkylating agent with good penetration of BBB and an excellent safety profile.[7] The clinical trials of EORTC (the European Organisation for Research and Treatment of Cancer) 22981/26981 and NCIC (the National Cancer Institute of Canada) CE.3 reported in 2005 and 2009 the increased postoperative median survival time (14.6 months versus 12.1 months) and annual survival rate (27.2% versus 10.9% at 2 years, 16.0% versus 4.4% at 3 years, 12.1% versus 3.0% at 4 years, 9.8% versus 1.9% at 5 years, respectively) by comparing radiotherapy concomitant temozolomide followed by six cycles of adjuvant temozolomide with radiotherapy alone.[78, 79] No definitive evidence supports superior survival benefit from increased dose or extended duration of TMZ in the newly diagnosed GBMs.[80-82] *MGMT* gene is located on chromosome 10q26 and codes MGMT protein. MGMT protein is a DNA repair enzyme that removes alkyl groups from the O^6 position of guanine. The promoter methylation status of *MGMT* gene is a strong prognostic predictor of both temozolomide chemotherapy and radiotherapy. GBM patient who has epigenetic silence of *MGMT* gene by promoter methylation exhibits inactivated MGMT protein and compromised DNA repair. This would trigger cytotoxicity and apoptosis. While unmethylated *MGMT* gene exhibits activated MGMT enzyme which can interfere with the effects of treatment.[83]

Gliadel® is a biodegradable polymers wafer by incorporation with carmustine. It is locally

implanted into the surgical cavity and gradually releases carmustine over several weeks to kill residual tumor cells.[84-86] However, Gliadel® is rarely used because of poor clinical benefit.[7] Bevacizumab, also named Avastin®, is a humanized anti-angiogenic monoclonal antibody to VEGF. It is well tolerated, shows superior radiographic response and reduces corticosteroid dosage dramatically in recurrent GBM patients.[87-89] Nonetheless, two phase III trials reported that the adding of bevacizumab to Stupp protocol in newly diagnosed GBM patients failed to demonstrate improved OS despite a clear 3-4 months benefit in PFS. Increased adverse events were higher with bevacizumab over times. [90, 91] Improved PFS may stem from reduced peritumoral edema by stabilization of the blood-brain barrier. This is named pseudoresponse.[92] Bevacizumab is approved for recurrent GBMs in Canada, USA (United States of America), Switzerland and other countries outside the European Union.[7]

1.1.5.11 Tumor-treating fields

TTFields (tumor-treating fields), also named Optune®, is a novel antimitotic treatment modality that interrupts GBM cell division and organelle assembly followed by cell apoptosis. TTFields delivers low-intensity, intermediate-frequency (200 kHz), alternated electric fields through 4 transducer arrays that connect to a portable device. It is continuously applied on the shaved scalp and should be used for more than 18 hours a day. A phase III trial reported improved PFS (6.7 months vs 4.0 months) and OS (20.9 months vs 16.0 months) by comparing with the adding of TTFields to Stupp protocol or not in newly diagnosed supratentorial GBM patients. Frequency of systemic adverse events was similar between 2 groups. Mild to moderate localized skin toxicity occurred in half of the TTFields group. [50, 93]

1.1.5.12 Other treatments

The novel experimental treatment modalities include targeted therapy, immunological therapy, gene therapy, as well as novel drug blood brain barrier delivery technologies. Decades of research produce numerous frustrating results. This may attributed to tumour heterogeneity, lack of validated biomarkers, redundancy of intracellular signalling pathways, and poor drug blood-brain barrier penetration.[94]

1.1.5.13 Palliative care

Palliative care is to improve the patient's quality of life and problems associated with life-threatening illness of their families. This can be performed by identification, assessment and treatment of physical, psychosocial and spiritual problems.[95] Palliative care should be initiated early and throughout their disease course, particularly in the end of life phase. Due to the life-limiting nature of GBMs, it is aimed to relieve symptoms and preserve or improve functions and quality of life instead of the prolongation of life or cure.[51]

1.1.5.14 Post-treatment monitoring, evaluation and follow-up

MRI is the standard diagnostic measurement for the evaluation of disease status and treatment response. Three months intervals are common practice initially for most patients, but longer intervals are appropriate in case of stable and vice versa.[7]

Pseudoprogression is a phenomenon to show increased enhancement and/or edema on imaging that reflects a transient effect in vessel permeability as a result of treatment. This indicates tumor progression without increased tumor activity. Pseudoprogression is most likely to occur during the first three months of chemoradiotherapy with temozolomide.[96] Radiation necrosis is a late radiation response which is similar to true tumor progression on imaging. Radiation necrosis often occurs 3-12 months after radiotherapy.[97] In the event of dubious tumor progression, recheck the MRI scan after 4-6 weeks of treatment to confirm whether progression is reasonable.[7] MRS, perfusion MRI and amino acid PET help to distinguish pseudoprogression and radio-induced necrosis from actual progression.[7, 8] Pseudoresponse is another phenomenon to show the decreased contrast-enhancement and/or edema on imaging. Pseudoresponse shows reduced vascular permeability without a true antitumor effect. It usually occurs after antiangiogenic therapies such as bevacizumab, cediranib. They induce rapid normalization of abnormally permeable blood vessels and regional cerebral blood flow.[36]

Macdonald criteria are used to assess the response after treatment of malignant gliomas. Macdonald criteria include 4 response categories that are complete response, partial response, stable disease, and progressive disease. Macdonald criteria are based on changes in tumor size by enhanced CT or MRI, corticosteroid dose and neurologic findings.[98] RANO (The Response Assessment in Neuro-Oncology working group) criteria are the updated standard for response

assessment. RANO criteria recommend additional assessment of non-contrast-enhancing areas and new lesions.[99]

1.1.5.15 Prognosis

Age, KPS of patient, methylation status of *MGMT* promoter and extent of surgical resection are the important therapy-independent and therapy-dependent prognostic factors of glioma, respectively.[7, 59] *IDH* mutation is the favorable core molecular marker of GBM prognostically.[7] Preoperative tumor size and location, pathology, postoperative neurological deficits are also associated with outcomes.[7, 33]

1.1.5.16 Progression and recurrence

According to RANO criteria, progression of malignant glioma is defined as any of the following: 25% or more increasement of enhancing area or a significant increasement of T2/FLAIR nonenhancing area on stable or increasing corticosteroid dosage by comparing with baseline imaging; the appearance of any new lesions; significant progression of nonmeasurable lesions; definite clinical deterioration without other reasons; fail to evaluate because of deteriorating condition or death.[99] After the treatment of Stupp protocol, the percentage of progression in GBM patients are 73.1% at 1 year, 88.8% at 2 years, 94.0% at 3 years, 94.4% at 4 years, 95.9% at 5 years, respectively. The median survival is 6.2 months after progression.[78, 79] Progression patterns include inside, margin, outside of the RT field. Progression inside of the RT field accounts for the majority and with a shorter PFS and OS. Patterns and time of progression are correlated with the status of *MGMT* methylation. CSF/spinal dissemination or distant recurrence are rare.[100]

No well established second-line standards of care for patients with recurrent GBMs, because of insufficiency of randomized controlled studies.[7, 8] Clinical decision-making is influenced by age, KPS, prior treatment, and progression patterns.[7]

Despite both prospective data and retrospective analyses show controversial results of prognostic impact on OS by second surgery.[101-103] Surgery debulking can alleviate mass effect, symptoms and confirm recurrent diagnosis, differential diagnosis and molecular testing.[33] Second surgical resection is recommended for 20-30% of patients with symptoms and

circumscribed lesions. It is performed more than 6 months interval from the initial surgery. Second surgery can be shorter interval for patients with symptoms after suboptimal preceding surgery.[7]

It is controversial for prognostic impact on OS and PFS by re-irradiation after GBM progression, because of the scarcity of prospective and randomized trials. Limited effect, radiation necrosis and neurocognitive impairment should be concerned.[103] Re-irradiation is recommended to maintain or improve neurological status and quality of life in GBM patients. Conventional re-irradiation regimen for recurrent GBMs is 30-35 Gy in 3-3.5 Gy fractions. Stereotactic hypofractionated radiotherapy dose is 30-36 Gy in 5-6 Gy fractions or a single dose of 15-20 Gy by radiosurgery.[104]

Re-chemotherapy is usually recommended for the majority of patients with GBM progression. These include nitrosoureas, TMZ, and bevacizumab.[7] Etoposide and platinum-based regimens may be useful only in certain circumstances.[8] Nitrosoureas were widely used in treatment of GBMs before 1999.[77] They are remained as the efficacy agents for recurrent GBMs.[103] Interstitial chemotherapy, such as carmustine polymers wafer, is a safe approach for patients with recurrent malignant gliomas showing moderate efficacy.[85] TMZ becomes the prioritized treatment in recurrent GBM patients because of effectiveness and favorable tolerability profile. This was demonstrated by two phase II trials at the beginning of this century.[105, 106] TMZ rechallenge is probably limited to GBM with *MGMT* promoter methylation.[107] No convincing efficacy of TMZ-based combination regimens precedes single agent activity of TMZ in recurrent GBM patients.[103] Bevacizumab is approved in United States for recurrent GBMs based on two phase II trials,[87, 88] but rejected by EMEA (European Medicines Agency).[108]

TTFields is controversy for recommendation, while still approved for recurrent GBM patients. Because there is no improvement of overall survival in TTFields group by comparing with chemotherapy alone. However, efficacy and activity as well as acceptable toxicity and better quality of life appear comparable to re-chemotherapy.[109]

No targeted agents have been proved efficacy that exceed alkylating agents so far. Immunotherapeutic approaches are under evaluation by promising preliminary data from rindopepimut.[103]

1.1.6 Molecular biology of GBM

1.1.6.1 Genome-wide level alterations

After the completion of the Human Genome Project, many consortia and laboratories endeavor efforts to survey human cancer genome alterations by using advanced genomic technologies. TCGA (the Cancer Genome Atlas) is a large-scale multidimensional analysis project of NIH (the National Cancer Institute's Center for Cancer Genomics) and NHGRI (the National Human Genome Research Institute), that aims to comprehensively analyze the genomic alterations of major cancers. These analyses include diverse molecular alterations of mRNA, miRNA (microRNA), DNA copy number, mutation, protein expression, DNA methylation, etc. GBM is one of the first cancer types to be systematically studied by TCGA.[4, 110]

Integrative analysis from the research result of TCGA reveals the complicated genetic profile of GBM. Three core signaling pathways and related genes are commonly deregulated which include RTK (receptor tyrosine kinases)/RAS (rat sarcoma)/PI3K oncogene pathway, p53 and Rb (retinoblastoma) tumor suppressor pathways.[4, 5] Other parallel study has determined similar alterations of critical genes and pathways.[111]

Many groups have tried to delineate subtype classifications of GBMs.[110, 112] One of the most important and widely used is the four-subtype classification on the basis of signature gene expression profiles from TCGA by Verhaak et al. These include proneural, neural, classical, and mesenchymal subtypes.[6] More in-depth and extensive molecular subtype classifications have also been established in recent years.[113]

1.1.6.2 Core molecular signal pathways and related genes

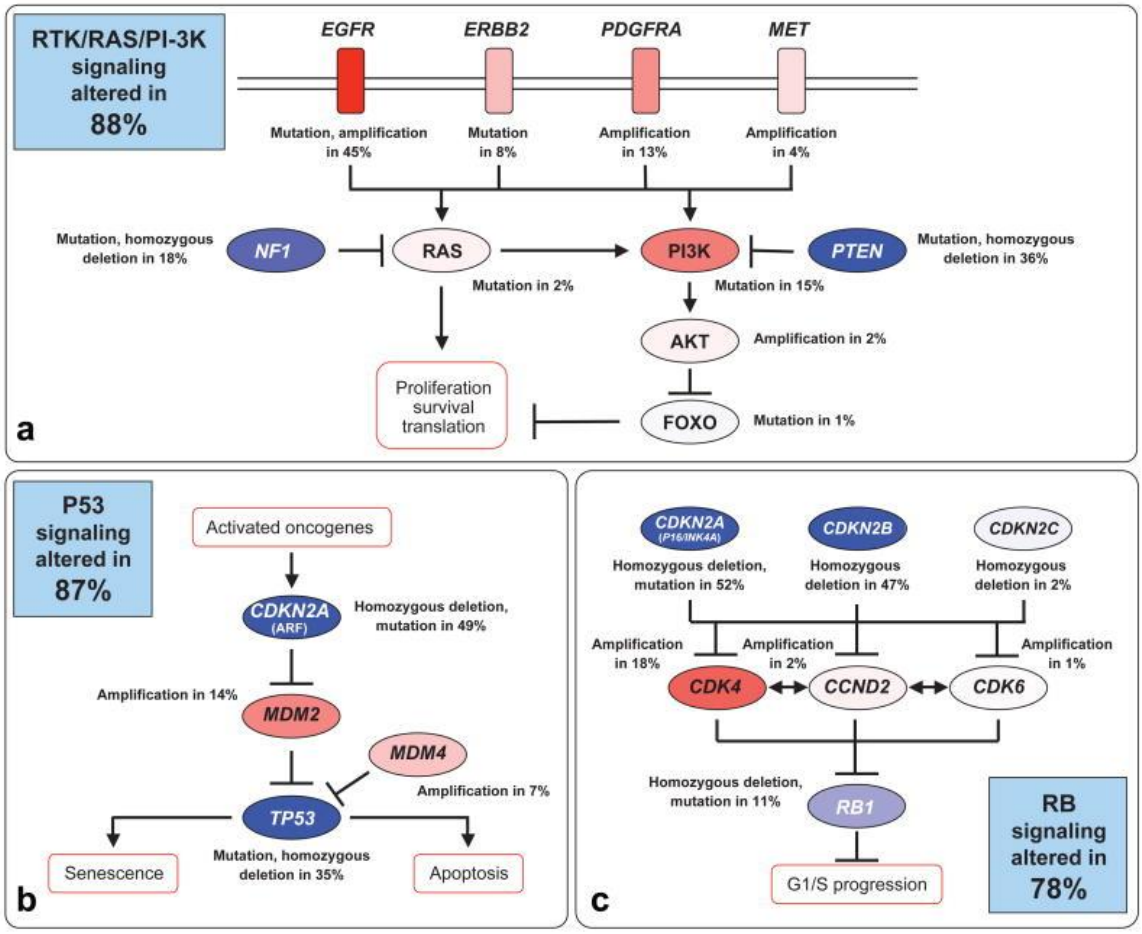

Figure 1.2 Frequent genetic alterations in three critical signaling pathways [4]

RTK signaling pathway includes GF (growth factor) and their receptor [e.g., EGF (epidermal growth factor)/EGFR, PDGF (platelet-derived growth factor)/PDGFR (platelet-derived growth factor receptor), VEGF/VEGFR (vascular endothelial growth factor receptor), HGF (hepatocyte growth factor)/HGFR (hepatocyte growth factor receptor, also named MET), etc]. They activate PI3K/Akt [(AKT serine/threonine kinase, also named PKB (protein kinase B)]/mTOR (mammalian target of rapamycin) and Ras/Raf/MAPK (mitogen-activated protein kinase) signaling pathways. RTK signaling pathway plays an important role in metabolism, proliferation, differentiation, and survival of cells.[114] GBMs often harbor amplification or mutation of RTKs.[4]

PTEN-PI3K/Akt/mTOR signaling pathway regulates normal cell function as well as

tumorigenesis which include proliferation, apoptosis, mobility and invasion of tumor cells. Activated PI3K converses PIP2 (phosphatidylinositol 4,5-bisphosphate) to PIP3 (phosphatidylinositol-3,4,5-triphosphate) and in turn activates Akt and downstream target mTOR. mTOR is the integrated signal for effector actions of various functions.[114] Almost all GBMs represent raised activity in some parts of PI3K pathway. *PTEN* negatively regulates PI3K pathway.[115] The aberrations of PI3K pathway mainly include mutations and deletions of *PTEN*, *PI3K* activating mutations, *mTOR1/2* activation.[114]

NF1-Ras/Raf/MAPK signaling pathway plays a vital role in cell proliferation, differentiation, apoptosis, growth, invasion and tumorigenesis. Activated RAS activates RAF kinase and in turn regulates downstream MEK [also named MAPKK (mitogen-activated protein kinase kinase)] and MAPK. *NF1* is the pivotal negative regulater of RAS. The aberrations of Ras pathway include tumor suppressor deleted or mutated of *NF1* gene, over-expression of *Ras*.[4, 5, 115]

p53 (coded by *TP53*) signaling pathway functions in cell cycle regulation, differentiation, apoptosis, and DNA damage repair.[115] p53 is a tumor suppressor that induces cell cycle arrest and apoptosis in response to various genotoxic and cytotoxic stresses. It is also a broad transcription factor that regulates many genes. *TP53* mutation is an early event in secondary GBM and is a secondary event of general genomic instability in primary GBM. MDM2 (mouse double minute 2 homolog) is an E3 ubiquitin ligase that negatively regulates p53 by transcriptional inhibition and protein degradation. MDM4 is another important negative regulator of p53. ARF (ADP ribosylation factor) ($p14^{ARF}$) is a tumor suppressor and encoded by *CDKN2A*. It regulates p53 by binding and inhibiting the function of MDM2. Inactivation of the p53 pathway occurs in the form of *CDKN2A/ARF* deletions, *MDM2* or *MDM4* amplifications, and *TP53* mutation.[4, 5, 114]

Rb signaling pathway plays an important role in the inhibition of cell cycle progression of G1 phase to S phase. Rb is a tumor suppressor that binds and inhibits E2F1 transcription factor. Rb is phosphorylated and inactivated by Cyclin D/CDK4 (cyclin dependent kinase)/CDK6. INK4a ($p16^{INK4a}$) is encoded by the *CDKN2A*. INK4a and CDKN2B negatively regulate Cyclin D/CDK4/CDK6. The Rb pathway is dysregulated by gene deletion and protein inactivating mutation of *CDKN2A/CDKN2B*, activating mutations or amplification of Cyclin D/CDK4/CDK6 as well as protein mutation or promoter methylation of *Rb*.[4, 5, 114]

1.1.6.3 Molecular subtype classifications of GBMs

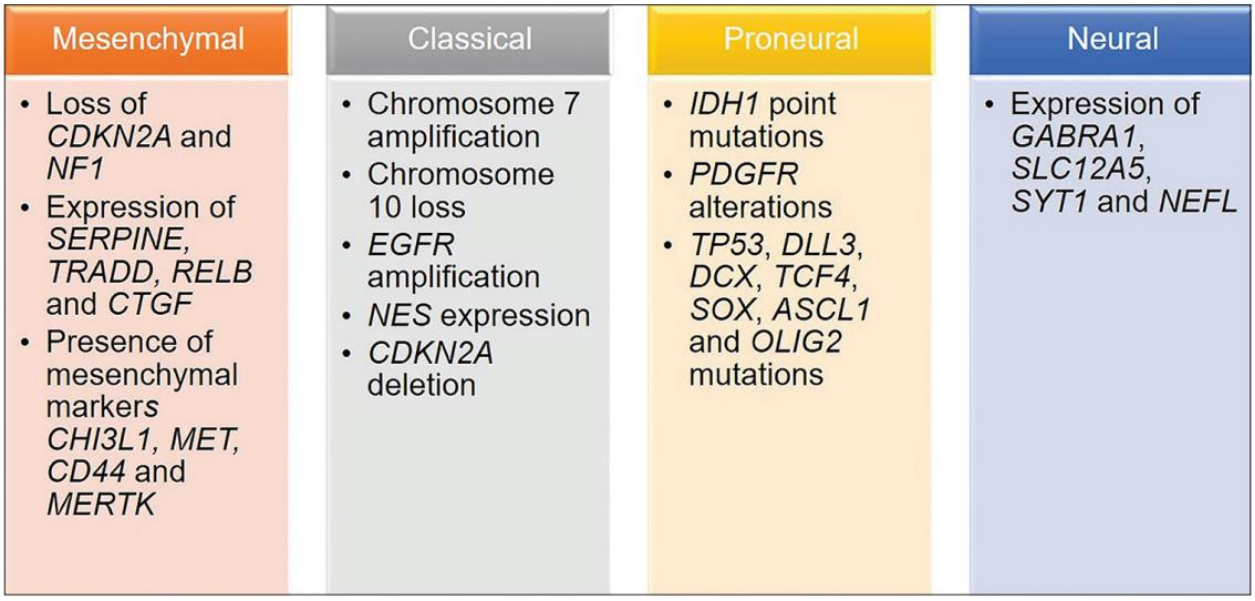

Figure 1.3 The most common genetic changes in the four molecular subtypes of GBMs described by Verhaak et al. [6, 116]

Classical subtype is typified by chromosome 10 loss (*PTEN*), and chromosome 7 amplification (*EGFR*). Loss of *CDKN2A* is also prevalent in classical subtype and mutually exclusive with aberrations of other components in Rb pathway. Classical subtype is highly expression of neural stem or precursor cell marker *NES* (nestin), Notch [*JAG1* (jagged canonical Notch ligand 1), *NOTCH3*, *LFNG* (LFNG O-fucosylpeptide 3-beta-N-acetylglucosaminyltransferase)] pathway, and Sonic hedgehog [*GAS1* (growth arrest specific 1), *SMO* (smoothened gene), *GLI2* (GLI family zinc finger 2)] pathway. Classical subtype shows the greatest benefit response to aggressive therapy.[6]

Mesenchymal subtype is featured as the loss of *NF1* located on 17q11.2. *NF1* and *PTEN* co-mutations are also found in mesenchymal subtype. Mesenchymal subtype is highly expression of mesenchymal markers [*CHI3L1* (chitinase-3-like protein 1) and *MET*], mesenchymal and astrocytic markers [*CD44*, *MERTK* (c-mer proto-oncogene tyrosine kinase)], genes in TNF (tumor necrosis factor) super family and NF-κB (nuclear factor kappa B) pathways [*TRADD* (tumor necrosis factor receptor type 1-associated death domain protein), *RELB* (v-rel reticuloendotheliosis viral oncogene homolog B), *TNFRSF1A* (TNF receptor superfamily member 1A)].[6] Mesenchymal subtype represents lower level of nonenhancement and an overall

higher level of necrosis than other tumor subtypes on imaging.[117]

Proneural subtype is largely defined by alterations of *PDGFR*A (platelet derived growth factor alpha) at 4q12 locus, *IDH1* point mutations, *TP53* mutations with heterozygosity loss and *PIK3CA* (the phosphatidylinositol-4,5-bisphosphate 3-kinase, catalytic subunit alpha)/*PIK3R1* (phosphatidylinositol 3-kinase regulatory subunit alpha) mutations. Alterations of *PDGFR*A include focal amplification, overexpression and mutation. Amplification of chromosome 7 paired with loss of chromosome 10 are less prevalent in proneural subtype. Proneural subtype is characterized by a high expression level of oligodendrocytic development genes [*PDGFRA*, *NKX2-2* (NK2 homeobox 2) and *OLIG2* (oligodendrocyte transcription factor 2)] and proneural development genes [*SOX* (SRY-related HMG-box), *DCX* (doublecortin), *DLL3* (delta-like 3), *ASCL1* (achaete-scute homolog 1), and *TCF4* (transcription factor 4)]. Proneural subtype shows no benefit response to aggressive therapy.[6] The proneural subtype can be further divided according to G-CIMP (glioma-CpG island methylator phenotype).[118] The positive G-CIMP group is tightly associated with *IDH1* mutations, *SOCS3* (suppressor of cytokine signaling 3) promoter hypermethylation, as well as a more favorable prognosis overall.[119] Proneural subtype shows remarkably lower level of contrast enhancement in the image.[117]

Neural subtype is characterized by expression of neuron markers [*NEFL* (neurofilament light polypeptide), *GABRA1* (gamma-aminobutyric acid receptor subunit alpha-1), *SYT1* (synaptotagmin 1) and *SLC12A5* (solute carrier family 12 member 5)] and is poorly defined.[6]

There are some associations between GBM subtypes and distinct neural cell types in accordance with enrichment of gene expression pattern. Classical subtype is strongly associated with astrocytic signature. Mesenchymal subtype is associated with cultured astroglial signature. Proneural subtype is enriched in oligodendrocytic signature. Neural subtype is association with oligodendrocytic, astrocytic and neurons differentiation signature. [6]

1.1.6.4 Molecular markers of GBMs

IDH is a metabolism-related gene, and it is a frequent mutation on genome level studies. It is strong associated with young patients, potentially tumorigenesis, secondary GBM and better outcome.[110, 111] *IDH1* R132H and *IDH2* R172H are the most common mutations and highly homologous. This is a single residue alteration of arginine (R) to histidine (H) or other amino acid substitution.[110, 115] Wild-type IDH enzyme converts isocitrate to normal products α-KG

(alpha-ketoglutarate) and NADPH (nicotinamide adenine dinucleotide phosphate). While the missense-mutant IDH enzyme results in excess 2-HG (2-hydroxyglutarate) substitution and reduced production of α-KG and NADPH. α-KG is used by PHD2 (prolyl hydroxylase domain protein 2) to catalyze the proteasome dependent degradation of HIF (hypoxia-inducible factor), which is important in angiogenesis and hypoxic gene regulation. 2-HG inhibits diverse α-KG dependent dioxygenases such as the TET (ten-eleven translocation) histone demethylase and elevates ROS (reactive oxygen species). TET enzyme facilitates the demethylation of 5-methylcytosine which is pivotal in retrotransposon-mediated gene silencing. *IDH1* R132H is strong associated with positive G-CIMP expression.[15, 110] The mutant IDH enzyme and gene can be detected by immunohistochemistry and DNA sequencing. DNA sequencing is recommended especially for negative immunohistochemistry result in younger patients.[15] It can be also used as gliomas classification.[12]

ATRX mutation or loss followed by reduced ATRX protein expression is closely correlated with *IDH* mutant and *p53* mutation, not 1p/19q co-deleted, in secondary GBMs.[12, 115] Mutation of ATRX protein causes telomerase-independent chromatin telomere maintenance mechanism which is named ALT (alternative lengthening of telomeres). ALT is the presumed precursor of genomic instability.[120, 121] Loss of nuclear ATRX expression can be detected by immunohistochemistry.[7, 115]

EGFR gene is amplified in approximately 40% of primary GBMs. Half of them harbor a constitutive active variant, named EGFR vIII (epidermal growth factor receptor variant III). The oncogenic mutation refers to in-frame deletion of exons 2-7, which encode part of the protein extracellular domain. Both wild-type EGFR and EGFR vIII proteins activate the Ras/RAF/MEK/MAPK and PI3K/Akt/mTOR pathways as well as the expression of Bcl-XL (B cell lymphoma extra large) that induce tumorigenicity, cell survival, proliferation, apoptosis resistance, cell cycle, invasion, angiogenesis, etc. It is reported that EGFR vIII-positive cells not only drive own proliferation, but also enhance the proliferation of wild-type EGFR-expressing neighboring cells. This may be attributed to the paracrine secretion of cytokines (e.g., interleukin-6 and/or leukemia inhibitory factor) by EGFR vIII-positive cells, and in turn activate cytokine co-receptor gp130 dependent expression of wild-type EGFR neighboring cells.[15, 110, 115]

PDGFRA is amplified in roughly 13% of GBMs and related to tumor development. This can be

performed by ligand-receptor binding in autocrine and paracrine signaling loops as well as ligand-independent active mutants. Intragenic deletion of exons 8 and 9, termed *PDGFRA*$^{\Delta 8,9}$, leads to a truncated extracellular domain. This induces the increased phosphorylation of downstream c-Jun in a ligand-independent manner. In-frame gene fusion of *VEGFR-2* extracellular domain and *PDGFRA* intracellular domain shows elevated tyrosine kinase activity.[122] *PDGFRA* point mutations are also observed in GBM patients.[15, 110]

hTERT is a catalytic subunit of telomerase complex. It is indispensable in regulating telomere DNA length and activity that function as cellular immortalization and tumorigenicity. h*TERT* promoter mutation occurs in 70-80 % of primary GBMs, and in more than 70% of oligodendrogliomas on genome level analysis.[15]

Ki-67 antigen, is a nuclear protein. It is expressed during the cell cycle of G1, S, G2, mitosis phases, and absent in G_0 phase. [123] It is used as a stable cell proliferation marker of GBM. Ki-67 labeling index, the positive tumor cells fraction, is associated with malignant progression and poor prognosis.[44, 124]

MGMT promoter methylation causes gene transcriptional silence followed by reduced MGMT protein level and sensitivity to alkylating agents. *MGMT* promoter methylation is found in approximately 40% of primary GBM patients. It can be tested and established by molecular genetic analyses (e.g., methylation-specific PCR, bisulphite-modified DNA pyrosequencing), but not by immunocytochemistry.[15, 83, 115] The binding of *miR-181d* to 3'-UTR (3′ untranslated region) of *MGMT* causes unstable and decreased expression of mRNA followed by reduced protein translation.[125, 126]

1.1.6.5 Heterogeneity and plasticity of GBMs

Intertumoral heterogeneity is defined as different genetic changes that occur in a single tumor originated from the same organ and allow these tumors to be classified into different molecular subtypes. Intratumoral heterogeneity refers to the diversity within individual tumor which can be certified by single cell transcriptome RNA-seq.[9, 127] The plasticity refers to the dedifferentiation and transdifferentiation of GBM cells as well as subtypes transition (e.g., epithelial-mesenchymal transition). It is an important driver that adds another level of complexity to GBM heterogeneity.[9, 10] GBMs represent extraordinary intertumoral and intratumoral heterogeneity on genome,[128] expression profiles,[6] metabolism,[129] extracellular

environment[130], stages,[127] morphologies,[9] histopathology and tumour location[131], etc. All of these contribute to the therapeutic resistance, tumor recurrence and poor prognosis.[9, 10]

1.1.6.6 BTICs and stem cell culture

BTICs are a small fraction of undifferentiated cell population that possess the ability of continuous self-renewal, long term proliferation or clonogenicity, multiple lineages differentiation, as well as tumors initiating.[10, 132] These cells are the basis for the so called stem cell hypothesis.[133] BTICs are maintained and promoted in distinct cancer stem cell niches such as perivascular and hypoxic niches.[18] The potential of tumor initiation *in vivo* and serial transplantation is the gold standard for the definition of BTICs. The newly formed tumor closely resembles the original parent tumor.[132] BTICs show symbiotic relationships with the oncogenic signaling pathways, epigenetic regulation and tumor microenvironment.[18]

The stem cell hypothesis started with the research of acute myeloid leukemia and later breast cancer, etc.[132] Stem cell hypothesis was also established in brain tumor later.[134, 135] BTICs are propagated under serum-free conditions[136] and express neural stem cell markers.[132] BTICs that possess stem cell characteristics provide insights into the heterogeneity and pathogenesis of GBMs.[9, 10]

Initially, BTICs were isolated and purified by fluorescence-activated magnetic cell sorting and flow cytometry based on the neural stem or precursor cell marker CD133 (cluster of differentiation 133, also known as prominin-1). Only the $CD133^+$ brain tumor cell subpopulation exhibited the stem cell-like properties for self-renewal, proliferation, sphere formation, and differentiating into tumor cells that mimiced the original tumor from the patient *in vitro*.[135] The injection of as few as 10^2 $CD133^+$ brain tumor cells could be serially transplanted and initiated tumors that resembled patient's original tumour phenotypically in xenograft assay of NOD-SCID (non-obese diabetic, severe combined immunodeficient) mouse brains. However, the injection of engrafted 10^5 $CD133^-$ brain tumor cells did not produce a tumour.[134] Subsequently, $CD133^-$ tumor cells were also demonstrated to have stem cell-like properties and xenograft tumor formation ability including GBM. [132, 137] $CD133^+$ and $CD133^-$ BTICs represented differences of molecular and biological growth patterns *in vitro* and *in vivo*.[137] Many additional candidate markers [such as A2B5, CD44, CD171 (L1CAM, L1 cell adhesion molecule), CD15 (SSEA1, stage-specific embryonic antigen-1), CD49f (integrin α6), Musashi, Nestin, Nanog, Oct4

(octamer-binding transcription factor 4), Sox2, ABC (ATP-binding cassette) transporters] were used for identifying BTICs over the last decade. But none of them are reliable and universal to date because of inconsistencies. Signaling pathways and related proteins [such as Notch, PI3K-Akt, Hedgehog-Gli, Bone morphogenetic proteins (BMPs), Wnt β-catenin, JAK (Janus kinases)-STAT3 (signal transducer and activator of transcription protein 3)] as well as transcription factors [such as Sox2, Oct4, Nanog, c-Myc (MYC proto-oncogene), OLIG2, and BMI1 (BMI1 proto-oncogene, also named polycomb ring finger)] also participate in the regulation of BTICs.[18]

GBM cells are traditionally cultured as adherent growth in medium with serum for *in vitro* study. They express differentiation markers and lost the invasive ability (some of them), and are not suitable for stem cell research. NSCs were discovered as neurospheres growth in defined, serum-free medium with growth factors. Later GBM cells were also demonstrated to form neurospheres in similar medium. A percentage of GBM cells in neurospheres express NSC genes and show the ability of self-renewal, proliferation, invasiveness, serial passages, multiple lineages differentiation. Therefore, neurospheres culture can be used for stem cell research. However, this is dependent on cell passage number, culture and dissociation time. Neurospheres also show differentiated progenies and necrosis. The dedifferentiated and differentiation states of some cells can be converted mutually and are serum-free medium dependent.[132]

The next generation stem cell culture was reported as monolayer adherent growth on bottom of culture flasks in the same serum-free medium for neurospheres culture [stem-cell permissive medium RHB-A supplemented with EGF/bFGF (basic fibroblast growth factor)]. The adherent culture allows all cells acquire nutrients and growth factors equally, which hinders the differentiation and apoptosis. The adherent cells express NSC genes and show stronger tumor formation ability.[136]

1.2 Cancer cellular metabolism reprogramming and TME acidification

1.2.1 Cancer cellular metabolism reprogramming

Cellular metabolism reprogramming is one of the emerging hallmarks of cancer.[138] Cancer cellular metabolism is featured as using opportunistic modes to acquire increased consumption of nutrients and relying on glycolysis and TCA (tricarboxylic acid) cycle intermediates as precursors

for biosynthesis and maintain viability. Cancer cellular metabolism reprogramming, gene alterations and TME are interactivated with each other mutually.[139] It becomes a renewed topic in the past 2 decades with the help of new biochemical and molecular biological tools.[139]

The first observation of tumor metabolic alteration is that tumor cells often have elevated increase of glucose consumption and lactic acid production even in the presence of oxygen.[140] This phenomenon is termed aerobic glycolysis or Warburg effect. Glycolysis is normally inhibited by the presence of oxygen in most mammalian cells. This appearance is named Pasteur effect.[141] Warburg effect canbe observed in a series of tumour types including GBM.[142] Glycolysis is inefficient for energy production by comparing with TCA cycle/mitochondrial OXPHOS (oxidative phosphorylation). The possible explaination of high aerobic glycolysis is that survival and proliferation of tumor cells are limited by local insufficient of oxygen initially. While periodic or persistent hypoxia give rise to evolutionary selection pressures that bring about constitutive upregulation of glycolysis by gene mutations or epigenetic modifications even under aerobic conditions. The consequence of increased glycolysis makes tumor cells acquire energy quickly, more adaptable to hypoxia, provides metabolic intermediates for significant proliferative advantage, TME acidification, as well as induces invasion and chemoradiation resistance.[143, 144]

Warburg and other scientists speculated that the enhanced aerobic glycolysis is caused by an irreversible mitochondrial respiration impairment in cancer for a long time.[139, 145] While recent investigations supported that mitochondrial respiration was not defective but intact and functional in most cancers.[146] GBMs were also demonstrated to utilize both glycolysis and TCA cycle/OXPHOS *in vitro* and cell line research *in vivo* as well as radioisotope labeled imaging studies of orthotopic models.[129, 147, 148] Novel specific inhibitors for OXPHOS were started for targeting GBM in the past two years.[149, 150]

While metabolic profile of BTICs is not fully defined because of intertumoral and intratumoral heterogeneity.[151] Very recent studies indicated that BTICs with mesenchymal subtype of this study were highly glycolytic (Seliger-Behme, submitted).

1.2.2 Tumor microenvironment acidification

The acidification is one of the characteristics of tumor microenvironment, and due to high metabolic demand and tortuous tumour vasculatures that prevent an efficient oxygen and nutrient

delivery.[152]

The intracellular alkaline and extracellular acidic natures of tumors were initially proved by electrode studies and ^{31}P NMR (nuclear magnetic resonance) measurements. This notion was further optimized and confirmed by selectively targeted studies of ^{31}P NMR with better spatio-temporal resolution.[153] Present consensus about pH value in most tumors is that pHi 7.4 or more alkaline and pHe range 6.5-7.0, although pHe as low as 6.0 has been reported.[152, 154] Extracellular titration of acids is mainly drived from lactic acid and carbonic acid accumulation via glycolysis and pentose phosphate pathway, TCA cycle/OXPHOS, glutaminolysis pathway.[152, 155, 156] Both lactic acid and carbonic acid should be considered as dissociated entities as H^+ ions plus lactate ions and bicarbonate ions.[152]

The alteration of pHe or pHi even as low as 0.1 pH unit may disrupt important biological and/or biochemical course of tumour cells.[154] Increased pHi is responsible for tumor cell proliferation and apoptosis evasion.[152] Decreased pHe promotes the evolution of an acid- and chemoradiation-resistant subtype of tumor cells, cell dedifferentiation, increased production of growth factors and increased invasive and migrative potential via ECM (extracellular matrix) degradation and angiogenesis.[143, 157] Exposure of normal cells to acidic environment results in their apoptosis or necrosis by p53- or caspase-dependent pathways.[143] Increased lactic acid levels induce immunosuppression by interacting with dendritic cells, T cells, monocytes, and macrophages.[139] Consequently, intracellular alkaline and extracellular acidic natures provide a crucial selective advantage of tumor cells.

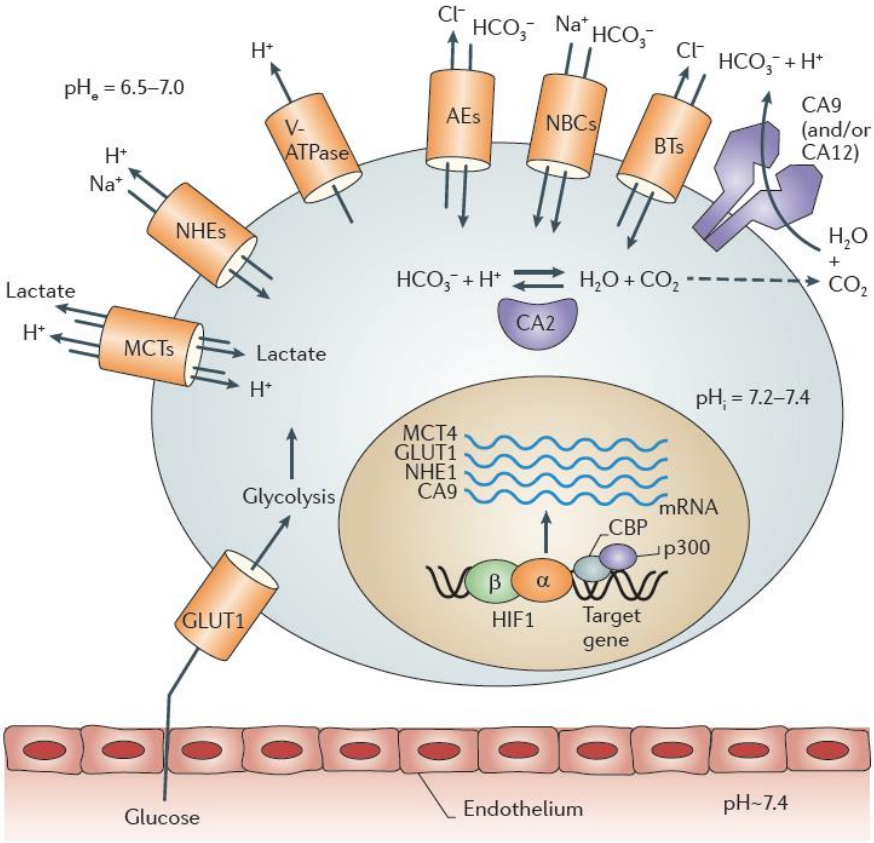

Figure 1.4 Involved pH regulating proteins of a tumour cell [154]

As mentioned above, tumors (including GBM) frequently show high glycolytic metabolic rate which should leads to a significant intracellular acidification, while it is alkaline paradoxically. This is mainly attributed to extrusion of H^+ ions into the extracellular milieu and/or influx of equivalent HCO_3^- with the help of pH regulating enzymes, ion transporters and exchangers as well as gas channels. These key pH regulators are CAs (carbonic anhydrase II, IX and XII), AEs (anion exchangers), NBCs (Na^+/HCO_3^- co-transporters), NHEs (Na^+/H^+ exchangers), NDCBEs (Na^+-driven Cl^-/HCO_3^- exchangers), MCTs (monocarboxylate transporters), V-ATPases (vacuolar ATPases), aquaporins and so on.[152, 154]

The comprehensive mechanisms are as follows: Initially, intracellular hydrogens and bicarbonate ions are converted to carbon dioxides catalyzed by cytoplasmic CAII to facilitate diffusion across the plasma membrane freely or by aquaporins. Later, extracellular CO_2 are hydrated back to bicarbonate ions and protons catalyzed by CAIX and CAXII. Protons will be left outside of the cell for the contribution of extracellular acidification. At last, bicarbonate ions are imported into

the cell via BTs (bicarbonate transporters) (including AEs, NBCs and NDCBEs) for the maintenance or slightly alkaline of the intracellular pH. Overall, each cycle has a net proton efflux without carbon extrusion. This is also known as Jacobs-Stewart cycle for recycling of bicarbonate ions and protons efflux.[158, 159] The spatial and functional coupling complexes formed by CAs and BTs are termed transport metabolons.[160] Another transport metabolon is constituted by CAIX and MCT. Proteoglycan-like domain of CAIX functions as a proton antenna for the transporter, which drives the efflux of both lactate ions and protons from cytoplasm.[161]

1.3 Tumor hypoxia and HIF-1 pathway

Intratumoral hypoxia is a universal phenomenon including GBM.[46, 162] Tumor hypoxia regulates the transcriptional expression of a series of genes that participate in metabolic reprogramming, angiogenesis, migration and invasion, immune evasion, cancer stem cell maintenance, and resistance to chemoradiation primarily by the increased activity of hypoxia-inducible factors.[163] HIF-1 was initially discovered in *EPO* (erythropoietin) gene study and functioned by HREs (hypoxia response elements), which were essential for the transcriptional activation in response to hypoxia.[162, 164-166]

HIF-1 is a heterodimer assembled by a hypoxia inducible α-subunit (HIF-1α/2α/3α) and a constitutive expressing β-subunit [HIF-1β/2β, also named ARNT (aryl hydrocarbon receptor nuclear translocator)].[162, 166] HIF-1α and HIF-2α subunits in responding to the majority of HIF-dependent transcriptions were first described in 1995 and 1997, respectively.[167] HIF-1α and HIF-2α share 48% identical amino acid sequence, as well as structural and biochemical similarities.[168] HIF-1α shows ubiquitous tissue expression and plays a crucial role in acute and severe hypoxia. HIF-2α shows restricted expression particularly in vascular areas and responds to chronic and moderate hypoxia. They also show shared and unique regulations of downstream target genes.[167, 169] GBM expresses both HIF-1α and HIF-2α.[170] HIF-3α and its differentially spliced variants regulate activity of other HIF complexes positively or negatively. HIF-2β (ARNT2) has also been identified. Both HIF-3α and HIF-2β have not been studied intensively in hypoxic tumor.[167] The role of HIF-1α/HIF-1β is widely accepted and in-depth studied in cancer progression.[171] HIF-1α and HIF-1β are bHLH (basic helix-loop-helix)-PAS [PER(Period)-ARNT-SIM(single minded)] domain protein.[172] HIF-1α and HIF-2α bind to HRE of *CAIX* in *in vivo* chromatin immunoprecipitation assay. While *CAIX*, distinct with most

other hypoxia inducible genes, is only responsive to HIF-1α.[173]

HIF-1α consists of 826 amino acids. Start from N- to C-terminal, amino terminus half possesses a basic helix-loop-helix domain (bHLH), two PER-ARNT-SIM domains (PAS-A and B) which are important for DNA binding and heterodimerization, respectively. Carboxy terminus half comprises oxygen-dependent degradation domain (ODDD), two transactivation domains (N-TAD and C-TAD) segregated by inhibitory domain (ID), which act as O_2-dependent instability, autonomous and negative regulated transactivation, respectively. In addition, there are two nuclear localization signal domains (NLS-N and NLS-C).[166]

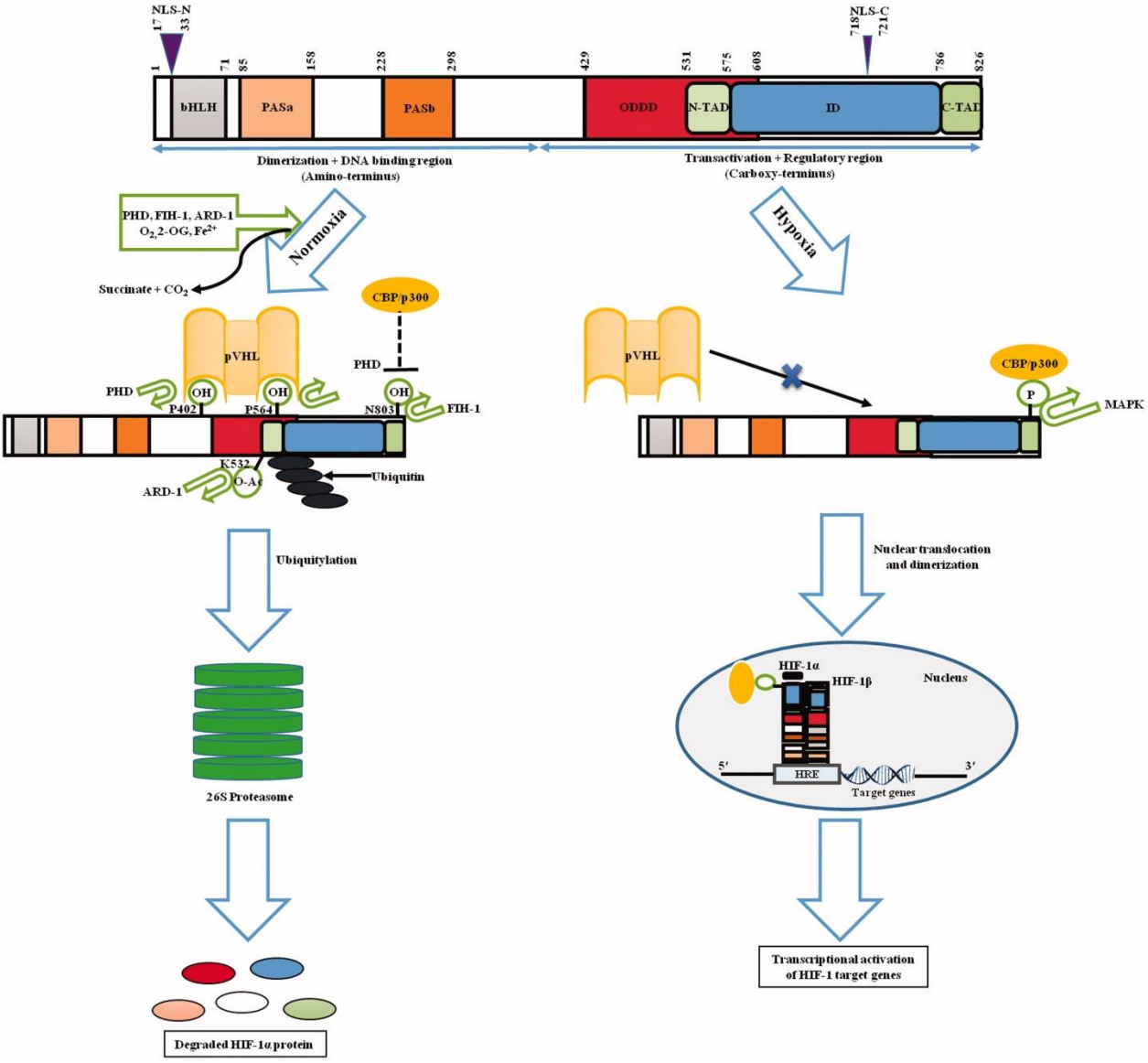

Figure 1.5 Schematic representation of structure and oxygen-dependent regulatory mechanism of HIF-1α [166]

Under hypoxia, N-TAD stabilizes HIF-1α, C-TAD binds to CH1 (cysteine-histidine rich domain) of p300/CBP (CREB-binding protein) or other histone acetyltransferases [SRC-1 (steroid-receptor co-activator-1) and TIF2 (transcription intermediary factor 2)] as co-activator for increasing transactivation. S-nitrosation of Cysteine-800 residue is also critical for co-activation. While CITED2 (CBP/p300 interacting transactivator with ED-rich tail 2) competitively inhibits binding between HIF-1α and p300/CBP. Stabilization and co-activation of HIF-1α lead to its nuclear translocation followed by dimerizing with HIF-1β. HIF-1α/1β heterodimer binds to HRE of target gene enhancer domain and activates their transcription.[166, 174] During normoxia, PHDs hydroxylate Proline 402 and 564 residues located at LXXLAP motif of ODDD domain. ARD-1(arrest defective-1) acetylates Lysine-532 residue of ODDD domain. Alterations above result in the binding of HIF-1α and β-domain of pVHL (von Hippel-Lindau protein) complex (an E3 ubiquitin ligase) at Leucine-574. In addition, FIH-1 (factor inhibiting HIF-1) hydroxylates Asparagine 803 residue for blocking C-TAD and CBP/p300 interaction. All these result in ubiquitylation and quick (half-life 5 minutes[162]) degradation of HIF-1α by 26S proteasome.[166] Futhermore, a small protein SUMO (Small ubiquitin-related modifier) is very similar to ubiquitin in 3D structure, and sumoylation of Lysine-391, -477, and -532 decreases transcriptional activity. Phosphorylation of 531 to 826 residues also affects expression of HIF-1α.[166, 174]

Many oncogenic pathways [e.g., GF/RTK, PI3K/AKT/mTOR/S6K (ribosomal protein S6 kinase beta-1), RAS/RAF/MEK/ERK (extracellular signal-regulated kinase, also named MAPK), tumor suppressor pathways (e.g., p53/MDM2) and factors [e.g., Hsp (heat shock protein) 90] regulate mRNA and protein synthesis of HIF-1α directly or indirectly. For example, ERK phosphorylates p300/CBP and increases HIF-1α/p300 complex formation followed by stimulating transcriptional activation function of HIF-1α.[162, 166]

1.4 Carbonic anhydrase IX

1.4.1 Overview of carbonic anhydrases

Carbonic anhydrase was first purified from erythrocytes in 1933.[175] CAs (Enzyme Commission Number: 4.2.1.1) comprise 7 distinct evolutionary classes (α, β, γ, δ, ζ, η, and θ) to

date in all life of nature and form a family of metalloenzymes that catalyze the reversible hydration of CO_2 to HCO_3^- and a proton.[176] Isoforms of α-class share a similar three-dimensional structure and a typical fold characterized by a central Zn^{2+} surround by an antiparallel β-sheet.[177] Humans express α-class CAs that include 15 isoforms which possess the identical tertiary spatial structure, while differ in amino acid sequence, expression levels, catalytic efficiency, tissue distribution, subcellular localization, sensitivity to inhibitors and physiological processes. 12 isoforms of CAs display catalytic activity because of essential zinc ions in catalytic center. These include cytosolic CAs (I-III, VII, XIII), membrane bound CAs (IV, IX, XII, XIV), secretory CA (VI), and mitochondrial CAs (VA, VB). The other 3 isoforms of CAs (VIII, X, and XI), named CA-RPs (CA-related proteins), are non-catalytic because of the lack of active site zinc ions and accompanied 3 important histidines. The biological functions of CA-RPs remain largly unclear.[178-180]

Cytosolic α-CAs isoforms show decreased expression in colorectal, hepatocellular and lung tumors when compared to corresponding normal tissues which indicate non-tumorigenesis contribution. Expression and activity of mitochondrial α-CA V are completely missing in tumors. CA-RPs are associated with lung and colorectal carcinomas and promote cancer cells proliferation and invasiveness, while they function independent of the catalytic activity and cannot be modulated by compounds that affect the enzyme activity.[180] There is an established tumor-related role of membrane bound CAIX/XII particularly under hypoxic condition over last decades.[178, 181] CAXII shows extensive and abundant expression in normal tissue, while lesser tumor and hypoxia relevance.[178, 180, 181] CAIX is one of the most efficient enzymes of all α-CAs.[178] High expression of CAIX is an independent prognostic factor for poor survival outcome of GBM patients,[182] CAXII is not an established prognostic marker.[178]

1.4.2 Discovery, normal and tumor tissues expression of carbonic anhydrase IX

A protein named MN was originally discovered by M75 monoclonal antibody in human HeLa cells in 1992.[183] The amino acid sequence analysis of cDNA (complementary DNA) coding for MN protein in 1994 showed a strong structural homology with carbonic anhydrases.[184] Therefore, MN protein was renamed CAIX because of the ninth identified CA in mammals.[185] Gene of *CAIX* was sequenced and characterized in the same year.[186]

CAIX is high expression in solid tumors contrasting with limited expression in normal tissues,

which make it attractive as anti-cancer target.[178, 180] In terms of normal adult human tissues, diffuse protein expression of CAIX was detected in lining cells of body cavity (reactive mesothelial cells), gastrointestinal system (gastric fundus/pyloric glands; ductal cells of the Brunner's glands in duodenum; crypt enterocytes of small intestine, duodenum, appendix; gland cells of cecum and ascending colon), gallbladder/biliary tract, reproductive system [testis (ductular efferens, rete testis); ovary (surface coelomic epithelium, rete ovarii)], basal cells of hair follicle of the skin, and choroid plexus in central nervous system. Focal protein expression of CAIX was detected in underling stellate stromal cells, salivary glands ductal cells, gastric pits, pancreas ductal cells, cartilaginous tissues near joint spaces, skeletal muscle, ventricle lining cells, and mesodermal cells of amniotic/chorionic plate in placenta.[181, 187] Expression of CAIX in normal tissues is closely related to the cell origin, proliferation, differentiation, cellular hypoxic condition, ion transport, as well as the biomarker of stemlike or transit amplifying cells.[173, 188] Many human malignancies were found CAIX expression which comprise cervical carcinoma, renal cell carcinoma, oesophageal tumour, colorectal neoplasm, non small cell lung cancer, head and neck squamous cell carcinoma, breast malignancy, soft tissue sarcoma, astrocytic tumor, vulvar carcinoma, tongue/oral squamous cell carcinoma, nasopharyngeal carcinoma, oligodendroglioma, malignant mesothelioma in an chronological order.[181]

1.4.3 Gene structure of carbonic anhydrase IX

CAIX gene is located in chromosome 9p13.3 and encompasses 10,898 base pairs (bp).[189] It is a single copy gene per haploid genome, and possesses 11 exons for coding sequence and 10 introns.[186] *CAIX* is highly inducible and is transcribed into a single 1.5 kilo base pairs (kb) mRNA by appropriate activation.[184] No mutations are detected between cancer cell lines and normal tissue cells by cDNA sequence analysis of *CAIX* which indicates the abnormal expression is due to amplification instead of mutation.[190]

GC-rich *CAIX* promoter (-173 to +31) possesses five protected regions (PRs) and a HBS (HIF-binding site) for nuclear proteins binding, and TATA box is not found.[191, 192] PR1 (-45 to -24) was indicated putative binding site for AP2 (activator protein 2) and SP1 (specificity protein 1) transcription factors by preliminary sequence analysis via transcription factor database. AP2 and SP1 share significant sequence similarity. Binding propensity of PR1 is complex because 4 complexes were generated with HeLa nuclear extract in competition EMSA

(electrophoretic mobility shift assay). Both SP1 and AP2 probes competed for complexes 1-2-4, while AP2 was less efficient. Further supershift EMSA identified that SP1 antibody recognized complex 1 and SP3 antibody recognized complexes 2-4, while AP2 antibody failed to supershift either of the PR1 complexes. Furthermore, SP1 site point mutation abrogated the PR1 function, while AP2 site point mutation showed minor effect. Later, it was once again proved the crucial role and orientation-independent function of SP site in PR1 in block-replacement mutagenesis assay. In conclusion, SP activity is necessary and sufficient in PR1. SP site represents the constitutive element in promoter that supports basal transcription especially in the absence of a TATA box.[191, 193, 194] PR2 (-71 to -56) possesses AP1 site by computer-assisted searching. PR2 produced a single complex band in competition EMSA. Binding AP1 to PR2 and transactivation function were proved in supershift EMSA and point mutation assay, respectively.[191] Therefore, AP1 activity is essential in PR2.[193] AP1 consists of heterodimers of c-Jun, c-Fos, ATF (activating transcription factor) which canbe induced by hypoxia via ERK/MAPK, PI3K signal pathways on a cell type specific manner.[173] Synergistic cooperation of SP and AP1 factors bind to PR1 and PR2 respectively which makes up 90% activity of the *CAIX* promoter, but neither of them alone is sufficient for transactivation.[193] PR3 (-101 to -85) shows a lesser extent of transcriptional activity[191] and no further available information about functional importance of it could be found.[173] PR4 (-134 to -110) is a promoter-, position-, and orientation-independent silencer,[191] while the presumed repressor binding with PR4 has not been determinated and maybe on a cell type specific manner.[173] PR5 (-163 to -145) shows significant sequence identity with PR1. They are functionally equivalent for SP1/SP3 binding, and the relative distance to the transcription start site contributes the difference for *CAIX* promoter activity.[194] HRE possesses a conserved consensus core sequence (G/ACGTG) named HIF-binding site. HBS is required but not sufficient for hypoxia induction which requires non-conserved flanking region of the HRE.[173] It is critical for *CAIX* transcriptional activation by constitutive binding of SP1/SP3 to PR1 incorporated with active HIF-1 which canbe regulated by PI3K and hypoxia.[194] Therefore, the cooperation of PR1-HRE is proposed to be a hypoxia-responsive enhancer in *CAIX* promoter.[173]

1.4.4 Promoter regulation of carbonic anhydrase IX

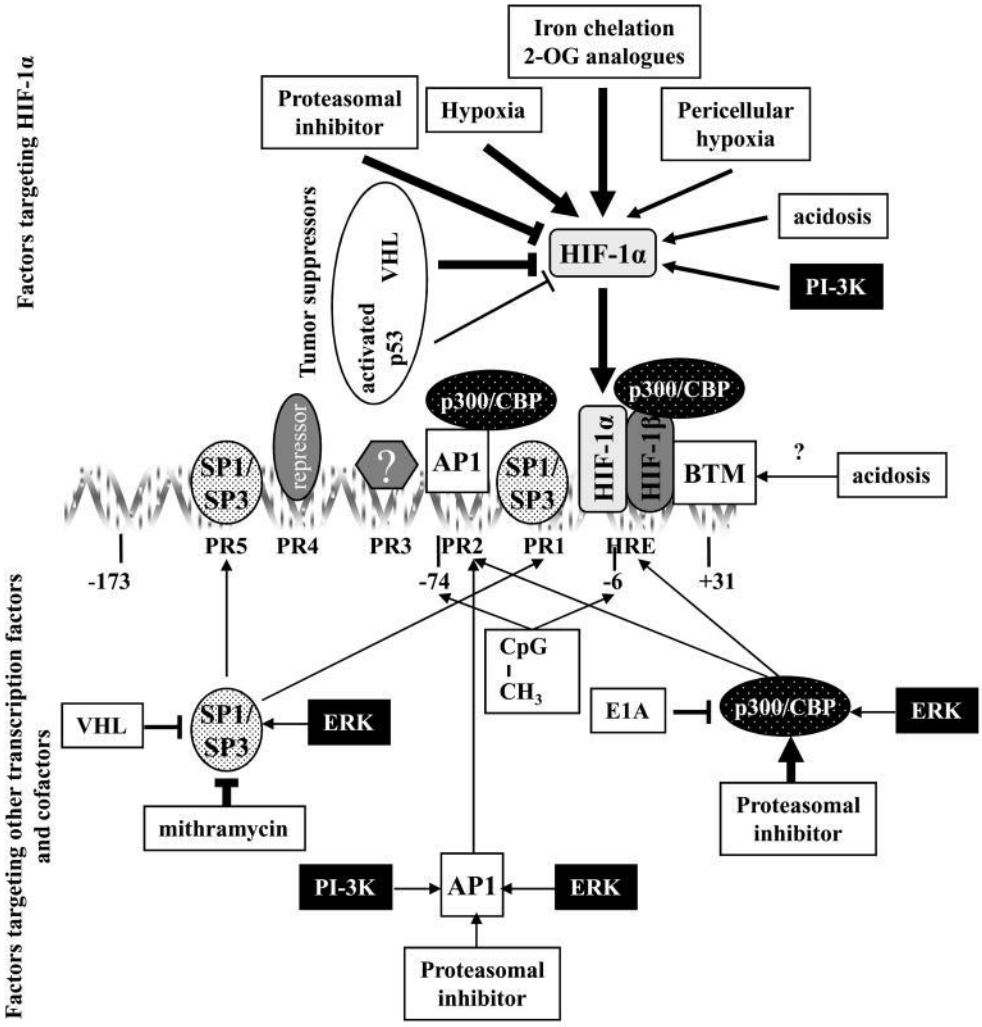

Figure 1.6 Pathways and factors regulating activity of *CAIX* promoter [173]

The primary mechanisms in charge of stability and transcriptional activity of *CAIX* promoter are widespread and highly inducible. After HRE was identified in *CAIX* promoter, the crucial role of HIF-1 pathway for *CAIX* regulation was established and supported by a large body of evidence generated by numerous research. Regulations of HIF-1 pathway by many pathways, factors, and proper experimental conditions are the converged integrators and central mediators of *CAIX* transcription.[173]

In addition to oxygen dependent regulation of HIF-1 pathway that controls CAIX expression, inactive mutation of VHL tumor suppressor or inhibitors of PHDs and FIH-1 hydroxylases result in impossibility of HIF-1α degradation followed by overexpression of CAIX.[195, 196] In

contrast, competitive inhibitor of p300/CBP downregulated CAIX expression.[195] The tumor suppressor *p53* downregulates the expression of HIF-1α and in turn CAIX via proteasome-dependent degradation and competition for cofactor p300/CBP.[197, 198] The interdependent of PI3K pathway activation and a minimal HIF-1 level induces CAIX expression in high-density culture of HeLa cells.[199] MAPK signaling increases the activation of HIF via p300/CBP.[200] Inhibition of MAPK signaling cascade reduces both the promoter activity and protein level of CAIX in dense culture and hypoxic condition.[201] PI3K also regulates the promoter of *CAIX* by stimulating the activity of AP1 in PR2.[202] ERK pathway regulates the expression of CAIX via activating HIF-1, SP1/SP3, and AP1, and shows less prominent, conspicuously manifestation and a cell type specific manner.[173]

Microenvironmental conditions (e.g., extracellular acidosis, reduced glucose or bicarbonate concentration) also influence expression of CAIX and on a cell type specific manner.[203] TME acidosis increases mRNA and protein levels of CAIX in GBM cells under normoxia. This is mediated by basic transcriptional machinery via stabilization of HIF-1α concurrent with the ERK pathway activation transiently as well as MAPK and PI3K pathways.[204] Promoter methylation status of CpG sites shows strong correlation with CAIX expression in human renal carcinoma cells.[205, 206] The hypomethylated status of CpG sites is also accompanied by overexpression of CAIX which in turn induces the increased invasiveness and migration in *in vitro* study of ovarian cancer.[207] Overexpression of MORC2 (microrchidia 2) downregulates the acetylation level of histone H3 in PR4 of *CAIX* promoter via histone deacetylase 4 in *in vitro* study of human gastric cancer and colorectal cancer.[208] However, there is no relevant report about epigenetic modification and CAIX expression in GBM so far.

1.4.5 Structure and function of carbonic anhydrase IX

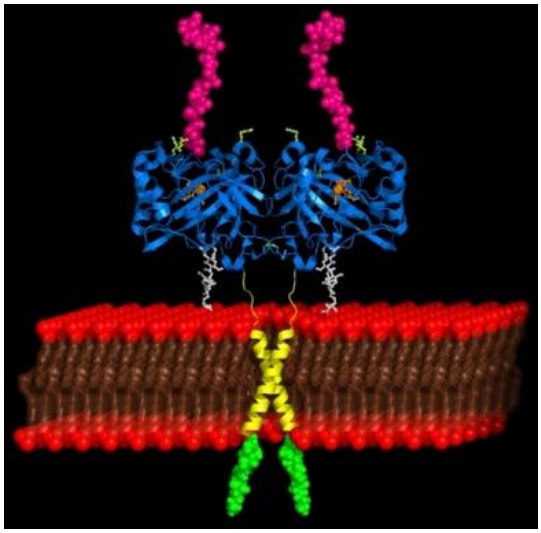

Figure 1.7 Structure schematic diagram of fulllength CAIX dimer on cell membrane [177]

CAIX (PDB ID: 3IAI)[177] exists as a homodimer of single-span transmembrane glycoprotein.[209] It is an acidic protein with p*I* of 4.39 (ranging from 4.7 to 6.3).[186] The dimerization is mediated by intermolecular disulfide bond formed between Cysteine 174 and Cysteine 409 residues,[180] and further stabilized by two hydrogen bonds and numerous Van der Waals forces.[177] CAIX can be figured out as 58/54 kDa double bands (monomeric form) in denatured state and 153 kDa single band (trimer form) in native condition by western blot assay.[180, 183]

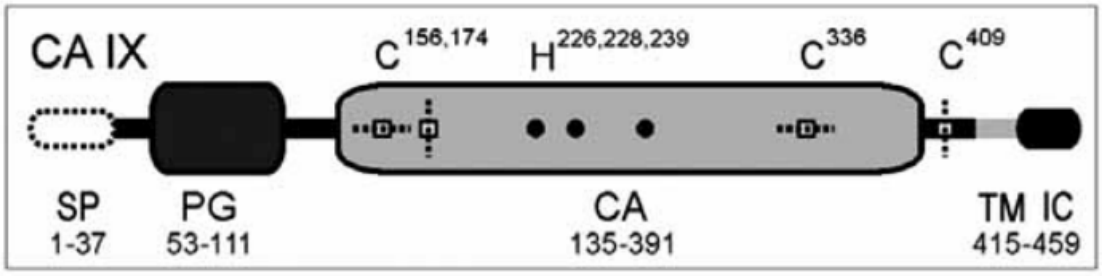

Figure 1.8 Scheme of the domain composition of CAIX based on amino acid sequence (primary structure) [180]

CAIX protein consists of 459 amino acids. CAIX canbe functionally divided into a signal peptide domain (SP) (range from 1-37 aa and 37 aa totally), a N-terminal extracellular proteoglycan-like

domain (PG) (range from 53-111 aa and 59 aa totally), a catalytic domain (CA) (range from 135-391 aa and 257 aa totally), transmembrane domain (TM) (range from 415–434 aa and 20 aa totally), and a C-terminal intracytoplasmic domain (IC) (range from 435–459 aa and 25 aa totally).[186] SP and PG domains are encoded by exon 1, CA domain is encoded by exon 2 to 8, TM and IC domains are encoded by exon 10 and 11, respectively.[186]

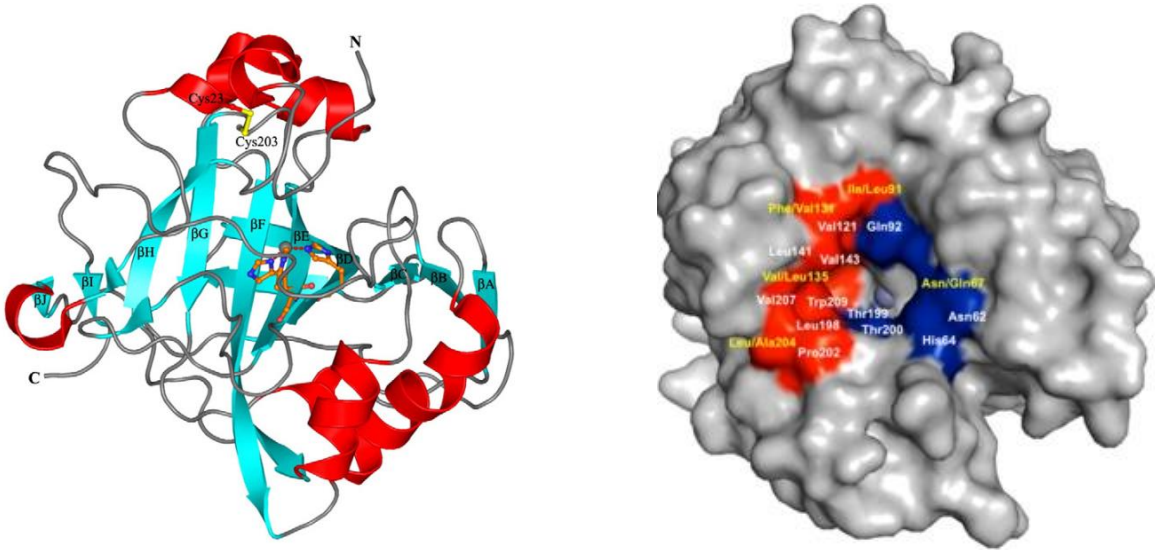

Figure 1.9 Secondary structure and surface rendition of CAIX catalytic domain [209, 210]

The CA domain is globular-shaped and approximately 47×35×42 $Å^3$ in size by an X-ray crystal structure analysis. A typical fold in CA domain is characterized by a central 10-stranded antiparallel β-sheet surround a zinc ion.[177] Intramolecular folding is stabilized by disulfide bridge between Cysteine 156 and Cysteine 336 residues.[211] The active site region that ranges from 125-137 amino acids is highly conservative and represents a "hot spot" to be considered for structure-based drug design.[210] It is characterized by a cone-shaped cavity formed by half hydrophobic region and contralateral half hydrophilic region. Zn^{2+} coordinated by 3 imidazole moieties of histidines (Histidine-226, -228 and -251) and a hydroxide ion are located in the base of the cavity of molecule centre tetrahedrally.[177, 209] A reasonable explanation for this unique "bipolar" architecture of active site is that the hydrophobic pocket is used for entrapping the hydrophobic gas molecule CO_2, while the hydrophilic half is used for assisting the binding and release of polar components (bicarbonates and protons). Proton transfer reaction is the rate determining step. After CO_2 is transformed into bicarbonate which is coordinated to the zinc ion, bicarbonate will be released into the environment by reacting with an incoming water molecule

because of the labile binding.[212]

PG domain in CAIX is unique contrasted with other isoforms of CAs and is in charge of cell adhesion and catalytic activity improvement.[209] CAIX protein was initially presumed for mediating cell-cell adhesion.[213] This was confirmed by the inhibition of M75 mAb and the location of M75 epitope (6-fold tandem repeat of GEEDLP) in PG domain.[214] Later, the PG domain mediated cell-cell adhesion was proved to be easily dissociated even under slightly acidic microenvironment.[215] Another group demonstrated that the ectopic overexpression of CAIX, function by PG domain, destabilized E-cadherin induced cell adhesion by interacting with β-catenin in tumor cells under calcium switch-triggered disruption and hypoxia condition.[216] PG domain is abundant in negatively charged amino acid residues. Therefore, it is presumed to interplay with positively charged amino acid residues that demarcate the vicinal active site and acts like a hat to open and close for controlling substrate entrance and assisting the proton shuttle reaction on the pH-dependent profile sterically. This is confirmed by kinetic assay that the pKa values are 7.01 and 6.49, and the turnover number (k_{cat}/s) are 3.8×10^5 and 1.1×10^6 for the comparation of CA domain alone and CA+PG domain.[177, 210] As mentioned above, PG domain of CAIX also functions like a proton antenna for facilitating the transport activity of MCTs.[161]

Intracellular tail of CAIX was proved to be involved in signal transduction. The phosphorylated tyrosine-449 moiety in IC domain of CAIX (location in the lipid rafts) can be elicited by EGFR and serves as docking site for p85 regulatory subunit [containing SH2 (Src homology 2) motifs] of PI-3-Kinase followed by Akt/mTOR activation. Cap-dependent translation is controlled by mTOR which further activates cyclin D1, c-myc, and HIF-1α in a hypoxia independent manner. Accumulation of HIF-1α upregulates (in addition to *CAIX*) *TGF-α* (transforming growth factor-α), *VEGF* and *PDGF* genes which in turn activate mTOR as a vicious cycle.[217] Under hypoxia, HIF-1 induces transcriptional activation of adenylyl cyclases VI and VII isoforms followed by prompting cancer-associated cAMP (cyclic adenosine monophosphate)/PKA (protein kinase A) signaling.[218] PKA phosphorylates Threonine 443 in IC domain for activation of CAIX, while the fullest activity also needs dephosphorylation of Serine 448.[219]

1.4.6 Carbonic anhydrase inhibitors, U104

Carbonic anhydrase inhibitors (CAIs) mainly include small molecule inhibitors, monoclonal

antibodies (mAbs) and PTK (protein tyrosine kinase) inhibitors.[154] Small molecule inhibitors, the largest and most diverse class of all CAIs, consist of sulphonamides, coumarins and their derivatives.[220] Small molecule inhibitors show non-immunogenic, economy and easily diffusion in tumours compared with mAbs (M75 and cG250) in spite of high specific binding with PG domain of CAIX.[154, 220] PTK inhibitors (e.g., Imatinib and Nilotinib) show less efficient and non-specific to CAIX.[221]

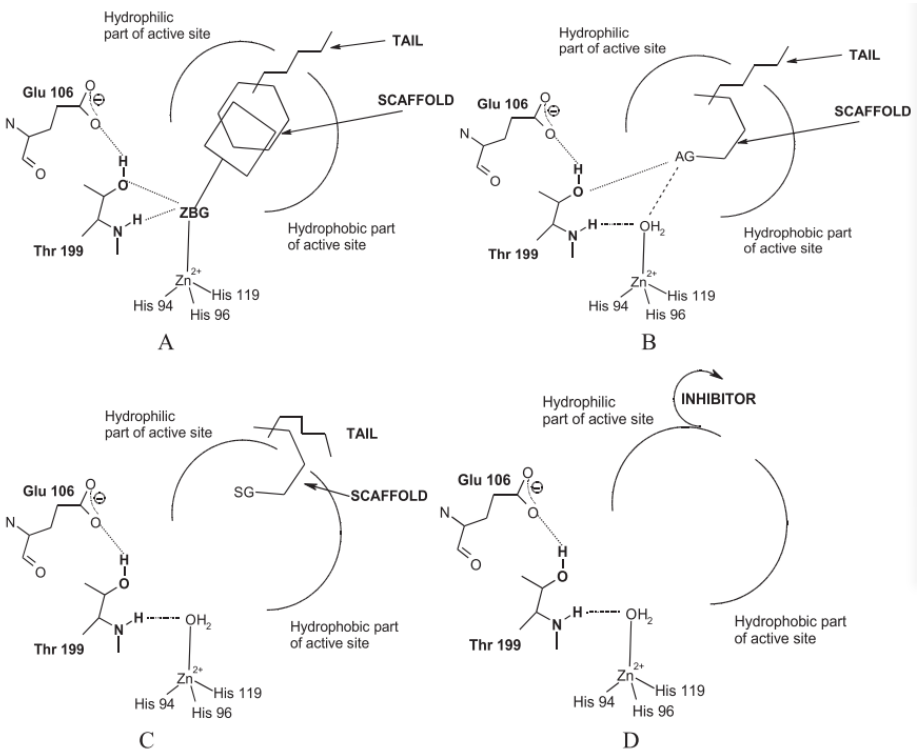

Figure 1.10 CA inhibition mechanisms of small molecule inhibitors [212]

(A) Zinc binding. (B) Anchoring to the metal ion coordinated water. (C) Occlusion of the active site entrance. (D) Out of the active site binding. ZBG (zinc-binding group), AG (anchoring group), SG (sticky group)

The inhibition mechanisms of small molecule inhibitors of carbonic anhydrases include: (A) Inhibitor possesses zinc-binding group (e.g., SO_2NH^- moiety of sulfonamide) for binding with zinc ion directly followed by blocking enzyme catalytic function. In addition, the scaffold of inhibitor may interact with one or both halves of the active site. The tail also binds to the exit of the active site cavity for enhancing the isoform selectivity. (B) Anchoring group of inhibitor anchors to hydroxide ion coordinated with zinc ion, followed by making additional hydrogen bonds with adjacent gate keeping residues. (C) Sticky group of inhibitor (e.g., OH, amino, COOH,

scaffold and tail of inhibitors, etc) irreversibly occludes the entrance of active site. The scaffold and tail of inhibitor of this group show the similar functions with mechanism A. (D) Inhibitor (e.g., benzoic acid derivative) binds the outside of active site cavity by blocking the proton shuttle residue. [212, 220, 222]

The classical inhibitors are promiscuous and potent, show non-specific for carbonic anhydrase isoforms and have a series of side effects.[154, 212] The highly homology of the catalytic domain of CAs makes them difficult to be designed for isoform specific CAIs.[220] In order to increase the specificity to different CAs and enhance the efficiency of inhibitors for imaging or therapeutic purpose, these can be realized by regulating the physical and chemical characteristics of the inhibitors (e.g., membrane permeability, molecular size/charge or surface topology, etc) via attachment of different side chains and other modifications (e.g., fluorescent tags or radioisotope labeled, glycosyl/thioureido/aromatic/heterocyclic modifications, positive charge, nanoparticles conjugated, etc).[154, 180, 220, 223] New generation inhibitors (e.g., U104) show more potent, selective inhibition and fewer side effects.[212]

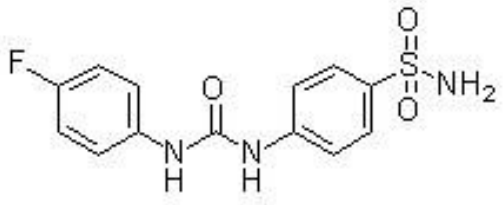

Figure 1.11 Chemical structure of U104 [224]

U104 is also known as SLC-0111, MST-104, and WBI-5111.[225] Its chemical name is (4-[[[(4-fluorophenyl)amino]carbonyl]amino]-benzenesulfonamide) and molecular formula is $C_{13}H_{12}FN_3O_3S$. It is one of the ureidobenzenesulfonamide inhibitors of CAIX/XII. The K_i value of U104 against CAIX is 45 nM.[224] The flexibility of the second ureido nitrogen linker may provide orientation in different subpockets of the active site cavities of CAs, which is possibile the determinant for the control of inhibitory power.[226] U104 shows significant potential of inhibition in *in vitro* and *in vivo* studies (e.g., breast carcinoma, rat prostate carcinoma, melanoma, colon cancer, etc) alone or with traditional radiotherapy and chemotherapy.[224] U104 is the first inhibitor that has completed clinical Phase I trial (NCT02215850) successfully and currently progresses in clinical Phase I/II trial (NCT03450018).

1.5 Invasion of GBM cells

1.5.1 Overview of glioma invasion

Cell migration is that cells move from one location to another and involve in both physiological and pathological conditions. Cell invasion is that cells become motile and navigate across the ECM in a tissue or infiltrate neighbouring tissues.[227] Alternatively, the definition of tumor cell invasion is the active translocation of tumor cells across cellular and ECM barriers and through tissue boundaries.[228] Although new therapeutic targeting of integrins and proteases appears to be expected to limit the invasion of GBM, inhibitors of these proteins have failed to improve patient prognosis. In this regard, the mechanism of GBM cell invasion still remains unclear.[229] Tumor cells invade and migrate in diverse modes by different mechanisms. These include individual cell mode (mesenchymal or amoeboid type) and collective mode (strands-, sheets-, files- or clusters-like type), and they can undergo transition or co-occurrence.[230] Both modes occur in GBM.[10] While GBM cells invade mainly by employing the mesenchymal mode of individual cell *in vivo* which is integrins and proteases dependent. Ameboid mode which is largely integrins and proteases independent has only been depicted *in vitro*.[229]

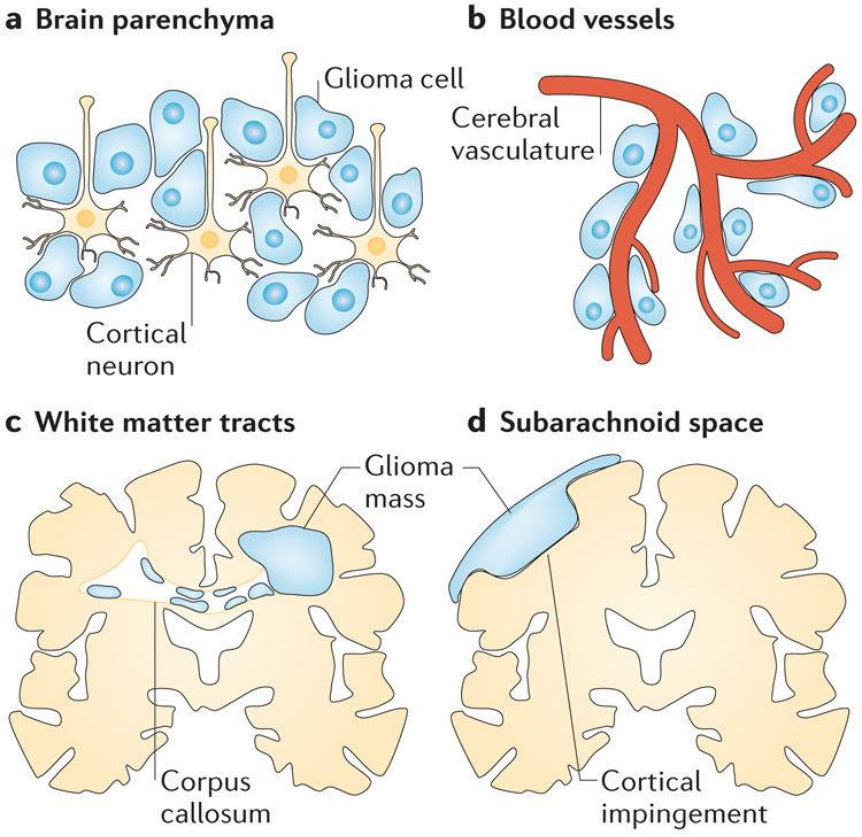

Figure 1.12 Routes of mesenchymal invasion mode of GBM cells [48]

(a) brain parenchyma, (b) pre-existing blood vessels, (c) white matter tracts (either perifascicularly intrafascicularly or interfibrillary) (d) subarachnoid space below the meningeal covering of the brain

Glioma cells prefer to invade along pre-existing brain structures which include brain parenchyma, perivascular space, white matter tracts and subarachnoid space.[48, 49] This feature was primaryly depicted by german neuropathologist Hans Joachim Scherer in 1938 and named Scherer's structures or secondary structures.[231] Very seldom gliomas metastasize outside the CNS and most of them are case reports in the literatures. This maybe attributed to glioma cells cannot intravasate the cerebrovascular and the absence of lymphatic system. Glioma cells may also require a specific milieu for survival and proliferation. Another reason is the extremely short survival of patients that not enough time for glioma cells to establish metastasis.[48, 232, 233]

1.5.2 Glioma microenvironment

The glioma microenvironment is a dynamic and intricate 3D network that encompasses diverse non-tumor cell types, stromal components, blood vessels, secreted factors, fluids and ECM. Glioma cells interact with adjacent microenvironment bi-directionally.[49, 234] There are many differences between brain and other tissues such as distinctive ECM composition (negligible fibrillar ECM proteins), unique tissue-resident cell types (e.g., microglia, astrocytes and neurons), physically protected barrier (the blood-brain barrier).[235] Width of the extracellular space is 38-64 nm in the rat brain neocortex, and is much smaller than the size of glioma cells for migration.[48, 236]

1.5.2.1 Structure and composition overview of neural extracellular matrix

Components of neural ECM are secreted by resident cells and serve as structural integrity, regulation of connectivity and communication for both cell-cell and cell-ECM, as well as growth factors and chemo-attractants isolation for cell motility regulation.[232] Neural ECM accounts for 20% volume of CNS[237] and is structurally and functionally distinct from other tissues of the body. Neural ECM comprises two principal compartments. They are the narrow and tortuous parenchymal ECM as well as the basement membranes that surround fluid-filled perivascular space and the subarachnoid space. The parenchymal ECM canbe further divided into diffusely

distributed dense neural interstitial matrix between cells and specialized structures around neurons. The specialized structures include condensed mesh-like perineural nets structures (PNN) that enwrap neuron soma and dendrites as well as the ECM circling the synapse and Ranvier nodes.[48, 232, 238-240]

The interstitial matrix is a highly compressible and motile-resistant network.[232] Major components of interstitial matrix are hyaluronan, proteoglycans, tenascins and link proteins. The minor components are adhesive glycoproteins (e.g., laminins and fibronectin) and fibrous proteins (e.g., collagens and elastin).[240] Perineural nets compose of hyaluronic acid, lecticans, aggrecan, tenascin R and link proteins principally. The ECM at the synapse mainly includes thrombospondin, brevican, pentraxin, hevin, cerebellin, neurexin, reelin, tenascin and hyaluronic acid. The ECM circling the Ranvier nodes is rich in brevican, versican, phosphacan, and tenascin R.[239] The basement membrane components consist laminin, collagen IV, nidogen, perlecan, fibronectin, and dystroglycan predominantly.[240]

1.5.2.2 Main molecular composition of parenchymal extracellular matrix

HA (hyaluronic acid), also named hyaluronan or hyaluronate, is the most abundant component of neural ECM. It is a very large unbranched linear glycosaminoglycan (GAG) polymer without protein core and sulfation. It is constituted by disaccharide units of D-glucuronic acid and N-acetylglucosamine. HA functions as back bone and hygroscopic carrier for binding with other molecules of ECM.[232] HA is produced at the inner-surface of the neuron cell membrane by hyaluronic acid synthetase. Other GAGs are produced in the Golgi apparatus.[238] HA anchors to the intracellular actin cytoskeleton via CD44, RHAMM (receptor for hyaluronan mediated motility) and hyaluronic acid synthase.[232, 238] CD44 is a single transmembrane glycoprotein. Its cytoplasmic domain links to cytoskeleton adapters and regulatory proteins (e.g., Src kinases and Rho GTPases). CD44 can be proteolyzed. The extracellular portion promotes glioma invasion and migration, and the intracellular fragment translocates into the cell nucleus that acts as a transcription factor for glioma cell adhesion. RHAMM is distributed in multiplex compartments of cell. Interactions of HA with RHAMM can activate a series of cellular signaling pathways involving PKC (protein kinase C), FAK (focal adhesion kinase), MAPK, Ras, PI3K, tyrosine kinases and cytoskeletal components.[238]

Proteoglycans take a large proportion of ECM in CNS.[239] Proteoglycans are constituted by a

protein core that covalently links to glycosaminoglycan side chains such as chondroitin sulfate (CS), keratan sulfate (KS), dermatan sulfate (DS), heparan sulfate (HS), etc.[238] Glycosaminoglycan is an anionic molecule that attracts Na^+ and other cations simultaneously with an osmotic water influx.[130] The most important proteoglycans in the CNS are chondroitin sulfate proteoglycans (CSPGs) and heparin sulfate proteoglycans (HSPGs).[239] CSPGs show variability of binding properties, distribution and function within CNS by variation of core protein, glycation and the number and position of sulfation.[232, 239] Disaccharide chain of CS-GAG (chondroitin sulfate glycosaminoglycan) consists of glucuronic acid and N-acetylgalactosamine linked by a β-glycosidic bond. In addition to the hygroscopic function abovementioned, CS-GAG acts as chemorepellent for inhibition of axon projection, cell motility and restriction of structural plasticity. CSPGs canbe cassified as lectican family [e.g., aggrecan, brevican (lectin), neurocan, and versican], phosphacan, and small leucine-rich proteoglycans.[232] HSPGs are expressed as membrane-bound (e.g., syndecans and glypicans) or secretory (e.g., perlecan, agrin, and collagen type XVIII). HSPGs are constituted by a core protein and HS glycosaminoglycan chains by O-linked covalent bonds. HSPGs play important roles in the ECM integrity and cell-cell or cell-ECM interactions by associating with various biomolecules (e.g., growth factors, chemokines, enzymes, and other ECM and plasma proteins). [241]

HAPLNs (hyaluronan and proteoglycan link proteins) family members [HAPLN1 (Crtl1), HAPLN2 (Bral1), and HAPLN4 (Bral2)] are found in the CNS and non-covalently link between HAs and CSPGs for the stabilization of PNN.[232, 239] HAPLN 1/4 interact with CSPGs and HA into a tripartite complex which forms an exoskeleton framework of PNN. HAPLN2 is produced by oligodendrocytes and interacts with verscian V2 around the Ranvier node.[239]

Tenascins are large multimeric glycoproteins.[238] Typical motifs of tenascins are a cysteine-rich amino acid terminal, a fibronectin type III domain, EGF repeats, and a fibrinogen β-like carboxy terminus. Tenascin-C and Tenascin-R are close related with the CNS. Tenascin-C (contactin) is a hexamer and is produced by both neurons and glia cells. The fibronectin motif is related to cell binding and neuronal migration. The EGF repeats are related to repulsive function. CSPGs are the main binding partner of Tenascin-C.[239] Tenascin-C also binds to integrins and affects cell behavior directly. The increased expression of Tenascin-C positively correlated with increasd glioma grade. Tenascin-R (restrictin) and other members of tenascin family are inversely correlated with the malignancy of GBMs.[238]

In addition to aforementioned CD44, other CAMs (cell adherein molecules) are also crucial for the invasion of glioma cells in CNS. These include integrins for glioma-ECM interaction, as well as cadherins, selectins, specific members of immunoglobulin superfamily for cell-cell interaction.[242] Furthermore, changed expression of axonal guidance molecules (e.g., netrins, ephrins, plexin, Slits/Robo, semaphorins/neuropilin) contribute gliomas cells invasion and migration to the special infiltration routes as well. [238]

1.5.2.3 Main molecular composition of basement membranes

BMs (basement membranes) are specialized, 50-100 nm thickness, dense ECM protein complex that predominantly associated with blood vessels and subarachnoid space in the brain.[243-245] BMs possess tiny pores of roughly 10-130 nanometer diameter which prevent cells from traversing the barrier except normal physiological functions.[243] The principal constituents and framework of brain BMs are two independent self-assembled, sheet-like network structures of collagen IV and laminin. They are bridged by nidogen (entactin) and perlecan (HSPG 2).[243, 245, 246] Different anatomical structures possess specific BM compositions within the CNS. Apart from the principal constituents, fibronectin and vitronectin can be found in cerebrovascular BMs. Type I, III collagens, fibronectin, and a variety of proteoglycans are found in glia limitans externa.[242] Fundamental ingredients of BMs are similar. While each ingredient, especially laminin, shows distinct amounts and isoforms as well as temporal and spatial distribution patterns which contribute to both heterogeneity and complexity structurally and functionally.[245, 246] The cross section of larger cerebrovascular, from inside to outside, is constituted by inner endothelial cell layer and its BM (laminins α4 and α5), meningeal epithelium with BM (laminin α1), outer astroglial BM (laminin α2) and astrocyte endfeet ultrastructurally. The meningeal and astroglial BMs are named parenchymal BMs collectively as they demarcate the boundary with the brain parenchyma. Microvessel cross section is sandwich-like structure and constituted by endothelial cells, BMs and astrocytic endfeets. Laminin α4, α5 and laminin α2 of BMs are secreted by two cell types above, respectively. BMs also encase pericytes and surround individual smooth muscle cell.[245] The neural BMs function as part of blood-brain barrier that isolates mesoderm-derived epithelial cells and ectoderm-derived neurons and glia, as well as structural support and cellular signaling pathways modulation.[48] Although the infiltration of glioma cells disrupts the parenchymal BMs, the endothelial BMs retain intact. Therefore, glioma cells fail to

traverse the BMs into the vessel lumen consistently.[242]

1.5.2.4 ECM-degrading enzymes and growth factors

Glioma cells produce and secrete ECM-degrading proteases and glycosidases for ECM remodeling and tumor invasion. ECM-degrading proteases also source from endothelial cells, stem cells, glioma-infiltrating microglial cells, etc. Proteases and relevant inhibitors can be modulated on transcriptional, post-transcriptional and epigenetic levels. Cleavage of the ECM components by proteases removes the physical barriers and releases growth factors followed by producing fragments with new biological activities. ECM-degrading proteases can be classified into subgroups by catalytic site. These include serine proteases [uPA/tPA (urokinase-type/tissue-type plasminogen activator) and their receptors], cysteine protease (cathepsin B), MMPs (metalloproteases) (e.g., gelatinases, collagenases, matrilysins, stromelysins and membrane-type MMP), ADAM (a disintegrin and metalloproteinase) and ADAMTS (ADAMs with a thrombospondin motif). Glycosidases (e.g., hyaluronidases and heparanases) catalyze the hydrolysis of glycosaminoglycans and proteoglycans. [229, 238]
Some auto- and paracrine growth factors (e.g., chemokines, TGF-β) are stored in ECM. They modulate ECM molecule expression and/or degradation as well as cell motility. Conversely, ECM structure and turnover significantly influence availability and activity of growth factors. [238]

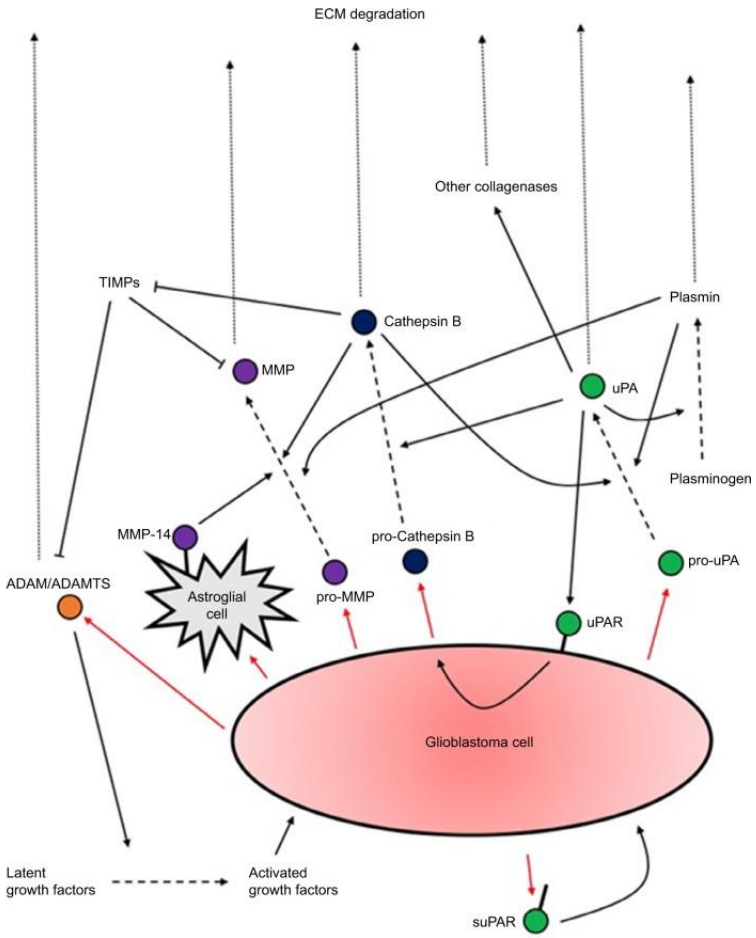

Figure 1.13 Proteases secretion and activation of GBM cells for invasion [247]

Acidic pHe induces the redistribution of active lysosomal proteinase cathepsin B to the invadopodia surface of tumor cells and in turn participates in the activation of uPA and MMPs. uPA converts plasminogen to plasmin and activates other collagenases. The convergent effects of proteinase activation cascade degrade all components of ECM. MT1-MMP (membrane-type MMP), ADAMs (transmembrane and secreted proteases), TIMPs (tissue inhibitor of metalloproteinases), suPAR (soluble urokinase-type plasminogen activator receptor), uPAR (urokinase plasminogen activator surface receptor) and growth factors also participate in the proteinase activation cascade and finally enhance invasion of tumor including GBM.[247, 248] Heparanase cleaves heparan sulfate proteoglycans and promotes tumor invasion at acidic pH.[249] Highly expressed heparanase also indicates poor survival of glioma patient.[250]

1.5.2.5 Non-neoplastic cell types in glioma microenvironment

In addition to glioma cells, many other non-neoplastic cell types are also found in glioma microenvironment. These include immune cells (tumor-associated macrophages and microglia, dendritic cells, monocytes, lymphoid cells, neutrophils and myeloid-derived suppressor cells), astrocytes, endothelial cells, non-tumour stem cells (neural stem cells, mesenchymal stem cells, and glioma-associated stem cells), etc. They play an important role in glioma invasion by many mechanisms. [49, 235]

1.5.3 The mechanism of mesenchymal invasion mode of individual glioma cell

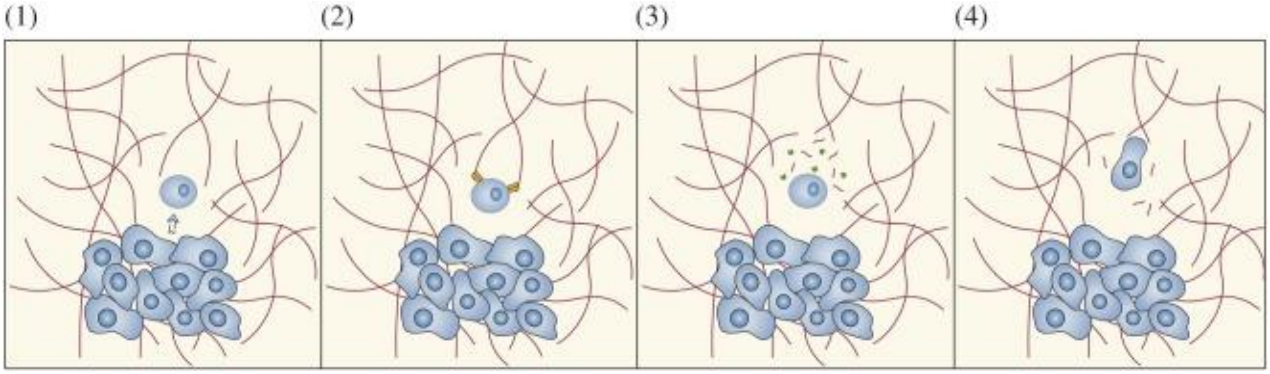

Figure 1.14 The mechanism of individual glioma cell mesenchymal invasion mode [251]

(1) The single glioma cell detaches from the primary tumor mass or trailing tail, (2) The formation of protrusion at leading edge and focal adhesion contacts to ECM components, (3) The proteolysis of ECM, (4) The glioma cell contraction and motility

The molecular biology mechanism of mesenchymal invasion mode of individual glioma cell canbe depicted as four principal steps. Each step involves several mechanisms.[49, 230, 252]

The first step is that single glioma cell detaches from the primary tumor mass or trailing tail. Extracellularly, glioma cell destabilizates and disassembles the cadherin-mediated and calcium-dependent transmembrane intercellular adherent junction complexes which combine the primary tumor mass together. The downregulation of connexin 43 results in the reduction of gap junction formation which is important for intercellular communication. ADAM cleaves CD44 which anchors the glioma cell to hyaluronic acid of ECM.[252] Integrins detach from ECM and are internalized by endocytotic vesicles for the recycling to the leading edge or deposition onto the ECM. Intracellularly, actin binding or severing proteins (e.g., gelsolin and cofilin) cap or

disassemble actin filaments, respectively. Phosphatases restrict cytoskeletal proteins assembly. Calpain cleaves cytoskeletal protein talin and cytoplasmic tail of integrin. FAK, proteolytic cleavage of adhesion receptors and degraded collagen fragments cause the disassembly of focal contact.[230]

The second step is the formation of protrusion at leading edge and the contaction of focal adhesion to ECM components.[230, 252] The binding of ARP2/3 complex (actin related protein 2/3 complex), WASP (Wiscott-Aldrich syndrome protein) and PIPs (phosphoinosites), located at the inner surface of plasma membrane, induces polymerization and branch of the actin-based filament nets. The nets are the fundamentals of lamellipodia and filopodia that push the cell membrane to outward direction.[230] Glioma cells secrete uPAs that upregulate the expression of αvβ3 integrins on an autocrine manner.[252] After the clustered integrins contact with ECM ligands, cytoplasmic tails of integrins interact with α-actinin, FAK, tensin, talin. All these proteins bind adaptor proteins, via SH2, SH3 or proline-rich domains, to recruit actin-binding proteins (α-actinin, vinculin and paxillin) and regulatory molecules (PI3K and Rho-family GTPases) for focal contacts.[230]

The third step is proteolysis of ECM.[252] The concentrated surface proteases at the focal contact sites cleave ECM components directly or pro-MMPs into active soluble MMPs (MMP2, MMP9) for the creation of invasive space.[230] Expression of MMPs are upregulated by uPA, LRP1 (low-density lipoprotein receptor-related protein 1), NF-κB, IGFBP-2 (insulin-like growth factor binding protein-2). Conversely, TIMP3 inhibits the activity of MMPs.[252]

The last step is glioma cell contraction and motility.[252] Actomyosin is the binding of active myosin II and actin filaments,[230] and is the principal source of cytoplasmic contractile force. Myosin II is activated and inactivated by phosphorylation and dephosphorylation of a serine residue of RLC (regulatory light chain) via MLC (myosin light chain) kinase and phosphatase, respectively. Small GTPases (e.g., RhoA, Rac, Cdc42) and RLC-interacting protein also influence the expression of myosin II.[252]

1.5.4 The influencing factors on invasion of glioma cells

1.5.4.1 The chemo-attractant enhances invasion

The migration and invasion of glioma cells are influenced by both the biochemical compositions

and biophysical inputs (e.g., density, rigidity and geometry) of ECM.[49] Cerebral vascular endothelial cells secrete bradykinin as a chemo-attractant that guides glioma cells to blood vessels via bradykinin 2 receptors and intracellular Ca^{2+} oscillations.[253] Glioma cells repurpose neurodevelopmental molecules such as pleiotrophin for invasion.[254] FBS (fetal bovine serum) is often used as chemo-attractant in invasion assay *in vitro*. Necrotic extract and growth factors (EGF, bFGF and PDGF-BB) are also reported to be used as chemo-attractants.[255-257]

1.5.4.2 The intracellular alkaline and extracellular acidic nature enhances invasion

The intracellular alkaline and extracellular acidic nature is resently known as a renewed major hallmark of tumours with the impetus of cancer metabolism study. The tumour acidosis that participates in invasion has shifted from a passive collateral effect to a key regulator of tumour progression. Tumor cell invasion is proposed to be mediated by dysregulated pH via various mechanisms.[152] The hypothesis of acid-mediated tumor invasion was introduced by Gatenby and Gawlinski in 1996.[258] CAIX is a major contributor to TME acidification and invasion. The inhibition of CAIX can be used as therapy of various cancers which mainly include renal, breast cancer and colon cancer.[259]

1.6 Intention and status of the research project

Despite in-depth research and understanding of invasion mechanism of GBM cells *in vitro* and *in vivo*, laboratory results have not been translated into effective clinical treatment.[10] For example, new therapeutic targeting of integrins and proteases appears to be expected to limit the invasion of GBM cells, inhibitors of these proteins have failed to improve patient prognosis. Therefore, the mechanism of GBM cell invasion is still unclear.[229] CAIX catalyzes the hydration reaction of CO_2 to carbonic acid that mediates the TME acidification.[153] Among all the human α-class carbonic anhydrases, CAIX shows highest catalytic activity, inducibility by hypoxia, extracellular membrane location and tumor-specific expression. This is why CAIX would be assumed as the potential "Achilles' heel" of GBM treatment. In addition, the research of CAIX on tumor invasion is limited to non-glioma or established GBM cell lines. After various omics research and new molecular subtype classification in recent years [4-6], there are seldom molecular subtype-based invasion studies of GBM cells. Further more, the next generation stem cell culture method of monolayer adherent growth shows great advantages, because it hinders the differentiation and

apoptosis of GBM cells which are more similar to the original GBM of paitients.[136]

1.7 Hypothesis

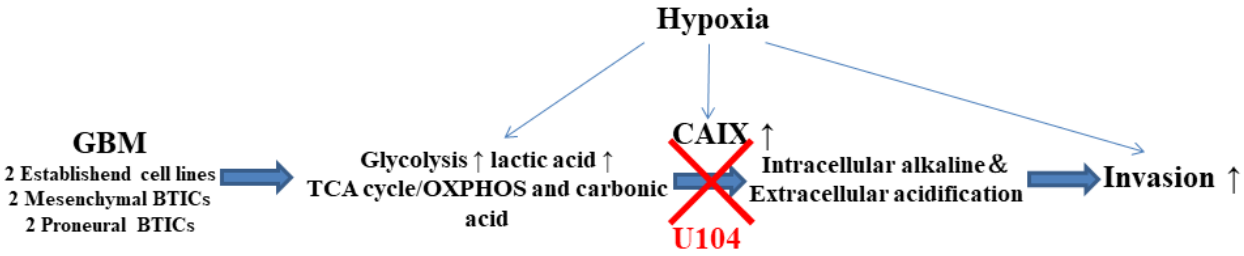

Figure 1.15 Technical route and hypothesis schematic diagram

We propose the following research hypothesis: GBMs are highly glycolytic and retain TCA cycle/OXPHOS which produce large mount of acid. CAIX promotes the nature of intracellular alkaline and extracellular acidification followed by the enhanced invasion of GBM cells. Both CAIX expression and cell invasion are upregulated by hypoxia. After the inhibition of CAIX by U104, the intracellular alkaline and extracellular acidic pH of GBM cells is disrupted, followed by the reduced invasion of GBM cells. The inhibition is more pronounced under hypoxia. All these are cellular molecular subtype dependent. Taken together, we hypothesize that carbonic anhydrase IX plays a role in the invasiveness of GBM cells.

1.8 Experimental design

Related experiments would be performed to investigate the expression of CAIX and corresponding GBM cell invasion. Mesenchymal and proneural BTICs would be incubated with next generation stem cell culture. Established GBM cell lines would be incubated in DMEM as control. 4.5g/L glucose of DMEM was used for the balance as RHB-A medium. Hypoxia induction and cell harvesting methods were inspected to optimize the experimental procedure. The expression of CAIX was examined under both normoxia and hypoxia on transcription and translation levels. Two single-isoform *VEGF*s were also tested to validate the experimental condition of hypoxia. Cell immunofluorescence staining was performed to specifically test the expression of membrane protein CAIX under normoxia and hypoxia. Cell viability experiment was conducted by treating cells with different concentrations of U104 and DMSO

(dimethylsulfoxid) to find the optimized concentration and action days for invasion assay before killing the cells. At last, cell invasion was investigated by Matrigel coated Transwell chamber and with or without inhibitor under normoxia and hypoxia.

2 Materials and Methods

2.1 Items list for experiment

2.1.1 Equipment, instruments and materials

Equipment, instruments and materials (Unit of measurement; Device model)	Manufacturers
Aspirator bottle (Duran)	Schott, Wertheim, Germany
Autoclave (VE-150)	Systec, Wettenberg, Germany
Autoclave (VX-150)	Systec, Linden, Germany
Bio vortex (V1)	Kisker-Biotech, Steinfurt, Germany
Biological safety cabinet (Hera Safe Class II)	Thermo Fisher, Langenselbold, Germany
Blood gas analyzer (ABL800 Flex)	Radiometer, Brønshøj, Denmark
Blot chamber	Renner, Dannstadt, Germany
Blotting paper (703)	VWR International, Vienna, Austria
BZO seal film	Biozym Scientific, Oldendorf, Germany
Cell counting slide (LUNA™ fl)	Logosbio, Gyeonggi-do, South Korea
Cell culture flask T75 (Standard) (CellStar®)	Greiner Bio-One, Frickenhausen, Germany
Cell culture flask T75/T175 (Standard/Vent. Cap)	Sarstedt, Nümbrecht, Germany
Cell culture insert 35/3097 (8.0µm pore size) (Falcon®)	Corning, New York, USA
Cell culture test plate (6-well, 24-well, 96-well)	TPP, Trasadingen, Switzerland
Centrifuge (5417C)	Eppendorf, Hamburg, Germany
Centrifuge (ROTINA 420R)	Hettich, Tuttlingen, Germany
Centrifuge tube (15ml/50ml) (CentriStar™)	Corning, Reynosa, Tamaulipas, Mexico
Comb (14-well, 1.5mm)	PeQLab, Erlangen, Germany
Companion plate 24-well (Falcon® 35/3504)	Corning, New York, USA
Constant temperature water bath 37°C (5A)	Julabo, Seelbach, Germany

Cotton swab (Bel premium)	Hartmann, Heidenheim, Germany
Counter	Infactory, Buggingen, Germany
Counter	IVO, Frauenfeld, Switzerland
Cover glasses (13mm)	Thermo Fisher, Braunschweig, Germany
Coverslip (Menzel Gläser)	Thermo Fisher, Braunschweig, Germany
Cryopreservation tube (2ml)	TPP, Trasadingen, Switzerland
Cuvette	NeoLab, Heidelberg, Germany
Developer (M35 X-OMAT Processor)	Kodak, Stuttgart, Germany
Digital-pH-Meter (647)	Knick, Berlin, Germany
Disposable bags	Carl Roth, Karlsruhe, Germany
Disposable cell scraper	Sarstedt, Newton, USA
Disposable nitrile gloves (VersaTouch®)	Ansell, Querétaro, Mexico
Drying cabinet (ED-115)	Binder, Tuttlingen, Germany
Dual fluorescence cell counter (LUNA™ fl)	Logosbio, Gyeonggi-do, South Korea
Electrophoresis chamber for PCR	PeQLab, Erlangen, Germany
Electrophoresis chamber for WB	Whatman Biometra, Göttingen, Germany
Extension tube	Bought from the University of Regensburg
Flake ice machine (AF-10)	Scotsman, Ipswich, Suffolk, UK (United Kingdom)
Foil sealing machine	Severin, Sundern, Germany
Freezing container (Cryo1°C)	Nalgene, Munich, Germany
Fume hood	Renggli Laboratory System, Rotkreuz Schweiz, Switzerland
Glass cylinder (Duran)	Schott, Wertheim, Germany
Heating circulator	Julabo EM, Seelbach, Germany
High performance chemiluminescence film (Hyperfilm™ ECL)	Cytiva Amersham, Buckinghamshire, UK
High pressure mercury burner (U-RFL-T-200)	Olympus, Tokyo, Japan
High temperature disinfection machine	Binder, Tuttlingen, Germany

(ED-115)	
Horizontal shaker (Titramax 1000)	Heidolph, Schwabach, Germany
Horizontal shaker (WS-10)	Edmund Bühler, Hechingen, Germany
Hypercassette™	Amersham Pharmacia Biotech, Buckinghamshire, UK
Incidine™ OxyWipe S	Ecolab, Monheim am Rhein, Germany
Incubator (Hera cell 150)	Thermo Fisher, Langenselbold, Germany
Inverted fluorescence microscope (IX70)	Olympus, Tokyo, Japan
Laboratory balance apparatus	Wägetechnik Dürnberger Acculab, Obertraubling, Germany
Laboratory dish washer (G7883 CD)	Miele, Gütersloh, Germany
Liner pipette (30-300µl)	Eppendoff, Hamburg, Germany
Liquid nitrogen tank (Thermolyne locator)	Thermo Fisher, Kerper Boulevard Dubuque, USA
Magnetic stirrer (MR2002)	Heidolph, Schwabach, Germany
Micro tube for reaction (0.5ml/1.5ml)	Sarstedt, Nümbrecht, Germany
Micro tube for storage (0.5ml/2ml)	Sarstedt, Nümbrecht, Germany
Microplate (96-well, F-bottom, chimney well, white) (lumitrac 600)	Greiner Bio-one, Schwerte, Germany
Microscope slides (25x 75x 1.0mm) (Superfrost® Plus)	Thermo Fisher, Braunschweig, Germany
Microwave oven	Privileg, Fürth, Germany
Milli-Q water machine (Q-POD®; Millipak® Express 40)	Millipore, Darmstadt, Germany
Mini rocker	Kisker, Steinfurt, Germany
Monitor (CCTV RMB92)	Rainbow, California, USA
Needle (0.9x 40mm, 0.7x 30mm)	Becton Dickinson Microlance, Fraga, Spain
Neubauer improved counting chamber	Marienfeld, Lauda-Königshofen, Germany
Nitrocellulose transfer membrane (300mm x 3m, Pore size 0.45µm) (Protran®)	Whatman, Dassel, Germany

Nitrogen 95% (+5% carbon dioxide)	Linde, Unterschleißheim, Germany
Parafilm	American National Can, Menasha, USA
Pasteur pipette (150mm)	John Poulten, Barking Essex, England
Pasteur pipette (230mm)	Carl Roth, Karlsruhe, Germany
PCR 96-well thin wall plate (0.2ml)	Biozym Scientific, Oldendorf, Germany
PCR soft tube (0.2ml)	Biozym Scientific, Oldendorf, Germany
Pipette (0.5-10µL; 10-100µL; 100-1000µL) (PhysioCare concept)	Eppendorf, Hamburg, Germany
Pipette controller	NeoLab, Heidelberg, Germany
Pipette controller (Accu-jet® pro)	Brand, Wertheim, Germany
Pipette tamping machine	IsmaTec, Glattbrugg-Zürich, Switzerland
Pipette tip (10µl; 200µl; 1000µl)	Sarstedt, Nümbrecht, Germany
Pipette tube cleaning machine	H. Hölzel, Hörlkofen, Germany
Plastic film	A.Hartenstein, Würzburg, Germany
Power supply (E835)	Consort, Turnhout, Belgium
Precision dispenser tip (4µl; 10µl; 50µl; 100µl)	Brand, Wertheim, Germany
Printer (DPU-414)	Seiko, Mihama-ku Chiba-shi Chiba, Japan
Printer (P93E)	Mitsubishi, Senai, Malaysia
Protective glasses	EAC uvex, Fürth, Germany
Refrigerator -20°C (MedLine)	Liebherr, Lienz, Austria
Refrigerator 4°C (Glass line)	Liebherr, Lienz, Austria
Refrigerator -80°C (Forma 900 Series)	Thermo Fisher, Marietta, USA
Repetitive pipette (Handy Step® S)	Brand, Wertheim, Germany
Repetitive tip (0.2ml) (Combitips advanced®)	Eppendorf, Berzdorf Wesseling, Germany
RNA/DNA calculator (GeneQuant II)	Pharmacia Biotech, Darmstadt, Germany
SafeSeal micro tube (2ml)	Sarstedt, Nümbrecht, Germany
Scanning and printing machine (Laser Jet 1536dnf MFP)	HP, Chinden Blvd Boise, Idaho, USA
Sealed box	Produced in the University of Regensburg

Steam indicator tape (Comply™)	3M, Saint Paul MN, USA
Syringe 1ml (Plastipak™)	Becton Dickinson, Madrid, Spain
Test tube rack (Rotilabo®)	Carl Roth, Karlsruhe, Germany
Thermo cycler for PCR (1732-1210)	VWR, Leuven, Belgium
Thermo cycler for qPCR (Mx3005p™)	Stratagene, Foster city, California, USA
Timer	Oregon Scientific, Shenzhen, PRC (People's Republic of China)
Tweezers	Aesculap, Tuttlingen, Germany
Ultraviolet transilluminator	PeQLab, Erlangen, Germany
Vacuum desiccator	VWR, Darmstadt, Germany
Vacuum pump	CE knf, Freiburg, Germany
Varioskan flash	Thermo Fisher, Vantaa, Finland
Video digital camera (XC10)	Olympus, Tokyo, Japan
Volumetric pipettes (5ml; 10ml; 20ml; 25ml; 50ml)	Brand, Wertheim, Germany

Table 2.1 Equipment, instruments and materials for experiment

2.1.2 Reagents

Reagents (Unit of measurement; Model)	Manufacturers
1x SDS (sodium dodecyl sulfate) Running buffer 1L	Bio-Rad, Munich, Germany
25x Protease inhibitor cocktail 100µl	Roche, Mannheim, Germany
2-Mercapto-Ethanol 100ml	Carl Roth, Karlsruhe, Germany
2-Propanol 70% 1000ml	B|Braun, Melsungen, Germany
6x Blue loading buffer (Bromophenol blue and xylene cyanol) 5ml	PeQlab, Erlangen, Germany
Accutase™ 100ml	PAA Laboratories , Cölbe, USA
Acrylamide/Bis solution 30% (37.5:1) 500ml	Bio-Rad, Munich, Germany

AEBSF (4-(2-aminoethyl)benzenesulfonyl fluoride hydrochloride) 25mg	Sigma-Aldrich, Saint Louis, USA
Agarose powder 500g	Biozym, Oldendorf, Germany
Aprotinin	Carl Roth, Karlsruhe, Germany
APS 10% (ammonium per sulfate) 25g	Sigma-Aldrich, Steinheim, Germany
Bio-Rad DC™ Protein Assay Reagent A 250ml Reagent S 5ml Reagent B 1L	Bio-Rad, California, USA
Boric acid 500g	Sigma-Aldrich, Steinheim, Germany
Bromophenol blue 5g	Merck, Darmstadt, Germany
BSA (bovine serum albumin) 100g	PAA, Pasching, Austria
CAIX antibody 1.0mg/ml	Novus Biologicals, Abingdon, UK
Cell Titer-Glo® Luminescent cell viability assay Cell Titer-Glo® substrate 1 vial powder. Cell Titer-Glo® buffer 100ml	Promega, Madison, USA
Chemiluminescent substrate SuperSignal™ West Pico PLUS stable peroxide solution 250ml SuperSignal™ West Pico Plus Luminol/Enhancer solution 250ml	Thermo Fisher, Rockford, USA
Crystal violet 25g	Carl Roth, Karlsruhe, Germany
DEPC (Diethyl pyrocarbonate) water 20ml	Carl Roth, Karlsruhe, Germany
Dk anti rbt Biotin (0.5mg/ml) (711-065-152)	Jackson Immuno-Research, Suffolk, England
DMEM (Dulbecco's Modified Eagle's Medium) 500ml $NaHCO_3$ 3.7g/L D-Glucose 4.5 g/L Low endotoxin	Merck Biochrom, Berlin, Germany
DMSO 1000ml	Carl Roth, Karlsruhe, Germany

dNTP (deoxy-ribonucleoside triphosphate)-Mix 1.0ml (Invitrogen)	Thermo Fisher, Carlsbad, USA
EDTA (ethylenediamine tetraacetic acid) 100g	Carl Roth, Karlsruhe, Germany
EGTA (ethylene glycol tetraacetic acid) 100g	Sigma-Aldrich, Steinheim, Germany
Electrolyte solution (3mol/L KCl) 200ml	WTW, Weilheim, Germany
Ethanol ≥99.8% 2.5L	Merck, Darmstadt, Germany
Ethidium bromide solution 1% (10mg/ml) 10ml	Carl Roth, Karlsruhe, Germany
FBS 500ml	Merck Biochrom, Berlin, Germany
Forward/reverse primers	Eurofins Genomics, Ebersberg, Germany
GAPDH (glyceraldehyde-3-phosphate dehydrogenase) antibody 10µg/50µl	Santa Cruz Biotechnology, Dallas, USA
GeneRuler™ DNA ladder (50-1050bp, 0.1µg/µl, 50µg)	Fermentas, Carlsbad, USA
Glycerol 100ml	Sigma-Aldrich, Steinheim, Germany
Glycine 1kg	Merck, Darmstadt, Germany
Hemacolor® rapid staining Solution 1 fixing solution 100ml Solution 2 color reagent red 100ml Solution 3 color reagent blue 100ml	Merck KGaA, Darmstadt, Germany
HEPES (4-(2-hydroxyethyl)-1-piperazineethanesulfonic acid) 1000g	ICN Biomedicals, Aurora, USA
HRP (horseradish peroxidase conjugates) antibody 0.40mg/ml	Bio Source, Camarillo, USA Santa Cruz Biotechnology, Dallas, USA
Human EGF、bFGF 100µg/500µg	Miltenyi Biotec, Bergisch Gladbach, Germany
KCl 1kg	Merck, Darmstadt, Germany
KH_2PO_4 1kg	Merck, Darmstadt, Germany
Leupeptin	Carl Roth, Karlsruhe, Germany

L-Glutamine (200mM) 100ml	Merck Biochrom, Berlin, Germany
Matrigel® (Cultrex® reduced growth factor basement membrane extract) (3433-005-01), 5ml	Bio-Techne, Wiesbaden, Germany
Mercaptoethanol 250ml	Carl Roth, Karlsruhe, Germany
Methanol 99.8% 2.5L	Merck, Darmstadt, Germany
Milk powder 250g	Carl Roth, Karlsruhe, Germany
Na_2HPO_4 1kg	Merck, Darmstadt, Germany
NaCl 1kg	VWR Chemicals, Leuven, Belgium
Nonidet P-40 100ml	ICN Biomedicals, Aurora, Ohio
Normal donkey serum (60mg/ml; 017-000-121) 10.0ml	Jackson ImmunoResearch Laboratories, Pennsylvania, USA
Orthovanadate	Sigma-Aldrich, Steinheim, Germany
PBS (phosphate buffered saline) 500ml	Sigma-Aldrich, Steinheim, Germany Invitrogen gibco, Paisley, UK
Penicillin (10.000U/ml)/ Streptomycin (10.000µg /ml)100ml	Merck Biochrom, Berlin, Germany
PFA (paraformaldehyde) 1kg	Sigma-Aldrich, Steinheim, Germany
Phospho-Akt antibody	R&D System, Minneapolis, USA
PMSF (phenylmethanesulfonylfluoride) 1g	Sigma-Aldrich, Steinheim, Germany
Polyclonal rbt anti CAIX (1mg/ml)	Novus Biologicals, Abingdon, UK
Ponceau S 10g	Sigma-Aldrich, St. Louis, USA
Primer random 1.0ml	Roche, Grenzach-Wyhlen, Germany
Protein marker IV 250µl (170~130~100~70~55~40~35~25~15~10) kDa	PeQlab, Erlangen, Germany
PVA (polyvinyl alcohol)-DABCO (1,4-diazobicyclo(2,2,2)-octane)10981-100ml	Merck, Darmstadt, Germany
QuantiFast™ SYBR® Green PCR kit SYBR® Green PCR master mix (2x 1.7ml) HotStarTaq® Plus DNA polymerase	Qiagen, Hilden, Germany

QuantiFast SYBR Green PCR buffer dNTP mix (dATP, dCTP, dGTP, dTTP) ROX™ passive reference dye RNase-free H_2O (1.9ml)	
Quantitas DNA marker (25-500bp)	Biozym Scientific, Hessisch Oldendorf, Germany
Rbt anti IgG (0.5mg/ml) (I5006)	Sigma-Aldrich, Missouri, USA
RHB-A 500ml Unknown ingredients	Takara Bio, kusatsu, Shiga, Japan
RNase ZAP® 250ml (Ambion® Invitrogen)	Thermo Fisher, Carlsbad, USA
RNase-free DNase set Buffer RDD (RNase-free DNA digest) 2ml DNase I, RNase free, lyophilized RNase free water 1.9ml	Qiagen, Hilden, Germany
RNase-free H_2O 1.9ml	Qiagen, Hilden, Germany
RNeasy® mini kit RLT lysis buffer 220ml RW1 wash buffer 220ml RPE wash buffer 55ml RNase-free water 50ml	Qiagen, Hilden, Germany
SDS 10% 250g	Serva, Heidelberg, Germany
Sodium acetate powder 250g (EMSURE®)	Millipore, Darmstadt, Germany
Sodium deoxycholic acid 25g	Sigma-Aldrich, Steinheim, Germany
Streptavidin-FITC (fluorescein isothiocyanate) (SA-5001; 1mg/ml)	Vector, Burlingame, USA
Stripping buffer 500ml (Restore™)	Pierce, Rockford, Germany
Super Script® II reverse transcriptase kit (Invitrogen) Super Script II reverse transcriptase 10,000U 5x First strand buffer 200µl 0.1M DTT (dithiothreitol) 500µl	Thermo Fisher, Carlsbad, USA

Taq PCR master mix kit Taq PCR master mix (250 units;1.7ml) RNase-free H_2O (1.9ml)	Qiagen, Hilden, Germany
TEMED (N,N,N',N'-Tetra-methyl ethylene-diamine) 5ml	Merck, Schuchardt, Hohenbrunn, Germany
Tris 1kg	Carl Roth, Karlsruhe, Germany
Triton®X-100 (t-Octylphenoxypoly-ethoxyethanol) 500ml	Sigma-Aldrich, Steinheim, Germany
Trypan blue 0.4% 100ml	Sigma-Aldrich, Steinheim, Germany
Trypsin/EDTA solution 100ml	Merck Biochrom, Berlin, Germany
TWEEN® 20 viscous liquid 500ml	Sigma-Aldrich, Steinheim, Germany
U104 50mg Catalog. No: 4540; Batch No:1A/179133	Tocris bioscience, Bristol, UK
Water 250ml	Sigma-Aldrich, Steinheim, Germany
Wortmannin (W1628-10MG)	Sigma-Aldrich, Rehovot, Israel
β-Actin antibody	Sigma-Aldrich, St. Louis, USA

Table 2.2 Reagents for experiment

2.1.3 Ingredients of chemical solutions

Chemical solutions	Ingredients
10x PBS (pH7.4,1M) 2L	KCL 4.0g KH_2PO_4 4.0g NaCl 160g Na_2HPO_4 x $2H_2O$ 28.8g
10x TBE buffer (Tris/Borate/EDTA) 1L	Tris 108g Boric acid 55g 0.5M EDTA 40ml
10x TBS (Tris-buffered saline) (pH7.5) 1L	Tris 24.2g NaCl 80g

5x RSB (reducing sample buffer)	1M Tris- HCl 0.6 ml 50% glycerol 5.0 ml 10% SDS 2.0 ml Mercaptoethanol 0.5 ml Sterile water 1.9 ml Bromophenol blue 1 spatula tip
Blotting buffer for pAkt 1L	Tris 25mM (pH 7.4) NaCl 0.15M 0.1% Tween
Crystal violet solution	Crystal violet powder 0.5g 20% Methanol 100ml
DMEM with/without FBS	DMEM 500ml Penicillin/Streptomycin solution 5ml L-Glutamine solution 5ml ±FBS 50ml
Lysis buffer for pAkt 500ml	Tris 1.2114g NaCl 4.383g EGTA 0.1902g EDTA 0.1461g Triton X-100 5ml Sodiumpyrophosphat 0.3323g
PBS-T (phosphate buffered saline with Tween)	1x PBS 1L Tween 20 1ml
Protease inhibitors for pAkt 1ml	Orthovanadate 1µl PMSF 10µl Leupeptin 1µl Aprotinin 1µl
Protease inhibitors for RIPA (radioimmunoprecipitation assay) buffer 1ml	AEBSF 2µl 25x protease inhibitor cocktail 40µl
RHB-A medium	RHB-A 500ml Penicillin/Streptomycin solution 5ml

	EGF 500µl FGF 500µl
RIPA buffer 100ml	10x PBS 10ml Nonidet P-40 1.0ml 20% SDS 0.5ml Sodium deoxycholic acid 500mg
Separating gel 12%	Milli Q H_2O 30% Acrylamide mix 1.5 M Tris（pH 8.8） 10% SDS 10% APS TEMED
Sodium acetate solution	Sodium acetate powder 0.8203g 50% Ethanol 100ml
Stacking gel 5%	Milli Q H_2O 30% Acrylamide mix 1.0 M Tris（pH 6.8） 10% SDS 10% APS TEMED
TBS-T (Tris-buffered saline with Tween)	1x TBS 1L Tween 20 1ml
Transfer buffer 1L	Glycine 2.93g Tris 5.81g SDS 0.38g Methanol 200ml

Table 2.3 Ingredients of chemical solutions for experiment

2.2 Cell line source and cell culture

2.2.1 Cell line source

Two mesenchymal and two proneural BTICs as well as two establishend cell lines were tested in this research. U87 and U251 were from the storage of our laboratory. BTICs were kindly provided by the Department of Neurooncology, Universitätsklinikum Regensburg.

Cell lines	Molecular subtypes	Growth characteristics	Medium
U87	established	adherent	DMEM
U251	established	adherent	DMEM
BTIC12	mesenchymal	adherent	RHB-A
BTIC13	mesenchymal	adherent	RHB-A
BTIC17	proneural	adherent and overlap growth	RHB-A
BTIC18	proneural	semi-adherent and spheres growth	RHB-A

Table 2.4 Characteristics and medium type of cell lines

Established cell line	Histology	Age at diagnosis (years)	Gender	Gene and expression information
U87	GBM	44	female	unknown
U251	GBM	75	male	unknown

Table 2.5.1 Patient information of established cell lines

BTIC	Original tumor				Patient characteristics				Primary cell culture					
	Histology	Molecular subtypes	*MGMT*-methyl.	*IDH1* (wt/mut)	Age at diagnosis(y)	Gender	Prior therapy	Survival (weeks)	*in vitro* growth	*MGMT*-methyl.	CD133 pos. (%)	*IDH1* (wt/mut)	Nestin	Sox2
12	GBM (prim.) Gliosarcoma	Mes.	meth.	wt	69	m	R/C	66	adherent	meth.	29	wt	+	-
13	GBM (sec.)	Mes.	unmeth.	pR132H	42	m	R/C	34	adherent	meth.	62	wt	+	-
17	GBM (prim.)	Pro.	meth.	wt	49	f	R/C	35	spheres	meth.	35	wt	+	+
18	GBM (prim.)	Pro.	unmeth.	wt	49	m	R/C	82	adherent	unmeth.	0	wt	+	+

Table 2.5.2 Patient information of BTICs

(prim.= primary, sec.= secondary, Mes.= mesenchymal, Pro.= proneural, meth.= methylated, unmeth.= unmethylated, wt= wild type, mut= mutant, m= male, f= female, R= Radiotherapy, C= Chemotherapy, y= years, pos.= positive)

Note: BTIC13 lost *IDH1* mutation and became wild type in primary cell culture.

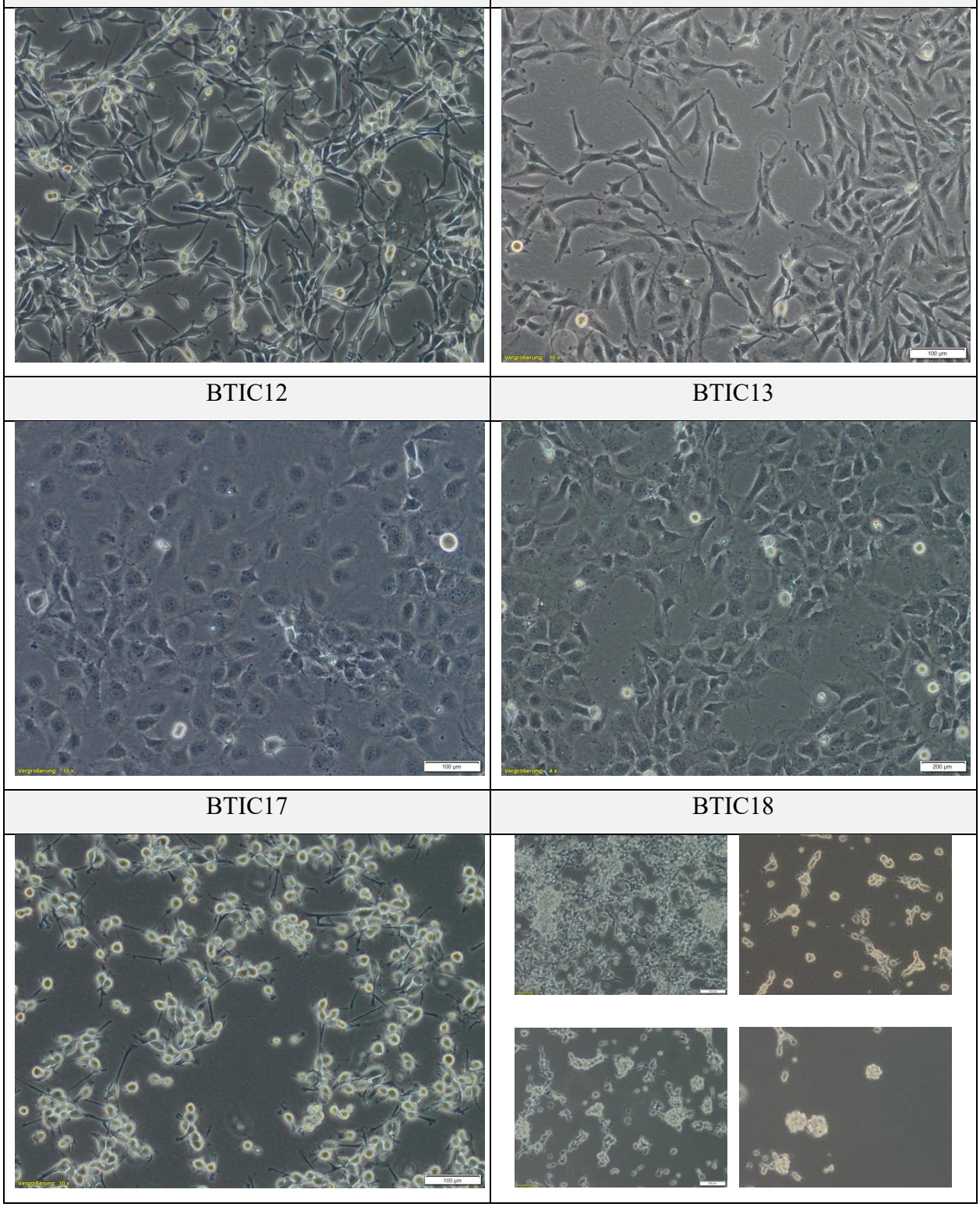

Figure 2.1 Morphology of all 6 cell lines (200x original magnification)

2.2.2 Cell culture

Cell culture was carried out with pre-warmed medium, PBS and digestive enzymes in a sterilized biological safety cabinet followed by incubation in the incubator of 37℃, 5% CO_2 and 95% humidity.

2.2.2.1 Cell resuscitation

The cryopreservation tube with desired cells was taken out from liquid nitrogen and transported on dry ice. 2-5ml medium was added in advance in a 50ml centrifuge tube. Cryopreservation tube was swirled in a 37°C water bath for thawing up until a small piece of ice (around 1/3 of total volume) remained in it. The cap should not be submerged to avoid contamination. After disinfection, the partially thawed cell suspension was poured into the 50ml centrifuge tube immediately. 6-10ml medium was pipetted and mixed with cell suspension slowly to dilute the DMSO for the protection of cells. After the tube was centrifuged 5 minutes at speed 1,200 rpm (revolutions per minute), the supernatant was aspirated away. Cell pellet was re-suspended with 10ml medium and the cell suspension was pipetted into a labeled culture flask. The culture flask was shaken gently for the even distribution of cells. After the observation under microscope, the culture flask was placed into the incubator.

2.2.2.2 Medium change

Medium was refreshed twice a week for the low and middle confluence growth of cells. The medium volume for the refreshment was based on the cell growth conditions, size of culture flask and medium types. DMEM was refreshed completely and RHB-A medium was refreshed by half. For adherent cells, care should be taken for not rinsing off cells on the flask bottom. For semi-adherent cells, the culture flask was tilted to precipitate cell spheres by gravity before operation.

2.2.2.3 Cell subculture

Cells should be passaged at no more than 80% confluence except confluence experiment. In the subculture process of adherent established cell lines, the old DMEM was aspirated completely

first without removing cells on the flask bottom. Cells were gently washed once with 3-5ml PBS, 3-5ml Trypsin was added and covered the whole bottom of culture flask. After the cell detachment for 4 minutes in the incubator, the side of culture flask was tapped gently on horizontal followed by the observation under the microscope. 6-10ml DMEM with FBS (2 times volume of Trypsin) was added into the culture flask and pipetted repeatedly to terminate the reaction. The cell suspension was transferred to a labeled 50ml centrifuge tube and centrifuged 5 minutes at 1200 rpm. 10-20ml DMEM with FBS was pre-added in the labeled culture flask. After centrifugation, the supernatant was aspirated completely, and the cell pellet was re-suspended by 1-5ml medium based on its size. A certain volume of cell suspension was used for experiment or continuous cell culture according to cell count result or ratio (1: X). The culture flask was shaken gently for the even distribution of cells. After the observation under microscope, the culture flask was placed into the incubator.

To save the expensive RHB-A medium for BTICs, the old medium was pipetted into the labeled 50ml centrifuge tube for the reaction termination of Accutase. 3-5ml mixture of Accutase and PBS (volume ratio 1:1) was used for the detachment of BTICs. BTIC18 grew in semi-adherent form and was operated in the same way as other BTICs.

2.2.2.4 Cell harvest

Trypsin/Accutase method

After the detachment of cells by Trypsin or Accutase, the collection of all cell suspensions was centrifuged 5 minutes at 1200rpm. Supernatant was removed and cell pellet was washed with 2.5ml pre-cooled PBS. Cells which were cultured in DMEM should be washed one more time because of phenol red. Finally, PBS was removed completely, and the cell pellet was kept on ice for short time or stored in -80℃ refrigerator for long time.

Cell scraper method

After aspirating the old medium completely, 5ml pre-cooled PBS was pipetted into the culture flask and all the cells on the bottom were scraped. After scraping, cell suspension was pipetted into a labeled 50ml centrifuge tube followed by the observation of flask bottom under the microscope. The bottom of flask should be washed and scraped again to increase the yield if necessary. The collection of all cell suspensions was centrifuged 5 minutes at 1200rpm, and the supernatant was discarded. Other steps were identical with Trypsin/Accutase method.

2.2.2.5 Cell count

The Neubauer counting chamber and the coverslip should be cleaned with 70% ethanol before operation. They were fixed right by seeing the Newtonian rings. 40µl re-suspended cell suspension was pipetted and mixed with 10µl Trypan blue in a 1.5ml micro tube. 10µl mixture was filled into the gap between the coverslip and the counting chamber fully without air bubbles or entering the side grooves. Cells in four quadrants were counted under microscope of 10x 10 times magnification. Deep stained cells were dead and could not be counted. Cells were counted at the lower left if they were on the grids. The clustered cells should be counted separately. The following formulas could be used for calculation.

Total cell number in cell suspension = (total cell number by counting ÷ 4 quadrants) x 1.25 dilution factor x 10^4 x volume of re-suspended medium

Volume required = (cell number required ÷ total cell number in cell suspension) x volume of re-suspended medium

2.2.2.6 Cell cryopreservation

The required volume of mixture (90% FBS or RHB-A and 10% DMSO) for cell cryopreservation should be calculated before operation according to the pellet size. The cell pellet was re-suspended by the calculated mixture, and the cell suspension was pipetted into the labeled cryopreservation tubes. The cryopreservation tubes with cells should be placed into the freezing container and transferred to the -80℃ refrigerator as soon as possible. After 24 hours, they were transferred into the nitrogen liquid for long time storage.

2.3 Hypoxia induction experiment

Hypoxia induction was optimized by testing different methods which included vacuum, gassing with 95% nitrogen or various combinations. More details please refer to 3.1.

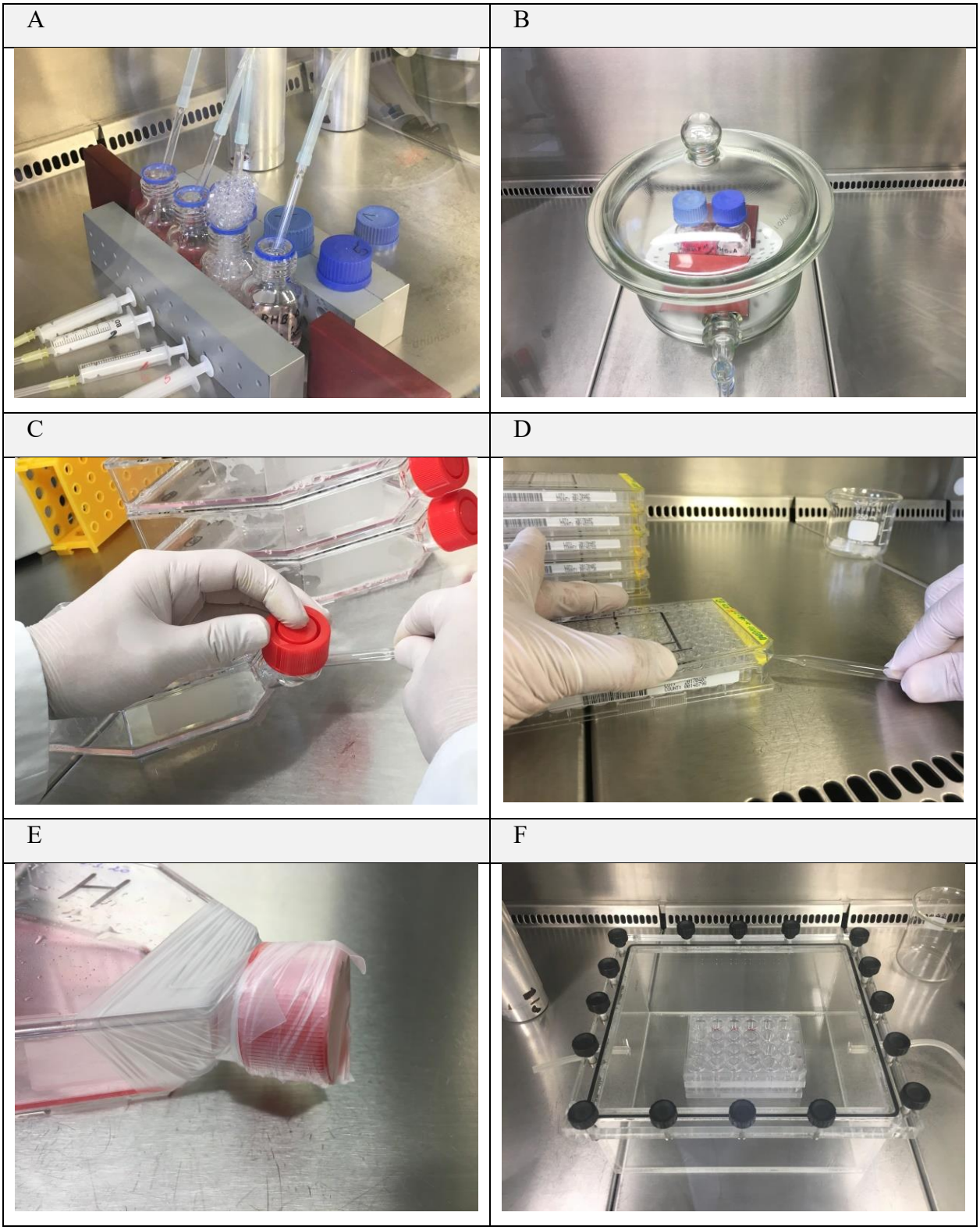

Figure 2.2 Photos of hypoxia induction process

(A) Gassing up to and into the medium of Duran bottles (B) Hypoxic medium preparation in vacuum desiccator (C) Gassing up to medium of culture flasks (D) Gassing up to medium in 96-well culture plates

(E) Wrap the culture flasks with parafilm after hypoxia induction (F) Gassing 24-well culture plates in pre-gassed sealed box.

The biological safety cabinet was switched off, and the inner surfaces of vacuum desiccator and sealed box were sterilized before hypoxia induction. In the process of hypoxic medium preparation under vacuum, rim of vacuum desiccator was greased for better sealing. Caps of Duran bottles were unscrewed to exhaust oxygen under vacuum. After the connection of extension tube and closing the lid and opening the tap of the desiccator, the vacuum pump was turned on. The stopcock of the tap was closed and the vacuum pump was turned off 20 minutes later. The vacuum state in desiccator would be lasted for 3 hours. Later, the desiccator was gassed with nitrogen and the stopcock of tap was opened very slowly to avoid the damage by quick pressure release. After removing the lid of desiccator, the caps of Duran bottles were closed quickly and tightly for the subsequent use.

Based on previous experiences in this laboratory, we took 5 minutes and 20 minutes for the hypoxic medium preparation by gassing culture flasks and Duran bottles, respectively. After hypoxia induction, the culture flasks were closed tightly and wrapped by parafilm followed by sustained 24 hours hypoxia in incubator. The medium gassed with nitrogen in Duran bottle was only used for hypoxic medium preparation. Later, the hypoxic medium would be transferred to culture wares.

In the process of hypoxia induction of medium in 24- and 96- well culture plates, the culture plates and the sealed box were gassed simultaneously for 5 minutes, and then the gassed culture plates were placed into the pre-gassed sealed box. After closing the sealed box tightly, 20 minutes gassing should be performed. Finally, the sealed box with culture plates was placed in incubator for sustained 24 hours hypoxia. Medium should be kept warm before the oxygen measurement with blood gas analyzer.

2.4 Scraper-Accutase/Trypsin comparative experiment

All cell lines were cultured for 3 days without medium change before harvest in Scraper-Accutase/Trypsin comparative experiment. Different cell numbers for seeding were tested in pre-experiments to avoid high cell confluence because of different growth rate between cell lines. The cell culture process was described in 2.2.2.2 and 2.2.2.3. The processes of two cell

harvesting methods were described in 2.2.2.4. Cells were counted according to 2.2.2.5 at harvest time. Measurement methods of total RNA yield and *CAIX* mRNA expression were described in 2.7. Measurement methods of total protein yield and CAIX protein expression were described in 2.8.1.

2.5 Low confluence experiment

The whole process of low confluence experiment was described in 2.2.2. To avoid high cell confluence and ensure sufficient final yield for further experiments, 3 identical culture flasks were seeded of each cell line. For eliminating the possible effect of high cell confluence and post-translational stability of proteins on the expression of CAIX, cell subculture was controlled at low-medium confluence (less than 70%) for 2 weeks before seeding. All cell lines were cultured for 3 days without medium change before harvest. Cell confluence was also controlled as low as 30-40% at harvest time. Methods of *CAIX* mRNA expression were described in 2.7. Methods of CAIX protein expression were described in 2.8.1.

2.6 Wortmannin inhibition experiment

The operator and working area should be protected, and the disposal of waste should also be careful because of the toxic Wortmannin. Cells were counted and seeded in labeled T75 culture flasks. Because the growth rates were different between cell lines, 1 million cells of U87/U251/BTIC12/BTIC13 and 1.5million cells of BTIC17/BTIC18 were seeded per culture flask. 6 hours later, cells were refreshed with 10ml medium or treated with 9,800µl medium and 200µl 1mM Wortmannin (final concentration 20µmol) per culture flask. Two conditions of U87 and U251 were cultured without FBS and they were washed with 3ml PBS before medium change. Cells were harvested after 17 hours treatment and incubation for the subsequent detection of mRNA and protein expression by PCR, qPCR and WB.

2.7 Transcriptional level experiments

2.7.1 Total RNA extraction and purification

All operations should be on ice especially before cell lysis and after RNA elution to prevent the degradation of RNA by RNase. The experimental workstation and all the items for use should be

dedicated and cleaned by RNase ZAP® before operation. Samples should not be vortexed in the whole process. The reagents for use were calculated and pipetted according to the protocol of manufacturer and the size of pellets.

Name of mixture	Composition and ratio
RLT cell lysis buffer mixture	RLT Lysis buffer 1000µl: 2-Mercapto-Ethanol 10µl
DNase I mixture	DNase I stock solution 10µl: Buffer RDD 70µl
RPE wash buffer mixture	RPE wash buffer 55ml +99.9%ethanol 220ml=275ml or RPE wash buffer 65ml +99.9%ethanol 260ml=325ml

Table 2.6 Composition and ratio of reagent mixture for total RNA extraction and purification

Cell pellet was taken out from -80℃ refrigerator and thawed. Excess PBS was removed by pipette carefully after centrifugation 5 minutes at 1200rpm under 4℃. The cell pellet was loosened thoroughly by flicking the tube.

During the process of cell lysis and RNA binding with silicone membrane in spin column, 350µl or 600µl RLT cell lysis buffer mixture was pipetted to each cell pellet in the first place. A needle was fixed to a 1ml RNase-free syringe and each pellet was homogenized 5 times. 70% ethanol 350µl or 600µl was added to each specimen and pipetted repeatedly. All cell lysates were transferred into RNeasy mini spin columns which were placed in 2ml collection tubes. The leaked liquid was discarded after centrifugation 15 seconds at 8000g.

To free the RNA from other impurities, 350µl RW1 wash buffer was pipetted to each spin column and the leaked liquid was discarded after centrifugation 15 seconds at 8000g. 80µl DNase I mixture was pipetted to each spin column and incubated 15 minutes at room temperature. 350µl RW1 wash buffer was pipetted to each spin column again and the leaked liquid was discarded after centrifugation 15 seconds at 8000g. 500µl RPE wash buffer mixture was pipetted to each spin column and the leaked liquid was discarded after centrifugation 15 seconds at 8000g. 500µl RPE wash buffer mixture was pipetted to each spin column again and the leaked liquid was discarded after centrifugation 2 minutes at 8000g. 2ml collection tubes were replaced with new tubes for spin columns. They were centrifuged 1 minute at full speed of 20800g to dry the spin column membrane and to remove the RPE carryover.

At last, 30µl RNase-free water was pipetted to each spin column. It was centrifuged 1 minute at 8000g and the RNA sample was collected into 1.5ml collection tube with labeled information.

The spin column membrane was re-eluted by the eluate of last step and centrifuged 1 minute at 8000g to increase the yield. RNA samples were stored in the -80℃ refrigerator after concentration measurement.

2.7.2 Determination of total RNA concentration

1:50 diluted RNA solution (RNA sample 2µl: DEPC water 98µl) of each sample was pipetted into a precision cuvette for the photometry measurement and the blank reference was set with DEPC water. The operation process was according to the manufacturer's protocol. Air bubbles should not be in the cuvette during measurement. The cuvette was rinsed twice with 100µl Milli-Q water after each measurement. The ratio of A260/A280 should between 1.9 and 2.1 which represented the high-quality purified RNA.

2.7.3 Reverse transcription (RT)

All the operations for reverse transcription should be on ice and in dedicated experimental workstation. According to the RNA concentration measured, the required volume of 1 µg RNA and compensated RNase-free water were calculated and pipetted to a total volume of 10µl per sample. RNA samples should not be vortexed. 10µl RNase-free H_2O was pipetted as cDNA negative control. 3 reagent mixture were calculated and pipetted according to the number of samples and manufacturer's protocol. Vortex and brief centrifugation were required after all reagents were mixed.

Sample+2		Reagent			Reagent			
	x1µl	dNTP-Mix		x1µl	Random Primer		2µl/sample	①
	x4µl	5x First Strand Buffer		x2µl	0.1M DTT		6µl/sample	②
	x1µl	SuperScriptII RT		x1µl	RNase-free H_2O		2µl/sample	③

Table 2.7 Volume calculation of reagent mixture for reverse transcription

After the preparation above, 2µl mixture ① was pipetted and mixed with each 10µl RNA sample solution in RNase free PCR soft tube. They were placed in the VWR Thermo cycler and the program was started. All the sample mixture were heated 5 minutes at 65℃ for denaturation. Later, they were cooled 1 minute at 4℃ to anneal the random primers with template RNA. 6µl

mixture ② was pipetted up and down into each PCR tube. The temperature was increased to 25℃ for 2 minutes. 2µl mixture ③ was pipetted up and down into each PCR tube. After a further 10 minutes at 25℃, the reverse transcription reaction was started at 42℃ for 50 minutes. The reaction could be terminated by inactivating the reverse transcriptase at 70℃ for 15 minutes. All sample reaction mixture were kept at 4℃. Finally, all 20µl cDNA sample solutions and negative control were diluted with 80µl RNase-free H_2O, aliquoted and stored at -20℃.

2.7.4 Polymerase chain reaction (PCR)

Name	Product length	Direction	Primer sequence
CAIX	252bp	forward	5'-CCG AGC GAC GCA GCC TTT GA-3'
		reverse	5'-GGC TCC AGT CTC GGC TAC CT-3'
VEGF isoform 165	224bp	forward	5'-ATC TTC AAG CCA TCC TGT GTG C -3'
		reverse	5'-CAA GGC CCA CAG GGA TTT TC -3'
VEGF isoform 121	118bp	forward	5'-ATA GAG CAA GAC AAG AAA AAT G -3'
		reverse	5'-ATC GTT CTG TAT CAG TCT TTC CT -3'
GAPDH	318bp	forward	5'-GGT CGG TGT GAA CGG ATT TG-3'
		reverse	5'-GTG AGC CCC AGC CTT CTC CAT-3'
RPL13A (ribosomal protein L13)	157bp	forward	5'-CAT AGG AAG CTG GGA GCA AG-3'
		reverse	5'-GCC CTC CAA TCA GTC TTC TG-3'

Table 2.8 Primers information for PCR

The whole process of preparation for PCR should be on ice and in dedicated experimental workstation. All the reagents should be mixed well before use to avoid localized different concentration. A certain volume of RNase-free H_2O was pipetted into the primer vial according to the manufacturer's protocol (final concentration: 100pmol/µl) for the preparation of primer stock solution. The primer stock solution was further diluted to 1:10 work solution by RNase-free H_2O for PCR reaction. After thawing, the reagent mixture was calculated and pipetted according to the number of samples and manufacturer's protocol.

Sample+2		Reagent
	x12.5µl	Taq PCR Master Mix
	x1.0µl	Primer forward
	x1.0µl	Primer reverse
	x9.5µl	RNase-free H_2O（Kit）

Table 2.9 Volume calculation of reagent mixture for PCR (total volume: 24µl /sample)

24µl reagent mixture was pipetted and mixed with each 1.0µl cDNA sample and control solution into RNase free PCR soft tube, respectively. A negative primer control (without template cDNA) should be included in every experiment. After all the RNase free PCR soft tubes were vortexed and briefly centrifuged, they were placed into the VWR thermal cycler. The reaction procedures were started according to the programs shown in the table below. Finally, 25µl specific DNA samples and control were stored in a 4°C refrigerator.

Primer name	Initial denaturation	Cycles	Denaturation	Annealing	Extension	Final elongation	Storage
CAIX	94°C 5min	30	94°C 30sec	66°C 1min	72°C 2min	72°C 8min	10°C Infinite
VEGF isoform 165	94°C 5min	35	94°C 30sec	59.7°C 30sec	72°C 2min	72°C 8min	10°C Infinite
VEGF isoform 121	94°C 5min	35	94°C 30sec	51.7°C 30sec	72°C 2min	72°C 8min	10°C Infinite
GAPDH	95°C 5min	33	94°C 45sec	57°C 45sec	72°C 45sec	72°C 8min	10°C Infinite

Table 2.10 Thermo cycler reaction programs for PCR of different primer pairs

2.7.5 Agarose gel electrophoresis

The 10x and 1x TBE buffer were prepared before the experiment started. The gel carrier was placed horizontally and 1-2 combs were inserted to create wells for loading samples. Appropriate volume of 1x TBE buffer was added into the electrophoresis chamber. 2g agarose powder and 100ml 1x TBE buffer were prepared into a glass conical flask. The mixture was heated in the

microwave until the powder was dissolved completely. 1% Ethidium Bromide solution 5μl was pipetted into agarose gel solution and mixed well. After cooling, the liquid gel was filled into the gel carrier. Bubbles were removed by tips. The gel should be protected from light during polymerizing for 20-30 minutes. Combs were removed carefully, and the gel carrier was aligned in the right current direction. More 1x TBE buffer was added to the FILL LINE of electrophoresis chamber to make sure that the gel was completely submerged during electrophoresis.

All samples, loading buffer, DNA ladder solution should be vortexed and briefly centrifuged before use. 6x loading buffer 2μl was pipetted and mixed with each 10μl specific DNA sample or control solution into 0.5ml tubes. 5μl DNA ladder solution and all the sample mixture were carefully loaded into the bottom of wells. Electrophoresis was carried out at 100V for 60 minutes. The DNA molecules could be visualized as clear bands under 230nm ultraviolet in transilluminator. After adjustment, related information was printed and marked. The remaining samples should be stored at 4℃ to repeat if necessary.

2.7.6 Quantitative real-time PCR (qPCR)

It was important to protect from light, operate on ice and in dedicated experimental workstation in the whole preparation process of qPCR. All reagent mixture should be vortexed and briefly centrifuged before use.

	CAIX (calibrators)		*RPL13A* (calibrators)		*CAIX* (samples)				*RPL13A* (samples)			
	1	2	3	4	5	6	7	8	9	10	11	12
A	pool	pool	pool	pool	1	2	13	14	25	26	37	38
B	1:3	1:3	1:3	1:3	3	4	15	16	27	28	39	40
C	1:9	1:9	1:9	1:9	5	6	17	18	29	30	41	42
D	1:27	1:27	1:27	1:27	7	8	19	20	31	32	43	44
E	1:81	1:81	1:81	1:81	9	10	21	22	33	34	45	46
F	1:243	1:243	1:243	1:243	11	12	23	24	35	36	47	48
G	NTC	NTC	NTC	NTC								
H												

Table 2.11 Layout of qPCR (e.g., 12 samples)

(NTC: no template control)

A certain volume of all cDNA sample solutions was calculated and pipetted into a calibrator pool according to the number of samples (e.g., 3µl/sample for 12 samples). The pool was diluted 5 times gradually by ratio 1:3 for the creation of standard curve. Reagent mixture was calculated and pipetted according to the layout and manufacturer's protocol.

Number of wells+4		Reagent
	x10µl	SYBR Green Master Mix
	x0.5µl	Primer forward
	x0.5µl	Primer reverse
	x5.0µl	RNase-free H_2O

Table 2.12 Volume calculation of reagent mixture for qPCR (total volume: 16µl /sample)

16µl reagent mixture of different primers (target gene and reference gene) was pipetted and mixed with each 4.0µl cDNA sample or calibrator solution into PCR 96-well plate respectively according to the layout. After being sealed by film, the PCR 96-well plate was centrifuged 1 minute at 2500 rpm at room temperature. The 96-well PCR plate was placed in the Thermo cycler and the reaction procedures were started according to the programs shown in the table below. Data was set and exported after the end of reaction.

Primer name	Initial denaturation 95°C	Cycles	Denaturation 95°C	Annealing	Extension 72°C	Melting curve temperature 95°C
CAIX	3min	40	15sec	63°C 20sec	30sec	30sec
VEGF isoform 165	3min	40	15sec	58°C 30sec	30sec	30sec
VEGF isoform 121	3min	40	15sec	52°C 30sec	30sec	30sec

Table 2.13 Thermo cycler reaction programs for qPCR of different primer pairs

2.8 Translational level experiments

2.8.1 Western blot (WB)

2.8.1.1 Total protein extraction (RIPA cell lysate method)

All the operations should be on ice and in dedicated experimental workstation for both protein lysis and concentration measurement. All reagent mixture should be vortexed and briefly centrifuged before use.

Before starting, the RIPA buffer which included 10ml 10x PBS, 1.0ml Nonidet P-40, 0.5ml 20% SDS, 500mg sodium deoxycholic acid was prepared and diluted with Milli Q H_2O to 100ml stock solution. 1:10 solution of RIPA buffer was also required. The required total volume of RIPA buffer with protease inhibitor mixture (100-200µl/sample) was calculated according to the number and size of pellets. The required volume of each component in the mixture should be calculated and pipetted by ratio (1:500 AEBSF and 1:25 25x protease inhibitor cocktail).

After all frozen cell pellets thawed, they were centrifuged at 1200rpm for 5 minutes under 4℃. The excess PBS was removed by pipette carefully. The cell pellets were loosened thoroughly by flicking the tube. 100-200µl RIPA buffer with protease inhibitor mixture was pipetted to each cell pellet in 15ml centrifuge tube. Cell pellets were lysed and disassociated by pipetting repeatedly until transparent and transferred into 1.5ml micro tubes. Later, cell lysates were incubated on horizontal shaker 15 minutes at speed 4 and centrifuged 15 minutes at 13,000rpm under 4℃. The supernatant that contained the extracted total protein was carefully transferred into new 1.5ml micro tubes.

The lysis buffer including protease inhibitors for protein extraction to analyze pAkt expression in Western blot was different compared to the analysis strategy for the unphosphorylated proteins.

2.8.1.2 Determination of total protein concentration (Bradford dye-binding method)

A calibration curve was required to convert the measured values of samples into the corresponding protein concentrations. Standard protein solutions could be achieved by the 1:2 serial dilution of 2000µg/ml BSA solution. The 2000µg/ml BSA solution was prepared by 150 times dilution of 30% BSA. 1:10 protein solution 25µl of each sample was calculated and pipetted. Both sample and standard protein solutions were diluted with 1:10 RIPA buffer.

Reagent A and S were calculated and pipetted by ratio 50:1 according to the total number of wells for measurement. 17.5µl reagent A+S mixture, 10µl standard protein solution, sample protein solution or Milli Q H_2O as blank, 140µl reagent B were pipetted into each well in sequence according to the layout. After the incubation on horizontal shaker 10 minutes at speed 3, the photometry of each sample was measured at 650 nm by VARIOSKAN. If the sample protein concentration was too high that exceeded the range of measurement, 1:20 dilution of sample protein solutions was required. The remaining protein samples should be aliquoted and stored at -80 ℃.

	1	2	3	4	5	6	7	8	9	10	11	12
A	2000	2000	0	0	1:10	1:10	1:20	1:20				
B	1000	1000	undiluted	undiluted	1:10	1:10	1:20	1:20				
C	500	500	undiluted	undiluted	1:10	1:10	1:20	1:20				
D	250	250	undiluted	undiluted	1:10	1:10	1:20	1:20				
E	125	125	undiluted	undiluted	1:10	1:10	1:20	1:20				
F	62.5	62.5	undiluted	undiluted	1:10	1:10	1:20	1:20				
G	31.25	31.25	undiluted	undiluted	1:10	1:10	2000	2000				
H	15.625	15.625	undiluted	undiluted	1:20	1:20	15.625	15.625				

Table 2.14 Layout of protein concentration measurement

2.8.1.3 SDS-PAGE (polyacrylamide gel electrophoresis) gel preparation

After the glass plates and sealing rubbers were cleaned and fixed, the system should be checked for leakage. 1cm under the comb teeth was marked as border of stacking gel and separating gel. After the 12% separating gel solution was pipetted according to the manufacturer's protocol, the separating gel solution was vortexed and filled into the gap between the glass plates to the marker immediately. Milli-Q H_2O was added to obtain a smooth edge and waited for gelling. Milli-Q H_2O was removed and the gap was dried with absorbent paper. After the 5% stacking gel solution was pipetted according to the manufacturer's protocol, the stacking gel solution was vortexed and filled into the gap between the glass plates to full immediately. Combs were inserted to create wells for loading samples and waited for gelling.

2.8.1.4 Loading samples, electrophoresis, blotting and Ponceau S staining

The electrophoresis chamber and its cooling system were prepared during gelling. All reagents were vortexed and briefly centrifuged before use. The required volume of 20µg per sample was calculated and prepared. Equal volume of 5x RSB was pipetted and mixed with each sample. 7µl marker solution was mixed with 13µl 5x RSB. After heating 5 minutes in boiled deionized water, all samples were placed on ice. Combs were taken out carefully, leftovers of gel and bubbles in the wells were removed with Milli-Q H_2O. The columns of gel had to be straight between wells. The sealing rubbers were removed and the glass plates with solidified gel were fixed to the electrophoresis chamber. 1x SDS running buffer was filled to the standard line. After a brief centrifugation, marker and samples were loaded with long tips. 10µl 2x RSB was pipetted into each of the remained wells.

Electrophoresis was started at 120V and the samples ran into the separating gel. The voltage was increased to 160V for protein separation. The voltage and electrophoresis time were adjusted according to actual condition. Electrophoresis was stopped when the blue strip ran to the bottom of the separating gel.

1 sheet of nitrocellulose membrane and 2x 5 sheets of blotting paper per gel were prepared according to the area of gel. They got wet with transfer buffer and placed in a tray. It was important to mark the nitrocellulose membranes for the front gel and back gel. The glass plates were detached carefully from each other by a spatula. The front gel and back gel were cut with scalpel and placed up to the nitrocellulose membranes. They were caught in the middle of 2x 5 sheets of blotting paper like sandwich. Care should be taken for the correct placement, current direction and no bubbles between them. They were placed to the blot chamber and pressurized by 1 kg liquid for a better connection. The current intensity was calculated according to the formula [current intensity (mA) = length (cm) x width (cm) x 2 gels x 0.8 coefficient] and transferred for 75 minutes.

Later, the membranes were stained with Ponceau S to ensure the successful blotting. Care should be taken that the side with protein of nitrocellulose membrane should face up. After development and record, Ponceau S was rinsed away by deionized water.

2.8.1.5 Blocking, primary and secondary antibodies incubation, development, stripping and storage

	Name and isoform of antibody	Order and lot number	Host and clonality	Molecular weight	Dilution ratio	Dilution buffer
Primary antibody	CAIX	NB100-417 Z1/Z3	Rabbit polyclonal antibody	55kDa	1:1,000	PBS-T or TBS-T
	pAkt S473	AF887 DZE13	Rabbit polyclonal antibody	65kDa	1:1,000	PBS-T
	GAPDH 0411	sc-47724 K1218	Mouse monoclonal antibody	37kDa	1:5,000	PBS-T
	β-actin	A 2066 061M4871	Rabbit	42kDa	1:5,000	PBS-T
Secondary antibody	Donkey anti mouse IgG HRP	AP192P 22040551			1:10,000	PBS-T or TBS-T
	Donkey anti goat IgG HRP	705-035-1 47 70689			1:5,000	PBS-T or TBS-T
	Goat anti Rabbit IgG HRP	ALI4404 3101			1:10,000	PBS-T
	m-IgGk BP-HRP	sc-516102 K1418			1:10,000	PBS-T

Table 2.15 Antibody information for Western blot

The nitrocellulose membranes were washed with PBS-T until colorless. They were incubated in 3% milk/PBS-T solution to block the non-specific binding on shaker 30 minutes at appropriate power.

The aliquot of primary antibody solution was briefly centrifuged before use. Primary antibody solution in PBS-T was calculated and pipetted at proper volume and dilution ratio. After the nitrocellulose membranes were placed in diluted primary antibody solution and sealed in plastic foil, they were shaken overnight for the incubation with appropriate power at 4°C.

In the next day morning, membranes were washed 3 times x 10 minutes with appropriate volume of PBS-T. The aliquot of secondary antibody solution was briefly centrifuged before use. Secondary antibody solution in PBS-T was calculated and pipetted at proper volume and dilution ratio. The membranes were placed in diluted secondary antibody solution and shaken 1 or 2 hours for the incubation with appropriate power at room temperature.

Membranes were washed 3 times x 10 minutes by PBS-T again. The chemiluminescent substrate (stable Peroxide Solution 4ml and Luminol/Enhancer Solution 4ml) was pipetted to membranes followed by 3 minutes incubation for the detection of HRP. Membranes were developed by using the X-ray films at appropriate time in darkroom. Information was marked on the films.

After washing membranes by PBS-T for 10 minutes, the bound specific antibodies were removed by stripping buffer for 10 minutes. The procedures above were also suitable for the detection of other proteins (e.g., GAPDH, β-actin). Finally, the membranes were sealed and stored with PBS-T in plastic foil.

It was worth to note that some antibodies were diluted by TBS-T.

A special blotting buffer to block, wash and dilute the antibody for pAkt in Western blot was important to use.

2.8.2 Cell immunofluorescence staining

Cover glasses were placed in 1M HCl solution overnight at 65℃ for the rough surface of cell adherence. In the next day morning, cover glasses were washed 3-4 times by Milli-Q H_2O and stored in 70% ethanol at room temperature for the subsequent use.

On the first day for cell culture, the dry cover glasses were placed on the bottoms of the wells first. Cells were counted and seeded (10,000cells/1ml/well) according to the layout and incubated 24 hours under normoxia for cell adherence.

On the second day, all cell lines were refreshed by 1000µl medium. On the third day, all cell lines were refreshed by 1000µl medium again and hypoxia induction was performed. Care should be taken for BTIC18 because of semi-adherent growth in most of the time and DMEM without FBS for established cell lines during medium change. Hypoxia was stopped after 24 hours. Cells were fixed with 300µl 4% PFA for 10 minutes and washed 3 times with 500µl PBS in each well of all 24-well plates at room temperature. 1000µl PBS was pipetted into each well, all 24-well plates were sealed with parafilm and stored at 4℃ until staining.

In the staining process of CAIX, all 24-well plates were taken out from 4℃ refrigerator and unsealed. All the wells were washed 1 time with 500µl PBS for 5 minutes on shaker slowly. The blocking solution for each plate was calculated and pipetted according to the following formula.

300µl x 24wells x 4times（block+ primary antibody+ secondary antibody+ FITC）

=28800µl→30ml (required)

Normal donkey serum was calculated (final 3%) and pipetted in blocking solution. 300µl blocking solution was pipetted into each well to block non-specific binding for 30 minutes.

U87	U251	BTIC12	BTIC13	BTIC17	BTIC18
CAIX	CAIX	CAIX	CAIX	CAIX	CAIX
CAIX	CAIX	CAIX	CAIX	CAIX	CAIX
IgG	IgG	IgG	IgG	IgG	IgG
IgG	IgG	IgG	IgG	IgG	IgG

Table 2.16 Layout of cell immunofluorescence staining on CAIX expression under normoxia or hypoxia

Primary antibody			Secondary antibody		
Antibody	Dilution ratio	Incubation time	Antibody	Dilution ratio	Incubation time
Polyclonal rabbit anti CAIX	1 :1000	overnight	Donkey anti rabbit Biotin	1 :300	2h
Rabbit IgG	1:500	overnight			

Table 2.17 Antibody information for cell immunofluorescence staining

Primary antibody solution was calculated and pipetted in blocking solution. Cells were incubated with primary antibody overnight at 4℃. Secondary antibody solution was calculated and pipetted in blocking solution. Cells were incubated with secondary antibody 2 hours at room temperature. 1:300 Streptavidin-FITC was calculated and pipetted in blocking solution. Cells were incubated with streptavidin-FITC 2 hours at room temperature. After each incubation, cells were washed 3 times with 500µl PBS on shaker for 10 minutes very slowly. A small drop of PVA-DABCO was pipetted onto the labeled microscope slides. The cover glasses were carefully inverted and fixed at the right positions of microscope slides. Microscope slides should be protected from light

when they were stored and dried overnight at room temperature. Long-term storage should be at 4°C. Finally, cells were observed and photographed of immunofluorescence at maximum excitation of 495-500 nm under microscope.

2.9 Cell viability experiments

2.9.1 Crystal violet assay

	1	2	3	4	5	6	7	8	9	10	11	12
A		Untreated	U104 10μM	U104 80μM	U104 180μM	DMSO 10μM	DMSO 80μM	DMSO 180μM				
B		Repeat 1	Repeat 1	Repeat 1	Repeat 1	Repeat 1	Repeat 1	Repeat 1				
C		Repeat 2	Repeat 2	Repeat 2	Repeat 2	Repeat 2	Repeat 2	Repeat 2				
D		Repeat 3	Repeat 3	Repeat 3	Repeat 3	Repeat 3	Repeat 3	Repeat 3				
E		Repeat 4	Repeat 4	Repeat 4	Repeat 4	Repeat 4	Repeat 4	Repeat 4				
F		Repeat 5	Repeat 5	Repeat 5	Repeat 5	Repeat 5	Repeat 5	Repeat 5				
G		Medium	Medium	Medium	Medium	Medium	Medium	Medium				
H												

Table 2.18 Layout of 96-well plate for one cell line (7500cells/100μl/well)

	1	2	3	4	5	6	7	8	9	10	11	12
A		Untreated	U104 40μM	U104 60μM	DMSO 40μM	DMSO 60μM	Untreated	U104 40μM	U104 60μM	DMSO 40μM	DMSO 60μM	
B		Repeat 1	Repeat 1	Repeat 1	Repeat 1	Repeat 1	Repeat 1	Repeat 1	Repeat 1	Repeat 1	Repeat 1	
C		Repeat 2	Repeat 2	Repeat 2	Repeat 2	Repeat 2	Repeat 2	Repeat 2	Repeat 2	Repeat 2	Repeat 2	
D		Repeat 3	Repeat 3	Repeat 3	Repeat 3	Repeat 3	Repeat 3	Repeat 3	Repeat 3	Repeat 3	Repeat 3	
E		Repeat 4	Repeat 4	Repeat 4	Repeat 4	Repeat 4	Repeat 4	Repeat 4	Repeat 4	Repeat 4	Repeat 4	
F		Repeat 5	Repeat 5	Repeat 5	Repeat 5	Repeat 5	Repeat 5	Repeat 5	Repeat 5	Repeat 5	Repeat 5	
G		Medium	Medium	Medium	Medium	Medium	Medium	Medium	Medium	Medium	Medium	
H												

Table 2.19 Layout of 96-well plate for two cell lines (7500cells/100μl/well)

Five repeats of same experimental condition were performed in crystal violet assay. In the

process of cell culture in 96-well plates for crystal violet assay, cells were counted and seeded according to the layout on the first day. Cells were washed with 100µl PBS (only for established cell lines) and refreshed with 100µl medium in each well on the second day. On the third day, old medium was removed, and cells were treated with different concentration of U104 and DMSO in 100µl fresh medium according to the layout followed by hypoxia induction. Hypoxia was stopped after 24 hours, and all cells were continuously cultured until staining. The medium used in established cell lines did not contain FBS.

During staining, it should be aware of the protection against toxic crystal violet solution. These included the protection of working area and operator and the disposal of waste. 96-well plates were taken out from incubator at specific time points. The specific time points of day 2, day 4 and day 6 started from hypoxia induction. 96-well plate was inverted and patted to discard old medium. 50µl 0.5% crystal violet solution was added into each well by repetitive pipette followed by 10 minutes incubation. 96-well plate was again inverted and patted to discard crystal violet solution, and then it was rinsed in deionized water 5 times in 2 directions. Many cells of BTIC18 were lost during wash step which led to instable and unreliable results, so one more time of ATP assay was performed. All the 96-well plates would be dried for 24 hours at room temperature before measurement.

During measurement, 50µl 0.1M sodium acetate solution was pipetted into each well by repetitive pipette and measured by VARIOSKAN FLASH.

2.9.2 ATP (adenosine triphosphate) assay

ATP assay was performed the same way with crystal violet assay in the layout of 96-well plate and the process of cell counting, seeding, treatment, hypoxia induction and specific time points for ATP measurement. 100µl ATP reagent mixture was added into each well by repetitive pipette. Cells were incubated 12 minutes on orbital shaker at speed 3 for cell lysis and the stable of luminescence signal. 150µl cell lysate from each well was pipetted by 8-channel liner pipette into a white microplate with the same layout. Finally, luminescence of lysate was measured by VARIOSKAN FLASH.

2.10 Invasion assay

One day before operation, Matrigel was transferred from -80°C to 4°C overnight for melting. All

items in contact with Matrigel in operation also should be cooled down at 4℃ overnight. All operations were performed on wet ice and in biological safety cabinet during the preparation process of Matrigel onto the membrane of Transwell inserts to avoid early gelling.

Sixteen repeats of same experimental condition were performed in invasion assay. Cell culture inserts were placed into the notched companion plates by sterile forceps first. 10mg/ml Matrigel solution of appropriate volume was prepared according to the layout and dilution factor. 50µl Matrigel solution was pipetted to the middle of membrane of each insert without damage. Bubbles should be punctured if necessary. All the plates were incubated 2 hours at 37℃ for gelling.

Medium with BSA (final 0.33%) was prepared according to actual needs. The medium used in established cell lines did not contain FBS. After cell count, required volume of cell suspension was pipetted into each labeled tube followed by centrifugation. Cells were washed by RHB-A medium 1 time or DMEM without FBS 2 times. Cell pellets were re-suspended by medium with BSA into desired densities of different cell lines. In option 1, U104 and DMSO were calculated and pipetted into cell suspension for treatment, and then 200µl cell suspension of different treatments was pipetted into each insert according to the layout. In option 2, 100µl cell suspension was pipetted into each insert first. After 4 hours incubation, 100µl medium with BSA and U104/DMSO was pipetted into corresponding insert according to the layout. The final densities of cells and concentrations of U104/DMSO were the same with option 1. Bubbles should be punctured if necessary and needles should be changed to avoid cross contamination.

After calculation, 600µl medium of different treatments was pipetted into each lower compartment according to the layout. No air bubbles were under the membrane of insert. The final concentrations of U104/DMSO in medium with BSA were the same in both upper and lower compartments. Started from Exp.2, chemo-attractant was investigated for the influence of cell invasion.

Hypoxia induction was performed after U104/DMSO treatment. Hypoxia was stopped after 24 hours, and cells of all conditions were continuously incubated for another 24 hours under normoxia.

At 48 hours, 500µl fix solution, 500µl reagent 1, 500µl reagent 2 were pipetted for staining, and 1000µl tap water was pipetted for washing in each well of a new 24-well plate. Matrigel with non-invasive cells was carefully removed by cotton swabs in one direction 2 times. Inserts were

placed into each dye and tap water one by one for 1 minute. After staining, inserts were placed in new notched companion plates with the same layout followed by drying more than 24 hours at room temperature. Finally, invaded cells were observed under microscope and blindly counted by Olympus cellsens Dimension software. Cells with clear morphology, pores deep stained, traces of cell morphology around the pore were all considered as invaded cells.

2.11 Ethical conduct of research

Our research was approved by the University of Regensburg Ethics Committee, Regensburg, Germany (No. 11-103-0182) and conducted in accordance with the ethical standards of the Helsinki Declaration. Patient's written consent was obtained whenever possible. All research results were stored and analyzed in an anonymous fashion.

2.12 Statistical analysis, imaging processing and graphical illustrations

SigmaPlot 13.0 was used for statistical analysis and graph making. Unpaired Student's t-test was used for the comparison between groups in Scraper-Accutase/Trypsin comparative experiment, Low confluence experiment, Wortmannin inhibition experiment, Normoxia and hypoxia comparative experiment, as well as DMSO and untreated groups in cell viability experiment. 2-way ANOVA (analysis of variance) was used in statistical analysis of cell viability and invasion experiments. Adobe Photoshop CS6 and Adobe illustrator CC 2019 were also used for figure making. Olympus cellsens Dimension was used for invasive cell counting by regulating pixel and threshold in invasion assay.

3 Results

3.1 Hypoxia induction experiment

Many methods were tested for choosing the best way for inducing hypoxia which was an important feature of GBM and a vital experimental condition of this study. Oxygen of medium in culture vessels would be exhausted as much as possible by gassing nitrogen, vacuum or various combinations. Oxygen pressure was tested immediately after operation (first and second exp.) and after 24-hour sustained hypoxia (third exp.).

First experiment		
No.	Different methods of hypoxia induction	mmHg
1	Gassing in DMEM of bottle (20 minutes)	68.7
2	Gassing up to DMEM of bottle (20 minutes)	55.2
3	Gassing up to DMEM of T75 flask (5 minutes)	71.8
4	Gassing in RHB-A medium of bottle (20 minutes)	73.7
5	Gassing up to RHB-A medium of bottle (20 minutes)	129
6	Gassing up to RHB-A medium of T75 flask (5 minutes)	66.5
7	Preparing hypoxic DMEM of bottle in vacuum tank (3 hours 20 minutes)	149
8	After vacuum, gassing up to DMEM of bottle (3 hours 20 minutes+20 minutes)	62.8
9	After vacuum, transfer by pipette and gas up to DMEM of T75 flask (3 hours 20 minutes+5 minutes)	58.8
10	Preparing hypoxic RHB-A medium of bottle in vacuum tank (3 hours 20 minutes)	150
11	After vacuum, gassing up to RHB-A medium of bottle (3 hours 20 minutes+20 minutes)	61.6
12	After vacuum, transfer by pipette and gas up to RHB-A medium of T75 flask (3 hours 20 minutes+5 minutes)	105

Table 3.1 The first experiment results of different hypoxia induction methods

In the first experiment, data of No. 1/4 illustrated that gassing in the medium was effective for exhausting oxygen. However, this operation generated many bubbles (especially in RHB-A medium) which resulted in protein denaturation and the possibility of contamination. Data of No.

7/10 illustrated that vacuum alone did not reduce oxygen levels significantly and indicated indirectly that gassing played a key role of hypoxia induction. This could be proved again by the non-significant difference between No.2/3-5/6 group and No.8/9-11/12 group. Furthermore, hypoxic medium preparation in bottle by vacuum was complex and dangerous. Therefore, No.2/3-5/6 or in sequence were selected to test again in the next experiment.

Second experiment		
No.	Different methods of hypoxia induction	mmHg
A	DMEM as blank control	172
B(2)	Gassing up to DMEM of bottle (20 minutes)	85.4
C(3)	Gassing up to DMEM of T75 flask (5 minutes)	60.7
D(2→3)	After the preparation by gassing up to DMEM in bottle and concurrent with gassing the empty T75 flask, transfer by pipette and gas up to DMEM again in T75 flask (20 minutes+5 minutes)	55.2
E	RHB-A medium as blank control	177
F(5)	Gassing up to RHB-A medium of bottle (20 minutes)	115
G(6)	Gassing up to RHB-A medium of T75 flask (5 minutes)	68.9
H(5→6)	After the preparation by gassing up to RHB-A medium in bottle and concurrent with gassing the empty T75 flask, transfer by pipette and gas up to RHB-A medium again in T75 flask (20 minutes+5 minutes)	69.5

Table 3.2 The second experiment results of different hypoxia induction methods

In the second experiment, data of B(2)/F(5) showed the similar results with the first experiment that gassing up to medium in bottle reduced oxygen level, but the result was not stable. No significant difference could be seen by comparing 1-step with 2-step operations (C to D and G to H). This might be attributed to reoxygenation during pipetting. Thence one more step for preparing hypoxic medium in bottle did not play a major role and it was more complex. Data of C(3)/G(6) illustrated that gassing up to the medium surface in flask directly was effective and stable. This was also corresponded with last experiment.

Third experiment		
No.	Different methods of hypoxia induction and 24-hour sustained hypoxia	mmHg
C(3)	Gassing up to DMEM of T75 flask (5 minutes)	44.8
D(2→3)	After the preparation by gassing up to DMEM in bottle and concurrent with gassing the empty T75 flask, transfer by pipette and gas up to DMEM again in T75 flask (20 minutes+5 minutes)	58.3
G(6)	Gassing up to RHB-A medium of T75 flask (5 minutes)	46.1
H(5→6)	After the preparation by gassing up to RHB-A medium in bottle and concurrent with gassing the empty T75 flask, transfer by pipette and gas up to RHB-A medium again in T75 flask (20 minutes+5 minutes)	49.3

Table 3.3 The third experiment results of different hypoxia induction methods

In the third experiment, all data were collected from 24-hour sustained hypoxia after hypoxia induction. These results were nice and stable. Once again, no significant difference could be seen between 1-step and 2-step operations. After unit conversion, the final oxygen level of 24-hour sustained hypoxia was about 6%. The following experimental results also proved it was sufficient in the comparison of CAIX expression under normoxia and hypoxia.

In conclusion, gassing up to the medium in T75 flask directly was effective and stable. This method could be used for subsequent hypoxia experiments. Based on the analysis above, this method was also used for hypoxia induction in 24- and 96- well culture plates. They were not tested because the small amount medium in the well was not easily tested and easily re-oxygenated.

3.2 Scraper-Accutase/Trypsin comparative experiment

Both scraper and digestive enzyme (Accutase/Trypsin) methods have advantages and disadvantages for cell harvest. Cell lines used in this study had different growth characteristics (adherent and semi-adherent). Therefore, total and CAIX yield of RNA and protein would be tested by comparative experiment to confirm which method was better.

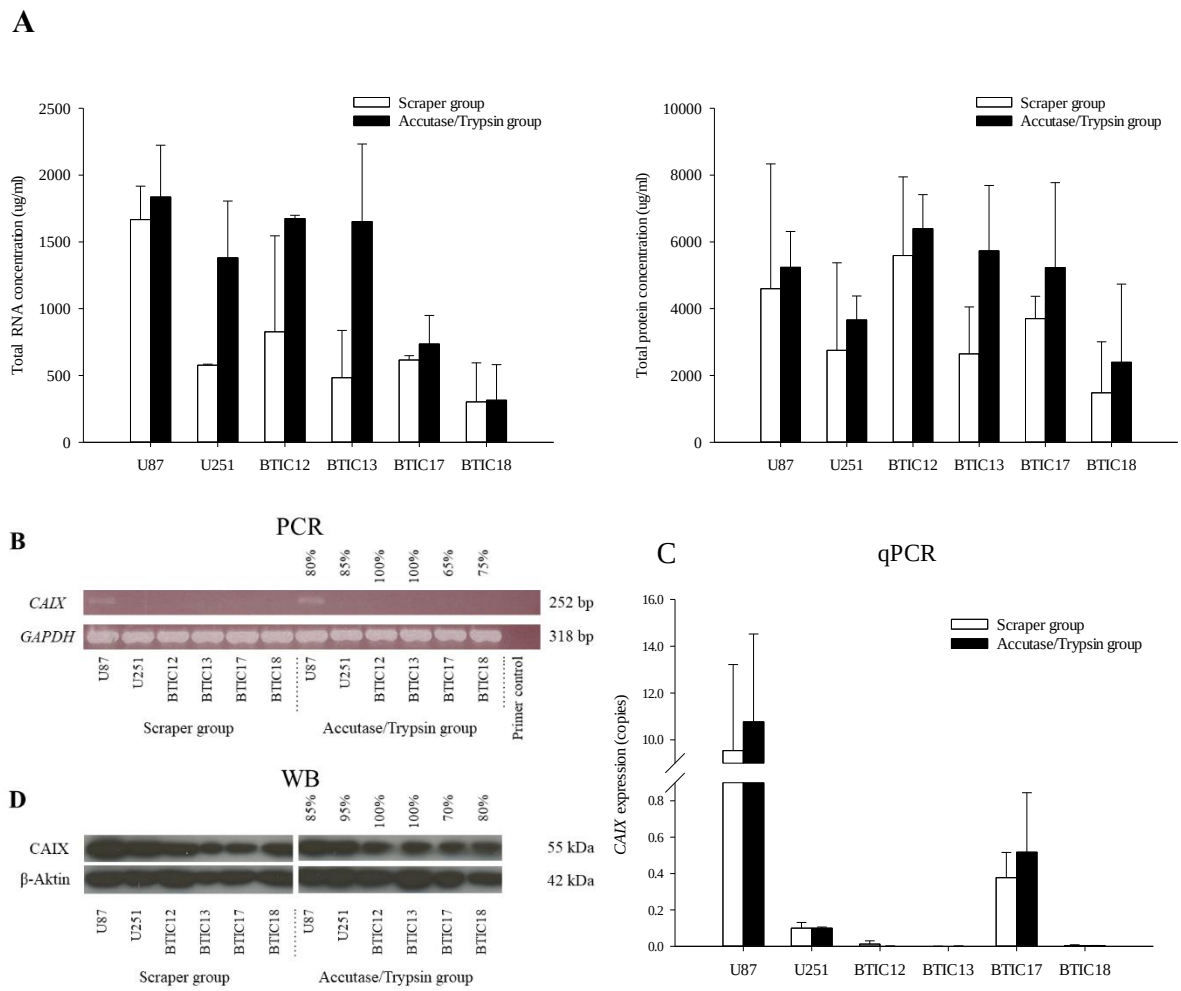

<u>Figure 3.1</u> The comparison of total RNA and protein yield as well as CAIX mRNA and protein yield by two cell harvest methods under normoxia

(A) The bar graphs present the comparison of total RNA concentration (left graph) and total protein concentration (right graph) by Scraper and Accutase/Trypsin harvest methods. (B) PCR result shows the bands of *CAIX* mRNA at 252 bp for the comparison of Scraper and Accutase/Trypsin harvest methods. *GAPDH* is used as reference gene at 318 bp for the equal loading in the lanes. The percentages are the highest cell confluence of corresponding cell line and both groups have the same cell confluence. (C) qPCR result shows the comparison of *CAIX* mRNA copies by Scraper and Accutase/Trypsin harvest methods. (D) WB result of whole cell lysate shows the bands of CAIX protein at 55 kDa for the comparison of Scraper and Accutase/Trypsin harvest methods. β-Aktin is used as reference protein at 42 kDa for the equal loading in the lanes. The percentages are the highest cell confluence of corresponding cell line and both groups have the same cell confluence. [Bar= mean ± SD (standard deviation), Student's t-test].

Overall, experimental data above illustrated that Accutase/Trypsin group had a higher yield of total RNA and total protein under normoxia. The total RNA yield of Accutase/Trypsin group was 1.04-3.42 times higher than scraper group (Figure 3.1 A left). The total protein yield of Accutase/Trypsin group was 1.14-2.17 times higher than scraper group (Figure 3.1 A right). mRNA and protein yield of CAIX showed no significant difference between two methods in PCR and WB (Figure 3.1 B, D). mRNA yield of *CAIX* again showed no statistical difference between two methods in qPCR by Student's t-test (Figure 3.1 C). This might be attributed to that scraper damaged the tightly adherent growth cells during operation which led to the losing of both total RNA and total protein partially. In addition, cell scraper method often required repeat operation to increase yield. Experimental data also illustrated that CAIX protein could not be destructed by digestive enzymes. Thence Accutase/Trypsin method would be used for subsequent cell harvest.

3.3 Low confluence experiment

All 6 GBM cell lines expressed CAIX protein under normoxia in Scraper-Accutase/Trypsin comparative experiment and other preliminary experiments or experimental exercises (data not shown). This was reminiscent that expression of CAIX was cell density-dependent (sparse or dense culture) and regulated by PI3K pathway in addition to HIF pathway in Hela cell line study.[199] Therefore, low confluence experiment and Wortmannin inhibition experiment were performed to test the expression of CAIX in all 6 GBM cell lines under normoxia.

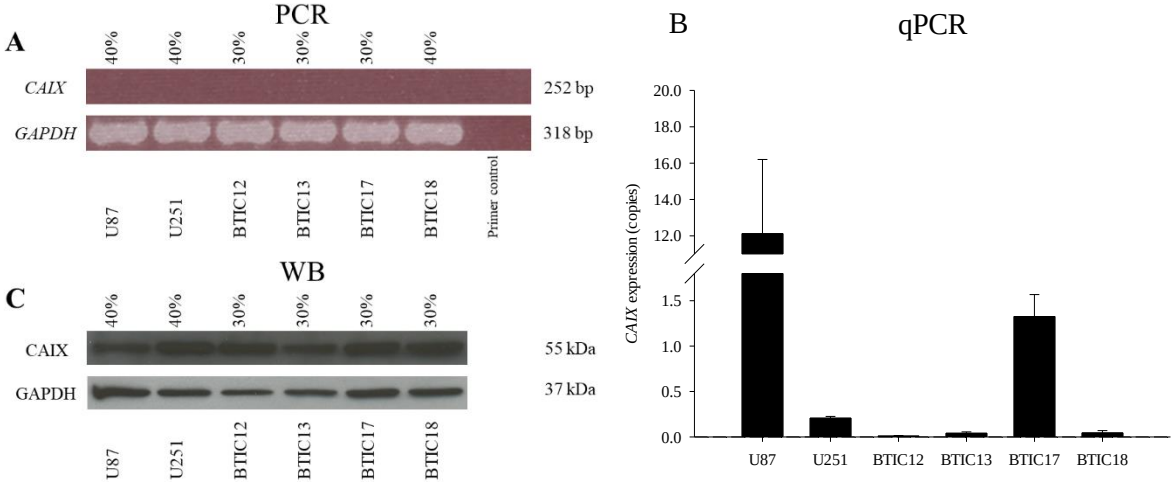

Figure 3.2 The expression of CAIX mRNA and protein in low confluence cell culture under normoxic condition.

(A) PCR result shows the bands of *CAIX* mRNA at 252 bp in low confluence cell culture. *GAPDH* is used

as reference gene at 318 bp for the equal loading in the lanes. The percentages are the lowest cell confluence of corresponding cell line. (B) qPCR result shows *CAIX* mRNA copies in low confluence cell culture. (C) WB result of whole cell lysate shows the bands of CAIX protein at 55 kDa in low confluence cell culture. GAPDH is used as reference protein at 37 kDa for the equal loading in the lanes. The percentages are the lowest cell confluence of corresponding cell line. (Bar= mean ± SD)

To eliminate the possible effect of high cell confluence and post-translational stability of proteins on the expression of CAIX, cell subculture was controlled at low-medium confluence (less than 70%) for 2 weeks before seeding. Cell confluence was also controlled as low as 30-40% at harvest time. Under both low or middle-high confluence of cell culture, PCR results showed no bands of *CAIX* mRNA in all cell lines except U87 which was cultured at 80% confluence (Figure 3.2 A and Figure 3.1 B). qPCR results also showed very low expression of *CAIX* in all cell lines except U87, and slightly higher expression in BTIC17 (Figure 3.2 B and figure 3.1 C). WB results showed baseline protein expression of CAIX in all cell lines of low confluence culture under normoxic condition (Figure 3.2 C).

In conclusion, all cell lines showed very low mRNA and baseline protein expression of CAIX under various confluence states and normoxia apart from *CAIX* mRNA in U87 under high confluence culture.

3.4 Wortmannin inhibition experiment

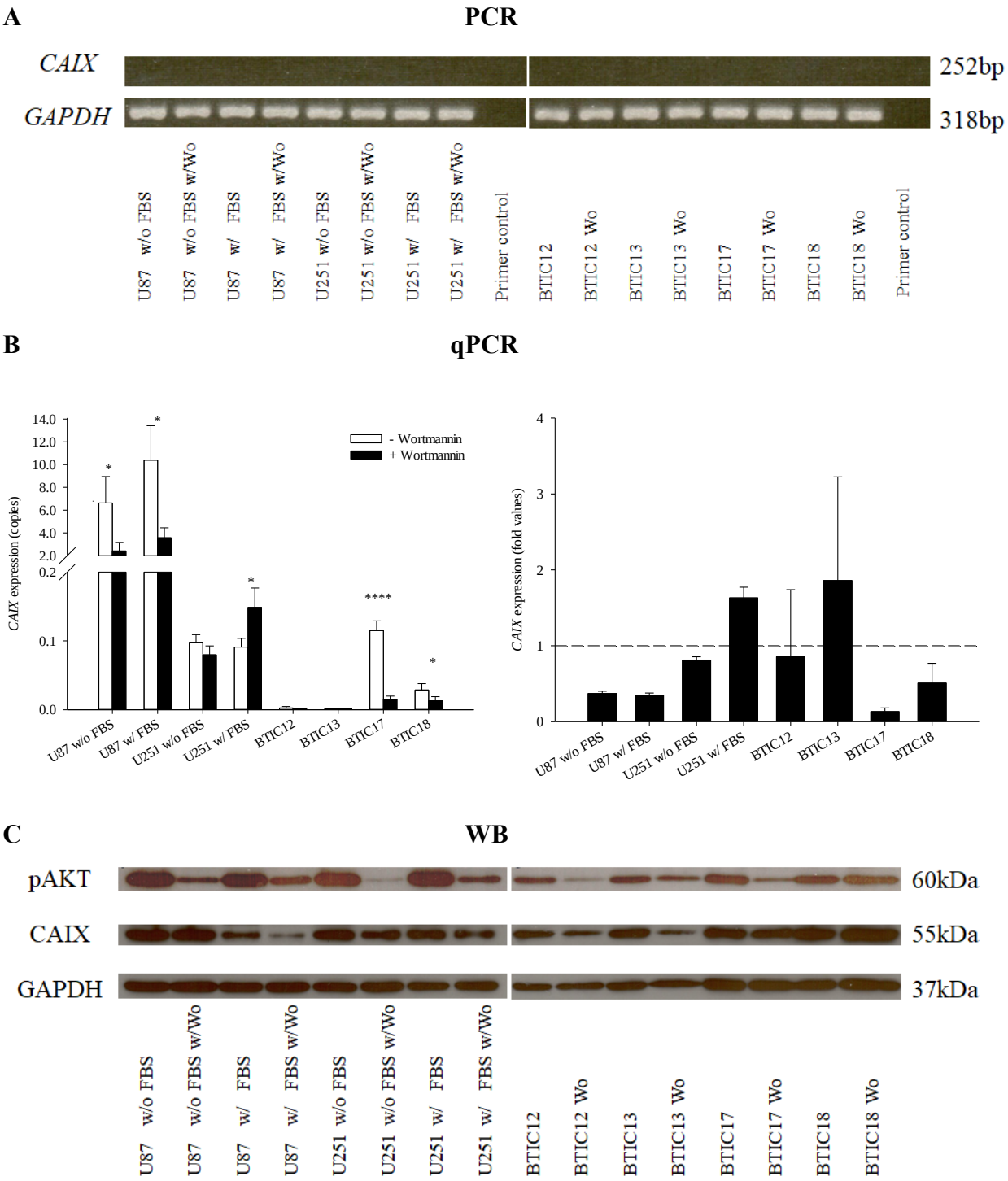

Figure 3.3 The comparison of CAIX expression without or with Wortmannin inhibition on transcription and translation levels under normoxia

(A) PCR result shows the bands of *CAIX* mRNA at 252 bp for comparing without or with Wortmannin

inhibition. *GAPDH* is used as reference gene at 318 bp for the equal loading in the lanes. (B) qPCR result presents the absolute value (left graph) and fold value (right graph) of *CAIX* mRNA for comparing without or with Wortmannin inhibition. The dash line represents the one time value (100%) by comparing the absolute value without and with Wortmannin. (C) WB result of whole cell lysate shows the bands of pAKT and CAIX protein at 60 kDa and 55 kDa respectively for comparing without or with Wortmannin inhibition. GAPDH is used as reference protein at 37 kDa for the equal loading in the lanes. (Bar= mean ± SD, *$p < 0.05$; ****$p < 0.0001$. Student's t-test) (w/: with, w/o: without, Wo: Wortmannin)

Results of WB showed that Wortmannin reduced expression of pAKT (a downstream protein of PI3K) in all cell lines except BTIC18 (Figure 3.3 C). This was a proof that Wortmannin was an effective inhibitor of PI3K pathway. No bands of *CAIX* mRNA could be seen in PCR (Figure 3.3 A) and this was consistent with the aforementioned experimental results. All cell lines showed down-regulation of *CAIX* mRNA by Wortmannin inhibition in qPCR except U251 with FBS and BTIC13 (Figure 3.3 B). The reduction of *CAIX* mRNA ranged from the lowest 18.6% in U251 without FBS to the highest 86.9% in BTIC17, and the increase of *CAIX* mRNA were 1.63 and 1.29 times in U251 with FBS and BTIC13, respectively. All cell lines showed down-regulation of CAIX protein by Wortmannin inhibition in WB except U87 without FBS and BTIC17/18 (Figure 3.3 C).

This experiment proved again that all 6 cell lines had very low mRNA and baseline protein expression of CAIX under normoxia. Most of the cell lines could be downregulated (not eliminated) by Wortmannin which meant PI3K pathway played an important role in the baseline expression of CAIX. This also indirectly indicated some other pathways might participate in the baseline expression regulation of CAIX and needed further investigation.

3.5 Experiment for CAIX and VEGF expression under normoxia and hypoxia (normoxia and hypoxia experiment)

Expression of CAIX was strong induced by hypoxia in established GBM cell lines which was reported everywhere, while there were seldom reports about BTICs. This experiment was performed to test whether CAIX could be induced by hypoxia in both established cell lines and BTICs on transcription and translation levels. The sustained hypoxia time of 24 hours was based on the preliminary work of this laboratory. The expression of two single-isoforms of *VEGF* mRNA was also investigated under normoxia and hypoxia, because *VEGF* had been established

to be a hypoxia-regulated gene.[166, 260]

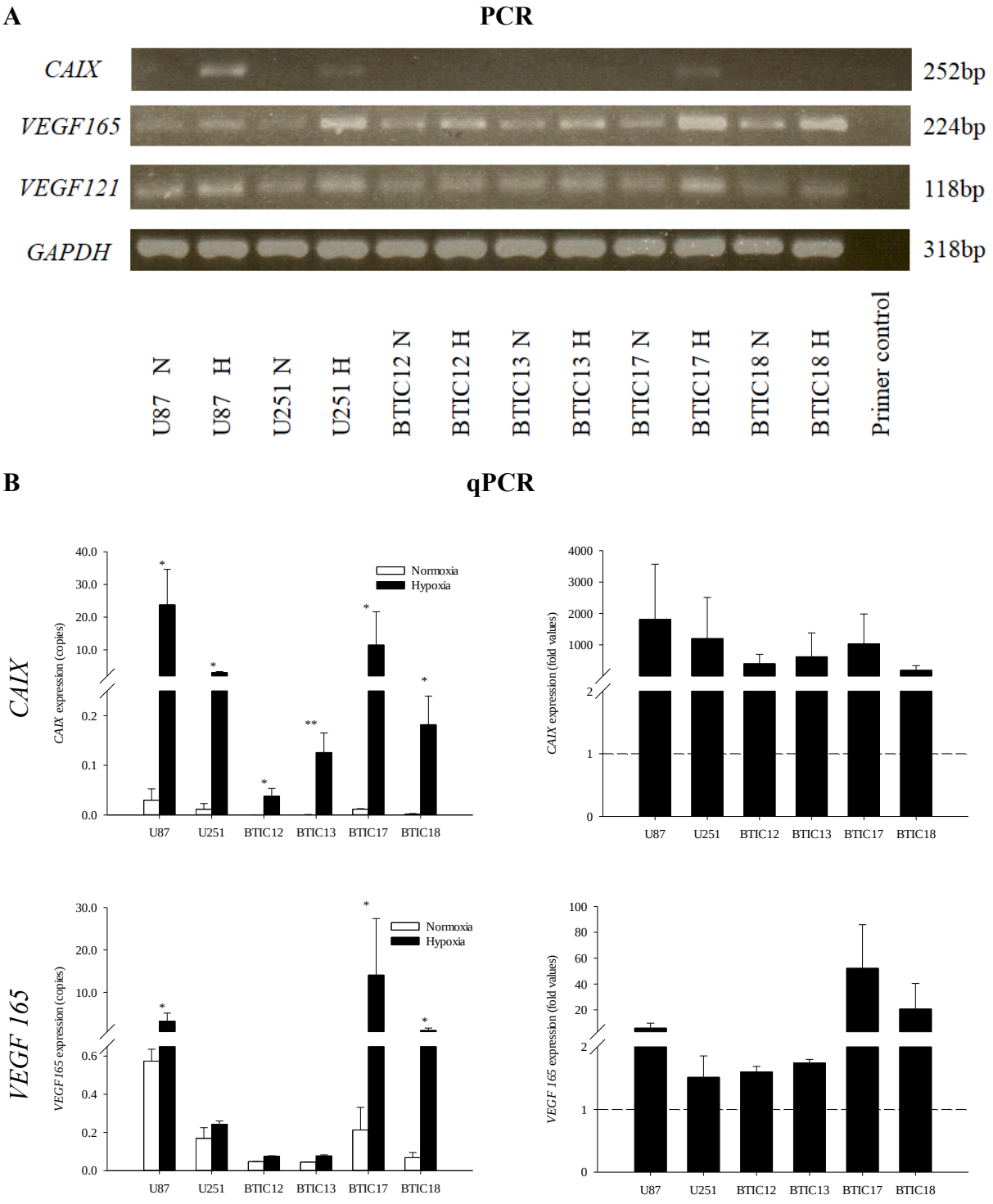

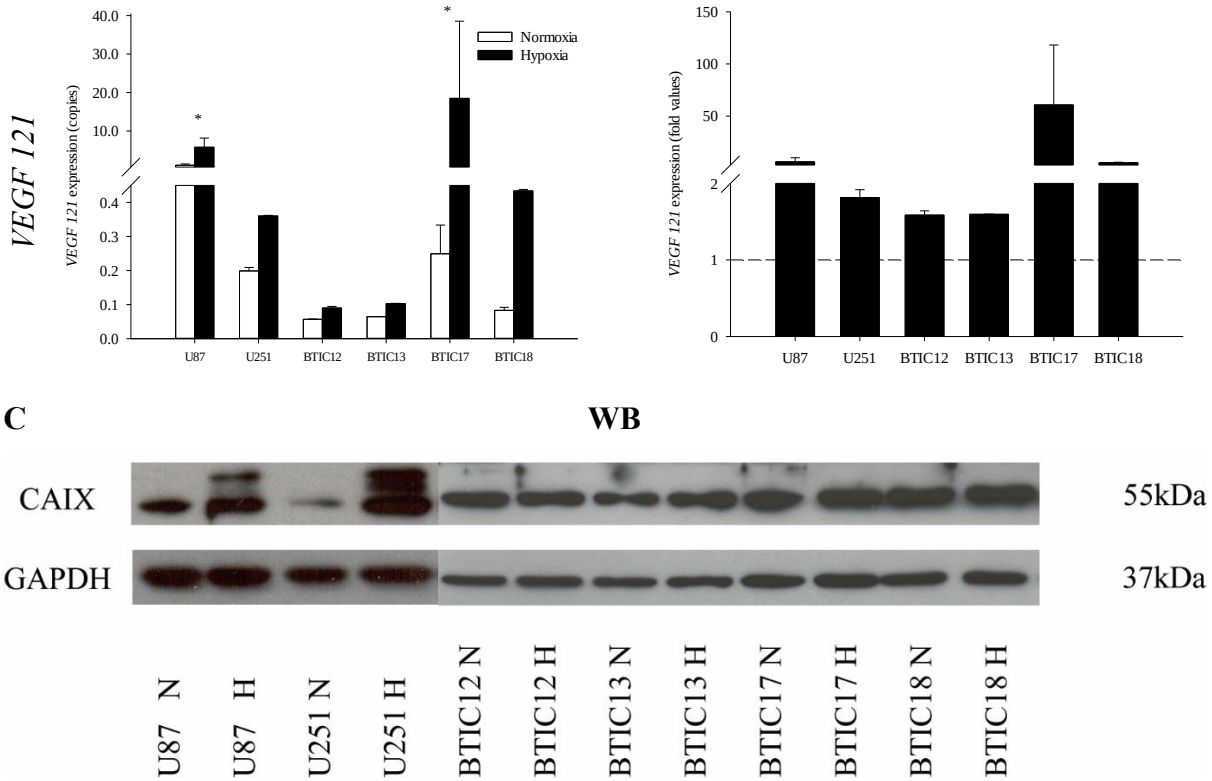

Figure 3.4 The expression of CAIX and VEGF on transcription and translation levels under normoxia and hypoxia

(A) PCR result shows the bands of *CAIX, VEGF 165, VEGF 121* mRNA at 252 bp, 224 bp, 118 bp, respectively under normoxia and hypoxia. *GAPDH* is used as reference gene at 318 bp for the equal loading in the lanes. (B) qPCR result shows the absolute value (left graphs) and fold value (right graphs) of *CAIX, VEGF 165, VEGF 121* mRNA under normoxia and hypoxia. The dash line represents the one time value by comparing with the absolute value under hypoxia and normoxia. (C) WB result of whole cell lysate shows the bands of CAIX protein at 55 kDa under normoxia and hypoxia. GAPDH is used as reference protein at 37 kDa for the equal loading in the lanes. (Bar= mean ± SD, *$p < 0.05$; **$p < 0.01$. Student's t-test) (N: normoxia, H: hypoxia)

PCR results showed no bands of *CAIX* mRNA in all cell lines under normoxia (Figure 3.4 A) and this was again consistent with the aforementioned experimental results. PCR results showed clear bands in U87/U251/BTIC17 under hypoxia, and no bands in BTIC12/13/18 under hypoxia because of low mRNA yield. PCR results also showed baseline and increased mRNA expression of *VEGF165* and *VEGF121* under normoxia and hypoxia, respectively (Figure 3.4 A). qPCR results showed increased mRNA expression of *CAIX/VEGF165/VEGF121* in all 6 cell lines under

hypoxia. Increased mean fold values of *CAIX* under hypoxia induction ranged from the lowest 188 times in BTIC18 to the highest 1811 times in U87. Increased mean fold values of *VEGF165* under hypoxia induction ranged from the lowest 1.51 times in U251 to the highest 52 times in BTIC17. Increased mean fold values of *VEGF121* under hypoxia induction ranged from the lowest 1.59 times in BTIC12 to the highest 61 times in BTIC17. Therefore, the fold value of *CAIX* mRNA induced by hypoxia was significantly higher than *VEGFs* (Figure 3.4 B). WB results showed significantly increased protein expression of CAIX in two established cell lines, mildly increased in BTIC13/17/18 and no significant change in BTIC12 under 24-hour sustained hypoxia (Figure 3.4 C).

3.6 Cell immunofluorescence staining

Whole cell lysate for WB was a mixture of total proteins which included membrane protein, cytoplasmic protein and nuclear protein. Immunofluorescence staining was a good method to detect the expression of membrane protein CAIX.

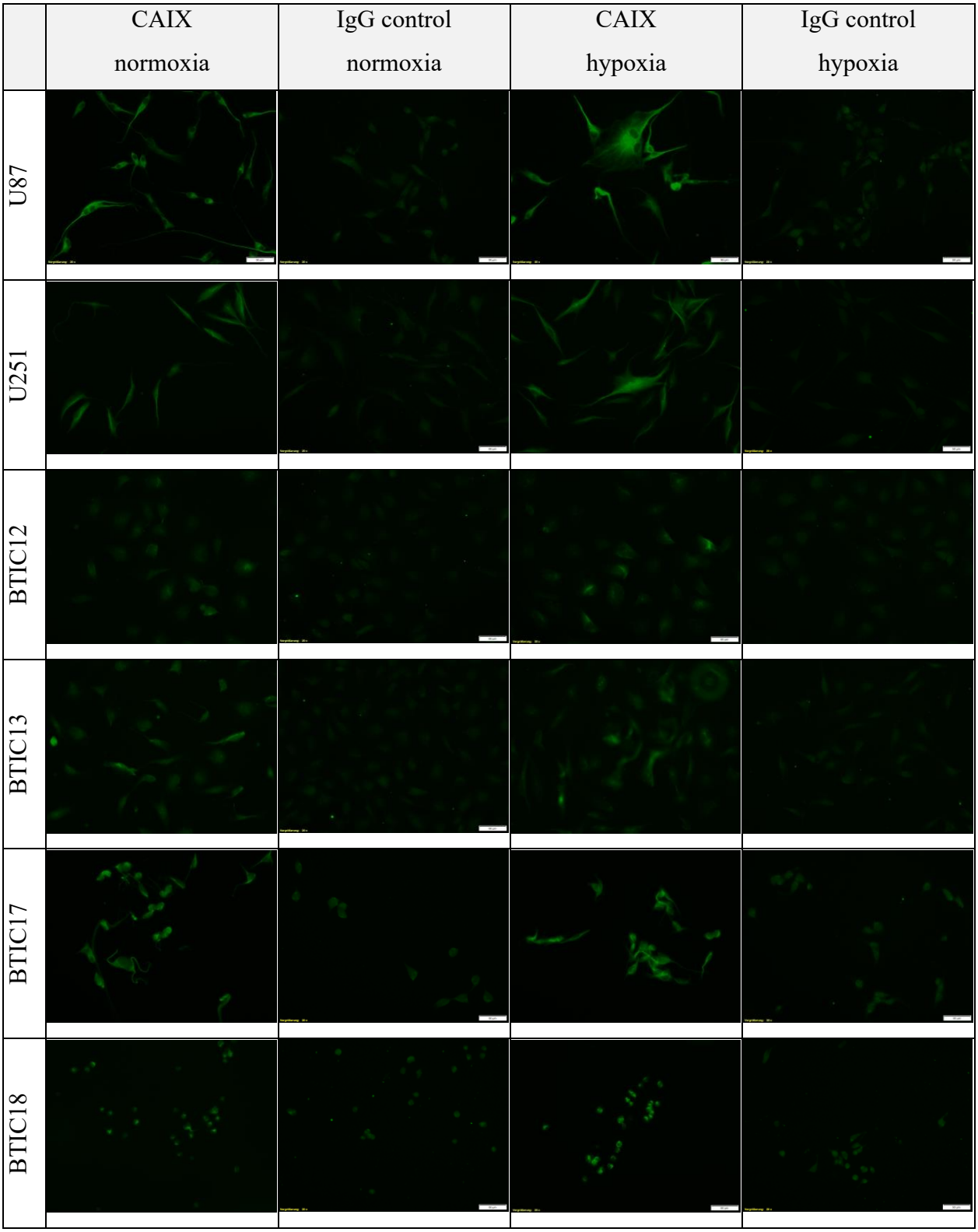

Figure 3.5 The expression of CAIX by cell immunofluorescence staining under normoxia and hypoxia

The result of cell immunofluorescence staining shows the CAIX expression by the fluorescence intensity

under normoxia and hypoxia. IgG antibody is used as negative control. (200x original magnification)

Results of immunofluorescence staining illustrated that all GBM cell lines expressed CAIX protein under both normoxic and hypoxic conditions by comparing with IgG control. Immunofluorescence staining results also showed significantly increased protein expression of CAIX in U87 and U251, as well as mildly increased CAIX expression in all BTICs after 24-hour sustained hypoxia. These results were roughly consistent with WB results in normoxia and hypoxia comparative experiment of CAIX expression. BTIC18 showed lesser cells because of cell loss caused by semi-adherent growth in the washing steps. No significantly morphological difference could be observed between normoxic and hypoxic conditions in all cell lines. (Figure 3.5)

3.7 Cell viability experiment

Cell viability experiment was performed to find the optimized concentration of U104 and action days under normoxia and hypoxia to start invasion assay before cell death, because the cells killed by the toxic inhibitor would not be able to invade anymore. To tease out the true anti-invasive effects of CAIX inhibition, we needed to rule out cell viability related effects. DMSO control was used in this experiment to eliminate its influence on cell viability, because U104 was diluted by DMSO. Boyd et al. reported 50μM concentration of U104 combined with temozolomide for the treatment of BTICs *in vitro* and *in vivo* effectively. [261] Xu et al. reported the combination therapy of 100μM U104 and temozolomide in established GBM cell lines U87 and U251 *in vitro*. [262] We started at a wider range of 10/80/180μM, and further tested 40/60μM (data not shown) according to the initial experimental results. In addition, this experiment was also used to elucidate whether there were different sensitivities to U104 in terms of cell viability between cell lines. Results of ATP assay were finally shown instead of results of crystal violet assay, because cell loss of BTIC18 during wash step led to the unstable experimental results of crystal violet assay.

	$p < 0.05$				
Comparison between cell lines	Untreated	DMSO	10μM	80μM	180μM
Day2 vs. day4	No	No	No	No	No
Day2 vs. day6	Yes	No	No	No	Yes
Day4 vs. day6	No	No	No	No	Yes

Table 3.4 Pairwise multiple comparisons between action days in different groups in terms of cell viability (Two-way ANOVA, Holm-Sidak method)

First of all, the results showed the differences between day 2/4/6 treatments (data not shown), while most differences were not statistically significant because of not enough power. (Table 3.4) Therefore, data of day 2/4/6 in same condition were pooled. Secondly, 10μM DMSO control groups were used in the comparative analysis with other treatment groups, because there were no statistically significant differences between DMSO control groups of different concentrations. (data not shown)

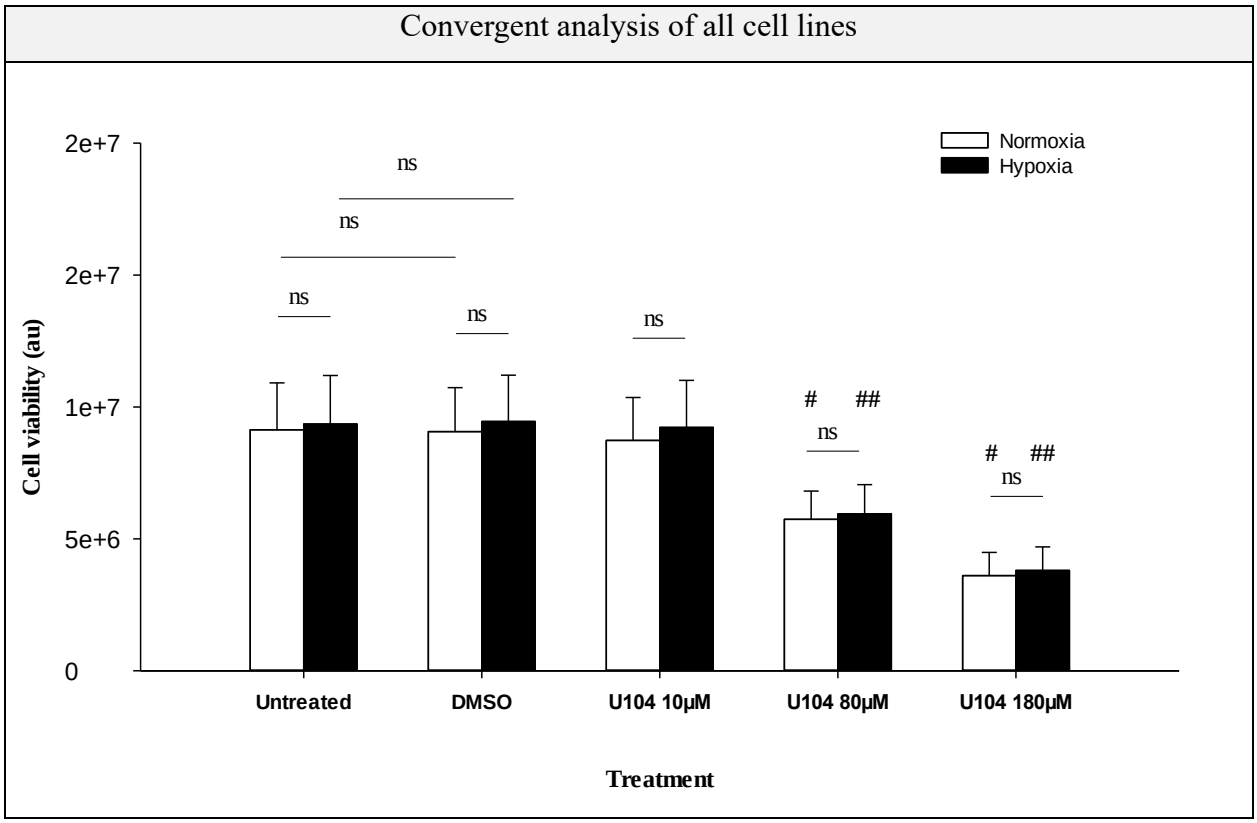

Figure 3.6 Convergent quantitative results of cell viability values of all GBM cell lines in different groups under normoxic and hypoxic conditions. (Bar = mean ± SD, # $p < 0.05$; ## $p < 0.01$ (vs DMSO

control), ns= not significant. Two-way ANOVA, Holm-Sidak method)

Convergent analysis (pooled data of all six GBM cell lines) showed no statistically significant of cell viability value changes between normoxia and hypoxia in all groups. The cell viability value started to decrease significantly from 80μM U104 treatment, and the cell viability value decreased 36.8% and 37.0% under normoxic and hypoxic conditions respectively in comparing with DMSO control ($p < 0.05$; $p < 0.01$). The cell viability value decreased 60.3% and 59.8% in 180μM U104 treatment under normoxic and hypoxic conditions respectively in comparing with DMSO control ($p < 0.05$; $p < 0.01$). Therefore, these results presented a dose-dependent toxic effect of U104 in the treatment of GBM cells. In addition, there was no statistically significant difference between DMSO group and untreated group under both normoxia and hypoxia. This meant DMSO did not affect cell viability of GBM cells during culture. (Figure 3.6)

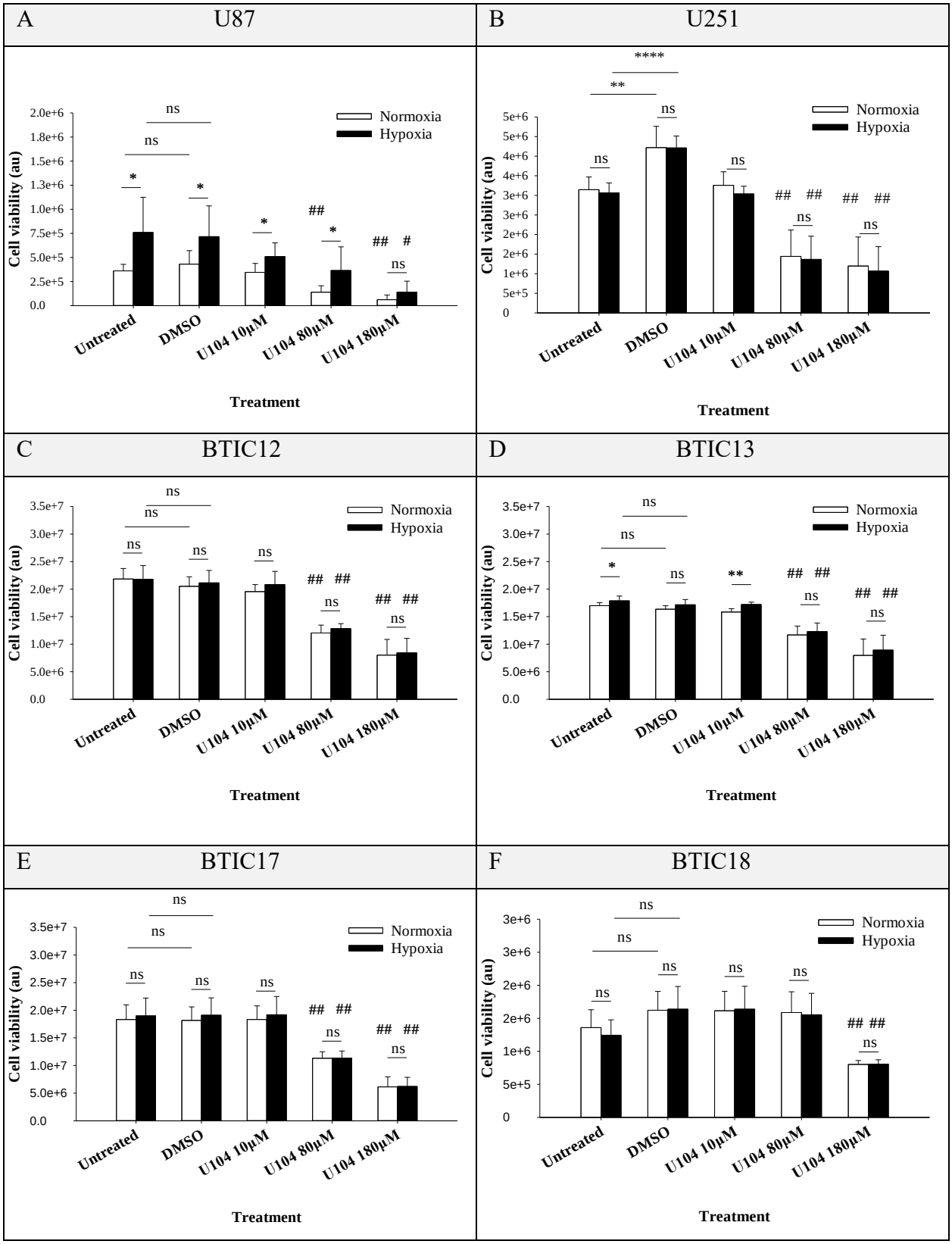

Figure 3.7 Cell viability value of each GBM cell line in different groups under normoxic and hypoxic conditions. (Bar = mean ± SD, *$p < 0.05$; **$p < 0.01$; ****$p < 0.0001$, # $p < 0.05$; ## $p < 0.01$ (vs DMSO

control), ns= not significant. Two-way ANOVA, Holm-Sidak method)

Results of Figure 3.7 presented the bar graphs and statistical comparisons of cell viability in six GBM cell lines separately. There were no statistically significant of cell viability value changes between normoxia and hypoxia in all groups of U251/BTIC12/BITC17/BTIC18. (Figure 3.7 B,C,E,F) There were statistically significant of cell viability value changes between normoxia and hypoxia in all groups ($p < 0.05$) (except 180μM group) of U87 (Figure 3.7 A), and in untreated group ($p < 0.05$) and 10μM group ($p < 0.01$) of BTIC13 (Figure 3.7 D). The statistically significant increasements ranged from the lowest 1.47 times in 10μM group to the highest 2.62 times in 80μM group of U87. The increasement was 2.11 times in untreated group of U87. (Figure 3.7 A) In addition, the increasements were gradual (1.05 and 1.09 times) in untreated group and 10μM group of BTIC13, yet statistically significant. (Figure 3.7 D) Interestingly, there were slight reductions of cell viability after hypoxia induction in all groups of U251 (Figure 3.7 B), untreated group of BTIC12 (Figure 3.7 C) as well as untreated group and 80μM group of BTIC18 (Figure 3.7 F), although no statistically significant differences could be seen.

Cell viability value started to decrease significantly from 80μM U104 treatment in U251/BTIC12/BTIC13/BTIC17 cell lines under both normoxic and hypoxic conditions in comparing with DMSO control ($p < 0.01$). (Figure 3.7 B-E) Cell viability value of U87 started to decrease significantly from 80μM U104 treatment only under normoxia ($p < 0.01$) and decrease significantly in 180μM U104 treatment under both normoxia ($p < 0.01$) and hypoxia ($p < 0.05$). There were no statistically significant differences for the comparison between 10μM group and DMSO control group as well as between 80μM group and DMSO control group under hypoxia, although 28.9% and 49.1% reduction of cell viability could be seen. This might because of the high standard deviation. (Figure 3.7 A) Cell viability value of BTIC18 started to decrease significantly from 180μM U104 treatment under both normoxia and hypoxia ($p < 0.01$). (Figure 3.7 F)

Additionally, there were statistically significant increasements of cell viability value 1.34 times ($p < 0.01$) and 1.37 times ($p < 0.0001$) after the addition of DMSO under normoxia and hypoxia respectively by comparing with untreated group in U251 cell line (unpaired Student's t-test). (Figure 3.7 B) DMSO also increased cell viability value of 1.19 times and 1.32 times under normoxia and hypoxia respectively by comparing with untreated group in BTIC18 cell line

(unpaired Student's t-test), however there were no statistically significant. (Figure 3.7 F) No statistically significant differences could be seen between DMSO and untreated groups in U87/BTIC12/BTIC13/BTIC17 cell lines under both normoxia and hypoxia. (unpaired Student's t-test) (Figure 3.7 A,C,D,E) Therefore, it was necessary to use DMSO as control for revealing the net effect of U104 because of its effect on cell viability in specific cell lines and experimental conditions.

	$p < 0.05$				
Comparison between cell lines	Untreated	DMSO	10μM	80μM	180μM
U251 vs. U87	Yes	Yes	Yes	No	No
U251 vs. BTIC18	Yes	Yes	Yes	No	No
BTIC18 vs. U87	No	No	Yes	No	No
BTIC17 vs. U87	Yes	Yes	Yes	Yes	Yes
BTIC17 vs. U251	Yes	Yes	Yes	Yes	Yes
BTIC17 vs. BTIC18	Yes	Yes	Yes	Yes	Yes
BTIC17 vs. BTIC13	No	Yes	Yes	No	Yes
BTIC13 vs. U87	Yes	Yes	Yes	Yes	Yes
BTIC13 vs. U251	Yes	Yes	Yes	Yes	Yes
BTIC13 vs. BTIC18	Yes	Yes	Yes	Yes	Yes
BTIC12 vs. U87	Yes	Yes	Yes	Yes	Yes
BTIC12 vs. U251	Yes	Yes	Yes	Yes	Yes
BTIC12 vs. BTIC18	Yes	Yes	Yes	Yes	Yes
BTIC12 vs. BTIC17	Yes	Yes	Yes	No	Yes
BTIC12 vs. BTIC13	Yes	Yes	Yes	No	No

Table 3.5 Pairwise multiple comparisons between cell lines in different groups in terms of cell viability (Two-way ANOVA, Holm-Sidak method)

	$p < 0.05$						
Comparison between treatments and DMSO	Convergent	U87	U251	BTIC12	BTIC13	BTIC17	BTIC18
Untreated vs. DMSO	No	No	No	No	No	No	No
10μM vs. DMSO	No	No	No	No	No	No	No
80μM vs. DMSO	Yes	No	Yes	Yes	Yes	Yes	No
180μM vs. DMSO	Yes	No	Yes	Yes	Yes	Yes	No

Table 3.6 Pairwise multiple comparisons between different treatment groups and DMSO control group in each cell line in terms of cell viability (Two-way ANOVA, Holm-Sidak method)

In view of no statistically significant of cell viability value changes between normoxia and hypoxia in convergent analysis of all groups of all cell lines (Figure 3.6), data of normoxia and hypoxia in same group were pooled and the cell viability values between cell lines were analyzed in different groups. There were statistically significant differences between most cell lines in all groups. No statistically significant differences could be seen only in 2 pairs (BTIC18 vs. U87; BTIC17 vs. BTIC13) of untreated group, 1 pair (BTIC18 vs. U87) of DMSO group, 6 pairs (U251 vs. U87; U251 vs. BTIC18; BTIC18 vs. U87; BTIC17 vs. BTIC13; BTIC12 vs. BTIC17; BTIC12 vs. BTIC13) of 80μM group, 4 pairs (U251 vs. U87; U251 vs. BTIC18; BTIC18 vs. U87; BTIC12 vs. BTIC13) of 180μM group. Results of untreated group indicated different basal cell viablility levels between cell lines. Some of the statistically significant differences between cell lines changed after the addition of different treatments. Therefore, this revealed the treatment heterogeneity between cell lines. (Table 3.5) In addition, BTIC12/13/17 showed relatively higher cell viability values in untreated groups than other cell lines which meant higher basal cell viablility levels, while this did not imply a higher proliferation rate in these cell lines.

Statistical analysis results of pooled values of normoxia and hypoxia also showed the comparisons between different concentration groups of U104 and DMSO control groups in each cell line or all cell lines. There were no statistically significant differences in all comparative groups of U87 and BTIC18, as well as untreated/10μM vs. DMSO groups in other cell lines. Therefore, U87 and BTIC18 were lesser sensitivity to the treatment of U104 in comparing with other cell lines. (Table 3.6)

In general, our results revealed that: 1. There was a dose and exposure time dependent toxic

effect of U104 in all cell lines. 2. Hypoxia increased cell viability only in specific cell lines (U87 and BTIC13) and experimental conditions. 3. There was a significant heterogeneity of sensitivity to U104 treatment between cell lines. U87 and BTIC18 were less sensitive to U104 in comparing with other cell lines.

3.8 Cell invasion experiment

3.8.1 Pre-experiment results of GBM cell invasion

Matrigel coated Transwell cell invasion assay is a classic and widely used method to investigate invasion ability of various tumor cells including GBM. [263, 264] 8.0μm pore size of cell culture insert was chosen in our experiment because of common use. Considering the growth pattern difference, different sensitivity to various inhibitor concentrations and other unknown impact factors between cell lines, eight pre-experiments were performed to find out the optimized experimental conditions. According to the protocol of company, results of cell viability experiment and previous work experience in our laboratory, 50μl 10mg/ml water diluted Matrigel per insert, $2x10^5$ cells in 200μl serum-free medium per upper compartment (culture insert), 600μl medium without chemo-attractant per lower compartment, 40μM U104/DMSO and 2 days for cell invasion were used at the beginning of pre-experiments. Two identical repeated wells were used in each condition in most instances.

Cell fluorescence and electronic resistance invasion assay methods were excluded not only because of the need to buy new expensive equipments, but also because of impossibility to observe the morphological changes during experiment process. Invasive cells detachment and insert membrane cutting for staining and measuring were also excluded because of impossibility of long-term observation, storage and complex operation.

No.		Purposes, conditions and procedures of pre-experiments
1	N/H	Experimental conditions: 200,000cells/insert; 40µmol U104/DMSO; day 2 Option 1: Cell seeding and treatment→ Hypoxia induction (4 hours later)→ Incubation 24hours Option 2: Cell seeding→ Cell treatment and hypoxia induction (4 hours later)→ Incubation 24hours Try ready-to-use pre-coated Matrigel inserts (BTIC12 without treatment)
2	N/H	1.Dilute Matrigel with water or medium 2.Test different cell number (10,000/50,000/100,000 per insert) of all cell lines for invasion without treatment 3.Observe the impact of punctured membrane on cell invasion 4.Test the invasiveness with/without chemo-attractant in lower compartment (BTIC13 without treatment)
3	N	Test the invasiveness with/without chemo-attractant and different cell number of all cell lines without treatment (50,000/100,000/200,000 per insert)
4	H	Test the invasiveness with fixed cell number and different concentration of U104/DMSO
5	N/H	Test the invasiveness with fixed cell number and fixed concentration of U104/DMSO
6	N/H	Repeat pre-Exp.5 and seed cells after 30 minutes treatment of U104/DMSO
7	H	Repeat pre-Exp.5/6 of 4 days for invasion (U251/BTIC12/BTIC17)
8	N	Use low generation and less passaged cells of all cell lines

Table 3.7 Brief introduction of purposes, conditions and procedures in all pre-experiments

(N: normoxia, H: hypoxia, No.: Number, pre-Exp.: pre-experiment)

3.8.1.1 Results of first pre-experiment

Medium change after seeding in inserts was impossible, because this operation might cause loss of cells and Matrigel. Hypoxia induction should be carried out after seeding and treatment immediately, because cells started to invade after seeding. Therefore, the procedure of invasion experiment was significaltly different from the previous CAIX expression under normoxia and

hypoxia experiment as well as cell viability experiment. Cell seeding, inhibitor treatment and hypoxia induction should be carried out in small time intervals. The detachment of cells by digestive enzymes and medium without FBS in established cell lines might lead to biological changes of GBM cells. In addition, immediate treatment with inhibitors and hypoxic condition might lead to excessive stress. The first pre-experiment was carried out in 2 options to determine whether 4-hour interval between seeding and U104 treatment helped to relieve stress of cells. The ready-to-use pre-coated Matrigel inserts were also investigated in BTIC12 without treatment for the comparation with self-made ones.

A	U87					
	Option 1			Option 2		
	Untreated	U104	DMSO	Untreated	U104	DMSO
Normoxia	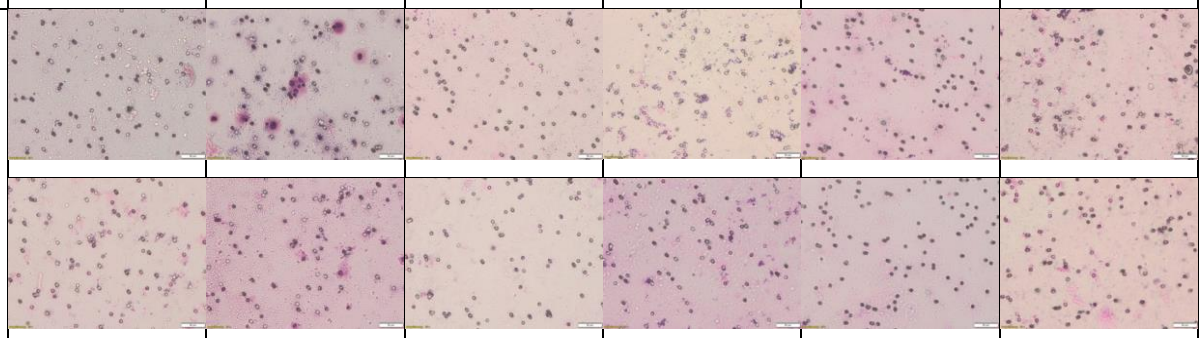					
Hypoxia	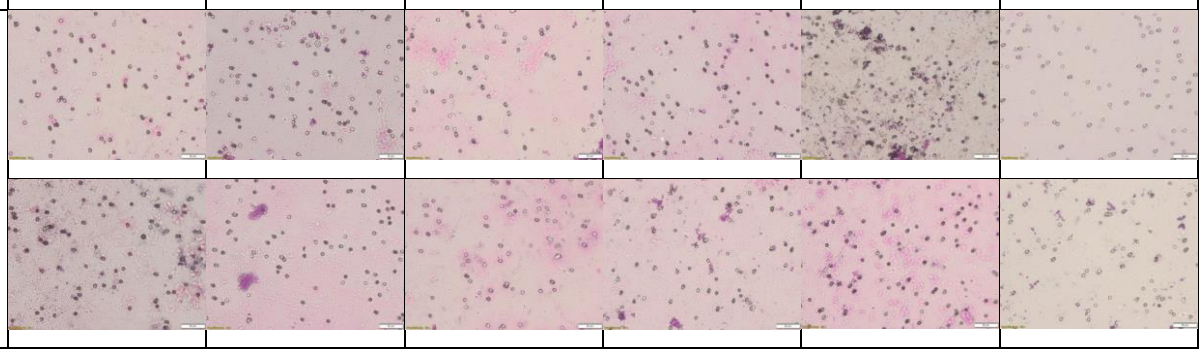					

B	U251					
	Option 1			Option 2		
	Untreated	U104	DMSO	Untreated	U104	DMSO
Normoxia	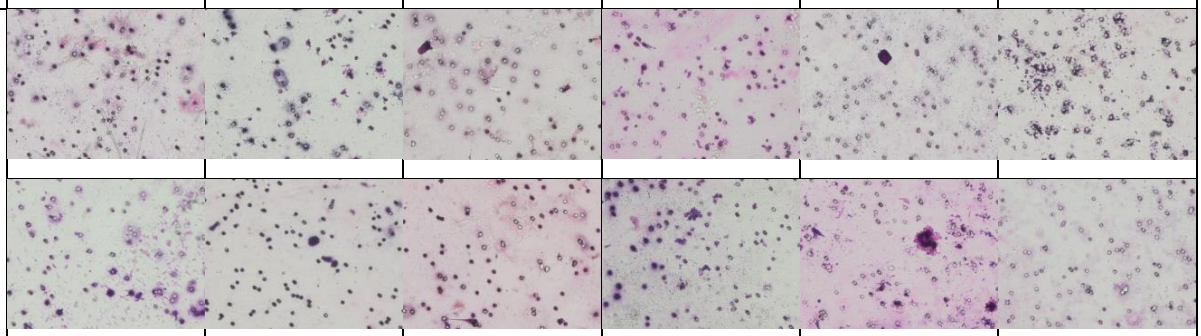					
Hypoxia	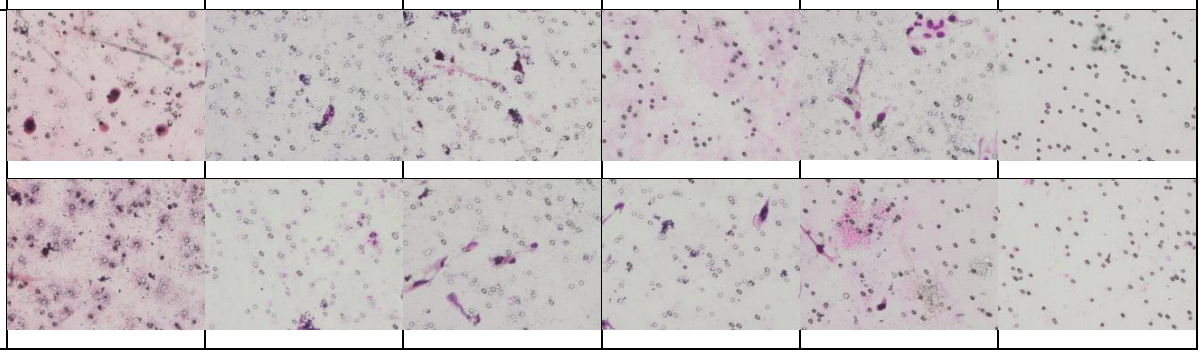					

C	BTIC12						
	Option 1			Option 2			Option 1+ pre-coated Matrigel insert
	Untreated	U104	DMSO	Untreated	U104	DMSO	Untreated
Normoxia	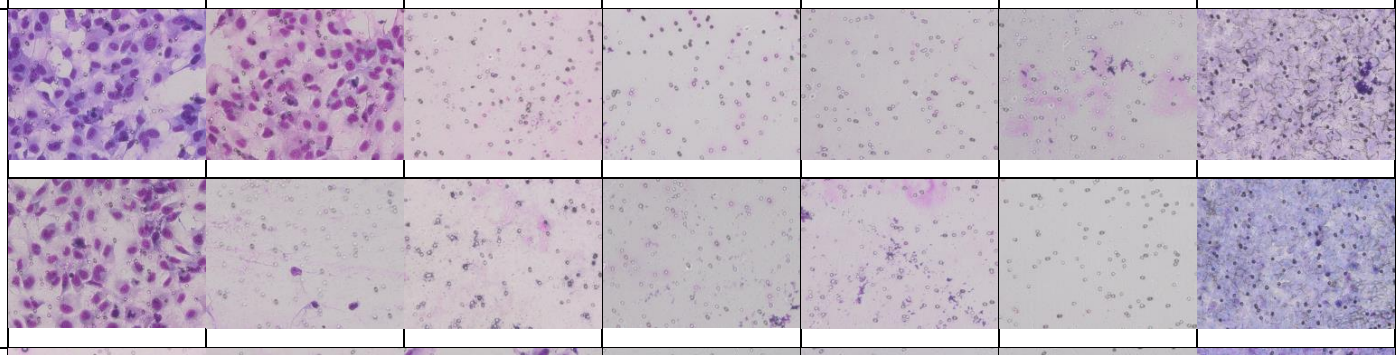						
Hypoxia	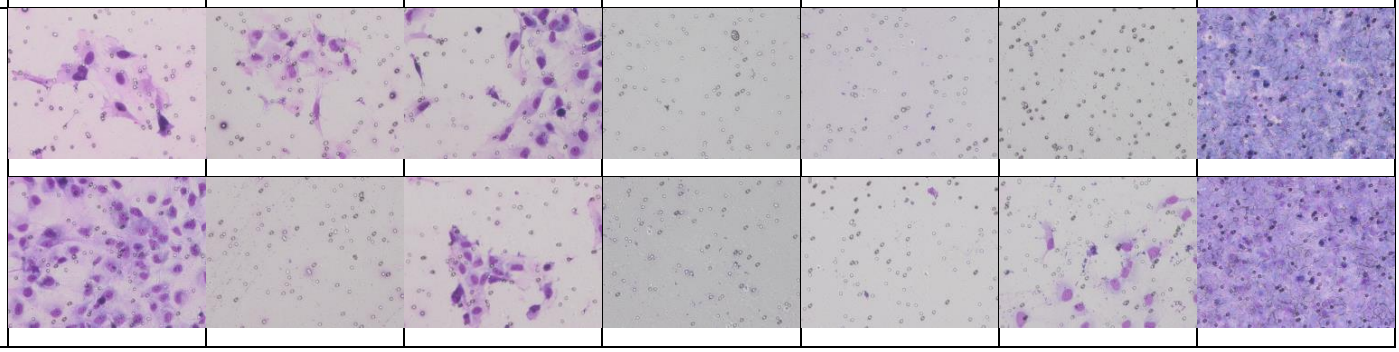						

D	BTIC13					
	Option 1			Option 2		
	Untreated	U104	DMSO	Untreated	U104	DMSO
Normoxia	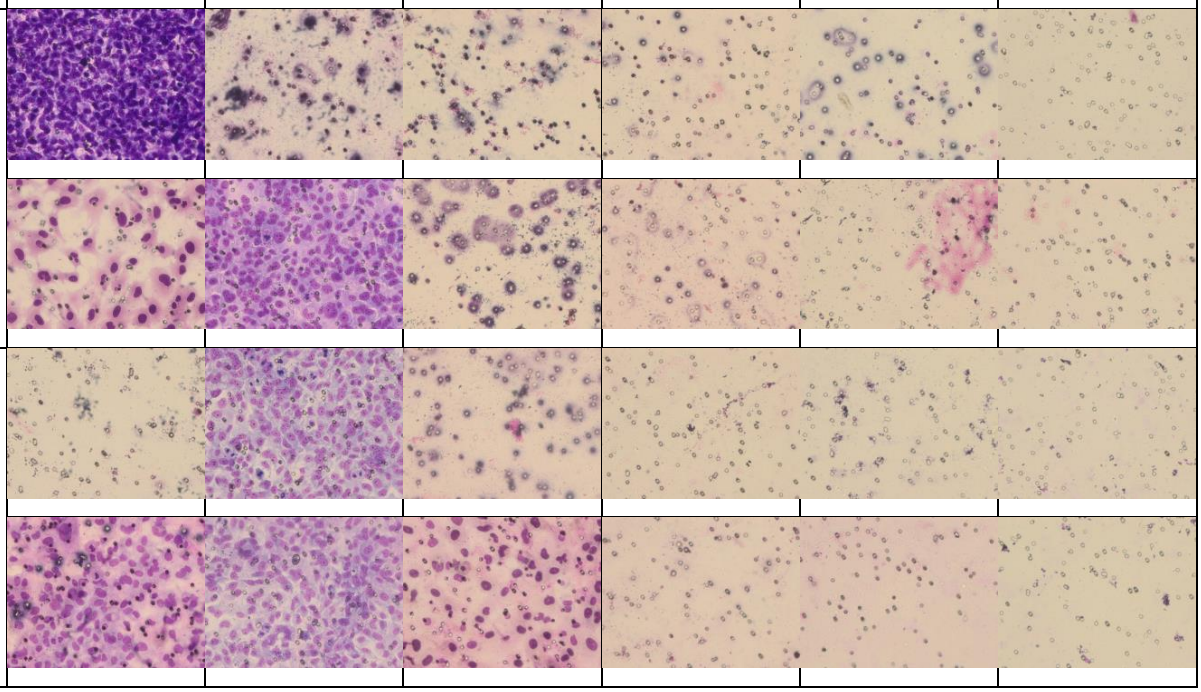					
Hypoxia						

E	BTIC17					
	Option 1			Option 2		
	Untreated	U104	DMSO	Untreated	U104	DMSO
Normoxia	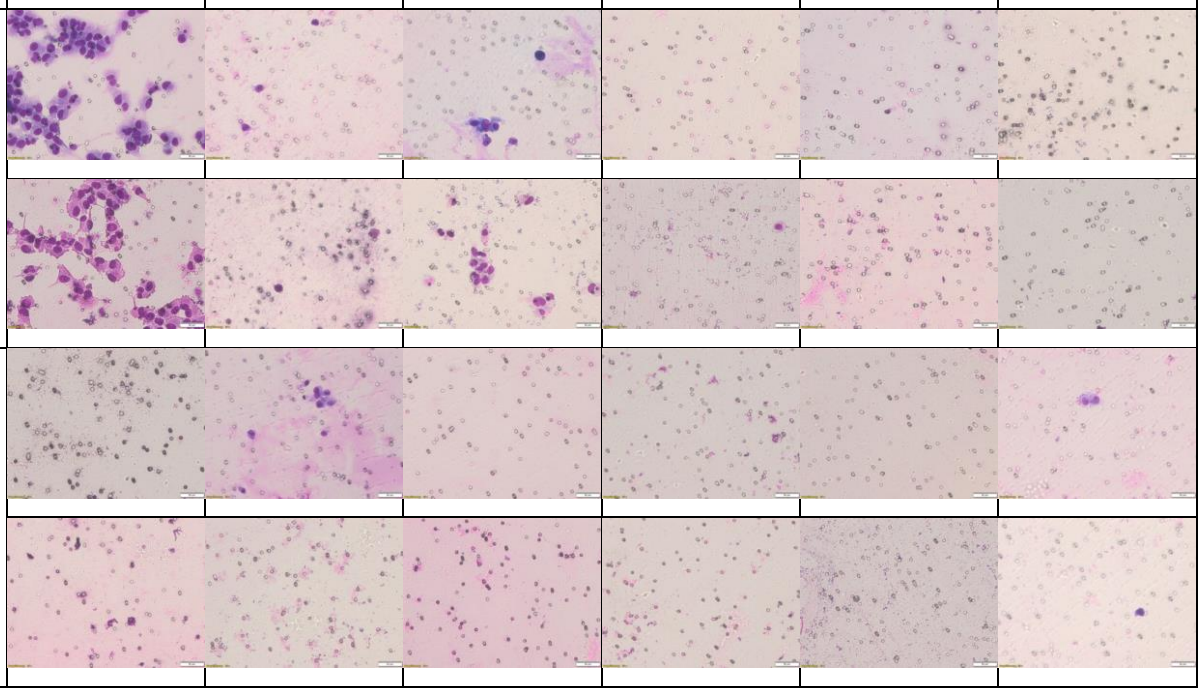					
Hypoxia						

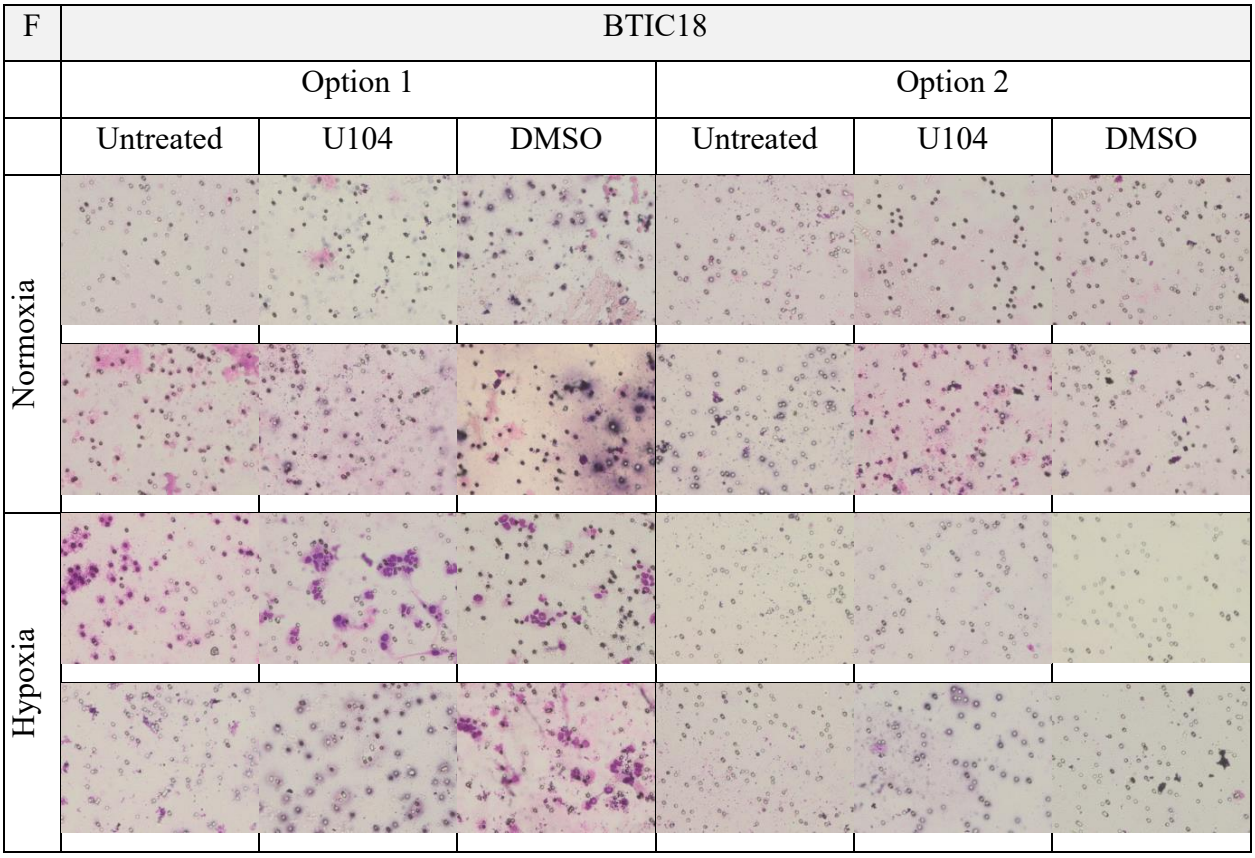

Figure 3.8 The first pre-experiment results of invasion

In the first pre-experiment, 200,000 cells are seeded in each insert of all cell lines. The concentration of U104/DMSO is 40μM. The whole process for cell invasion takes 2 days. Option 1: cell seeding and treatment are operated simultaneously, and hypoxia induction is carried out 4 hours later. Option 2: 4 hours after cell seeding, inhibitor treatment and hypoxia induction are carried out simultaneously. 24 hours sustained hypoxia incubation is performed after hypoxia induction in both options. The most typical area of cell invasion in each culture insert is photographed and showed. (200x original magnification)

Although no much difference of cell and cluster morphology could be observed between option 1 and option 2 under microscope during the growth and invasion process after seeding (data not shown), very rare cells invaded in option 2 of all cell lines. U87/U251 seldom invaded in both options. Mesenchymal BTIC12/13 of some experimental conditions invaded profoundly in option 1. Proneural BTIC17/18 of some experimental conditions invaded moderately and mildly respectively in option 1. In general, invasion ability of all cell lines was significantly stronger in option 1 than in option 2. Therefore, option 1 was selected and used in subsequent experiments.

Hypoxia seemed more important in enhancing invasion in BTIC18 and reducing invasion in BTIC17. Both U104 and DMSO played a big role in the inhibition of cell invasion. However, this was no statistical significance because of small samples. In addition, there was an obviously heterogeneous invasive performance even in same cell line and same experimental condition, as well as between repeated experiments (data not shown). The morphology of invasive cells (BTIC12 without treatment) were not clear by using ready-to-use pre-coated Matrigel insert, self-made Matrigel coated insert would be used in subsequent experiments.

3.8.1.2 Results of second pre-experiment

The second pre-experiment was carried out without inhibitor treatment to investigate: first, whether cells invaded more in the medium diluted Matrigel (referenced from Li et al [265]); second, the optimized cell number for invasion of each cell line; third, if the punctured membrane played a role in local cell invasion; fourth, invasiveness of BTIC13 in the presence of chemo-attractant in lower compartment. The usage of human serum as chemo-attractant was referenced from experimental protocol of Ries et al.[266], and was also because of homologous to human GBM in comparing with FBS. Different cell number for seeding (depending on cell lines) was also reported by Higa et al.[267] and Kahlert et al.[268], because too many invaded cells were not easy for quantitative analysis.

A		U87			U251		
		10,000cells	50,000cells	100,000cells	10,000cells	50,000cells	100,000cells
Normoxia	Water	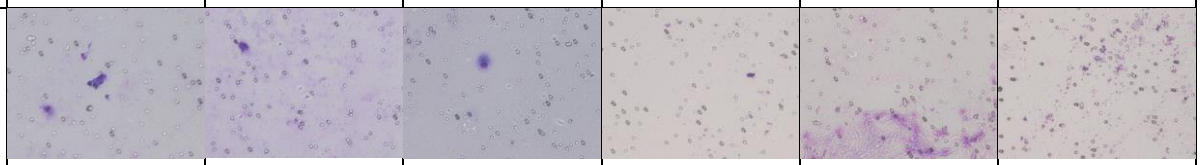					
	Medium	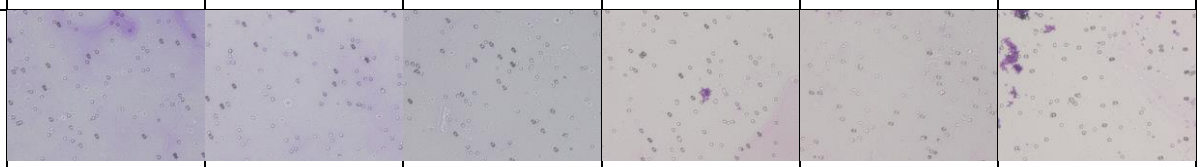					
Hypoxia	Water	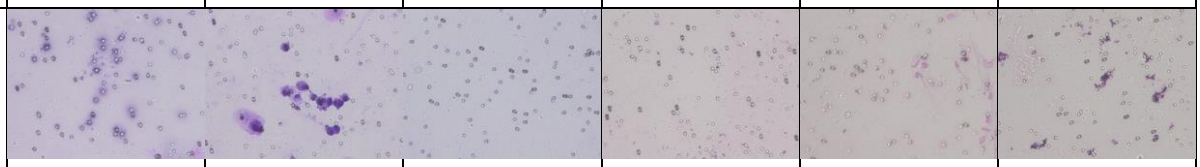					
	Medium	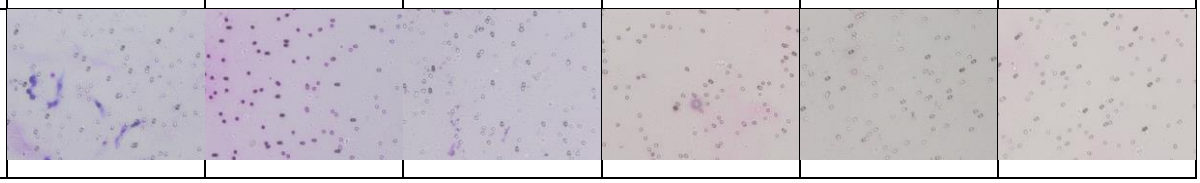					

B		BTIC12			BTIC13		
		10,000cells	50,000cells	100,000cells	10,000cells	50,000cells	100,000cells
Normoxia	Water	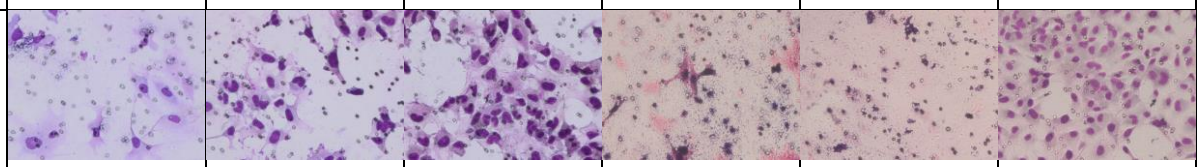					
	Medium	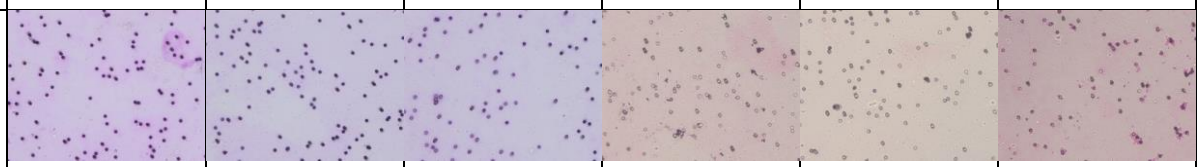					
Hypoxia	Water	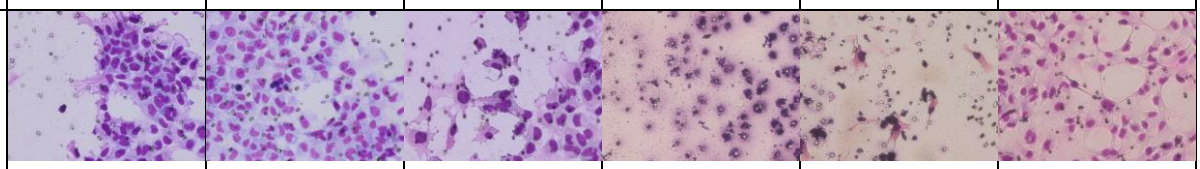					
	Medium	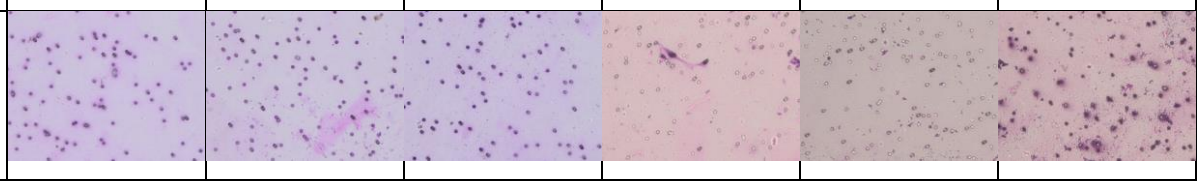					

C		BTIC17			BTIC18		
		10,000cells	50,000cells	100,000cells	10,000cells	50,000cells	100,000cells
Normoxia	Water	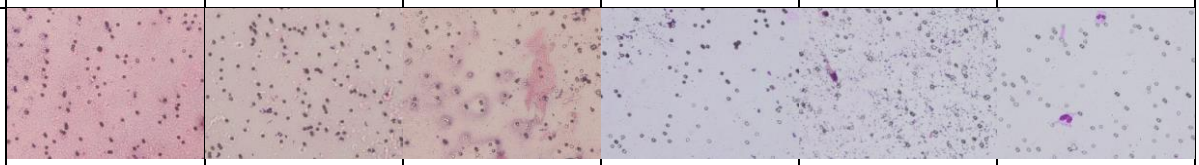					
	Medium	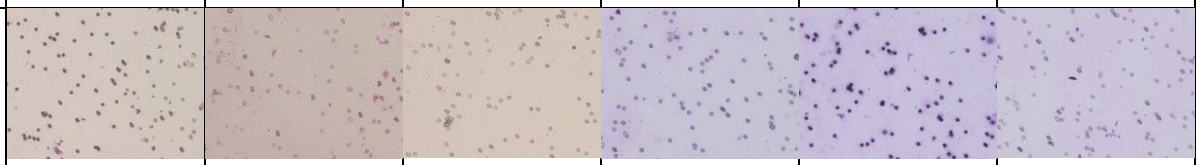					
Hypoxia	Water	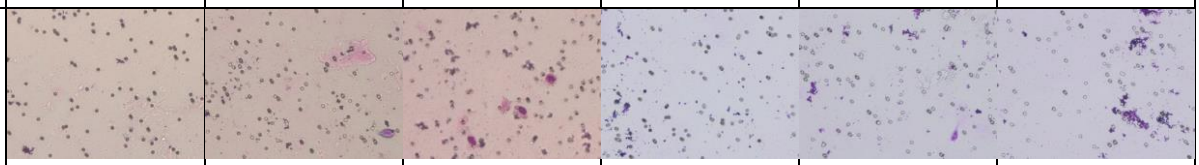					
	Medium	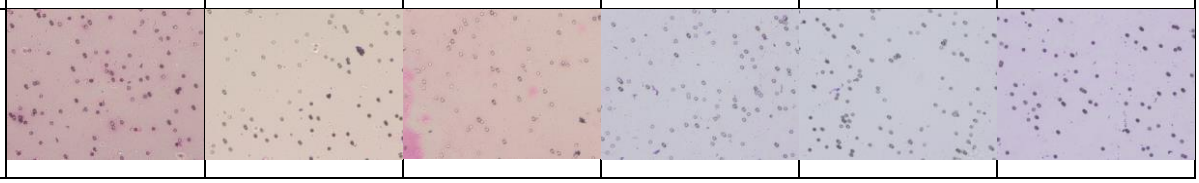					

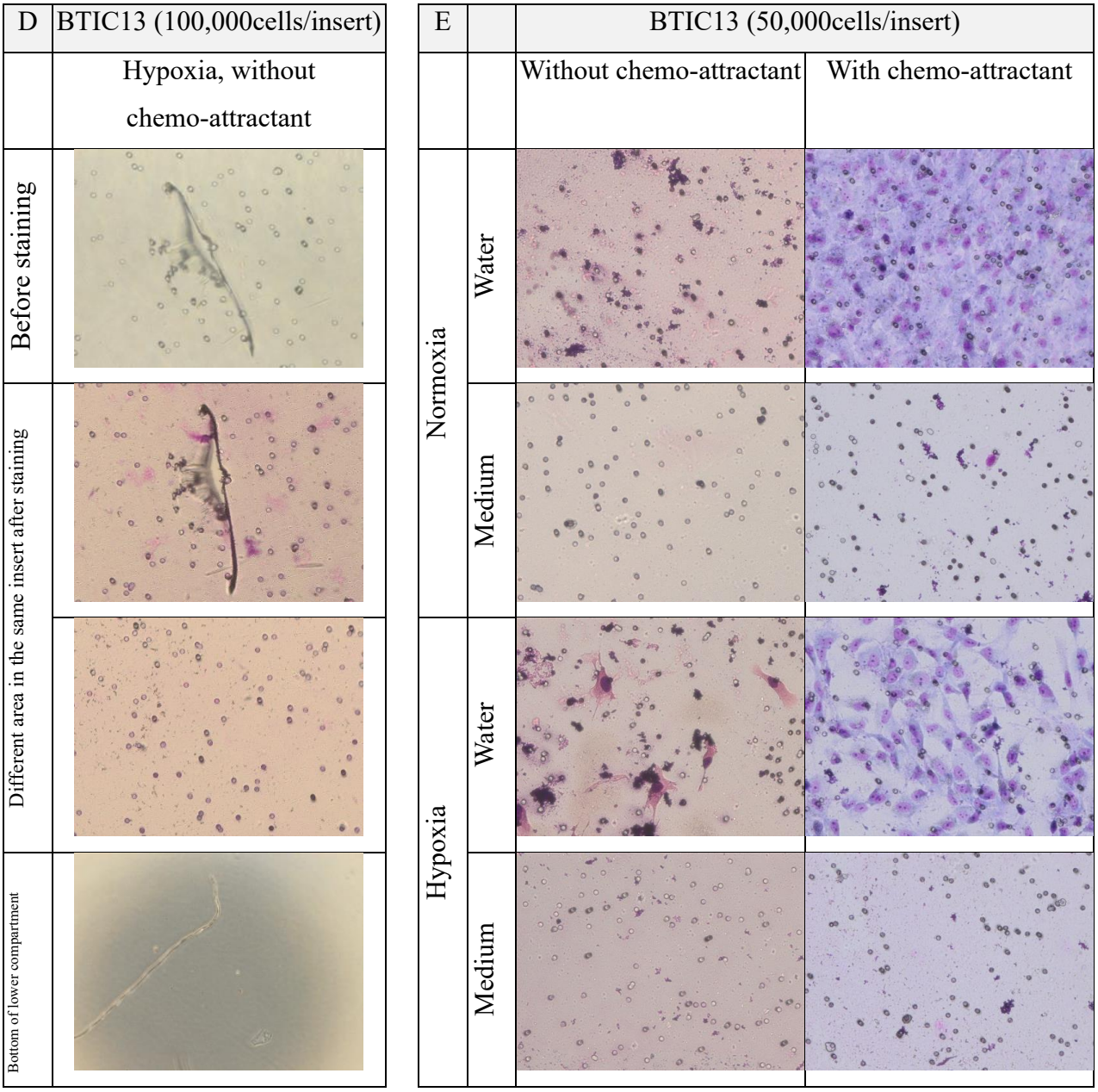

Figure 3.9 The second pre-experiment results of invasion

(A to C) Cells are seeded with different number under normoxia and hypoxia without inhibitor treatment. Water or medium diluted Matrigel are also investigated. Other processes are the same with option 1 in the first pre-experiment. (D) Photos represent the invasiveness of BTIC13 in the punctured membrane area before and after staining, as well as other area in the same membrane and bottom of lower compartment. (E) The invasiveness of BTIC13 is tested with or without chemo-attractant, as well as different dilution solutions of Matrigel under normoxia and hypoxia. The most typical area of cell invasion in each culture insert is photographed and showed. (200x original magnification) Bottom of lower compartment (20x original magnification)

Not much difference of cell and cluster morphology could be seen between water and medium diluted Matrigel groups under microscope during the growth and invasion process after seeding (data not shown), while very rare cells invaded in medium diluted Matrigel of all cell lines. Seldom cells of U87/U251 invaded in water diluted Matrigel which was consistant with the results of first pre-experiment. Mesenchymal BTIC12/13 invaded much in water diluted Matrigel, and this was also consistant with the results of first pre-experiment. Proneural BTIC17/18 seldom invaded in water diluted Matrigel, and this was different with the first pre-experiment. In general, cell invasion was significantly stronger in water diluted Matrigel than in medium diluted Matrigel. Therefore, water diluted Matrigel would be used continually in subsequent experiments. Hypoxia and cell number seemed play a moderate role of invasion in invasive Mesenchymal BTICs. Accidentally punctured membrane did not affect the result of cell invasion. The difference of invasive performance in the same membrane again presented the heterogeneity. Chemo-attractant in lower compartment significantly enhanced the invasion ability of BTIC13.

3.8.1.3 Results of third pre-experiment

In view of the strong chemotaxis of human serum in the second pre-experiment, and in order to maintain the balance of the experimental conditions in all cell lines, the third pre-experiment was carried out to investigate the effect of without or with chemo-attractant on invasion of all cell lines under normoxia. This was also in line with the experimental methods reported in the literatures everywhere. Because of the powerful chemotaxis of chemo-attractant, cell number for seeding should be optimized again in each cell line.

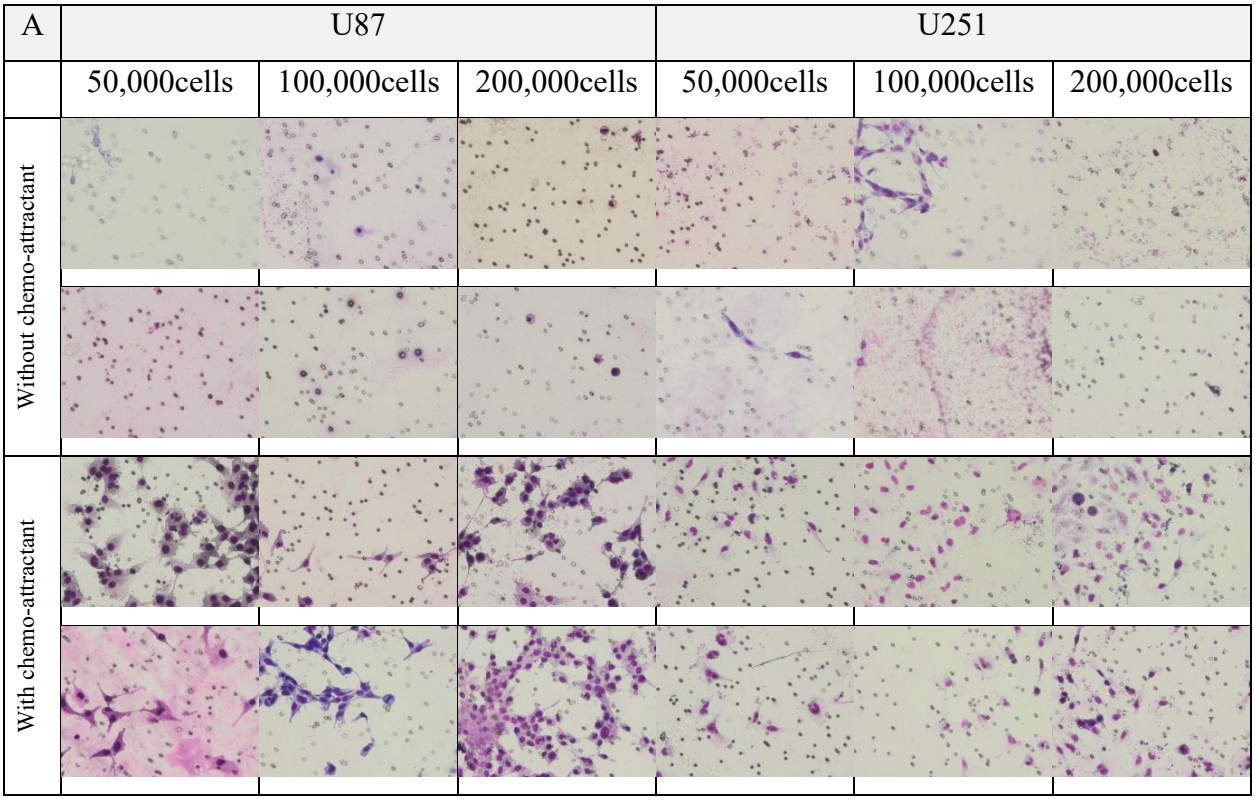
A
U87
U251
50,000cells
100,000cells
200,000cells
50,000cells
100,000cells
200,000cells
Without chemo-attractant
With chemo-attractant

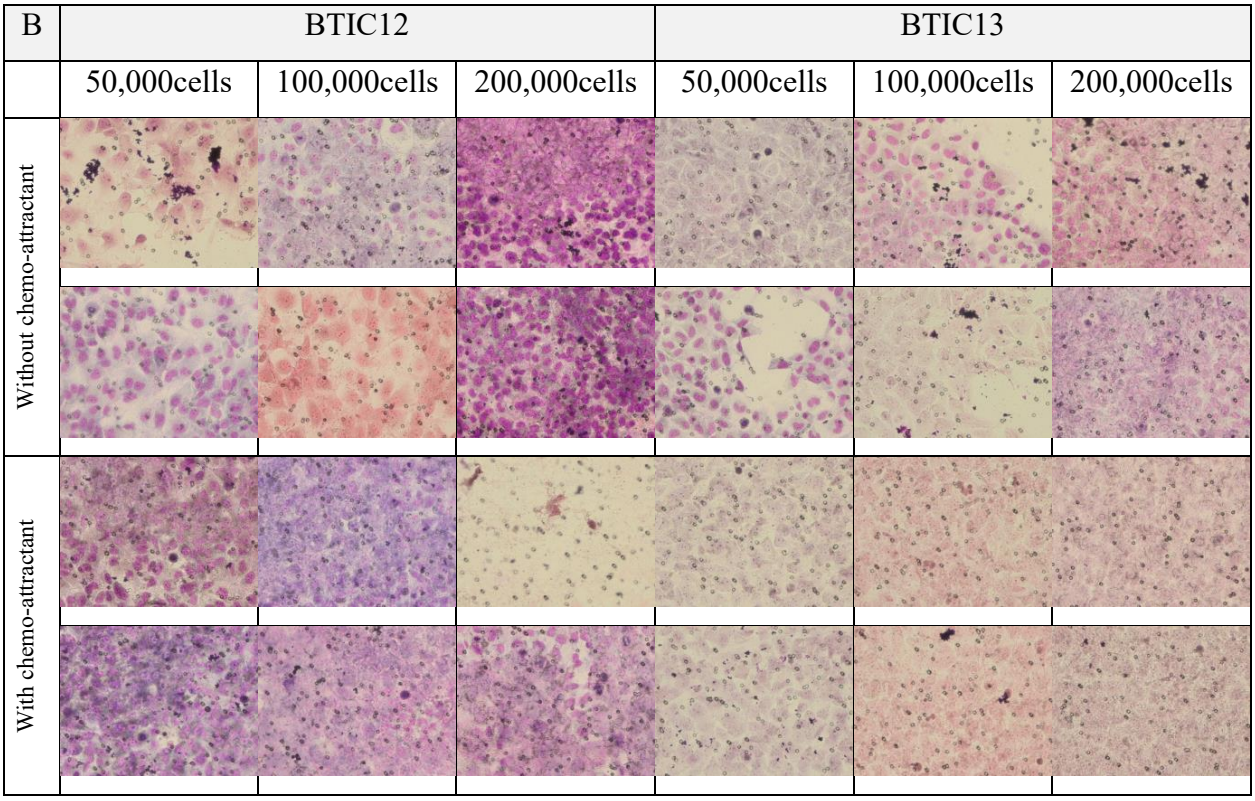
B
BTIC12
BTIC13
50,000cells
100,000cells
200,000cells
50,000cells
100,000cells
200,000cells
Without chemo-attractant
With chemo-attractant

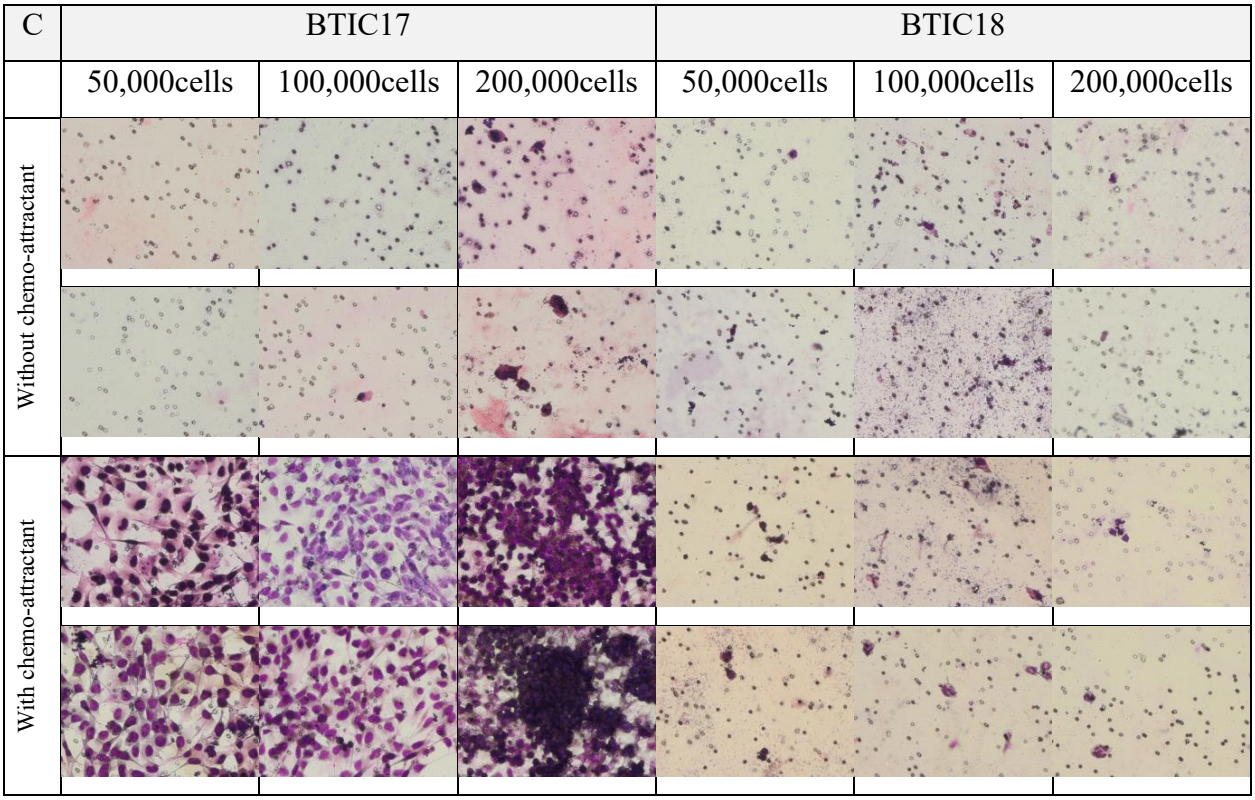

Figure 3.10 The third pre-experiment results of invasion

Cells are seeded with different number under normoxia without inhibitor treatment. Medium in lower compartment without or with chemo-attractants are also investigated. Other processes are the same with option 1 in the first pre-experiment. The most typical area of cell invasion in each culture insert is photographed and showed. (200x original magnification)

No distinct performance change of cell and cluster morphology could be observed between groups of absence and presence of chemo-attractant under microscope during the growth and invasion process after seeding (data not shown), while different degree of enhanced invasion ability in all cell lines could be seen in chemo-attractant groups compared with none chemo-attractant groups. The invasiveness of all cell lines in condition without chemo-attractant was consistent with the results of second pre-experiment. That was Mesenchymal BTIC12/13 invaded much, both established cell lines and Proneural BTICs invaded much less profoundly. In condition with chemo-attractant, U87/U251 invaded moderate, BTIC12/13 invaded much despite high before, BTIC17 also invaded much and presented the most sensitivity to chemo-attractant, BTIC18 showed no sensitivity to chemo-attractant. In general, chemo-attractant showed a strong chemotaxis in all cell lines except BTIC18. Therefore, subsequent pre-experiments and actual

experiments would be carried out with the use of chemo-attractant. Cell number seemed played a moderate and variable role of invasion. Heterogeneity of invasive performance was also presented in this pre-experiment.

3.8.1.4 Results of fourth, fifth, sixth, seventh and eighth pre-experiments

Based on the results of third pre-experiment that BTIC12/13/17 invaded much in the presence of chemo-attractant, cell numbers for seeding of BTIC12/13/17 were reduced drastically in the fourth pre-experiment, cell numbers for seeding of established cell lines were also reduced. This was because too many invasive cells were not easy for quantitative analysis. After rechecking the results of cell viability experiment, different concentrations of U104 and DMSO were investigated in the fourth pre-experiment under hypoxia. Fine-tuning of cell number for seeding was carried out in fifth and sixth pre-experiments under normoxia and hypoxia. Ries et al. reported an experimental protocol that cells were pre-incubated for 30 minutes with inhibitor before being pipetted in the upper compartment. [266] Thence, cell invasion was tested by seeding after 30 minutes treatment of U104/DMSO in sixth pre-experiment. This might help to relieve stress of cells. However, waiting for 30 minutes treatment before seeding did not play a role in experimental results. The optimized cell number and U104/DMSO concentration for cell invasion was showed in Table 3.8

Cell lines	Number of cells for seeding/insert	U104/DMSO concentration
U87	100,000/insert	60μM
U251	50,000/insert	60μM
BTIC12	20,000/insert	60μM
BTIC13	20,000/insert	60μM
BTIC17	20,000/insert	100μM
BTIC18	200,000/insert	100μM

Table 3.8 Optimized cell number and U104/DMSO concentrations for cell invasion

Two extra phenomena were discovered in the fourth, fifth and sixth pre-experiments. One phenomenon was that the invasiveness of cells was not much influenced with the use of U104. This was reminiscent that whether the inhibitor effect time was possibly too short. Therefore, cell invasion of U251/BTIC12/BTIC17 with 4 days of inhibitor action was investigated in the seventh

pre-experiment. No better experimental result could be seen. (data not shown) Another phenomenon was that most cell lines showed reduced invasion ability as the increased cell passage number in conditions with chemo-attractant under both normoxia and hypoxia. For instance, U251 seldom invaded since the fifth pre-experiment. BTIC12/13/17 represented significantly reduced invasion ability gradually, and BTIC17 did not invade anymore after the seventh pre-experiment (data not shown for the failed actual experiment of BTIC17). U87 also showed reduced invasion ability gradually. BTIC18 seldom invaded in all conditions. The eighth pre-experiment was carried out by using low generation and less passaged cells of all cell lines under normoxia. All cell lines (including BTIC18) invaded like early pre-experiments. (data not shown) In addition, obvious heterogeneity could be observed again in identical repeated inserts, cell line and experimental condition (data not shown).

3.8.1.5 Morphological changes of clusters and cells

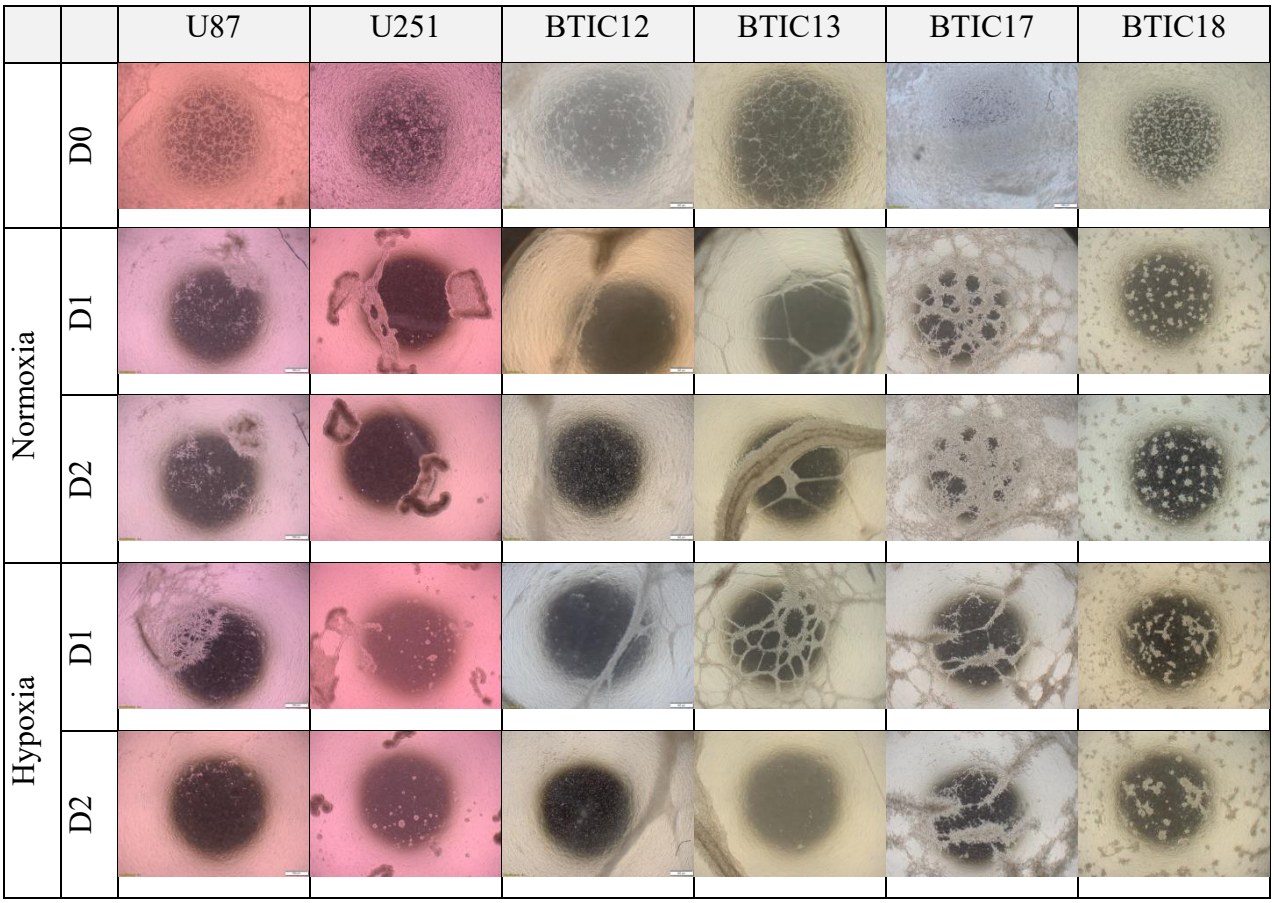

Figure 3.11 The cluster morphology of all cell lines during the growth and invasion process after seeding (20x original magnification)

The morphology of cell cluster in upper compartment during invasive process was photographed. U87/U251 showed clusterd growth and BTIC12/13/17 showed doming growth like bundles. BTIC18 showed small cluster-like growth. The clusterd and doming growth pattern increased with time. Heterogeneity of cluster morphology could be seen (data not shown). The morphological changes of cluster were recorded because some cell lines did not invade in the initial pre-experiments. Based on the 'go-or-grow' theory, if the seeded cells clustered and proliferated locally, they did not invade anymore. After checking and comparing all the photos of cluster morphology during invasive process, there was no obvious correlation between growth patterns or cluster morphology and cell invasion ability. Clusterd and doming growth cells were actually non-invasive cells. This also illustrated that not all BTICs invaded in the same cell line, and this might be attributed to some cell biology characteristics changed after seeding in some BTICs. In addition, it could be seen from the photos of Day 0 in all cell lines that seeded cells were evenly distributed in each insert. By focusing on pores of membrane under 200-time magnification, the morphology of cells in upper compartment during invasive process was photographed (data not shown). However, it could not be determined whether these cells had passed through the membrane without staining. Futhermore, because some invasive cells might detach and drop onto the basement, the basement of lower compartment was also photographed in all invasion experiments (data not shown). No cells could be seen on the basement of lower compartment in most instances. In the condition of mesenchymal cell line with the use of chemo-attractant, dozens of cells could be seen on the basement of lower compartment, while they could be negligible by comparing with the thousands of invasive cells. This might be attributed to the strong adherence of all cell lines except BTIC18, as well as the short invasion time. Invasive cells might not have enough time to detach and drop onto the basement.

In general, many experimental conditions and operating steps had been optimized in pre-experiments. Overall, results of all pre-experiments showed heterogeneity of cell invasion. Established cell line U87/U251 seldom invaded in the absence of chemo-attractant and moderate invaded in the presence of chemo-attractant. Mesenchymal BTIC12/13 represented the strong invasive ability in both absence and presence of chemo-attractant. The invasive ability of proneural BTIC17 was strong only in the presence of chemo-attractant. Proneural BTIC18 rarely invaded in pre-experiment 1-7 in both absence and presence of chemo-attractant. With the increase of cell passage number, cell invasion ability reduced gradually in most cell lines and

even disappeared in BTIC17. Low generation and less passaged cells of all cell lines (including BTIC18) invaded like early pre-experiments. In addition, no obvious cell morphological changes could be seen under microscope between normoxia and hypoxia in pre-experiments. There was also no obvious correlation between growth patterns or cluster morphology and cell invasion ability.

3.8.2 Actual experiment results of GBM cell invasion

Cell morphology of each condition and cell line was photographed to exhibit the possible influence by 24-hour hypoxia and treatments.

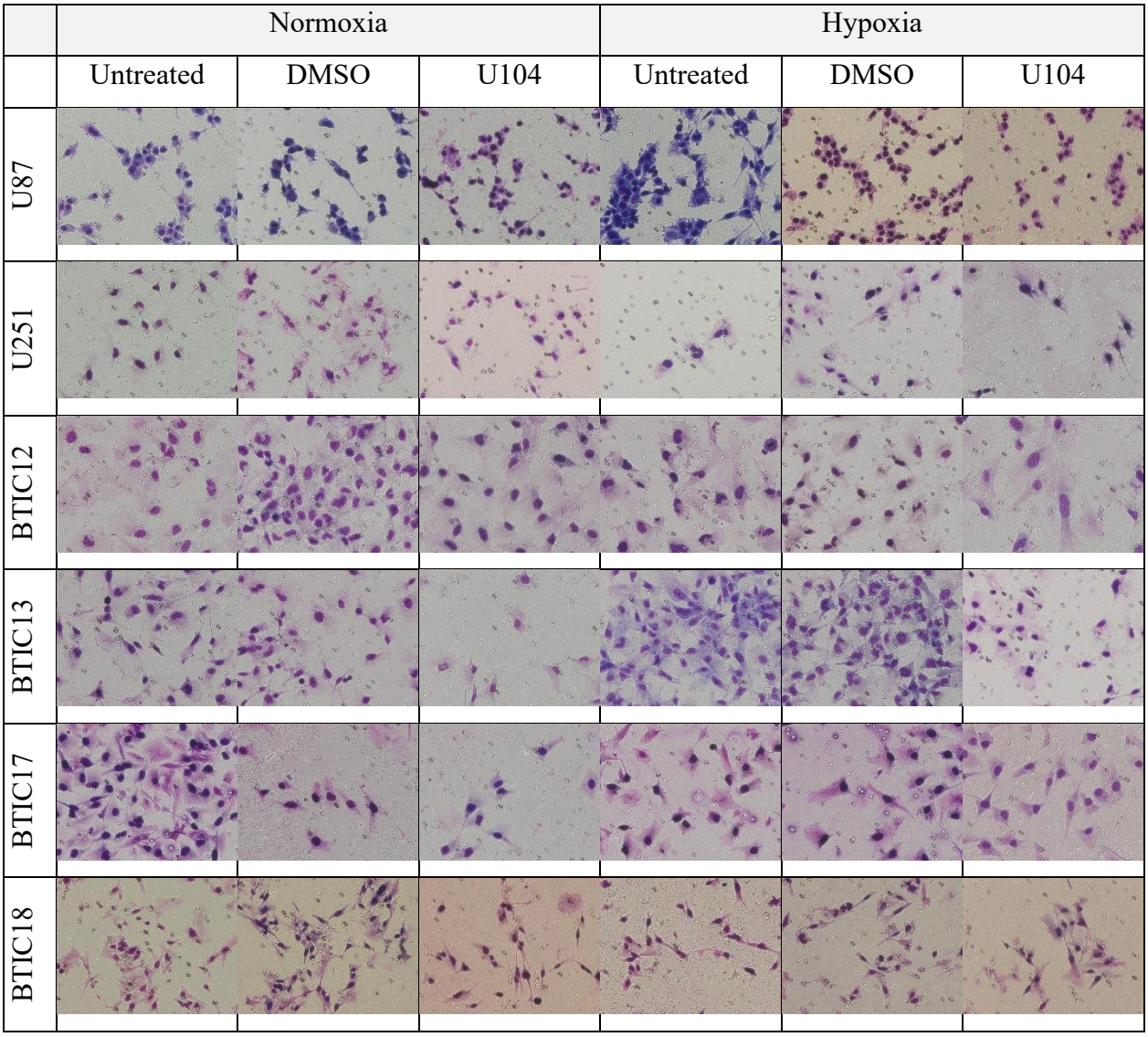

Figure 3.12 Representative invaded cell morphology of each cell line in different groups under normoxic and hypoxic conditions (200x original magnification)

Note: Photos mainly display the cell morphology, and the quantitative results of cell invasiveness please refer to Figure 3.14.

Heterogeneity caused by artificial staining could be seen, while this did not affect the observation of cell morphology. No obvious morphological changes of invaded cells could be observed between different treatment groups as well as normoxia and hypoxia in same cell line under optical microscope in actual experiments. This was consistent with the results of pre-experiments. Long protrusion of cells could be seen in both normoxia and hypoxia. Established cell lines, mesenchymal BTICs and proneural BTIC17 represented similar cell morphology with normal cell culture. It was worth noting that BTIC18 showed mesenchymal-like fusiform which was different with sphere or clusterd morphology in normal cell culture (Figure 2.1).

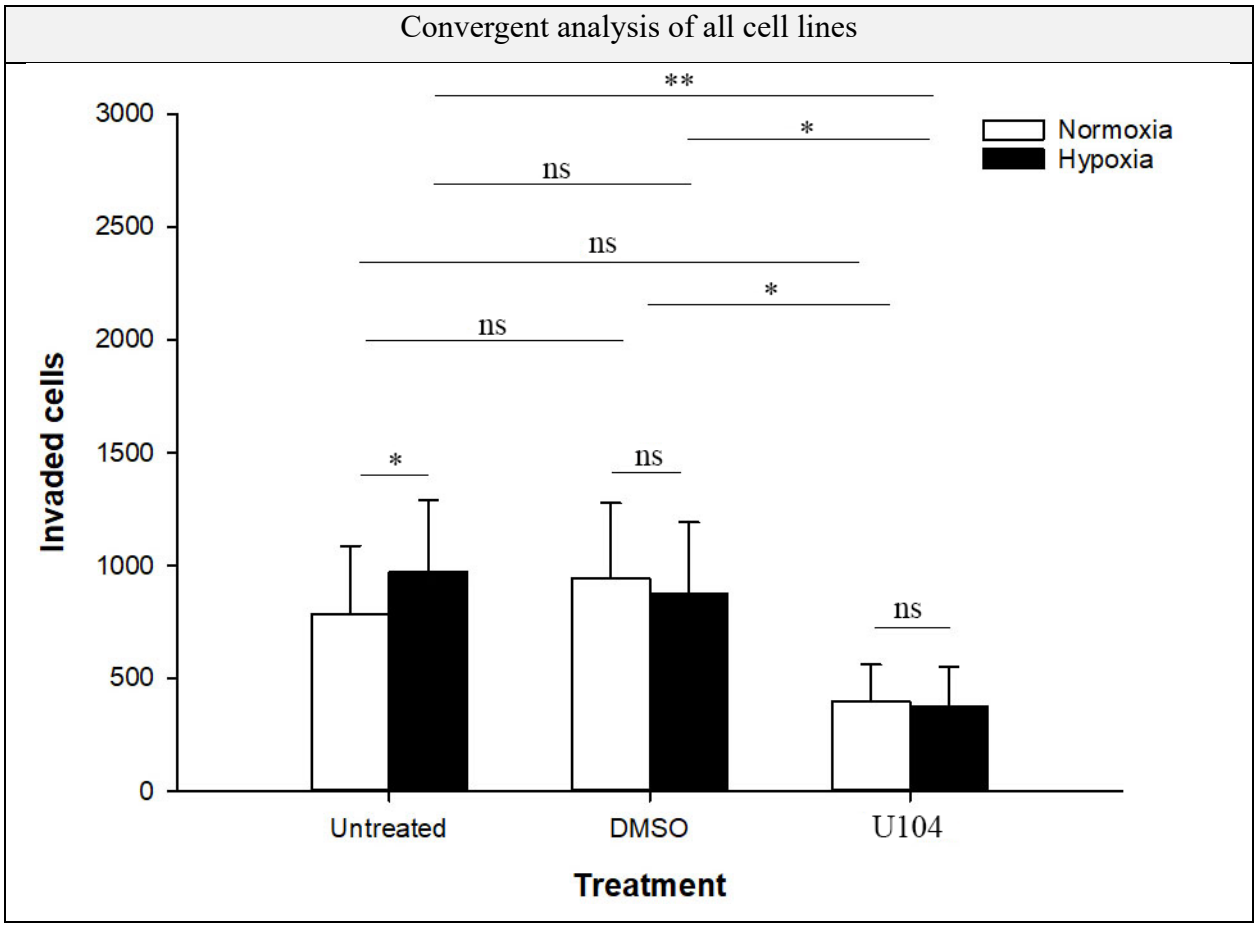

Figure 3.13 Convergent quantitative results of cell invasion of all GBM cell lines in different groups under normoxia and hypoxia (Bar= mean ± SD, *$p < 0.05$; **$p < 0.01$, ns= not significant. Two-way ANOVA, Holm-Sidak method)

Convergent analysis (pooled data of all six GBM cell lines) showed statistically significant increment (1.24 times) of cell invasion by comparing hypoxia and normoxia in untreated group ($p < 0.05$). Meanwhile, no statistically significant differences could be seen in DMSO and U104 groups (Three labels above and close to SD bars). Three lower left labels represented the comparison between groups under normoxic condition. There were no statistically significant differences of cell invasion between U104 and untreated groups as well as between DMSO and untreated groups, although clear reduction and increment respectively could be seen. Most importantly, there was statistically significant reduction of cell invasion between U104 and DMSO groups ($p < 0.01$). Three upper right labels represented the comparison between groups under hypoxic condition. In contrast, there was no statistically significant difference of cell invasion between DMSO and untreated groups. Meantime, there were statistically significant reductions between U104 and DMSO groups ($p < 0.05$), as well as between U104 and untreated groups ($p < 0.01$). Invaded cell number reduced 57.8% and 57.3% in U104 treatment under normoxic and hypoxic conditions respectively in comparing with DMSO control. Therefore, these results illustrated that U104 instead of DMSO played an important role in the inhibition of cell invasion of GBM cell lines under both normoxic and hypoxic conditions. (Figure 3.13)

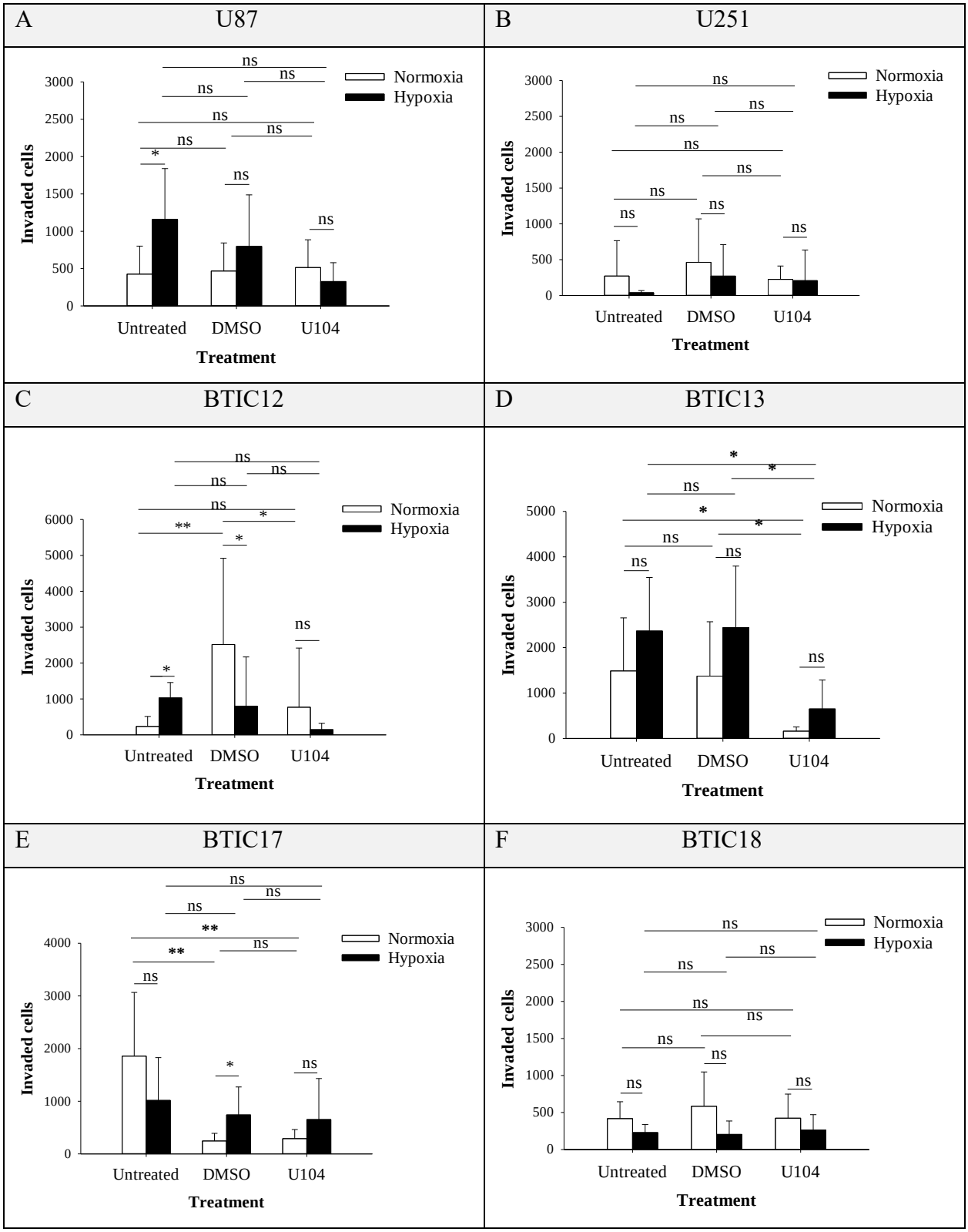

Figure 3.14 Separate quantitative results of cell invasion of each GBM cell line in different groups under normoxia and hypoxia (Bar= mean ± SD, *$p < 0.05$; **$p < 0.01$, ns= not significant. Two-way ANOVA)

Results of Figure 3.14 presented the bar graphs and statistical comparisons of cell invasion with various treatments under normoxic and hypoxic conditions in six GBM cell lines separately.

In U87 (Figure 3.14 A), there were no statistically significant differences between various intergroup comparisons except 2.72 times increment by comparing hypoxia with normoxia in untreated group ($p < 0.05$), despite there were clear reductions after the addition of DMSO and U104 under hypoxic condition.

In U251 (Figure 3.14 B), there were no statistically significant differences between various intergroup comparisons which included normoxia and hypoxia as well as different treatments. This might be because of the high standard deviation.

In BTIC12 (Figure 3.14 C), there were a statistically significant increment (4.40 times) of cell invasion by comparing hypoxia and normoxia in untreated group, as well as a statistically significant reduction (68.2%) in DMSO group ($p < 0.05$). There was no statistically significant in U104 group, although a clear reduction could be seen after 24-hour hypoxia (three labels above and close to SD bars). In addition, no statistically significant differences could be seen between groups under hypoxic condition, although gradual decreasements were there (three upper right labels). Under normoxic condition (three lower left labels), there was statistically significant increment (10.75 times) of cell invasion with the use of DMSO in comparing with untreated group ($p < 0.01$). There was also statistically significant reduction (69.4%) with the addition of U104 in comparing with DMSO group ($p < 0.05$). Meanwhile, no statistically significant difference was observed between U104 and untreated groups. This implicated that the enhancing effect of DMSO on cell invasion was offset by the inhibitory effect of U104.

In BTIC13 (Figure 3.14 D), there were no statistically significant differences between normoxia and hypoxia (three labels above and close to SD bars), although the increments of cell invasion could be seen in all groups. This might attribute to the high standard deviation. In addition, no statistically significant differences could be seen between DMSO and untreated groups under both normoxic and hypoxic conditions. There were statistically significant reductions of cell invasion with the addition of U104 in comparing with DMSO group and untreated group under both normoxia and hypoxia ($p < 0.05$). The reductions were 88.4% and 89.3% respectively under normoxia. The reductions were 73.4% and 72.6% respectively under hypoxia.

In BTIC17 (Figure 3.14 E), there were clear reduction in untreated group and increments in DMSO and U104 groups by comparing the cell invasion under normoxia and hypoxia, however

only DMSO group showed statistically significant ($p < 0.05$). Additionally, no statistically significant differences could be observed between all groups under hypoxia (three upper right labels). Under normoxic condition, there were statistically significant reductions by comparing DMSO group with untreated group (86.8%) ($p < 0.01$), as well as comparing U104 group with untreated group (84.4%) ($p < 0.01$). Meanwhile, there was no statistically significant difference between U104 and DMSO groups. (three lower left labels) This meant the statistically significant reduction of cell invasion was attributable to the inhibitory effect of DMSO instead of U104.

In BTIC18 (Figure 3.14 F), there were no statistically significant differences between all intergroup comparisons, although clear reductions of cell invasion could be seen by comparing hypoxia and normoxia in all groups.

In general, there were statistically significant increments of cell invasion after 24-hour hypoxia only in untreated group of U87 and BTIC12 as well as DMSO group of BTIC17. There was statistically significant reduction in DMSO group of BTIC12 under hypoxia. There were no statistically significant reductions after addition of U104 by comparing with DMSO control in established cell lines (U87, U251), mesenchymal BITC12 under hypoxic condition and proneural cell lines (BITC17, BTIC18). Meanwhile, there were statistically significant reductions after addition of U104 in mesenchymal BITC12 of normoxic condition and BTIC13. In addition, DMSO played a role in statistically significant increment in BTIC12 and reduction in BTIC17 under normoxic condition. Therefore, the use of DMSO as control was very necessary to show the net effect of U104 because of its effect on cell invasion in specific cell lines and experimental conditions. These experimental data and statistical analysis illustrated the influences on invasion by U104 as well as DMSO and hypoxia were cell line dependent. Mesenchymal BTIC12 (normoxia)/13 (normoxia and hypoxia) were the most sensitive to CAIX inhibitor in all tested GBM cell lines of different molecular subtypes. Proneural BTICs were the most insensitive to U104 because of the use of the highest inhibitor concentration (Table 3.8).

	Mean of invaded cell number / Seeded cell number = Standardized ratio of cell invasion		
Cell lines	Normoxia	Hypoxia	Normoxia+ Hypoxia
U87	$425.44/100*10^{3}=4.25*10^{-3}$	$1157.88/100*10^{3}=11.58*10^{-3}$	$791.66/100*10^{3}=7.92*10^{-3}$
U251	$271.25/50*10^{3}=5.43*10^{-3}$	$38.81/50*10^{3}=0.78*10^{-3}$	$155.03/50*10^{3}=3.10*10^{-3}$
BTIC12	$234.06/20*10^{3}=11.70*10^{-3}$	$1029.06/20*10^{3}=51.45*10^{-3}$	$631.56/20*10^{3}=31.58*10^{-3}$
BTIC13	$1487.13/20*10^{3}=74.36*10^{-3}$	$2367.56/20*10^{3}=118.38*10^{-3}$	$1927.34/20*10^{3}=96.37*10^{-3}$
BTIC17	$1857.75/20*10^{3}=92.89*10^{-3}$	$1015.06/20*10^{3}=50.75*10^{-3}$	$1436.41/20*10^{3}=71.82*10^{-3}$
BTIC18	$416.75/200*10^{3}=2.08*10^{-3}$	$228.25/200*10^{3}=1.14*10^{-3}$	$322.50/200*10^{3}=1.61*10^{-3}$

Table 3.9 Standardized ratio of cell invasion in untreated group of each cell line under normoxia and hypoxia

BTIC13/17 without any treatments showed relatively higher number of invaded cells under normoxia or pooled values (numerators in the left and right columns) than other cell lines. U87 and BTIC12/13/17 without any treatments showed relatively higher number of invaded cells under hypoxia (numerators in the middle column). U251 showed the lowest number of invaded cells under all conditions. However, this did not mean that they had relatively higher or lower cell invasive ability because of different cell number for seeding (denominators). Therefore, standardized ratios of cell invasion by using mean of invaded cell number divided by seeded cell number were calculated. Standardized ratios showed that mesenchymal BTIC12/13 and proneural BTIC17 possessed much higher invasive ability than other cell lines under normoxia and hypoxia as well as pooled analysis. Meanwhile, proneural BTIC18 possessed the much lower invasive ability in all conditions. This was consistent with the results of pre-experiments. (Table 3.9)

	$p < 0.05$		
Comparison between cell lines	Untreated	DMSO	U104
U87 vs. U251	No	No	No
U87 vs. BITC18	No	No	No
U87 vs. BITC12	No	Yes	No
BITC18 vs. U251	No	No	No
BITC17 vs. U87	No	No	No
BITC17 vs. U251	Yes	No	No
BITC17 vs. BITC18	Yes	No	No
BITC17 vs. BITC12	No	Yes	No
BITC13 vs. U87	Yes	Yes	No
BITC13 vs. U251	Yes	Yes	No
BITC13 vs. BITC18	Yes	Yes	No
BITC13 vs. BITC17	No	Yes	No
BITC13 vs. BITC12	Yes	No	No
BITC12 vs. U251	No	Yes	No
BITC12 vs. BITC18	No	Yes	No

Table 3.10 Pairwise multiple comparisons between cell lines in different groups in terms of cell invasion (Two-way ANOVA, Holm-Sidak method)

	$p < 0.05$						
Comparison between treatment groups	Convergent	U87	U251	BTIC12	BTIC13	BTIC17	BTIC18
Untreated vs. DMSO	No	No	No	Yes	No	Yes	No
U104 vs. untreated	Yes	No	No	No	Yes	Yes	No
U104 vs. DMSO	Yes	No	No	Yes	Yes	No	No

Table 3.11 Pairwise multiple comparisons between different treatment groups in each cell line in terms of cell invasion (Two-way ANOVA, Holm-Sidak method)

Data of normoxia and hypoxia in same group were also pooled, and the cell invasion between cell

lines were analyzed in different groups. There were statistically significant differences in 6 pairs (BITC17 vs. U251；BITC17 vs. BITC18；BITC13 vs. U87；BITC13 vs. U251；BITC13 vs. BITC18；BITC13 vs. BITC12) of untreated group, 8 pair (U87 vs. BITC12；BITC17 vs. BITC12；BITC13 vs. U87；BITC13 vs. U251；BITC13 vs. BITC18；BITC13 vs. BITC17；BITC12 vs. U251；BITC12 vs. BITC18) of DMSO group. No statistically significant differences could be seen in all comparisons between cell lines in U104 group. Some of the statistically significant differences between cell lines changed after the addition of DMSO and U104. This uncovered the heterogeneity of influence by different treatments on cell invasion between cell lines. (Table 3.10)

Statistical analysis results of pooled values of normoxia and hypoxia showed the comparisons between different treatment groups in each cell line or all cell lines. There were statistically significant differences between U104 and DMSO in BTIC12/13. This meant only mesenchymal BTICs were sensitive to U104 in comparing with other cell lines. In addition, DMSO did play a role in cell invasion of BTIC12/17. (Table 3.11)

In general, our results revealed that: 1. Hypoxia increased cell invasiveness only in specific cell lines (U87 and BTIC12) and experimental conditions. 2. There was a significant heterogeneity in the invasiveness of all cell lines. Mesenchymal BTIC12/13 and proneural BTIC17 (only in condition with the use of chemo-attractant) displayed a significant higher invasiveness than other cell lines. Proneural BTIC18 possessed much lower invasive ability. 3. CAIX inhibitor U104 reduced cell invasion which was cell line dependent and only in mesenchymal BTIC12 (normoxia)/13(normoxia and hypoxia).

4 Discussion

The extensivelly infiltrative and invasive nature of GBM is an important reason that GBM cannot be cured and always recur.[49, 57, 58] CAIX is overexpressed in GBM but is virtually absent in the normal brain.[181, 269] CAIX participates in extracellular acidification and promotes invasion of tumor cells.[153] The inhibition of CAIX is inferred as a potential target for antitumor treatment.[270] In this scenario, the impact of CAIX inhibition on molecular and biofunctional changes in GBM needed to be investigated, because it may potentially reveal a new therapeutic target.

In our present study, we demonstrated that in most GBM cell lines the surprisingly high normoxic CAIX expression levels were related to the PI3K pathway rather than cell confluence on both transcription and translation levels. In addition, and as expected, the mRNA expression of *CAIX* was strongly induced by hypoxia in all cell lines. In contrast, the CAIX protein expression was induced by hypoxia only in the established cell lines U87 and U251, which might be attributed to the high protein stability post-transcriptionally. To clarify the effect of CAIX on GBM cell viability and invasion, we performed experiments to detect the CAIX related biofunctional changes by using small molecule inhibitor U104. Experimental results showed the inhibition effect of U104 on cell viability and invasion in GBM cells but were cell line dependent. U87 and BTIC18 displayed a lower sensitivity to U104 than other cell lines in cell viability assay. Looking at invasive behavior, only the mesenchymal BTICs were sensitive to U104 and displayed a much higher invasion ability compared to other cell lines.

Collectively, our research demonstrates that CAIX is a potential metabolic target for the treatment of patients with GBM but only in specific cell lines.

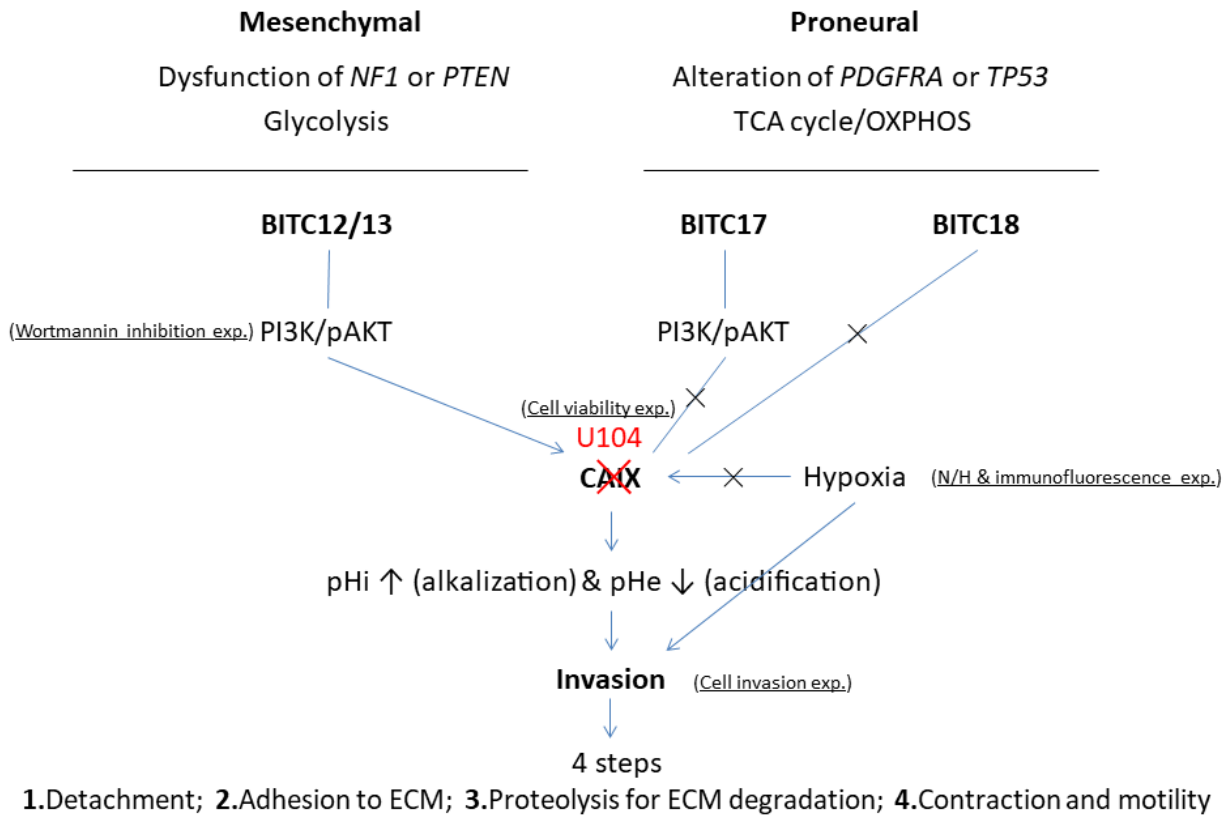

Figure 4.1 Schematic diagram of this research (exp.= experiment)

4.1 Expression of CAIX under normoxia and hypoxia

Before the actual experiments addressing the main hypothesis of this project, we optimized the experimental conditions such as methods of hypoxia induction and cell harvest. From the experimental result of Scraper-Accutase/Trypsin comparative experiment, we could see a clearly baseline expression of CAIX in all 6 GBM cell lines under normal oxygen condition. Subsequent low confluence and Wortmannin inhibition experiments showed same results. These results conflict with CAIX as a good hypoxia marker.[173] Actually, several experimental results confirmed that some cell lines showed a baseline CAIX expression under normoxic condition. While other experimental results represent negative expression of CAIX under normoxia.

Said et al. reported that early-passage of U87 and U251 cultured in DMEM with FBS had no bands of *CAIX* mRNA under 24 hours normoxia by Northern blot analysis. The expression of

CAIX mRNA was strongly upregulated at different intensity and duration of hypoxia, and showed cell-line specific patterns. On the protein level, U87 exhibited baseline expression of both CAIX and HIF-1α protein under normoxia, and no significant changes under various intensities and durations of hypoxia. U251 also represented a baseline expression of CAIX protein under normoxia. The increased CAIX protein expression was parallel to the prolonged hypoxia. HIF-1α protein was also constitutively expressed under normoxia, while exhibited more prounced induction under hypoxia. Therefore, they proposed that the expression of CAIX was regulated by both oncogene related signaling pathway and hypoxia.[271] In the same year, it was interesting that the same group reported U251 and two other established GBM cell lines showed weak bands of baseline *CAIX* mRNA expression under normoxia by comparing with previous and later experiments, although *CAIX* mRNA was still significantly upregulated under hypoxia. The author had no relevant explanation for that.[272] When investigating other hypoxia-related genes one year later, they repeated and confirmed the same result of the first report.[273] Three and six years later, Said et al. cooperated with Supuran et al. tested the same cell lines with the application of various inhibitors under 0.1% hypoxia by PCR and WB analysis. Same experimental results as in the first report were seen.[274, 275] They found undetectable bands of *CAIX* mRNA under normoxia and clear bands after 24 hours sustained hypoxia, as well as constitutive stable expression and hypoxia inducible expression of CAIX protein in U87 and U251 respectively. No detailed information was given regarding the glucose concentration of the medium, and the confluence of cell culture. These results are consistent to our results except that the CAIX protein expression of U87 was less reactive to hypoxia in Said's experiment compared to BTICs in our experiment. McIntyre et al. showed very low and low expression of mRNA and protein of CAIX respectively in U87 under normoxic condition, while both mRNA and protein were strongly induced by 72 hours hypoxia.[276] Huang et al. also showed lower baseline expression of CAIX under normoxia and highly inducible under hypoxia in both U87 and U251 on protein level.[277] Both results of McIntyre et al. and Huang et al. are consistent with our results in established cell lines on transcription and translation levels. The established cell lines display numerous changes in genomic and transcriptomic make up and are therefore poorly representative of primary GBMs. This may be the reason for the diverse expression of CAIX abovementioned.[136, 278, 279] Therefore, the investigation of CAIX expression in BTICs is necessary. Amiri et al. showed the baseline CAIX expression of both BTICs in 10-day

neurosphere 3D culture and U251 in traditional DMEM with FBS under normoxia. BTICs had a higher baseline expression of CAIX than U251. The expression of CAIX under hypoxic condition was not investigated in the experiment of Amiri et al.[280] There are no experimental reports so far about CAIX expression under normoxia and hypoxia based on the molecular classification of BTICs which are cultured in stem cell culture medium of monolayer adherent growth.

To verify the validity of our *in vitro* hypoxia technique, we tested the expression of *VEGF*, which is one of the most important and established hypoxia inducible genes in tumors including GBM.[166, 281] Expression of *VEGF* 165 and *VEGF* 121, the main isoform of *VEGF* expressed in CNS[260], were tested in our research. Our results showed baseline mRNA expression under normoxia and increased expression level after 24-hour sustained hypoxia of both *VEGF165 and VEGF121* in all 6 GBM cell lines. This fully proved the method of hypoxia induction actually worked in our experiment. Bache et al. reported relatively low expression of *CAIX* mRNA by qPCR in compared with other hypoxia induced genes (including *VEGF*) in GBM tissue.[282] This is consistent with our experimental results of very low expression of *CAIX* mRNA and baseline expression of *VEGF* mRNA under normoxia in both establishend cell lines and BTICs. (Figure 3.4 A) In addition, although Chédeville et al. did not show the absolute value of baseline mRNA expression under normoxia, ten to hundred folds increase of *CAIX* mRNA under hypoxia could be seen in both biopsy-derived primary culture GBM cell lines and U87.[283] The high fold value of *CAIX* mRNA induced under hypoxic condition by Chédeville et al. is consistent with our experimental result. In other words, the fold value of *CAIX* mRNA induced by hypoxia is significantly higher than other genes such as *VEGF* (Figure 3.4 B).

Most of the GBM cells used in this research grew very fast, the cell confluence was generally controlled to be less than or equal to 80% before seeding, although local high confluence within the culture was tolerated. The cell confluence marked in Figure 3.1 of PCR and WB results were the highest confluence among all experimental operation exercises and pre-experiments. Kaluz et al. proved that PI3K pathway activity was significantly increased in dense culture of Hela cell compared with sparse cell culture. The expression of CAIX is cell density-dependent and regulated by both PI3K pathway and a minimal level of HIF-1α.[199] Therefore, we performed the low confluence experiment to verify the effect of cell confluence on the expression of CAIX in GBM cells. In order to eliminate the possible influence of CAIX accumulation caused by high confluence and post-translational stability of proteins, all cell lines were subcultured in

low-medium confluence (less than 70%) for 2 weeks before seeding, and controlled as low as 30-40% confluence at harvest time. The experimental results still showed a baseline protein expression of CAIX. In contrast, there were no bands of *CAIX* mRNA by PCR in all cell lines of low confluence culture. (Figure 3.2) Collectively, although no direct comparison was done in one experiment in terms of CAIX expression between low and high confluence conditions, our results showed extremely low mRNA expression and baseline protein expression in various confluence conditions, except the significantly increased mRNA expression of U87 in the high confluence state. No direct experimental evidence and reports could be found about the comparison of influence on CAIX expression between low-medium-high confluence of cultured GBM cells.

Given that PI3K pathway has a positive impact on CAIX expression of Hela cells. The Wortmannin inhibition experiment was performed in GBM cells. All cell lines showed reduced pAKT expression after adding Wortmannin except BTIC18. The expression of CAIX was also reduced with Wortmannin inhibition in most cell lines. This suggests that PI3K pathway participates in the baseline expression of CAIX in low-medium confluence under normoxia in most cell lines. Shafee et al. speculated that the activity of PI3K/Akt had variable cell-specific effects on the expression of CAIX in human cancer cell lines.[284] This could serve as an explanation of diverse expression of pAKT and CAIX in our experiment. The result above also indirectly proves that other pathways and factors may participate in the baseline expression of CAIX (See 1.4.4). At the same time, according to the PCR result of Wortmannin inhibition experiment, there are no bands of *CAIX* mRNA which are consistent with the aforementioned experiments.

The post-translational stability of CAIX may play a major role in the baseline expression of CAIX. There are no reports about the protein half life of CAIX in GBM. Rafajová et al reported the post-translational stability and 38.4 hours half life of CAIX protein in HeLa cell cultured in DMEM with FBS. The mRNA transcription was prolonged and present after 24 hours reoxygenation. New CAIX molecules were also produced in the period of reoxygenation.[203] Therefore, the post-translational stability aided by the new synthesis which constitutes the compensation of the degraded protein during reoxygenation, finally results in the overlay convergence of CAIX protein. This partially explains the reason of the detectable high expression of CAIX several days after reoxygenation. In our experiments, we did not test CAIX under reoxygenation. The high protein expression under both normoxic and hypoxic conditions may

largely due to the stability of CAIX protein as well as the continuous synthesis regulated by oncogene signal pathway. The increase of CAIX protein expression is not significant in BTICs after hypoxia induction may attributed to the continuous aggregated protein content is already relatively high.

In most published research papers, whole cell lysates are used for the measurement of CAIX expression in Western blot analysis. However, whole cell lysates are a mixture of membrane protein, cytoplasmic protein, and nuclear protein. This may make Western blot results hard to interpret, when investigating a strictly membrane-bound protein such as CAIX. Immunofluorescence staining may therefore be an alternative method to evaluate protein expression especially for membrane protein. Western blot and immunofluorescence staining in this research showed similar results. This again confirms the CAIX expression under both normoxia and hypoxia. CAIX can be upregulated significantly in established cell lines and mildly increased in BTICs after 24-hour sustained hypoxia.

In conclusion, the diverse expression of CAIX may be attributed to cell types and experimental conditions. These include different molecular subtype of cell lines, genome instability caused by multiple cell passages, non-hypoxic/oncogene regulation of CAIX, type of medium, with or without FBS, glycose concentration, etc. It may also because that the transcriptional activity of *CAIX* promoter are widespread and highly inducible[173] as well as the post-translational stability of CAIX protein. In general, all GBM cell lines (except U87 under high confluence) present very low *CAIX* mRNA expression which canbe significantly upregulated under hypoxic condition. However, due to different genetic background, post-translational stability of CAIX protein and specific experimental conditions, all GBM cell lines showed baseline CAIX expression which canbe upregulated significantly by hypoxia only in establishend cell lines instead of BTICs.

4.2 CAIX inhibitor U104 reduces viability of GBM cells under normoxia and hypoxia

Cell viability experiments such as MTT [3-(4,5-Dimethylthiazol-2-yl)-2,5-diphenyltetrazolium bromide], CCK8 (cell counting kit-8) are commonly used in the detection of cytotoxicity of various bioactive molecules in GBM cells. Each experimental method has its own advantages and disadvantages. ATP assay shows more sensitive, fast, flexible, homogeneous, stable, as well as lesser handling steps and lesser interference by ATPase than other methods of cell viability

assay.[285] Initial purpose of the cell viability experiment is to choose the optimized concentration and exposure time of CAIX inhibitor before cell death in order to differentiate between the true anti-invasive effect and the induction of cell death by this inhibitor. The confounding factors such as DMSO and hypoxia on cell viability would also be evaluated. In addition, there might be different sensitivities to U104 between cell lines. Our experimental results illustrated DMSO and hypoxia, as well as different time of exposure affected cell viability only in specific cell lines and experimental conditions. Meanwhile these results presented a dose-dependent cytotoxicity of U104 in all cell lines. In addition, these results also presented different sensitivity to various treatments between cell lines. U87 and BTIC18 were lesser sensitivity to U104 in comparing with other cell lines.

According to the results above, U104 may be considered as a potentially effective drug for the treatment of GBM. In fact, U104 has been tested in clinical trials of metastatic pancreatic ductal adenocarcinoma and other advanced solid tumours (refer to 1.4.6). However, research reports on GBM treatment with U104 are scarce. Boyd et al. proved that U104 concurrent with temozolomide decreased cell growth and induced cell cycle arrest by DNA damage *in vitro*, as well as inhibited the BTICs enrichment by the measurement of CD133 expression and the capacity of neurosphere formation. The treatment combination also delayed the growth of patient-derived xenografts, as well as shifted tumor bioenergetic metabolism to a suppressed state *in vivo*. The effect of combination treatment was greater than each single treatment. Cell viability was measured by SYTOX™ Blue staining. In addition, the expression pattern of *CAIX* mRNA is in accordance with our result, while CAIX protein shows significant increasement under 2% hypoxia of 72 hours in cell lines tested.[261] This is possible attributed to the use of pediatric and recurrent adult patient-derived xenograft cells of neurosphere culture in DMEM/F12 supplemented with B27 which are much different from our experimental conditions. Xu et al. also reported the combinatorial therapy of CAIX inhibitor U104 and temozolomide in U87 and U251 GBM cell lines *in vitro* which were cultured in DMEM with FBS. Their results showed the positive synergistic effect of cell apoptosis induction in comparing with temozolomide treatment alone. The effect also synchronized with the decreased expression of SOX9. The potential underlying mechanism of enhanced chemosensitivity involves the reduction of both SOX9 and CAIX expression, which in turn markedly decreases Akt phosphorylation followed by downregulating and upregulating expression of apoptotic signaling molecules Bcl-2 and BAX

(Bcl-2-associated X) respectively on transcription and translation levels. However, no single treatment with U104 was reported in the research of Xu et al. Cell viability was measured by propidium iodide staining. In addition, their result also showed the baseline expression of CAIX under normoxic condition which was consistent with our experimental result.[262] Different GBM cell lines show diverse sensitivity to the cytotoxicity of U104 from our experimental results, and established cell line U87 and proneural BTIC18 require a larger dose of U104 to work for the reduction of cell viability. This is partly consistent with that proneural subtype shows no benefit in response to aggressive therapy.[6] BTIC18 shows the least sensitivity to U104 which also may be the difficulty to reach the center of sphere because of spherical growth in addition to inherent resistance. BTIC18 has a much slower growth rate than other faster growing GBM cell lines in this research, and this maybe another reason to explain the insensitivity to anti-proliferative effect of U104. However, this explanation does not suitable for U87 cell line. There are unequal glioma-CpG island methylator phenotype in proneural subtype[118] and different positive percentage of CD133 expression between cell lines (refer to Table 2.5.2). However, whether these differences of epigenetics and biomarker play master regulatory effects in the different sensitivities to U104 between cell lines need to be further proved. Results of Zhou et al. showed that cell viability of U87 stem cells was a little bit higher than U251 stem cells without any treatment in the incubation process of 72 hours under normoxia. However, there was no statistical analysis of differences between them.[286] No published papers were found about molecular subtype-based and inter-subtypes comparative analysis of cell viability in GBM cells.

Although DMSO is widely used as an organosulfur solvent for various inhibitors and shows low toxicity to cells, it still may have some impacts on cell biology. Our experimental results showed that DMSO did in fact increase cell viability of U251 cell line. Therefore, DMSO was used as a control to show the net effect of U104.

Our results indicated that the cell viability value changes were not statistically different between normoxia and hypoxia in all different groups of all GBM cell lines except specific groups of U87 and BTIC13. Li et al. reported that the cell growth did not show obvious changes in U87 and even mildly reduced in GSCs (glioma stem cells) under 1% hypoxia in the incubation process of 72 hours in comparing with normoxia, and there was no statistical analysis.[265] Heiland et al. also reported decreased cell viability of three BTICs under 3% hypoxia of 24 hours by MTT assay *in vitro*, although no statistically significant could be seen.[257] There is obvious difference

between U87 cell lines in different laboratories, probably based on the high heterogeneity of this cell line. However, results of Li et al. and Heiland et al. are partly consistent with our results. That is 24 hours hypoxia does not play a major role in cell viability changes of some GBM cell lines. This may due to the involvement of hypoxia-independent oncogene and tumor suppressor gene signaling pathways.

In conclusion, CAIX inhibitor U104 can potentially be used as a targeted drug therapy of GBM cells, particularly if the cells show a mesenchymal subtype. More detailed molecular mechanisms of cytotoxicity caused by U104 in GBM cells need to be further elucidated.

4.3 All six cell lines show diverse invasive ability and heterogeneity in pre-experiments

Results of pre-experiments represented versatile invasive performance among cell lines and experimental conditions. However, no statistical analysis of comparison results of different invasive performance can be established because of small samples. In addition, a high degree of heterogeneity could be seen in all respects.

The obvious invasive heterogeneity was first discovered in the exercise of invasion experiment for learning before the pre-experiments. This recalled us about whether the heterogeneity was caused by irregular operation. In the operation process of pre-experiments, many steps were more carefully operated. For example, diluted Matrigel was pipetted onto the middle of membrane without membrane touching. Immediately after pipetting, bubbles in Matrigel were punctured without membrane damaging. All the coated inserts in companion plate were gently tilted and rotated horizontally for the even distribution of Matrigel on the whole membrane especially at the edge. Cell suspension for seeding was also carefully pipetted onto the middle of gelatinous Matrigel drop by drop. No bubbles could be seen in the upper and lower compartments especially below the membrane. Each step was observed under microscope to ensure the strictness and accuracy of operation. Therefore, heterogeneity of invasive performance caused by irregular operation could be ruled out, and experimental protocol was further optimized in subsequent pre-experiments.

Although widely used, Matrigel coated Transwell invasion assay is possibly to unidimensional and may fail to recapitulate the complexity of native neural microenvironment.[264] The reason of invasive heterogeneity may be attributed to the significant difference between neural ECM and matrices in other tissues of the body structurally and functionally, such as abundant HA

components instead of fibrillar proteins, special biophysical properties, etc. The primary ingredients of Matrigel or collagen-based matrices used in Transwell invasion assay are mainly present in the basal membrane.[263] Furthermore, GBM cells represented hugely different invasion performance in two-dimensional and three-dimensional systems. These include changes of cell micro-morphology, different responses to protease inhibitors, different requirements of certain molecules and signaling pathways for the motility of GBM cells.[229] In addition, the absence of cellular components in Transwell invasion assay also devoids of the evaluation of intercellular interactions. The adaptation to the unique glioma microenvironment and ECM remodling of GBM cells as well as the varied composition and structure among different brain compartments make invasion performance of GBM cells *in vivo* more complicated. With the development of polymeric materials, surface science and microfabrication, many new technologies and methods have been applied to the research of GBM cell invasion. These include artificial matrices of bioengineered scaffolds (e.g., hyaluronan based synthetic hydrogels of multiple ingredient combinations) and cerebral organoids in 3D *in vitro* invasion models, microfluidic co-culture models, *ex vivo* organotypic brain tissue slice models and *in vivo* orthotopic xenograft animal models, microfabricated ECMs, etc. While each method has advantages and disadvantages.[264, 287] The addition of human serum, FBS or other chemo-attractants in the lower compartment also results in accelerated migration and invasion. This may not be relevant to physiological conditions.[264]

It is well established that cells undergo senescence as well as changes of phenotype and genotype potentially in serial cell culture *in vitro* because of selective pressures especially for primary cell cultures.[288] These changes include proliferation and differentiation ability, innate characteristics, morphology, production of heterochromatin foci, and altered sensitivity to cell cycle inhibitors.[289] Liao et al. reported that the abilities of cell spreading and migration increased first at early passages and decreased after 15 passages in the research of human umbilical vein endothelial cells.[290] There was a clear gradual reduction of cell invasion ability in all cell lines with the increase of cell passage number in pre-experiments. Therefore, the importance was proved again that both established cells and BTICs should be worked up in short-term passage for maintaining biological ability or resembling original tumor cells maximally. However, there was still report of 20-40 passages of primary gliblastoma stem cells culture for invasion research.[291]

4.4 All six cell lines show invasive heterogeneity, diverse invasive ability, different sensitivity to hypoxia and U104 in actual experiments

4.4.1 Heterogeneity within cell lines

Results of actual experiments again showed heterogeneity of invasion even in same experimental condition which was consistent with results of pre-experiments. At the same time, the reason for heterogeneity caused by different batches of Matrigel was also excluded. Vollmann et al. indicated that Transwell assays generated high standard deviations of results.[10] Results of Qiu et al. presented high standard deviations of invasion in both differentiated glioma cells and BTICs experimentally.[292] There are two major possible reasons for invasive heterogeneity. The first major reason is the inherent deficiencies of Matrigel coated Transwell invasion assay itself which is explained in chapter 4.3 in detail. In addition, the low ratio of invaded cells devided by seeded cells indicates that the invaded cells only account for a small part of the seeded cells. Therefore, these results indirectly indicate the influences of biological characteristics of GBM cells by the experimental microenvironment of Matrigel coated Transwell invasion assay largely. The second major reason is the heterogeneity in the same molecular subtypes as well as the heterogeneity of intercommunications and interactions between cells randomly. Therefore, further classification of molecular subtype is necessary.

4.4.2 Morphology changes after 24-hour hypoxia

Our observations represented no obvious changes of cell morphology under optical microscope between normoxia and hypoxia in both pre-experiments and actual experiments.

Li et al. also reported that under optical microscope, there were no morphology changes after 24 hours hypoxic incubation (1% O_2) in both established cell lines and GSCs, while obvious cell morphology changes such as the absence of cell processes and aggregated oval cells in masses could be seen after 72 hours hypoxic incubation. Additionally, under transmission electron microscopy, ultrastructure changes such as reduction of collagen fibers, present of nucleolus and mitochondria could be seen after 24 hours hypoxic incubation. Significant ultrastructure changes such as reduced organelles, absence collagen fibers, presence of nucleolus and double nucleoli could be observed after 72 hours hypoxia. [265] Joseph et al. also reported that established GBM cell lines U87 and SNB75 but not U251 underwent phenotypic conversion which was

characterized by more elongated and stretched morphology under 1% hypoxia of 72 hours. [293] Qiu et al. found that invaded GSCs preferd to aggregate and reform new tumor spheres after penetrating Matrigel and pores followed by adherenting onto the lower side of the insert membrane. On the contrary, the differentiated progeny cells were more scattered and possessed extended processes. These were different from our experimental observations. The first thinking is whether the invaded cells differentiate during the contaction of human serum in the lower compartment which leads to the formation of spindle cells in our experiment. This phenomenon is more obvious in the morphological change of BTIC18 which changes from spherical growth to fusiform (Figure 2.1 vs. Figure 3.12). However, Qiu et al. also used FBS as chemo-attractant in the lower compartment. The possible explanation might be the incubation time of 40 hours which was longer than our experimental condition as well as the different cell lines and medium. No more molecular information of GSCs could be found except CD133 by Qiu et al.[292]

4.4.3 GBM cell invasion affected by 24-hour hypoxia

Our experimental results elucidated that hypoxia increased invasion of GBM cells in convergent statistical analysis. Only the invasive ability of U87 and mesenchymal BTIC12 cell lines was enhanced under hypoxia in the analysis of individual cell line.

Hypoxia increases invasion of GBM cells has been reported everywhere, but mostly in established cell lines. Heiland et al. reported statistically significant increased invasive capacity of BTICs under 3% O_2 with the use of PDGF-BB as chemo-attractant *in vitro*.[257] Papale et al. reported both increased and decreased invasive capacity of two BTICs under 1% oxygen *in vitro*.[255] No molecular subtype related information could be found about tested BTICs.

There are many related mechanisms that hypoxia increases invasion of GBM cells such as the regulation of oncogene and tumor suppressor gene signals, transcription factors, adherent interaction of cell-cell and cell-ECM, ECM degradation, cytoskeleton dynamics, EMT (epithelial mesenchymal transition), extracellular active molecules, and so on.

Hypoxia promotes invasiveness and EMT via HIF-2α-EPHB2 (Ephrin type-B receptor 2)-paxillin axis.[294] Huang et al. reported hypoxia activated the PI3K/Akt/mTOR pathway and expression of HIF-1α followed by enhancement of migration and invasion of U87 cells.[295] Jiao et al. reported that hypoxia (1% O_2) increased U251 cell invasion via RhoA/JNK (Jun NH2-terminal kinase)/c-Jun and activated MMP2.[296] Hypoxia inhibits expression of TIPE2 (tumor necrosis

factor-a-induced protein 8-like 2) and in turn upregulates Wnt/β-catenin signaling followed by enhancing EMT as well as migration and invasion of U251 cells.[297] Hypoxia induces the expression of FTL (ferritin light chain) via binding to HRE-3 promoter region and following activation of AKT/GSK3β (glycogen synthase kinase 3β)/β-catenin pathway for the increased EMT and glioma invasion *in vivo* and *in vitro*.[298] Higher expression and activation of CBF1 (also known as recombination signal binding protein for immunoglobulin kappa J, RBPJ) could be found in hypoxic regions of GBM samples and cultured glioma cells under hypoxia *in vitro*. CBF1 contributes to the upregulation of activators of EMT and invasiveness of GBM cells.[299] Hypoxia enhances migration and invasion of both established GBM cell lines and GBM neurosphere cell lines by promoting EMT which is also mediated by HIF1α-ZEB1 (zinc finger E-box binding homeobox 1) axis.[268, 293] TWIST (twist family bHLH transcription factor) is high expression in pseudopalisading necrotic areas of human GBM tissue[300], and can be upregulated by HIF-1α under hypoxia.[301] TWIST1 promotes GBM cell invasion *in vitro* and *in vivo* via mesenchymal change instead of EMT.[302] Hypoxia downregulates GLTSCR2 (glioma tumor suppressor candidate region gene 2 protein) via JNK and in turn increases invasiveness of GBM cells.[303] Hypoxia (1% and 5% O_2) accelerates motility and invasion of established GBM cell lines via c-src mediated phosphorylation of NWASP (neural Wiskott-Aldrich syndrome protein) in collagen and matrigel coated Transwell assays as well as organic mouse brain slice culture assay.[304] Liu et al. reported that established GBM cell lines with EGFRvIII showed enhanced invasiveness under microenvironment of hypoxia and vitronectin. This process was interceded by EGFRvIII/integrin β3/SRC/FAK signaling as well as subsequently activated ERK/AKT/STAT3 signaling and upregulated MMPs.[305] Hypoxia upregulates and activates the protein translation of cell-cell adhesion molecule cadherin-22 via eIF4E2 (eukaryotic initiation factor 4) instead of mTORC1 followed by driving glioma cell migration and invasion.[306] Hypoxia induces expression of PLOD2 (procollagenlysine 2-oxoglutarate 5-dioxygenase 2) via HIF-1α followed by FAK-mediated enhancement of migration and invasion in established glioblastoma cells. This is proved by transwell and 3D spherical assay *in vitro* as well as orthotopic xenografts assay *in vivo*.[307] Cyclin G2 is high expression in pseudopalisades and is upregulated by hypoxia. Mechanistically, cyclin G2 recruits and phosphorylates cortactin at the leading edge in the presence of SFKs (src family kinases), as well as connects with filamentous actin followed by the formation of membrane ruffles and enhanced invasion of GBM cells *in*

vitro and *in vivo*.[308] Hypoxia significantly elevates the expression of eHsp90/LRP1 signaling and subsequently activates src/AKT/EphA2 signaling followed by the formation of lamellipodia and enhanced motility and invasion of GBM cells.[309] Hypoxia activates Notch1 signaling and in turn upregulates expression of TRPC6 (transient receptor potential 6). TRPC6 causes a continuously intracellular Ca^{2+} entry and activates calcineurin-NFAT (nuclear factor of activated T-cell) signaling-mediated invasion of GBM cells.[310] Hypoxia (0.5% O_2) increases the production of adenosine extracellularly and in turn facilitates HIF2/PAP (prostatic acid phosphatase)-dependent activation of A3AR (A3 adenosine receptor) and enhancement of migration and invasion of GSCs *in vivo* and *in vitro*.[311] Hypoxia promotes the release of intracellular HMGB1 (high mobility group box 1) and subsequently activates AKT and ERK signaling pathways followed by enhancing invasion of GBM cells in a autocrine pathway.[312] Hypoxia positively regulates TF (tissue factor)/FVIIa (factor VIIa)/PAR-2 (protease-activated receptor 2)/ERK axis for increasing migration and invasion of GBM cells *in vitro*.[313] Hypoxia promotes secretion of CCL4 (chemokine C-C motif ligands 4)-CCR5 (C-C chemokine receptor type 5) in macrophages followed by increased expression of MMP9 and enhanced invasion of GBM cells.[314]

There is no direct experimental evidence that hypoxia enhances glycolysis and extracellular acidification followed by increased invasion capacity of BTICs which is mediated by CAIX. Proescholdt et al. reported that hypoxia enhanced invasion of established GBM cell lines which were under enhanced glycolytic metabolism condition.[182] However, this could not explain why hypoxia response works only in BTIC12 instead of BTIC13, because both BTIC12/13 are glycolysis. No relevant genetic and metabolic information could be found about U87. BTIC12 was diagnosed gliosarcoma apart from mesenchymal subtype. However, it is unknown whether BTIC12 continues to maintain the gliosarcoma phenotype and genotype during primary cell culture. Therefore, this may not be the solid evidence that invasion of BTIC12 is more sensitive to hypoxia. Further molecular mechanism studies on the difference between BTIC12 and other BTICs are necessary. Proescholdt et al. also reported that the mechanism was mediated by CAIX, and the inhibition of CAIX repressed invasion and was more prounced under hypoxia.[182] However, this still does not explain the difference between BTIC12 and BTIC13 in terms of sensitivity to hypoxia, because they have similar expression of CAIX.

4.4.4 Mesenchymal BTICs possess the strongest invasion ability and possible mechanism

Actual experimental results showed that mesenchymal BTIC12/13 and proneural BTIC17 possessed much higher invasive ability than other cell lines. Meanwhile, proneural BTIC18 always exhibited much lower invasive ability. This is consistent with the results of third to eighth pre-experiments. However, these were all carried out with the use of human serum as chemo-attractant. According to the results of first and second pre-experiments, if the human serum is taken out which is more close to the physiological microenvironment, mesenchymal BITC12/13 have the strongest invasion ability in all cell lines undoubtedly. Proneural BTIC17 is the most sensitive to chemo-attractant. Proneural BTIC18 seldom invades in all invasion experiments with different conditions.

Mesenchymal BTICs display more aggressive phenotypes than proneural BTICs which are reported everywhere[315], especially in PMT (proneural to mesenchymal transition). While more aggressive can refer to upregulated proliferation and growth *in vitro*, faster growth of xenograft and increased angiogenesis or necrosis *in vivo* with a shorter median survival, etc. Many low-grade gliomas also have extensive infiltration into normal brain tissue. Therefore, high aggressiveness is not equal to high invasiveness.

Cheng et al. reported that GSCs derived from both surgical specimens and xenografts possessed stronger invasive ability than paired non-stem GBM cells *in vitro* (4-5 folds quantitatively) and *in vivo*. GSCs endued the invasive phenotype of GBM. In addition, some invasion-associated proteins [such as L1CAM, MMP16, ADAMTS1 and SEMA3C (semaphorin 3C)] were identified in the differential expression between GSCs and non-stem GBM cells. No cell subtype classification-based molecular information of GSCs could be found by Cheng et al.[316] Qiu et al. also reported that GSCs from surgical specimens were more invasive than matched differentiated GBM progeny cells *in vitro* (0.5-2.5 fold greater or 1.25 fold on average quantitatively). [292] Results of *in vitro* experiments above are partially consistent with our observations only in the comparation of invasive ability between BTICs and differentiated cell lines. However, there are no subtype classification-based analysis in the experiments of Cheng et al. and Qiu et al. The quantitative results cannot be evaluated, because we cannot simply pool the data of mesenchymal BTICs and proneural BTICs as GSCs for the comparison with differentiated cells.

Binda et al. reported mesenchymal BTICs were more invasiveness than proneural BTICs in

Transwell assay *in vitro* and intracranial xenograft mouse model *in vivo*. They also proved this mechanism was due to high expression of Wnt5a which was a noncanonical member of Wnt family. Because they found that Wnt5a was statistically significant higher overexpression in mesenchymal subtype than in proneural subtype from GBM surgery specimens and their BTICs on both transcription and translation levels. This is consistent with our experimental results. [317] Saito et al. reported mesenchymal BTICs exhibited higher invasive ability than other subtypes of BTICs in orthotopic injection xenografts of BTICs into mouse brain caudate nucleus *in vivo*. The reason of higher invasive ability in mesenchymal subtype was attributed to higher expression of TGF-β pathway components as well as the deactivation of Notch and Wnt pathways by bioinformatics analysis. [318]

In contrast, De Bacco et al. reported diverse invasion performance between mesenchymal and proneural subtypes of BTICs in conditions without any treatments *in vitro*. Transwell assay was performed in both upper and lower compartments supplemented with 1% FBS culture medium. It is not clear whether FBS causes BTICs differentiation or other biological function changes after 24 hours incubation in spite of low concentration.[319] While experiment of Saito et al. clearly showed that BTICs underwent differentiation in the presence of 1μM retinoic acid and 1% FBS after 5 days. [318]

Previous work in our laboratory demonstrated that proneural BTIC17/18 heavily relied on TCA cycle/oxidative phosphorylation compared to mesenchymal BTIC12/13 which were more glycolysis. Therefore, different metabolic phenotype may contribute to the different invasion ability. This implies that upregulated glycolysis promotes invasion of BTICs compared to TCA cycle/oxidative phosphorylation. No direct experimental evidence has been found regarding the comparison of invasion ability between glycolytic BTICs and TCA cycle/oxidative phosphorylated BTICs.

Beckner et al. demonstrated that glycolytic ATP was the primary source of energy and sufficient to support migration of human metastatic melanoma cell line (A2058). The inhibition of glycolysis repressed cell motility at all glucose concentrations. The production of glycolytic CO_2 was directly related to cell motility. In contrast, the production of mitochondrial CO_2 was inversely correlated with glucose concentration.[320] Later, same group proved abundantly increased glycolytic enzymes and decreased mitochondrial enzymes in the pseudopodia of U87 cells. This further supports the important role of glycolysis during the migration of glioma

cells.[321] In the same year, they demonstrated that glycolysis alone could support migration and invasion of established glioma cell lines (U87 and LN229) *in vitro* without the participation of mitochondria. This was aided by loss of *PTEN* which upregulated the PI3K/Akt pathway followed by the phosphorylation of GSK3. Interestingly, loss of *PTEN* is a predominant character of Mesenchymal BTICs.[322] Kathagen-Buhmann et al. also reported that glycolysis enzymes were elevated in various migrating cells (including glioma cell lines U87 and G55, human mesenchymal stem cells gbMSC and TB869, pseudopalisading cells), and knockdown of Aldolase C by short hairpin RNA decreased migration *in vitro* but not *in vivo*.[323] Furthermore, bevacizumab resistant GBM cells are more invasiveness accompanying a significantly increased glycolytic phenotype and reduced mitochondria under electron microscopy.[324] Basanta et al. found that the glioma invasive phenotype was prone to evolve from the anaerobic glycolytic phenotype based on evolutionary game theory.[325] In addition, upregulated glycolysis produces large amounts of lactic acid. Aggregated lactic acid is responsible for the inducible expression of KLHDC8A (kelch domaincontaining 8A) followed by the increased migration and invasion of glioma cells (U87MG and U251).[326] Lactic acid also promotes migration of glioma cell via TGF-β2 dependent regulation of MMP2 and integrin αvβ3.[327]

There are also some other possible mechanisms to explain that mesenchymal BTICs possess stronger invasive ability than proneural BTICs such as differential expression of biomarker, cytokine, chemokine, transporter, ion channel, metabolic microenvironment, non-coding RNA, etc. However, all these possible mechanisms are based on bioinformatics analysis or subtype-associated and invasion-related molecular markers instead of direct experimental evidence in the comparison of invasive ability between different subtypes of BTICs. Whether these mechanisms and molecular markers play dominant regulatory effects in the invasiveness of mesenchymal BTICs instead of proneural BTICs need to be further proved experimentally.

4.4.5 CAIX inhibitor U104 represses invasion of GBM cells only in mesenchymal BTICs

Our results showed that CAIX inhibitor U104 statistically significant reduced cell invasion under both normoxia and hypoxia in convergent analysis of all GBM cell lines. Furthermore, U104 played an inhibitory effect only in mesenchymal BTIC12 (normoxia) and BTIC13 (normoxia and hypoxia) in the analysis of individual cell line. Therefore, experimental results illustrated only the invasion of mesenchymal BTICs was associated with the functional inhibition of CAIX.

4.4.5.1 Possible mechanism of CAIX inhibition reduces invasion of GBM cells

As early as 2000, Parkkila et al. reported that acetazolamide, a non-specific inhibitor of carbonic anhydrase (including inhibition of CAIX), suppressed the invasion ability of renal cancer cells *in vitro* and on a concentration-depndent manner.[328] The inhibition of CAIX suppresses the invasion which is also reported in breast tumor [329] pancreatic cancer [330] nasopharyngeal carcinoma [331] ovarian carcinoma [207] and so on. There is also report about the inhibition of CAIX by RNAi (RNA interference) that exhibits no statistically significant effect on invasion in specific breast carcinoma cell line.[332] Direct experimental evidence are very seldom about CAIX inhibition on invasion of GBM cells. Proescholdt et al. reported that knockdown of CAIX by siRNA (small interfering RNA) resulted in a statistically significant reduction of cell invasion in established GBM cell line U251 under normoxia (high glucose) and hypoxia (both high and low glucose).[182]

The molecular mechanism research of CAIX inhibition on cell invasion are mainly focused on non-glioma cell lines. CAIX promotes formation of active invadopodia and ECM degradation proteolytically. This is supported by co-distribution of CAIX with cortactin, MMP14, NBCe1, pPKA in invadopodia and related biological experiments. This process is pH-dependent and interplayed with actin polymerization regulatory mechanistically. The silencing or inhibition of CAIX reduces invadopodia formation and ECM degradation as well as invasion of non-CNS tumor *in vivo*.[333] CAIX colocalizes with paxillin followed by promoting the turnover of initial transient adhesion to mature adhesion in focal contacts by proteoglycan and catalytic domains in sequence. This process is mediated by ROCK1 (RhoA-associated protein kinase 1)/myosin II and is dependent on the pHe regulated by CAIX catalytic activity, and finally contributes to the enhanced cell migration. The inhibition of CAIX reverses the process above.[334] CAIX increases cell migration through catalytic domain as well as colocalizes and interacts with bicarbonate transporters (sodium bicarbonate co-transporters and anion exchangers) in leading edge of lamellipodia on HGF-independent and dependent manners.[335] Depletion of CAIX by shRNA (short hairpin RNA) reduces cell invasion by focal adhesion pathway in fibrosarcoma cells under 72 hours hypoxia, and the mechanism may be related to the reduction of MMP9.[336] CAIX is promoted by COX-2 (cyclooxygenase-2)/PGE2 (prostaglandins E2)/ERK1/2 axis and the pathway can be triggered by high cell density and hypoxia. The interplay of CAIX and COX-2 promotes invasion of colorectal cancer cells, and the knowdown reduces invasiveness

accompanied by the reduced level of active MMP2.[337] In addition, CAIX colocalizes and enhances MMP14-modulated catalytic degradation of type I collagen by directly providing hydrogen ions in mature invadopodia followed by increasing migration and invasion of breast and pancreatic cancers. CAIX-specific inhibitor U104 reverses the process above on a dose-dependent manner.[338] Overexpression of CAIX activates MMP9-mediated increasement of invasion in the research of human oral squamous carcinoma cell lines. The mechanism relates to FAK/Src and ERK signaling pathways followed by the increased binding capacity of transcription factor NF-κB and AP-1 (c-Jun and c-Fos) with *MMP9* gene promoter.[339] Pharmacological inhibition of CAIX by U104 reduces the invasiveness of breast and lung cancer cell lines *in vitro* via inhibition of proteolytic activity of MMP2 accompanied by upregulation and release of TIMP2.[340] CAIX weakens cytoskeleton-linked and E-cadherin-mediated adhesion on lateral membrane of MDCK cells by interaction with β-catenin. Function of E-cadherin is closely linked to tumor cell invasion.[216] Chu et al. reported upregulation of CAIX was closely related to increased invasive capacity of breast cancer cell lines at 72 hours under $CoCl_2$-induced hypoxia in comparing with normoxia group *in vitro*. The mechanism was attributed to changed expression levels of MMP2, MMP9, E-cadherin and vimentin.[341] Ditte et al. reported that extracellular acidification modulated by fullest activity of CAIX was mediated via phosphorylation of Threonine 443 and dephosphorylation of Serine 448 at the intracellular domain followed by the changes of cell migration. The phosphorylation was controlled by c-AMP-dependent PKA which was elevated under hypoxia.[219] The knockdown of CAIX by shRNA blocks the secreted hypoxia-induced stanniocalcin-1 glycoprotein which promotes invasiveness in a subgroup of triple-negative breast cancer cell line.[342] Kim et al. reported that overexpressed CAIX significantly enhanced invasion of human umbilical vein endothelial cells and the effect was reduced by DKK-1 (dickkopf-1, a negative regulator Wnt pathway). The process was mediated by directly binding of Methionine 1-Glycine 120 site of CAIX with Valine 60-Tyrosine 168 site of DKK-1 followed by the interruption of FAK/PI3K/mTOR pathway.[343] Overexpression of CAIX induces actin cytoskeletal remodeling, weakens focal cell adhesion complex and augments motility of human cervical carcinoma cell line via Rho-GTPase signaling. The inhibition of CAIX has the opposite effect.[270] CAIX promotes cell invasion of human nasopharyngeal carcinoma *in vivo* and *in vitro* by the activation of mTOR pathway. The promotion effect can be inhibited by shRNA.[331] Overexpression of CAIX induces cell

invasiveness in human ovarian carcinoma cell mice xenografts. This is proved to be because of the hypomethylation at CpG sites in the *CAIX* promoter. The inhibition of DNA methyltransferase increases the expression of CAIX and invasiveness in non-invasive tumor cells.[207]

4.4.5.2 Possible mechanism of intracellular alkaline and extracellular acidification facilitate invasion of GBM cells

Although the pH values were not measured in our experiments, the inhibitory mechanism of U104 on CAIX is the direct blockage on the catalytic active site cavity of enzyme (refer to 1.4.6). It is unknown whether other functions of CAIX are suppressed or not, such as signal transduction of IC domain, cell adhesion and catalytic activity improvement of PG domain (refer to 1.4.5). Therefore, the blockage of catalytic function of CAIX accompanied with the disturbation of intracellular alkaline and extracellular acidification might influence invasion of GBM cells. Current research of intracellular and extracellular changes of pH-dependent invasion were still mainly performed in non-CNS tumors. These mechanisms include different sensitivity of various pH-dependent proteins (also called pH sensors) and posttranslational protein modifications that involve in the molecular mechanism of invasion.

Protonation, a kind of post-translational modification, changes side chains charge of amino acids and drives conformation and function changes of proteins. Many of them involve cell invasion process.[344] Dbs (Dbl's big sister), an Dbl (diffuse B-cell lymphoma) family member of GEFs (guanine nucleotide exchange factors), binds PI(4,5)P2 and is pH dependent. The maximal specific binding ability is at pH 6.5 and reduced significantly at pH 7.5 and 8.0. This means a lower affinity at higher pH. Alkaline of pHi promotes the release of GEF followed by catalyzing the binding of GTP (guanosine triphosphate) and Cdc42. Cdc42 is a Rho GTPase and is crucial for polarity of migrating cells.[345] Cofilin, an actin-binding protein, severs and increases actin free barbed ends for the *de novo* assembly of branched actin filament network followed by driving formation of membrane protrusion in the fronts of migrating cells. PI(4,5)P2 binds and inhibits the actin severing activity of cofilin. The binding ability of PI(4,5)P2 and cofilin is pH-dependent and decreases at pHi 7.5 in comparing with pHi 6.5.[346] Locally increased pHi results in the release of activated cofilin from phosphorylated cortactin followed by regulating the dynamic protrusion and retraction cycles of invadopodia which is indispensable for actin

polymerization and cell invasion of breast carcinoma.[347] Talin, a focal adhesion-associated protein, binds actin filaments for the stabilization of cell-substrate adhesions. The binding process of talin and actin is the rate-limiting step of cell migration and is pH-dependent. The binding affinity is 2-fold greater at pH 6.5 than at pH 7.5. Higher pHi increases the turnover of focal adhesion.[348] FAK is a pH sensor and is activated by autophosphorylation of Tyrosine 397 at higher pHi followed by focal adhesion remodeling. Histidine 58 is proved vital for pH sensing of FAK by mutagenesis studies.[349]

Paradise et al. reported that low pHe influenced cell morphology, adhesion and migration by protonation of Aspartate β127 residue and opened the headpiece of integrin αvβ3 for its activation. This is proved by both computational analysis and experiments.[350] Extracellular acidification promotes formation, increased number and length of invadopodia as well as invadopodia-dependent ECM degradation followed by facilitating invasion of breast carcinoma cells.[351] Acidic pHe promotes redistribution to cell periphery and secretion of active lysosomal protease Cathepsin B for the local proteolysis which facilitates tumor cell invasion. This process is also proved dependent on the microtubular system.[352] Bourguignon et al. also reported acidic pHe promoted activation of hyaluronidase-2 and cathepsin B mediated matrix degradation and increased cell invasion of breast tumor.[353] In addition, acidic microenvironment (pH 5.6) contributes to cathepsin B mediated release and activation of tumor-shed microvesicles and gelatinase MMP2/9 which are responsible for proinvasive activity of cells. The application of Cathepsin B inhibitor or siRNA suppresses the proinvasive activity.[354] Kato et al. reported that mouse metastatic melanoma cells secreted gelatinases in acidic culture medium (pH 5.4-6.1) instead of neutral culture medium (pH 7.1-7.3). The acid-induced secretion extent of gelatinases is positively consistent with their invasion potentials. Meanwhile, human lung adenocarcinoma and fibrosarcoma cells show higher level secretion of gelatinases at pH 6.8 than pH 7.3.[355] Acidic pHe-mediated activation of MMP9 is proved to be induced by PLD (phospholipase D)/MAPKs (p38 and ERK1/2)/NF-κB axis.[356] ASICs (acid-sensing ion channels) are transiently activated at low pHe. ASICs interact and colocalize with subunits of ENaC (epithelial sodium channel) followed by mediating active amiloride-sensitive current in human high grade glioma cells. The inhibition of ASICs reduces migration of glioma cells.[357] Low pHe increases CAIX expression of GBM cells on both transcriptional and translational levels under normoxia (independ on hypoxia). This is mediated by stabilization of HIF-1α concurrent with the

transiently activated ERK pathway as well as MAPK and PI3K pathways.[204]
The expression and activity of pH-sensitive proteins as well as their impacts on invasion of GBM cells need to be further elucidated by experimental evidence. In addition, it is worth noting the deficiency of convergent analysis due to intratumoral and intertumoral heterogeneity especially the unknown ratio of different subtypes in a specific tumor. Simple convergent analysis could not represent the real situation of tumors *in vivo*.

4.4.5.3 Possible mechanism of CAIX inhibition reduces cell invasion of mesenchymal BTICs instead of proneural BTICs

Although CAIX inhibitor U104 statistically significant repressed cell invasion under both normoxia and hypoxia in convergent experimental result analysis of all GBM cell lines, individual analysis of each cell line elucidated this only worked in mesenchymal BTIC12 (normoxia) and BTIC13 (normoxia and hypoxia) statistically. No relevant genetic information could be found about U87 and U251. Therefore, the different sensitivity to U104 between mesenchymal and proneural BTICs would be discussed. There are many possible mechanisms such as differential metabolism phenotype and genetic background.
As mentioned above, mesenchymal BTIC12/13 are more glycolysis, and proneural BTIC17/18 heavily relay on TCA cycle/OXPHOS. Therefore, different metabolic phenotype may contribute to the different sensitivity to CAIX inhibitor in terms of invasiveness.
In the study of Proescholdt et al., knockdown of *CAIX* reduced invasion of established GBM cell lines. Although the inherent metabolic phenotype was unknown and might also change in established GBM cell lines, the experimental conditions of normoxia with high glucose as well as hypoxia with both high and low glucose might enhance intracellular glycolysis level.[182] Xu et al. reported gene silencing of *CAIX* by shRNA decreased cell migration in the research of clear cell renal cell carcinoma *in vitro*. This mechanism was due to downregulate amino acid transporters and cell motility associated proteins as well as increase associated proteins synthesis and biogenesis of mitochondrial oxidative phosphorylation and reverse Warburg effect.[358] No direct experimental evidence could be found that the invasion of glycolytic BTICs could be repressed by CAIX inhibitor instead of TCA cycle/oxidative phosphorylated BTICs. There is a small amount of evidence in non-CNS tumors that the expression, inhibition and function of CAIX are positively correlated with the level of intracellular glycolysis and the large amounts of

lactic acid produced. Choi et al. reported that many metabolism-related proteins were differentially expressed in the different molecular subtypes of breast cancer. The significantly increased expression of CAIX was associated with glycolytic phenotype.[359] Gibadulinova et al. reported that downregulation of CAIX attenuated glycolysis and promoted mitochondrial function via modulating *let-7* (lethal-7)/LIN28 (Lin-28 homolog A) axis and downstream metabolic enzymes [PDK1 (pyruvate dehydrogenase kinase 1) and PDH (pyruvate dehydrogenase)] in the research of breast cancer cells under hypoxic microenvironment.[360] Jamali et al. demonstrated that CAIX augmented flux of lactic acid extracellularly by a non-catalytic function. Knockdown of CAIX by siRNA reduced proliferation of human breast cancer cells significantly *in vitro*.[361] However, whether the inhibition of CAIX causes a decrease of invasion ability only in glycolytic cells needs to be further elucidated. The evidence that the inhibition of CAIX reduced cell invasiveness in non-glioma tumors were discussed deeply in chapter 4.4.5.1, while the cell metabolic phenotypes were unclear.

According to our experimental results that the inhibition of CAIX reduced invasiveness only in glycolytic BTICs, there might be close relationship between the function of membrane protein CAIX and intracellular glycolysis in terms of cell invasiveness. This fully supports our hypothesis that the expression and function of CAIX may accelerate the efflux of large amounts of lactic acid produced by glycolysis, and subsequently cause some or all of the changes in the 4 steps of the invasion mechanism (such as enhancing the lysis of matrix protein, etc.), which in turn enhance tumor cell invasion. Therefore, the functional inhibition of CAIX only affects the invasiveness of glycolytic BTICs. Meanwhile, glycolytic BTICs possess the strongest invasive ability, and this may imply that CAIX inhibition is more effective.

Mutational and transcriptional background of different cell subtypes may also play a pivotal role in the different sensitivity to CAIX inhibitor for the invasion of gliblastoma cells. These include upstream and downstream molecules and signaling pathways centered on subtype-associated mutations. No experimental evidence-based mechanisms regarding genetic background could be found that CAIX inhibition reduces invasion of mesenchymal BTICs but not proneural BTICs.

Mesenchymal subtype is predominantly characterized by focal hemizygous deletions and mutations of *NF1* gene at 17q11.2 instead of methylation. Co-mutations of *NF1* and *PTEN* which intersect with AKT pathway are also common in Mesenchymal subtype. Typical Mesenchymal markers are *CHI3L1* (*YKL40*), *MET*, *CD44*, *MERTK*, genes in TNF and NF-κB pathways

(*TRADD*, *RELB*, *TNFRSF1A*). (refer to 1.1.6.3)

Pre-GRD (GAP-related domain) region (3489 bp for amino acids 1-1163) of neurofibromin which is encoded by *NF1* gene, negatively regulates Rac1 (Rac family small GTPase 1)/Pak1 [p21 (Rac1) activated kinase 1]/LIMK1 (LIM domain kinase 1)/cofilin pathway followed by the disassembly of actin stress fibers and focal adhesion for the reduced migration in GBM concomitantly. Effects of this process are independent of Ras signaling pathway accompanied with active Ras-GTP and increased cell proliferation. [362] Higher intracellular pH participates in the increased cofilin-dependent *de novo* assembly of actin filament network.[346] Therefore, loss-of-function mutations of *NF1* gene in mesenchymal BTICs may be the reason of more sensitive to the invasion inhibition by U104. In addition, LRD (leucine-rich domain) region of neurofibromin also negatively regulates glioma cell invasiveness independent of Ras signaling.[363]

In the research of *PTEN* gene transfection in GBM cells *in viv*o and *in vitro*, PTEN inhibits cell invasion by suppressing proteolysis of ECM via reducing enzymatic activities of MMP2/9 and upregulating TIMP2. PTEN also reduces migratory activity of cells by inactivating and decreasing Rac/Cdc42 and pFAK.[364] Most of these cell invasion-related molecules are pH-dependent (refer to 4.4.5.2). Therefore, loss-of-function mutations of *PTEN* gene and associated regulation of invasion may be another reason of more sensitive to U104 in mesenchymal BTICs. Daniel et al. demonstrated PI3K activation was sufficient for gliomagenesis while simultaneous deletion of *PTEN* was required for invasion of BTICs in a mouse model. This effect can be suppressed by inhibition of downstream transcription factor CREB (cAMP response element binding protein).[365] *PTEN* deletion leads to upregulation and activation of PI3K/PKCι pathway and RhoB-dependent invasion of GBM cells.[366] PKCι promotes the cytoskeleton remodeling for the formation of lamellipodia with a single leading edge by inactivating and dissociating cytoskeletal protein Lgl [lethal (2) giant larvae] from non-muscle myosin II mechanically. This is comfirmed by shRNA transfection and pharmacological inhibition assays. [367] In addition, PTEN represses migration of GBM cells by its C2 domain which is independent on the lipid phosphatase activity for the regulation of PI3K.[368] Later, Dey et al. proved that PTEN suppressed kinases of src family followed by inhibiting vitronectin-mediated GBM cell migration by its protein phosphatase activity.[369] Alam et al. reported PTEN suppressed SPARC (secreted protein acidic and rich in cysteine) induced migration and invasion

of GBM cells mediated by P38MAPK/pMAPKAPK2 (MAPK activated protein kinase 2) /Hsp 27 signaling pathway, as well as Shc/Ras/Raf/MEK/ERK1/2 and Akt signaling.[370] Loss of *PTEN* induces AKT/mTOR signal for stabilizing ARL4C (ADP-ribosylation factor like-4C) via inhibition of ubiquitination followed by enhancing RAC1-mediated filopodium formation and invasion of GBM cells.[371] PREX2a (phosphatidylinositol-3,4,5-trisphosphate-dependent Rac exchange factor 2a) is significantly high expression in glioma on both transcription and translation levels. Knockdown of PREX2a by siRNA inhibits the invasion of glioma cells *in vitro*. This mechanism is mediated by PREX2a-induced upregulation of PTEN activity and inhibition of PI3K signaling. [372] NLRP3 (nucleotide-binding domain leucine-rich family pyrin-containing 3) is also reported overexpression in high grade glioma, and significantly increases PTEN/AKT signaling followed by cell invasion and epithelial-mesenchymal transition *in vitro*. Knockdown of NLRP3 reverses the effects above.[373] HIF-1α upregulates long noncoding RNA H19 under hypoxia by HIF-1α or SP1 (HIF-1α-induced) binding to the H19 promoter directly or indirectly. Upregulated H19 promotes migration and invasion of GBM cells by increasing EMT-related proteins. For instance, H19 binds miR-181d for relieving inhibition of β-catenin. While PTEN reverses the effects of H19 by attenuating HIF-1α.[374] Numerous non-coding RNAs are reported to play roles in regulating invasion of GBM cells by targeting PTEN signaling directly or indirectly, which include miRs (microRNAs), lncRNAs (long non-coding RNA) and circRNAs (circular RNAs). These miRs comprise miR-21[375], miR-29a[376], miR-92b[377], miR-494-3p[378], miR-301a[379], mir-130b[380], synergistic effects of miR-10b and miR-222[381], miR-193a-5p via NOVA1 (neuro-oncological ventral antigen 1) [382], miR-216b[383] and miR-379[384] via metadherin, and so on. Related lncRNA involve GAS5 via miR-106b [385] and miR-10b[386], LINC00657 via miR-190a-3p[387], MEG3 via miR-19a[388] and miR-377[389], MT1JP[390], etc. Associated circRNA consists of circFBXW7 via miR-23a-3p[391].

Proneural subtype is feagured as focal amplification and high gene expression of *PDGFRA* at 4q12, point mutations in *IDH1*, *TP53* mutations and loss of heterozygosity, *PIK3CA/PIK3R1* mutations. Proneural markers mainly include oligodendrocytic development genes (*PDGFRA*, *NKX2-2*, *OLIG2*) and proneural development genes (*SOX*, *DCX*, *DLL3*, *ASCL1*, *TCF4*). (refer to 1.1.6.3) BTIC13 losts *IDH1* mutation in primary cell culture and all the BTICs used in this research are *IDH1* wild type. Therefore, the possibility of *IDH1* mutation which causes the

different sensitivity to CAIX inhibitor between mesenchymal and proneural BTICs canbe excluded.

PDGFRα-dependent research are mainly focused on development of normal brain, as well as proliferation, tumorgenesis, molecular diagnosis and prognosis of GBM. Instead, PDGFRβ preferentially informs stemness, self-renewal, cell plasticity, survival, growth, and invasion of GBM cells.[392]

The formation of gangliosides GD3/PDGFRα/Yes (Src kinase) complex in glycolipid-enriched rafts of lamellipodia promotes invasiveness of GBM cells derived from p53-deficient gene-engineered mice model.[393] Dock180, also known as Dock1, belongs to Dock (dedicator of cytokinesis) family of GEFs. PDGFRα specifically phosphorylates Dock180 at tyrosine 1811 and dependents on Src. p-Dock180^{Y1811} recruits CrkII/p130^{Cas} and activates Rac1 followed by subsequent migration and invasion of GBM cells *in vitro*.[394]

TP53 gene and pathway mainly involve in DNA repair, cell cycle arrest, senescence, apoptosis, stem-cell differentiation in response to stress signals such as DNA damage, genotoxicity, oncogene activation, aberrant growth signals, hypoxia and so on. *TP53* gene and pathway also participate in additional roles which include regulation of cellular metabolism, stemness, autophagy, invasion, microenvironment, and immunity of GBM cells.[395]

Functional impairment of p53 results in the activation of invasion/migration-associated genes through upregulating proto-oncogene Ets-I (erythroblast transformation specific-I) transcription factor.[396] PTEN even exerts oncogenic effects mediated by mut-p53. This mechanism is based on formation of mut-p53/CBP/NFYA (nuclear transcription factor Y subunit alpha) transcriptional complex followed by binding and activating the promoters of oncogenes c-Myc and Bcl-XL as well as increasing cell proliferation, survival, invasion, and clonogenicity of GBM cells.[397] USP7 (ubiquitin specific peptidase 7) promotes invasiveness of GBM cells by the inhibition of ubiquitylation and stabilization of LSD1 (lysine-specific demethylase 1) which is mediated via inhibition of the p53 signaling pathway.[398] p48 isoform of Ebp1 (a human homologue of the mouse protein p38-2AG4) is an ErbB3 (receptor tyrosine-protein kinase erbB-3) binding protein. p48 as a cofactor binds to HDM2 (a p53 E3 ligase of human homologue of MDM2) for promoting polyubiquitination and degradation of p53 followed by enhancing invasion of gliobalstoma cells.[399] Many non-coding RNAs are reported to play roles in regulating invasion of GBM cells by targeting *TP53* signaling directly or indirectly, which

include miR-34a [400], miR-15b via HOTAIR (HOX transcript antisense RNA) [401], miR-16[402], as well as lncRNA LINC00467 via DNMT1 (DNA methyltransferase 1)[403], lncRNA GHET1 (gastric carcinoma highly expressed transcript 1) via miR-216a.[404], lncRNA TP73-AS1 via miR-124[405].

In addition to distinct metabolic and genetic backgrounds, differential expression of invasion-related proteins in mesenchymal and proneural BTICs (refer to 4.4.4) may be another reason for the different sensitivity to CAIX inhibitor U104. However, whether all these differences mechanically on invasion of GBM cells which are affected by inhibition of CAIX or disturbation of alkaline pHi/acidic pHe need to be further elucidated by experiments.

Moreover, CAIX itself does not participate in the process of proton efflux, the inhibition of its catalytic function does not change proton flux. Instead, the cooperation of CAIX with transporters (such as MCT family) dominates the process. Ion transporters also exhibit differential expression between molecular subtypes in the research of breast cancer. [406] Therefore, CAIX-mediated regulation of tumor cell invasion is a dynamic and interrelated course. The cooperation with other transporters may be one more reason of the contribution of different sensitivity to U104.

5 Conclusion

Expression of CAIX in GBM cells is regulated by hypoxia, PI3K, cell confluence, etc. and is cell line dependent. *CAIX* mRNA represents very low expression in all cell lines under normoxia and strong induced by hypoxia. CAIX protein shows baseline expression in all cell lines under normoxia and is strong induced by hypoxia only in established cell lines instead of BTICs. CAIX plays an important role in viability and invasion of GBM cells and is cell line dependent. Functional inhibition of CAIX by U104 can be used as a targeted drug for cytotoxicity and invasion repression in the treatment of GBM cells but only in specific cell lines. Taken together, our hypothesis is confirmed that carbonic anhydrase IX plays a role in the invasiveness of GBM cells but only in specific cell lines.

6 Limitations of research and prospects

The molecular mechanism of GBM cell invasion likes a huge three-dimensional net, and many aspects are unknown and needed to be futher elucidated. Direct experimental evidence of CAIX on GBM invasion is seldom. Additionally, the mechanism and biological performance are much different between CNS and non-CNS tumor and related microenvironment. This subject is a groundbreaking research which fully proves the role of CAIX in subtype-based glioblastma cell invasion under hypoxia. However, there are still some shortcomings in this research which need to be noticed in future experimental design.

1. Experimental conditions that more close to the physiological microenvironment of CNS would be applied to the research of GBM invasion *in vitro* and *in vivo* in the future.
2. Although there is a molecular subtype classification-dependent analysis in this research, a significant heterogeneity can be seen between cell lines in the same subtype. Therefore, more detailed molecular-dependent research is necessary.
3. More related markers, pathways are necessary to be further tested and elucidated for involving in cell killing and cell invasion by U104.
4. It is better to elucidate the function of CAIX by using more specific CAIX inhibitor instead of the inhibitor of both CAIX and CAXII in the future.

7 Bibliography

1. Thamburaj, V.A., *Textbook of Contemporary Neurosurgery (Volumes 1 & 2)*. 2012: JP Medical Ltd.
2. Wen, P.Y. and S. Kesari, *Malignant gliomas in adults.* N Engl J Med, 2008. **359**(5): p. 492-507.
3. Ostrom, Q.T., et al., *CBTRUS Statistical Report: Primary Brain and Other Central Nervous System Tumors Diagnosed in the United States in 2011-2015.* Neuro Oncol, 2018. **20**(suppl_4): p. iv1-iv86.
4. Cancer Genome Atlas Research, N., *Comprehensive genomic characterization defines human glioblastoma genes and core pathways.* Nature, 2008. **455**(7216): p. 1061-8.
5. Brennan, C.W., et al., *The somatic genomic landscape of glioblastoma.* Cell, 2013. **155**(2): p. 462-477.
6. Verhaak, R.G.W., et al., *Integrated genomic analysis identifies clinically relevant subtypes of glioblastoma characterized by abnormalities in PDGFRA, IDH1, EGFR, and NF1.* Cancer cell, 2010. **17**(1).
7. Weller, M., et al., *European Association for Neuro-Oncology (EANO) guideline on the diagnosis and treatment of adult astrocytic and oligodendroglial gliomas.* Lancet Oncol, 2017. **18**(6): p. e315-e329.
8. Nabors, L.B., et al., *NCCN Clinical Practice Guidelines in Oncology (NCCN Guidelines®)Central Nervous System Cancers.* 2020.
9. Friedmann-Morvinski, D., *Glioblastoma heterogeneity and cancer cell plasticity.* Critical reviews in oncogenesis, 2014. **19**(5): p. 327-336.
10. Vollmann-Zwerenz, A., et al., *Tumor Cell Invasion in Glioblastoma.* International journal of molecular sciences, 2020. **21**(6).
11. Bailey, P. and H. Cushing, *A classification of the tumors of the glioma group on a histogenetic basis with a correlated study of prognosis*. 1926, Philadelphia: J. B. Lippincott. 146-167.
12. Louis, D.N., et al., *The 2016 World Health Organization Classification of Tumors of the Central Nervous System: a summary.* Acta Neuropathol, 2016. **131**(6): p. 803-20.
13. Fritz, A., et al., *International Classification of Diseases for Oncology. World Health Organization.* Geneva: Butler & Tanner, 2000.

14. Louis, D.N., et al., *The 2007 WHO classification of tumours of the central nervous system.* Acta Neuropathol, 2007. **114**(2): p. 97-109.
15. Aldape, K., et al., *Glioblastoma: pathology, molecular mechanisms and markers.* Acta neuropathologica, 2015. **129**(6): p. 829-848.
16. Ohgaki, H. and P. Kleihues, *Genetic pathways to primary and secondary glioblastoma.* The American journal of pathology, 2007. **170**(5): p. 1445-1453.
17. Ostrom, Q.T., et al., *The epidemiology of glioma in adults: a "state of the science" review.* Neuro Oncol, 2014. **16**(7): p. 896-913.
18. Schonberg, D.L., et al., *Brain tumor stem cells: Molecular characteristics and their impact on therapy.* Molecular aspects of medicine, 2014. **39**.
19. Bradshaw, A., et al., *Cancer Stem Cell Hierarchy in Glioblastoma Multiforme.* Frontiers in surgery, 2016. **3**: p. 21.
20. Ferris, S.P., et al., *Characterization of gliomas: from morphology to molecules.* Virchows Arch, 2017. **471**(2): p. 257-269.
21. Braganza, M.Z., et al., *Ionizing radiation and the risk of brain and central nervous system tumors: a systematic review.* Neuro Oncol, 2012. **14**(11): p. 1316-24.
22. McCarthy, B.J., et al., *Assessment of type of allergy and antihistamine use in the development of glioma.* Cancer Epidemiol Biomarkers Prev, 2011. **20**(2): p. 370-8.
23. Scheurer, M.E., et al., *Long-term anti-inflammatory and antihistamine medication use and adult glioma risk.* Cancer Epidemiol Biomarkers Prev, 2008. **17**(5): p. 1277-81.
24. Scheurer, M.E., et al., *Effects of antihistamine and anti-inflammatory medication use on risk of specific glioma histologies.* Int J Cancer, 2011. **129**(9): p. 2290-6.
25. Lahkola, A., et al., *Mobile phone use and risk of glioma in 5 North European countries.* Int J Cancer, 2007. **120**(8): p. 1769-75.
26. Hardell, L. and K.H. Mild, *Cellular telephones and risk of brain tumours.* Lancet, 2001. **357**(9260): p. 960-1.
27. Baan, R., et al., *Carcinogenicity of radiofrequency electromagnetic fields.* Lancet Oncol, 2011. **12**(7): p. 624-6.
28. Yang, M., et al., *Mobile phone use and glioma risk: A systematic review and meta-analysis.* PLoS One, 2017. **12**(5): p. e0175136.
29. Goodenberger, M.L. and R.B. Jenkins, *Genetics of adult glioma.* Cancer genetics, 2012.

205(12): p. 613-621.

30. Farrell, C.J. and S.R. Plotkin, *Genetic causes of brain tumors: neurofibromatosis, tuberous sclerosis, von Hippel-Lindau, and other syndromes.* Neurologic clinics, 2007. **25**(4).
31. Rice, T., et al., *Understanding inherited genetic risk of adult glioma - a review.* Neurooncol Pract, 2016. **3**(1): p. 10-16.
32. Zachariah, M.A., et al., *Blood-based biomarkers for the diagnosis and monitoring of gliomas.* Neuro-oncology, 2018. **20**(9): p. 1155-1161.
33. Davis, M.E., *Glioblastoma: Overview of Disease and Treatment.* Clin J Oncol Nurs, 2016. **20**(5 Suppl): p. S2-8.
34. Wen, P.Y., et al., *Medical management of patients with brain tumors.* J Neurooncol, 2006. **80**(3): p. 313-32.
35. Ellingson, B.M., et al., *Consensus recommendations for a standardized Brain Tumor Imaging Protocol in clinical trials.* Neuro Oncol, 2015. **17**(9): p. 1188-98.
36. Ahmed, R., et al., *Malignant gliomas: current perspectives in diagnosis, treatment, and early response assessment using advanced quantitative imaging methods.* Cancer Manag Res, 2014. **6**: p. 149-70.
37. Johnson, D.R., et al., *Case-Based Review: newly diagnosed glioblastoma.* Neurooncol Pract, 2015. **2**(3): p. 106-121.
38. Ellor, S.V., T.A. Pagano-Young, and N.G. Avgeropoulos, *Glioblastoma: background, standard treatment paradigms, and supportive care considerations.* J Law Med Ethics, 2014. **42**(2): p. 171-82.
39. Chamberlain, M.C., *Radiographic patterns of relapse in glioblastoma.* J Neurooncol, 2011. **101**(2): p. 319-23.
40. Young, G.S., *Advanced MRI of adult brain tumors.* Neurol Clin, 2007. **25**(4): p. 947-73, viii.
41. la Fougere, C., et al., *Molecular imaging of gliomas with PET: opportunities and limitations.* Neuro Oncol, 2011. **13**(8): p. 806-19.
42. Albert, N.L., et al., *Response Assessment in Neuro-Oncology working group and European Association for Neuro-Oncology recommendations for the clinical use of PET imaging in gliomas.* Neuro Oncol, 2016. **18**(9): p. 1199-208.

43. Moton, S., et al., *Imaging Genomics of Glioblastoma: Biology, Biomarkers, and Breakthroughs.* Top Magn Reson Imaging, 2015. **24**(3): p. 155-63.
44. Jiang, T., et al., *CGCG clinical practice guidelines for the management of adult diffuse gliomas.* Cancer Lett, 2016. **375**(2): p. 263-273.
45. Alexander, B.M. and T.F. Cloughesy, *Adult Glioblastoma.* Journal of clinical oncology : official journal of the American Society of Clinical Oncology, 2017. **35**(21): p. 2402-2409.
46. Rong, Y., et al., *'Pseudopalisading' necrosis in glioblastoma: a familiar morphologic feature that links vascular pathology, hypoxia, and angiogenesis.* Journal of neuropathology and experimental neurology, 2006. **65**(6): p. 529-539.
47. Caiazzo, A. and I. Ramis-Conde, *Multiscale modelling of palisade formation in gliobastoma multiforme.* Journal of theoretical biology, 2015. **383**: p. 145-156.
48. Cuddapah, V.A., et al., *A neurocentric perspective on glioma invasion.* Nature reviews. Neuroscience, 2014. **15**(7): p. 455-465.
49. Manini, I., et al., *Role of Microenvironment in Glioma Invasion: What We Learned from In Vitro Models.* International journal of molecular sciences, 2018. **19**(1).
50. Stupp, R., et al., *Effect of Tumor-Treating Fields Plus Maintenance Temozolomide vs Maintenance Temozolomide Alone on Survival in Patients With Glioblastoma: A Randomized Clinical Trial.* JAMA, 2017. **318**(23): p. 2306-2316.
51. Pace, A., et al., *European Association for Neuro-Oncology (EANO) guidelines for palliative care in adults with glioma.* The Lancet. Oncology, 2017. **18**(6): p. e330-e340.
52. Rossetti, A.O. and R. Stupp, *Epilepsy in brain tumor patients.* Current opinion in neurology, 2010. **23**(6): p. 603-609.
53. Perry, J.R., *Thromboembolic disease in patients with high-grade glioma.* Neuro-oncology, 2012. **14 Suppl 4**: p. iv73-iv80.
54. Gerber, D.E., S.A. Grossman, and M.B. Streiff, *Management of venous thromboembolism in patients with primary and metastatic brain tumors.* Journal of clinical oncology : official journal of the American Society of Clinical Oncology, 2006. **24**(8): p. 1310-1318.
55. Streiff, M.B., B. Holmstrom, and D. Angelini, *NCCN Clinical Practice Guidelines in Oncology (NCCN Guidelines®)Cancer-Associated Venous Thromboembolic Disease.* 2019.

56. Ryken, T.C., et al., *Surgical management of newly diagnosed glioblastoma in adults: role of cytoreductive surgery.* Journal of neuro-oncology, 2008. **89**(3): p. 271-286.
57. Sahm, F., et al., *Addressing diffuse glioma as a systemic brain disease with single-cell analysis.* Archives of neurology, 2012. **69**(4): p. 523-526.
58. Osswald, M., et al., *Brain tumour cells interconnect to a functional and resistant network.* Nature, 2015. **528**(7580): p. 93-98.
59. Haj, A., et al., *Extent of Resection in Newly Diagnosed Glioblastoma: Impact of a Specialized Neuro-Oncology Care Center.* Brain sciences, 2017. **8**(1).
60. Li, X.-Z., et al., *Prognostic implications of resection extent for patients with glioblastoma multiforme: a meta-analysis.* Journal of neurosurgical sciences, 2017. **61**(6): p. 631-639.
61. Kreth, F.W., et al., *Gross total but not incomplete resection of glioblastoma prolongs survival in the era of radiochemotherapy.* Annals of oncology : official journal of the European Society for Medical Oncology, 2013. **24**(12): p. 3117-3123.
62. Kuhnt, D., et al., *Correlation of the extent of tumor volume resection and patient survival in surgery of glioblastoma multiforme with high-field intraoperative MRI guidance.* Neuro-oncology, 2011. **13**(12): p. 1339-1348.
63. Chaichana, K.L., et al., *Establishing percent resection and residual volume thresholds affecting survival and recurrence for patients with newly diagnosed intracranial glioblastoma.* Neuro-oncology, 2014. **16**(1): p. 113-122.
64. Sanai, N., et al., *An extent of resection threshold for newly diagnosed glioblastomas.* Journal of neurosurgery, 2011. **115**(1): p. 3-8.
65. de Leeuw, C.N. and M.A. Vogelbaum, *Supratotal resection in glioma: a systematic review.* Neuro-oncology, 2019. **21**(2): p. 179-188.
66. Li, Y.M., et al., *The influence of maximum safe resection of glioblastoma on survival in 1229 patients: Can we do better than gross-total resection?* Journal of neurosurgery, 2016. **124**(4): p. 977-988.
67. Yordanova, Y.N., S. Moritz-Gasser, and H. Duffau, *Awake surgery for WHO Grade II gliomas within "noneloquent" areas in the left dominant hemisphere: toward a "supratotal" resection. Clinical article.* Journal of neurosurgery, 2011. **115**(2): p. 232-239.
68. D'Amico, R.S., et al., *Extent of Resection in Glioma-A Review of the Cutting Edge.* World neurosurgery, 2017. **103**: p. 538-549.

69. Vogelbaum, M.A., et al., *Application of novel response/progression measures for surgically delivered therapies for gliomas: Response Assessment in Neuro-Oncology (RANO) Working Group.* Neurosurgery, 2012. **70**(1).

70. Barani, I.J. and D.A. Larson, *Radiation therapy of glioblastoma.* Cancer treatment and research, 2015. **163**: p. 49-73.

71. Hochberg, F.H. and A. Pruitt, *Assumptions in the radiotherapy of glioblastoma.* Neurology, 1980. **30**(9): p. 907-911.

72. Shapiro, W.R., et al., *Randomized trial of three chemotherapy regimens and two radiotherapy regimens and two radiotherapy regimens in postoperative treatment of malignant glioma. Brain Tumor Cooperative Group Trial 8001.* Journal of neurosurgery, 1989. **71**(1): p. 1-9.

73. Walker, M.D., T.A. Strike, and G.E. Sheline, *An analysis of dose-effect relationship in the radiotherapy of malignant gliomas.* International Journal of Radiation Oncology, Biology, Physics, 1979. **5**(10): p. 1725-31.

74. Salazar, O.M., et al., *High dose radiation therapy in the treatment of malignant gliomas: final report.* International journal of radiation oncology, biology, physics, 1979. **5**(10): p. 1733-1740.

75. Keime-Guibert, F., et al., *Radiotherapy for glioblastoma in the elderly.* The New England journal of medicine, 2007. **356**(15): p. 1527-1535.

76. Galanis, E. and J. Buckner, *Chemotherapy for high-grade gliomas.* British journal of cancer, 2000. **82**(8): p. 1371-1380.

77. Weller, M., et al., *Standards of care for treatment of recurrent glioblastoma--are we there yet?* Neuro-oncology, 2013. **15**(1).

78. Stupp, R., et al., *Radiotherapy plus concomitant and adjuvant temozolomide for glioblastoma.* N Engl J Med, 2005. **352**(10): p. 987-96.

79. Stupp, R., et al., *Effects of radiotherapy with concomitant and adjuvant temozolomide versus radiotherapy alone on survival in glioblastoma in a randomised phase III study: 5-year analysis of the EORTC-NCIC trial.* Lancet Oncol, 2009. **10**(5): p. 459-66.

80. Gilbert, M.R., et al., *Dose-dense temozolomide for newly diagnosed glioblastoma: a randomized phase III clinical trial.* Journal of clinical oncology : official journal of the American Society of Clinical Oncology, 2013. **31**(32): p. 4085-4091.

81. Blumenthal, D.T., et al., *Is more better? The impact of extended adjuvant temozolomide in newly diagnosed glioblastoma: a secondary analysis of EORTC and NRG Oncology/RTOG.* Neuro-oncology, 2017. **19**(8): p. 1119-1126.
82. Gramatzki, D., et al., *P08. 30 Extended temozolomide for newly diagnosed glioblastoma: an analysis of the German Glioma Network.* 2016. **18**(Suppl 4): p. iv47.
83. Hegi, M.E., et al., *MGMT gene silencing and benefit from temozolomide in glioblastoma.* The New England journal of medicine, 2005. **352**(10).
84. Westphal, M., et al., *A phase 3 trial of local chemotherapy with biodegradable carmustine (BCNU) wafers (Gliadel wafers) in patients with primary malignant glioma.* Neuro-oncology, 2003. **5**(2): p. 79-88.
85. Brem, H., et al., *Placebo-controlled trial of safety and efficacy of intraoperative controlled delivery by biodegradable polymers of chemotherapy for recurrent gliomas. The Polymer-brain Tumor Treatment Group.* Lancet (London, England), 1995. **345**(8956): p. 1008-1012.
86. Westphal, M., et al., *Gliadel wafer in initial surgery for malignant glioma: long-term follow-up of a multicenter controlled trial.* Acta neurochirurgica, 2006. **148**(3).
87. Kreisl, T.N., et al., *Phase II trial of single-agent bevacizumab followed by bevacizumab plus irinotecan at tumor progression in recurrent glioblastoma.* Journal of clinical oncology : official journal of the American Society of Clinical Oncology, 2009. **27**(5): p. 740-745.
88. Friedman, H.S., et al., *Bevacizumab alone and in combination with irinotecan in recurrent glioblastoma.* Journal of clinical oncology : official journal of the American Society of Clinical Oncology, 2009. **27**(28): p. 4733-4740.
89. Vredenburgh, J.J., et al., *Corticosteroid use in patients with glioblastoma at first or second relapse treated with bevacizumab in the BRAIN study.* 2010. **15**(12): p. 1329.
90. Gilbert, M.R., et al., *A randomized trial of bevacizumab for newly diagnosed glioblastoma.* The New England journal of medicine, 2014. **370**(8): p. 699-708.
91. Chinot, O.L., et al., *Bevacizumab plus radiotherapy-temozolomide for newly diagnosed glioblastoma.* The New England journal of medicine, 2014. **370**(8): p. 709-722.
92. Schiff, D. and P.Y. Wen, *The siren song of bevacizumab: swan song or clarion call?* Neuro-oncology, 2018. **20**(2): p. 147-148.

93. Stupp, R., et al., *Maintenance Therapy With Tumor-Treating Fields Plus Temozolomide vs Temozolomide Alone for Glioblastoma: A Randomized Clinical Trial.* JAMA, 2015. **314**(23): p. 2535-2543.

94. Lapointe, S., A. Perry, and N.A. Butowski, *Primary brain tumours in adults.* Lancet (London, England), 2018. **392**(10145): p. 432-446.

95. World Health Organization %J World Health Organization, h.w.w.i.c.p.d.e., *Cancer: WHO definition of palliative care.* 2011.

96. Brandsma, D., et al., *Clinical features, mechanisms, and management of pseudoprogression in malignant gliomas.* The Lancet. Oncology, 2008. **9**(5): p. 453-461.

97. Walbert, T. and T. Mikkelsen, *Recurrent high-grade glioma: a diagnostic and therapeutic challenge.* Expert review of neurotherapeutics, 2011. **11**(4): p. 509-518.

98. Macdonald, D.R., et al., *Response criteria for phase II studies of supratentorial malignant glioma.* Journal of clinical oncology : official journal of the American Society of Clinical Oncology, 1990. **8**(7): p. 1277-1280.

99. Wen, P.Y., et al., *Updated response assessment criteria for high-grade gliomas: response assessment in neuro-oncology working group.* Journal of clinical oncology : official journal of the American Society of Clinical Oncology, 2010. **28**(11): p. 1963-1972.

100. Brandes, A.A., et al., *Recurrence pattern after temozolomide concomitant with and adjuvant to radiotherapy in newly diagnosed patients with glioblastoma: correlation With MGMT promoter methylation status.* Journal of clinical oncology : official journal of the American Society of Clinical Oncology, 2009. **27**(8): p. 1275-1279.

101. Nava, F., et al., *Survival effect of first- and second-line treatments for patients with primary glioblastoma: a cohort study from a prospective registry, 1997-2010.* Neuro-oncology, 2014. **16**(5): p. 719-727.

102. Clarke, J.L., et al., *Is surgery at progression a prognostic marker for improved 6-month progression-free survival or overall survival for patients with recurrent glioblastoma?* Neuro-oncology, 2011. **13**(10): p. 1118-1124.

103. Seystahl, K., W. Wick, and M. Weller, *Therapeutic options in recurrent glioblastoma--An update.* Critical reviews in oncology/hematology, 2016. **99**: p. 389-408.

104. Ryu, S., et al., *The role of radiotherapy in the management of progressive glioblastoma : a systematic review and evidence-based clinical practice guideline.* Journal of

neuro-oncology, 2014. **118**(3): p. 489-499.

105. Yung, W.K., et al., *A phase II study of temozolomide vs. procarbazine in patients with glioblastoma multiforme at first relapse.* British journal of cancer, 2000. **83**(5): p. 588-593.
106. Brada, M., et al., *Multicenter phase II trial of temozolomide in patients with glioblastoma multiforme at first relapse.* Annals of oncology : official journal of the European Society for Medical Oncology, 2001. **12**(2): p. 259-266.
107. Weller, M., et al., *MGMT Promoter Methylation Is a Strong Prognostic Biomarker for Benefit from Dose-Intensified Temozolomide Rechallenge in Progressive Glioblastoma: The DIRECTOR Trial.* Clinical cancer research : an official journal of the American Association for Cancer Research, 2015. **21**(9): p. 2057-2064.
108. Wick, W., et al., *Bevacizumab and recurrent malignant gliomas: a European perspective.* Journal of clinical oncology : official journal of the American Society of Clinical Oncology, 2010. **28**(12).
109. Stupp, R., et al., *NovoTTF-100A versus physician's choice chemotherapy in recurrent glioblastoma: a randomised phase III trial of a novel treatment modality.* European journal of cancer (Oxford, England : 1990), 2012. **48**(14): p. 2192-2202.
110. Bastien, J.I.L., K.A. McNeill, and H.A. Fine, *Molecular characterizations of glioblastoma, targeted therapy, and clinical results to date.* Cancer, 2015. **121**(4): p. 502-516.
111. Parsons, D.W., et al., *An integrated genomic analysis of human glioblastoma multiforme.* Science (New York, N.Y.), 2008. **321**(5897): p. 1807-1812.
112. Phillips, H.S., et al., *Molecular subclasses of high-grade glioma predict prognosis, delineate a pattern of disease progression, and resemble stages in neurogenesis.* Cancer cell, 2006. **9**(3): p. 157-173.
113. Zhang, P., et al., *Current Opinion on Molecular Characterization for GBM Classification in Guiding Clinical Diagnosis, Prognosis, and Therapy.* Frontiers in molecular biosciences, 2020. **7**: p. 562798.
114. Mao, H., et al., *Deregulated signaling pathways in glioblastoma multiforme: molecular mechanisms and therapeutic targets.* Cancer investigation, 2012. **30**(1): p. 48-56.
115. Ludwig, K. and H.I. Kornblum, *Molecular markers in glioma.* Journal of neuro-oncology,

2017. **134**(3): p. 505-512.

116. Jovčevska, I., *Genetic secrets of long-term glioblastoma survivors.* Bosnian journal of basic medical sciences, 2019. **19**(2): p. 116-124.
117. Gutman, D.A., et al., *MR imaging predictors of molecular profile and survival: multi-institutional study of the TCGA glioblastoma data set.* Radiology, 2013. **267**(2): p. 560-569.
118. Noushmehr, H., et al., *Identification of a CpG island methylator phenotype that defines a distinct subgroup of glioma.* Cancer cell, 2010. **17**(5): p. 510-522.
119. Feng, Y., et al., *SOCS3 promoter hypermethylation is a favorable prognosticator and a novel indicator for G-CIMP-positive GBM patients.* PloS one, 2014. **9**(3): p. e91829.
120. Heaphy, C.M., et al., *Altered telomeres in tumors with ATRX and DAXX mutations.* Science (New York, N.Y.), 2011. **333**(6041): p. 425.
121. Kannan, K., et al., *Whole-exome sequencing identifies ATRX mutation as a key molecular determinant in lower-grade glioma.* Oncotarget, 2012. **3**(10): p. 1194-1203.
122. Ozawa, T., et al., *PDGFRA gene rearrangements are frequent genetic events in PDGFRA-amplified glioblastomas.* Genes & development, 2010. **24**(19): p. 2205-2218.
123. Bruno, S. and Z. Darzynkiewicz, *Cell cycle dependent expression and stability of the nuclear protein detected by Ki-67 antibody in HL-60 cells.* Cell proliferation, 1992. **25**(1): p. 31-40.
124. Jaros, E., et al., *Prognostic implications of p53 protein, epidermal growth factor receptor, and Ki-67 labelling in brain tumours.* British journal of cancer, 1992. **66**(2): p. 373-385.
125. Kreth, S., et al., *In human glioblastomas transcript elongation by alternative polyadenylation and miRNA targeting is a potent mechanism of MGMT silencing.* Acta neuropathologica, 2013. **125**(5): p. 671-681.
126. Zhang, W., et al., *miR-181d: a predictive glioblastoma biomarker that downregulates MGMT expression.* Neuro-oncology, 2012. **14**(6): p. 712-719.
127. Patel, A.P., et al., *Single-cell RNA-seq highlights intratumoral heterogeneity in primary glioblastoma.* Science, 2014. **344**(6190): p. 1396-1401.
128. Sottoriva, A., et al., *Intratumor heterogeneity in human glioblastoma reflects cancer evolutionary dynamics.* Proceedings of the National Academy of Sciences of the United States of America, 2013. **110**(10): p. 4009-4014.

129. Griguer, C.E., C.R. Oliva, and G.Y. Gillespie, *Glucose metabolism heterogeneity in human and mouse malignant glioma cell lines.* Journal of neuro-oncology, 2005. **74**(2): p. 123-133.

130. Bellail, A.C., et al., *Microregional extracellular matrix heterogeneity in brain modulates glioma cell invasion.* The international journal of biochemistry & cell biology, 2004. **36**(6): p. 1046-1069.

131. Perrin, S.L., et al., *Glioblastoma heterogeneity and the tumour microenvironment: implications for preclinical research and development of new treatments.* Biochemical Society transactions, 2019. **47**(2): p. 625-638.

132. Gilbert, C.A. and A.H. Ross, *Cancer stem cells: cell culture, markers, and targets for new therapies.* Journal of cellular biochemistry, 2009. **108**(5): p. 1031-1038.

133. Moeckel, S., et al., *Response-predictive gene expression profiling of glioma progenitor cells in vitro.* PloS one, 2014. **9**(9): p. e108632.

134. Singh, S.K., et al., *Identification of human brain tumour initiating cells.* Nature, 2004. **432**(7015): p. 396-401.

135. Singh, S.K., et al., *Identification of a cancer stem cell in human brain tumors.* Cancer research, 2003. **63**(18): p. 5821-5828.

136. Pollard, S.M., et al., *Glioma stem cell lines expanded in adherent culture have tumor-specific phenotypes and are suitable for chemical and genetic screens.* Cell stem cell, 2009. **4**(6): p. 568-580.

137. Beier, D., et al., *CD133(+) and CD133(-) glioblastoma-derived cancer stem cells show differential growth characteristics and molecular profiles.* Cancer research, 2007. **67**(9): p. 4010-4015.

138. Hanahan, D. and R.A. Weinberg, *Hallmarks of cancer: the next generation.* Cell, 2011. **144**(5): p. 646-674.

139. Pavlova, N.N. and C.B. Thompson, *The Emerging Hallmarks of Cancer Metabolism.* Cell metabolism, 2016. **23**(1): p. 27-47.

140. Warburg, O., F. Wind, and E. Negelein, *THE METABOLISM OF TUMORS IN THE BODY.* The Journal of general physiology, 1927. **8**(6): p. 519-530.

141. Racker, E., *History of the Pasteur effect and its pathobiology.* Molecular and cellular biochemistry, 1974. **5**(1-2): p. 17-23.

142. Potter, M., E. Newport, and K.J. Morten, *The Warburg effect: 80 years on.* Biochemical Society transactions, 2016. **44**(5): p. 1499-1505.

143. Gatenby, R.A. and R.J. Gillies, *Why do cancers have high aerobic glycolysis?* Nature reviews. Cancer, 2004. **4**(11): p. 891-899.

144. Smallbone, K., et al., *Metabolic changes during carcinogenesis: potential impact on invasiveness.* Journal of theoretical biology, 2007. **244**(4): p. 703-713.

145. Warburg, O., *On respiratory impairment in cancer cells.* Science (New York, N.Y.), 1956. **124**(3215): p. 269-270.

146. Zheng, J., *Energy metabolism of cancer: Glycolysis versus oxidative phosphorylation (Review).* Oncology letters, 2012. **4**(6): p. 1151-1157.

147. Marin-Valencia, I., et al., *Analysis of tumor metabolism reveals mitochondrial glucose oxidation in genetically diverse human glioblastomas in the mouse brain in vivo.* Cell metabolism, 2012. **15**(6): p. 827-837.

148. Marin-Valencia, I., et al., *Glucose metabolism via the pentose phosphate pathway, glycolysis and Krebs cycle in an orthotopic mouse model of human brain tumors.* NMR in biomedicine, 2012. **25**(10): p. 1177-1186.

149. Shi, Y., et al., *Gboxin is an oxidative phosphorylation inhibitor that targets glioblastoma.* Nature, 2019. **567**(7748): p. 341-346.

150. Molina, J.R., et al., *An inhibitor of oxidative phosphorylation exploits cancer vulnerability.* Nature medicine, 2018. **24**(7): p. 1036-1046.

151. Libby, C.J., et al., *The pro-tumorigenic effects of metabolic alterations in glioblastoma including brain tumor initiating cells.* Biochimica et biophysica acta. Reviews on cancer, 2018. **1869**(2): p. 175-188.

152. Corbet, C. and O. Feron, *Tumour acidosis: from the passenger to the driver's seat.* Nature reviews. Cancer, 2017. **17**(10): p. 577-593.

153. Swietach, P., R.D. Vaughan-Jones, and A.L. Harris, *Regulation of tumor pH and the role of carbonic anhydrase 9.* Cancer metastasis reviews, 2007. **26**(2): p. 299-310.

154. Neri, D. and C.T. Supuran, *Interfering with pH regulation in tumours as a therapeutic strategy.* Nature reviews. Drug discovery, 2011. **10**(10): p. 767-777.

155. Newell, K., et al., *Studies with glycolysis-deficient cells suggest that production of lactic acid is not the only cause of tumor acidity.* Proceedings of the National Academy of

Sciences of the United States of America, 1993. **90**(3): p. 1127-1131.

156. Helmlinger, G., et al., *Acid production in glycolysis-impaired tumors provides new insights into tumor metabolism.* Clinical cancer research : an official journal of the American Association for Cancer Research, 2002. **8**(4): p. 1284-1291.
157. Böhme, I. and A.K. Bosserhoff, *Acidic tumor microenvironment in human melanoma.* Pigment cell & melanoma research, 2016. **29**(5): p. 508-523.
158. Sedlakova, O., et al., *Carbonic anhydrase IX, a hypoxia-induced catalytic component of the pH regulating machinery in tumors.* Frontiers in physiology, 2014. **4**: p. 400.
159. Potter, C.P.S. and A.L. Harris, *Diagnostic, prognostic and therapeutic implications of carbonic anhydrases in cancer.* British journal of cancer, 2003. **89**(1): p. 2-7.
160. Becker, H.M., *Carbonic anhydrase IX and acid transport in cancer.* British journal of cancer, 2020. **122**(2): p. 157-167.
161. Ames, S., S. Pastorekova, and H.M. Becker, *The proteoglycan-like domain of carbonic anhydrase IX mediates non-catalytic facilitation of lactate transport in cancer cells.* Oncotarget, 2018. **9**(46): p. 27940-27957.
162. Masoud, G.N. and W. Li, *HIF-1α pathway: role, regulation and intervention for cancer therapy.* Acta pharmaceutica Sinica. B, 2015. **5**(5): p. 378-389.
163. Schito, L. and G.L. Semenza, *Hypoxia-Inducible Factors: Master Regulators of Cancer Progression.* Trends in cancer, 2016. **2**(12): p. 758-770.
164. Semenza, G.L., et al., *Hypoxia-inducible nuclear factors bind to an enhancer element located 3′ to the human erythropoietin gene.* Proceedings of the National Academy of Sciences of the United States of America, 1991. **88**(13): p. 5680-5684.
165. Semenza, G.L. and G.L. Wang, *A nuclear factor induced by hypoxia via de novo protein synthesis binds to the human erythropoietin gene enhancer at a site required for transcriptional activation.* Molecular and cellular biology, 1992. **12**(12): p. 5447-5454.
166. Soni, S. and Y.S. Padwad, *HIF-1 in cancer therapy: two decade long story of a transcription factor.* Acta oncologica (Stockholm, Sweden), 2017. **56**(4): p. 503-515.
167. Keith, B., R.S. Johnson, and M.C. Simon, *HIF1α and HIF2α: sibling rivalry in hypoxic tumour growth and progression.* Nature reviews. Cancer, 2011. **12**(1).
168. Ke, Q. and M. Costa, *Hypoxia-inducible factor-1 (HIF-1).* Molecular pharmacology, 2006. **70**(5): p. 1469-1480.

169. Holmquist-Mengelbier, L., et al., *Recruitment of HIF-1alpha and HIF-2alpha to common target genes is differentially regulated in neuroblastoma: HIF-2alpha promotes an aggressive phenotype.* Cancer cell, 2006. **10**(5): p. 413-423.

170. Man, J., et al., *Hypoxic Induction of Vasorin Regulates Notch1 Turnover to Maintain Glioma Stem-like Cells.* Cell stem cell, 2018. **22**(1).

171. Balamurugan, K., *HIF-1 at the crossroads of hypoxia, inflammation, and cancer.* International journal of cancer, 2016. **138**(5): p. 1058-1066.

172. Wang, G.L., et al., *Hypoxia-inducible factor 1 is a basic-helix-loop-helix-PAS heterodimer regulated by cellular O2 tension.* Proceedings of the National Academy of Sciences of the United States of America, 1995. **92**(12): p. 5510-5514.

173. Kaluz, S., et al., *Transcriptional control of the tumor- and hypoxia-marker carbonic anhydrase 9: A one transcription factor (HIF-1) show?* Biochimica et biophysica acta, 2009. **1795**(2): p. 162-172.

174. Mazure, N.M., et al., *HIF-1: master and commander of the hypoxic world. A pharmacological approach to its regulation by siRNAs.* Biochemical pharmacology, 2004. **68**(6): p. 971-980.

175. Stadie, W.C. and H. O'Brien, *The catalysis of the hydration of carbon dioxide and dehydration of carbonic acid by an enzyme isolated from red blood cells.* Journal of Biological Chemistry, 1933. **103**(2): p. 521-529.

176. Supuran, C.T., *Carbonic Anhydrases and Metabolism.* Metabolites, 2018. **8**(2).

177. Alterio, V., et al., *Crystal structure of the catalytic domain of the tumor-associated human carbonic anhydrase IX.* Proceedings of the National Academy of Sciences of the United States of America, 2009. **106**(38): p. 16233-16238.

178. Mboge, M.Y., et al., *Carbonic Anhydrases: Role in pH Control and Cancer.* Metabolites, 2018. **8**(1).

179. Aggarwal, M., et al., *Structural annotation of human carbonic anhydrases.* Journal of enzyme inhibition and medicinal chemistry, 2013. **28**(2): p. 267-277.

180. Pastorekova, S., M. Zatovicova, and J. Pastorek, *Cancer-associated carbonic anhydrases and their inhibition.* Current pharmaceutical design, 2008. **14**(7): p. 685-698.

181. Ivanov, S., et al., *Expression of hypoxia-inducible cell-surface transmembrane carbonic anhydrases in human cancer.* The American journal of pathology, 2001. **158**(3): p.

905-919.

182. Proescholdt, M.A., et al., *Function of carbonic anhydrase IX in glioblastoma multiforme.* Neuro-oncology, 2012. **14**(11): p. 1357-1366.

183. Pastoreková, S., et al., *A novel quasi-viral agent, MaTu, is a two-component system.* Virology, 1992. **187**(2): p. 620-626.

184. Pastorek, J., et al., *Cloning and characterization of MN, a human tumor-associated protein with a domain homologous to carbonic anhydrase and a putative helix-loop-helix DNA binding segment.* Oncogene, 1994. **9**(10): p. 2877-2888.

185. Hewett-Emmett, D. and R.E. Tashian, *Functional diversity, conservation, and convergence in the evolution of the alpha-, beta-, and gamma-carbonic anhydrase gene families.* Molecular phylogenetics and evolution, 1996. **5**(1): p. 50-77.

186. Opavský, R., et al., *Human MN/CA9 gene, a novel member of the carbonic anhydrase family: structure and exon to protein domain relationships.* Genomics, 1996. **33**(3): p. 480-487.

187. Saarnio, J., et al., *Immunohistochemistry of carbonic anhydrase isozyme IX (MN/CA IX) in human gut reveals polarized expression in the epithelial cells with the highest proliferative capacity.* The journal of histochemistry and cytochemistry : official journal of the Histochemistry Society, 1998. **46**(4): p. 497-504.

188. Liao, S.-Y., M.I. Lerman, and E.J. Stanbridge, *Expression of transmembrane carbonic anhydrases, CAIX and CAXII, in human development.* BMC developmental biology, 2009. **9**: p. 22.

189. Nakagawa, Y., et al., *Radiation hybrid mapping of the human MN/CA9 locus to chromosome band 9p12-p13.* Genomics, 1998. **53**(1): p. 118-119.

190. Pastoreková, S., et al., *Carbonic anhydrase IX, MN/CA IX: analysis of stomach complementary DNA sequence and expression in human and rat alimentary tracts.* Gastroenterology, 1997. **112**(2): p. 398-408.

191. Kaluz, S., et al., *Transcriptional regulation of the MN/CA 9 gene coding for the tumor-associated carbonic anhydrase IX. Identification and characterization of a proximal silencer element.* The Journal of biological chemistry, 1999. **274**(46): p. 32588-32595.

192. Wykoff, C.C., et al., *Hypoxia-inducible expression of tumor-associated carbonic*

anhydrases. Cancer research, 2000. **60**(24): p. 7075-7083.

193. Kaluzová, M., et al., *Characterization of the MN/CA 9 promoter proximal region: a role for specificity protein (SP) and activator protein 1 (AP1) factors.* The Biochemical journal, 2001. **359**(Pt 3): p. 669-677.
194. Kaluz, S., M. Kaluzová, and E.J. Stanbridge, *Expression of the hypoxia marker carbonic anhydrase IX is critically dependent on SP1 activity. Identification of a novel type of hypoxia-responsive enhancer.* Cancer research, 2003. **63**(5): p. 917-922.
195. Grabmaier, K., et al., *Strict regulation of CAIX(G250/MN) by HIF-1alpha in clear cell renal cell carcinoma.* Oncogene, 2004. **23**(33): p. 5624-5631.
196. Schofield, C.J. and P.J. Ratcliffe, *Signalling hypoxia by HIF hydroxylases.* Biochemical and biophysical research communications, 2005. **338**(1): p. 617-626.
197. Kaluzová, M., et al., *DNA damage is a prerequisite for p53-mediated proteasomal degradation of HIF-1alpha in hypoxic cells and downregulation of the hypoxia marker carbonic anhydrase IX.* Molecular and cellular biology, 2004. **24**(13): p. 5757-5766.
198. Blagosklonny, M.V., et al., *p53 inhibits hypoxia-inducible factor-stimulated transcription.* The Journal of biological chemistry, 1998. **273**(20): p. 11995-11998.
199. Kaluz, S., et al., *Lowered oxygen tension induces expression of the hypoxia marker MN/carbonic anhydrase IX in the absence of hypoxia-inducible factor 1 alpha stabilization: a role for phosphatidylinositol 3'-kinase.* Cancer research, 2002. **62**(15): p. 4469-4477.
200. Sang, N., et al., *MAPK signaling up-regulates the activity of hypoxia-inducible factors by its effects on p300.* The Journal of biological chemistry, 2003. **278**(16): p. 14013-14019.
201. Kopacek, J., et al., *MAPK pathway contributes to density- and hypoxia-induced expression of the tumor-associated carbonic anhydrase IX.* Biochimica et biophysica acta, 2005. **1729**(1): p. 41-49.
202. Laderoute, K.R., *The interaction between HIF-1 and AP-1 transcription factors in response to low oxygen.* Seminars in cell & developmental biology, 2005. **16**(4-5): p. 502-513.
203. Rafajová, M., et al., *Induction by hypoxia combined with low glucose or low bicarbonate and high posttranslational stability upon reoxygenation contribute to carbonic anhydrase IX expression in cancer cells.* International journal of oncology, 2004. **24**(4).

204. Ihnatko, R., et al., *Extracellular acidosis elevates carbonic anhydrase IX in human glioblastoma cells via transcriptional modulation that does not depend on hypoxia.* International journal of oncology, 2006. **29**(4): p. 1025-1033.

205. Cho, M., et al., *Hypomethylation of the MN/CA9 promoter and upregulated MN/CA9 expression in human renal cell carcinoma.* British journal of cancer, 2001. **85**(4): p. 563-567.

206. Grabmaier, K., et al., *Renal cell carcinoma-associated G250 methylation and expression: in vivo and in vitro studies.* Urology, 2002. **60**(2): p. 357-362.

207. Sung, H.Y., W. Ju, and J.-H. Ahn, *DNA hypomethylation-mediated overexpression of carbonic anhydrase 9 induces an aggressive phenotype in ovarian cancer cells.* Yonsei medical journal, 2014. **55**(6): p. 1656-1663.

208. Shao, Y., et al., *Involvement of histone deacetylation in MORC2-mediated down-regulation of carbonic anhydrase IX.* Nucleic acids research, 2010. **38**(9): p. 2813-2824.

209. Mahon, B.P., M.A. Pinard, and R. McKenna, *Targeting carbonic anhydrase IX activity and expression.* Molecules (Basel, Switzerland), 2015. **20**(2): p. 2323-2348.

210. De Simone, G. and C.T. Supuran, *Carbonic anhydrase IX: Biochemical and crystallographic characterization of a novel antitumor target.* Biochimica et biophysica acta, 2010. **1804**(2): p. 404-409.

211. Hilvo, M., et al., *Biochemical characterization of CA IX, one of the most active carbonic anhydrase isozymes.* The Journal of biological chemistry, 2008. **283**(41): p. 27799-27809.

212. Supuran, C.T., *Structure and function of carbonic anhydrases.* The Biochemical journal, 2016. **473**(14): p. 2023-2032.

213. Zavada, J., et al., *Transient transformation of mammalian cells by MN protein, a tumor-associated cell adhesion molecule with carbonic anhydrase activity.* International journal of oncology, 1997. **10**(4): p. 857-863.

214. Závada, J., et al., *Human tumour-associated cell adhesion protein MN/CA IX: identification of M75 epitope and of the region mediating cell adhesion.* British journal of cancer, 2000. **82**(11): p. 1808-1813.

215. Zavadova, Z. and J. Zavada, *Carbonic anhydrase IX (CA IX) mediates tumor cell interactions with microenvironment.* Oncology reports, 2005. **13**(5): p. 977-982.

216. Svastová, E., et al., *Carbonic anhydrase IX reduces E-cadherin-mediated adhesion of MDCK cells via interaction with beta-catenin.* Experimental cell research, 2003. **290**(2): p. 332-345.

217. Dorai, T., et al., *The role of carbonic anhydrase IX overexpression in kidney cancer.* European journal of cancer (Oxford, England : 1990), 2005. **41**(18): p. 2935-2947.

218. Simko, V., et al., *Hypoxia induces cancer-associated cAMP/PKA signalling through HIF-mediated transcriptional control of adenylyl cyclases VI and VII.* Scientific reports, 2017. **7**(1): p. 10121.

219. Ditte, P., et al., *Phosphorylation of carbonic anhydrase IX controls its ability to mediate extracellular acidification in hypoxic tumors.* Cancer research, 2011. **71**(24): p. 7558-7567.

220. Lau, J., K.-S. Lin, and F. Bénard, *Past, Present, and Future: Development of Theranostic Agents Targeting Carbonic Anhydrase IX.* Theranostics, 2017. **7**(17): p. 4322-4339.

221. Parkkila, S., et al., *The protein tyrosine kinase inhibitors imatinib and nilotinib strongly inhibit several mammalian alpha-carbonic anhydrase isoforms.* Bioorganic & medicinal chemistry letters, 2009. **19**(15): p. 4102-4106.

222. Supuran, C.T., *How many carbonic anhydrase inhibition mechanisms exist?* Journal of enzyme inhibition and medicinal chemistry, 2016. **31**(3): p. 345-360.

223. Supuran, C.T. and J.-Y. Winum, *Carbonic anhydrase IX inhibitors in cancer therapy: an update.* Future medicinal chemistry, 2015. **7**(11): p. 1407-1414.

224. Williams, K.J. and R.G. Gieling, *Preclinical Evaluation of Ureidosulfamate Carbonic Anhydrase IX/XII Inhibitors in the Treatment of Cancers.* International journal of molecular sciences, 2019. **20**(23).

225. Bozdag, M., et al., *Discovery of 4-Hydroxy-3-(3-(phenylureido)benzenesulfonamides as SLC-0111 Analogues for the Treatment of Hypoxic Tumors Overexpressing Carbonic Anhydrase IX.* Journal of medicinal chemistry, 2018. **61**(14): p. 6328-6338.

226. Pacchiano, F., et al., *Inhibition of β-carbonic anhydrases with ureido-substituted benzenesulfonamides.* Bioorganic & medicinal chemistry letters, 2011. **21**(1): p. 102-105.

227. *https://www.nature.com/subjects/cell-invasion*.

228. Kohn, E.C. and L.A. Liotta, *Molecular insights into cancer invasion: strategies for prevention and intervention.* Cancer research, 1995. **55**(9): p. 1856-1862.

229. Vehlow, A. and N. Cordes, *Invasion as target for therapy of glioblastoma multiforme.* Biochimica et biophysica acta, 2013. **1836**(2): p. 236-244.

230. Friedl, P. and K. Wolf, *Tumour-cell invasion and migration: diversity and escape mechanisms.* Nature reviews. Cancer, 2003. **3**(5): p. 362-374.

231. Scherer, H., *Structural development in gliomas.* The American Journal of Cancer, 1938. **34**(3): p. 333-351.

232. Turner, S.G., M. Ahmad, and S.A. Toms, *Mechanisms of glioma cell invasion.* Neurooncology-Newer Developments, 2016.

233. Lun, M., et al., *The natural history of extracranial metastasis from glioblastoma multiforme.* Journal of neuro-oncology, 2011. **105**(2): p. 261-273.

234. Li, G., et al., *Tumor Microenvironment in Treatment of Glioma.* Open medicine (Warsaw, Poland), 2017. **12**: p. 247-251.

235. Quail, D.F. and J.A. Joyce, *The Microenvironmental Landscape of Brain Tumors.* Cancer cell, 2017. **31**(3): p. 326-341.

236. Thorne, R.G. and C. Nicholson, *In vivo diffusion analysis with quantum dots and dextrans predicts the width of brain extracellular space.* Proceedings of the National Academy of Sciences of the United States of America, 2006. **103**(14): p. 5567-5572.

237. Nicholson, C. and E. Syková, *Extracellular space structure revealed by diffusion analysis.* Trends in neurosciences, 1998. **21**(5): p. 207-215.

238. Ferrer, V.P., V. Moura Neto, and R. Mentlein, *Glioma infiltration and extracellular matrix: key players and modulators.* Glia, 2018. **66**(8): p. 1542-1565.

239. Krishnaswamy, V.R., et al., *Demystifying the extracellular matrix and its proteolytic remodeling in the brain: structural and functional insights.* Cellular and molecular life sciences : CMLS, 2019. **76**(16): p. 3229-3248.

240. Lau, L.W., et al., *Pathophysiology of the brain extracellular matrix: a new target for remyelination.* Nature reviews. Neuroscience, 2013. **14**(10): p. 722-729.

241. Xiong, A., S. Kundu, and K. Forsberg-Nilsson, *Heparan sulfate in the regulation of neural differentiation and glioma development.* The FEBS journal, 2014. **281**(22): p. 4993-5008.

242. Goldbrunner, R.H., J.J. Bernstein, and J.C. Tonn, *ECM-mediated glioma cell invasion.* Microscopy Research and Technique, 1998. **43**(3): p. 250-257.

243. Jayadev, R. and D.R. Sherwood, *Basement membranes.* Current biology : CB, 2017. **27**(6): p. R207-R211.

244. Yao, Y., *Basement membrane and stroke.* Journal of cerebral blood flow and metabolism : official journal of the International Society of Cerebral Blood Flow and Metabolism, 2019. **39**(1).

245. Hallmann, R., et al., *Expression and function of laminins in the embryonic and mature vasculature.* Physiological reviews, 2005. **85**(3).

246. Morris, A.W.J., et al., *The Cerebrovascular Basement Membrane: Role in the Clearance of β-amyloid and Cerebral Amyloid Angiopathy.* Frontiers in aging neuroscience, 2014. **6**: p. 251.

247. Hatoum, A., R. Mohammed, and O. Zakieh, *The unique invasiveness of glioblastoma and possible drug targets on extracellular matrix.* Cancer management and research, 2019. **11**: p. 1843-1855.

248. Peppicelli, S., F. Bianchini, and L. Calorini, *Extracellular acidity, a "reappreciated" trait of tumor environment driving malignancy: perspectives in diagnosis and therapy.* Cancer metastasis reviews, 2014. **33**(2-3): p. 823-832.

249. Toyoshima, M. and M. Nakajima, *Human heparanase. Purification, characterization, cloning, and expression.* The Journal of biological chemistry, 1999. **274**(34): p. 24153-24160.

250. Kundu, S., et al., *Heparanase Promotes Glioma Progression and Is Inversely Correlated with Patient Survival.* Molecular cancer research : MCR, 2016. **14**(12): p. 1243-1253.

251. Alfonso, J.C.L., et al., *The biology and mathematical modelling of glioma invasion: a review.* Journal of the Royal Society, Interface, 2017. **14**(136).

252. Onishi, M., et al., *Angiogenesis and invasion in glioma.* Brain tumor pathology, 2011. **28**(1): p. 13-24.

253. Montana, V. and H. Sontheimer, *Bradykinin promotes the chemotactic invasion of primary brain tumors.* The Journal of neuroscience : the official journal of the Society for Neuroscience, 2011. **31**(13): p. 4858-4867.

254. Qin, E.Y., et al., *Neural Precursor-Derived Pleiotrophin Mediates Subventricular Zone Invasion by Glioma.* Cell, 2017. **170**(5).

255. Papale, M., et al., *Hypoxia, Inflammation and Necrosis as Determinants of Glioblastoma*

Cancer Stem Cells Progression. International journal of molecular sciences, 2020. **21**(8).

256. Lulli, V., et al., *Mir-370-3p Impairs Glioblastoma Stem-Like Cell Malignancy Regulating a Complex Interplay between HMGA2/HIF1A and the Oncogenic Long Non-Coding RNA (lncRNA) NEAT1.* International journal of molecular sciences, 2020. **21**(10).
257. Heiland, D.H., et al., *Microenvironment-Derived Regulation of HIF Signaling Drives Transcriptional Heterogeneity in Glioblastoma Multiforme.* Molecular cancer research : MCR, 2018. **16**(4): p. 655-668.
258. Gatenby, R.A. and E.T. Gawlinski, *A reaction-diffusion model of cancer invasion.* Cancer research, 1996. **56**(24): p. 5745-5753.
259. McDonald, P.C., et al., *Recent developments in targeting carbonic anhydrase IX for cancer therapeutics.* Oncotarget, 2012. **3**(1): p. 84-97.
260. Merrill, M.J. and E.H. Oldfield, *A reassessment of vascular endothelial growth factor in central nervous system pathology.* Journal of neurosurgery, 2005. **103**(5): p. 853-868.
261. Boyd, N.H., et al., *Addition of carbonic anhydrase 9 inhibitor SLC-0111 to temozolomide treatment delays glioblastoma growth in vivo.* JCI insight, 2017. **2**(24).
262. Xu, X., et al., *Association between SOX9 and CA9 in glioma, and its effects on chemosensitivity to TMZ.* International journal of oncology, 2018. **53**(1): p. 189-202.
263. Benton, G., et al., *Matrigel: from discovery and ECM mimicry to assays and models for cancer research.* Advanced drug delivery reviews, 2014. **79-80**.
264. de Gooijer, M.C., et al., *An Experimenter's Guide to Glioblastoma Invasion Pathways.* Trends in molecular medicine, 2018. **24**(9): p. 763-780.
265. Li, P., et al., *Hypoxia enhances stemness of cancer stem cells in glioblastoma: an in vitro study.* International journal of medical sciences, 2013. **10**(4): p. 399-407.
266. Ries, C., et al., *MMP-2, MT1-MMP, and TIMP-2 are essential for the invasive capacity of human mesenchymal stem cells: differential regulation by inflammatory cytokines.* Blood, 2007. **109**(9): p. 4055-4063.
267. Higa, N., et al., *Formin-like 1 (FMNL1) Is Associated with Glioblastoma Multiforme Mesenchymal Subtype and Independently Predicts Poor Prognosis.* International journal of molecular sciences, 2019. **20**(24).
268. Kahlert, U.D., et al., *ZEB1 Promotes Invasion in Human Fetal Neural Stem Cells and Hypoxic Glioma Neurospheres.* Brain pathology (Zurich, Switzerland), 2015. **25**(6): p.

724-732.

269. Proescholdt, M.A., et al., *Expression of hypoxia-inducible carbonic anhydrases in brain tumors.* Neuro-oncology, 2005. **7**(4): p. 465-475.

270. Shin, H.-J., et al., *Carbonic anhydrase IX (CA9) modulates tumor-associated cell migration and invasion.* Journal of cell science, 2011. **124**(Pt 7): p. 1077-1087.

271. Said, H.M., et al., *Distinct patterns of hypoxic expression of carbonic anhydrase IX (CA IX) in human malignant glioma cell lines.* Journal of neuro-oncology, 2007. **81**(1): p. 27-38.

272. Said, H.M., et al., *Expression patterns of the hypoxia-related genes osteopontin, CA9, erythropoietin, VEGF and HIF-1alpha in human glioma in vitro and in vivo.* Radiotherapy and oncology : journal of the European Society for Therapeutic Radiology and Oncology, 2007. **83**(3): p. 398-405.

273. Said, H.M., et al., *Rapid detection of the hypoxia-regulated CA-IX and NDRG1 gene expression in different glioblastoma cells in vitro.* Oncology reports, 2008. **20**(2): p. 413-419.

274. Said, H.M., et al., *Modulation of carbonic anhydrase 9 (CA9) in human brain cancer.* Current pharmaceutical design, 2010. **16**(29): p. 3288-3299.

275. Said, H.M., et al., *Hypoxia induced CA9 inhibitory targeting by two different sulfonamide derivatives including acetazolamide in human glioblastoma.* Bioorganic & medicinal chemistry, 2013. **21**(13): p. 3949-3957.

276. McIntyre, A., et al., *Carbonic anhydrase IX promotes tumor growth and necrosis in vivo and inhibition enhances anti-VEGF therapy.* Clinical cancer research : an official journal of the American Association for Cancer Research, 2012. **18**(11): p. 3100-3111.

277. Huang, B.-R., et al., *CAIX Regulates GBM Motility and TAM Adhesion and Polarization through EGFR/STAT3 under Hypoxic Conditions.* International journal of molecular sciences, 2020. **21**(16).

278. Lee, J., et al., *Tumor stem cells derived from glioblastomas cultured in bFGF and EGF more closely mirror the phenotype and genotype of primary tumors than do serum-cultured cell lines.* Cancer cell, 2006. **9**(5): p. 391-403.

279. Li, A., et al., *Genomic changes and gene expression profiles reveal that established glioma cell lines are poorly representative of primary human gliomas.* Molecular cancer

research : MCR, 2008. **6**(1): p. 21-30.

280. Amiri, A., et al., *Inhibition of carbonic anhydrase IX in glioblastoma multiforme.* European journal of pharmaceutics and biopharmaceutics : official journal of Arbeitsgemeinschaft fur Pharmazeutische Verfahrenstechnik e.V, 2016. **109**: p. 81-92.
281. Tamura, R., et al., *The role of vascular endothelial growth factor in the hypoxic and immunosuppressive tumor microenvironment: perspectives for therapeutic implications.* Medical oncology (Northwood, London, England), 2019. **37**(1): p. 2.
282. Bache, M., et al., *mRNA expression levels of hypoxia-induced and stem cell-associated genes in human glioblastoma.* Oncology reports, 2015. **33**(6): p. 3155-3161.
283. Chédeville, A.L., et al., *Investigating Glioblastoma Response to Hypoxia.* Biomedicines, 2020. **8**(9).
284. Shafee, N., et al., *PI3K/Akt activity has variable cell-specific effects on expression of HIF target genes, CA9 and VEGF, in human cancer cell lines.* Cancer letters, 2009. **282**(1): p. 109-115.
285. Riss, T.L., et al., *Cell viability assays*, in *Assay Guidance Manual [Internet]*. 2016, Eli Lilly & Company and the National Center for Advancing Translational Sciences.
286. Zhou, D.X., et al., *Inhibition of JMJD6 expression reduces the proliferation, migration and invasion of neuroglioma stem cells.* Neoplasma, 2017. **64**(5): p. 700-708.
287. Rape, A., B. Ananthanarayanan, and S. Kumar, *Engineering strategies to mimic the glioblastoma microenvironment.* Advanced drug delivery reviews, 2014. **79-80**: p. 172-183.
288. *https://www.phe-culturecollections.org.uk/*.
289. Hong, S.H., et al., *Stem cell passage affects directional migration of stem cells in electrotaxis.* Stem cell research, 2019. **38**: p. 101475.
290. Liao, H., et al., *Effects of long-term serial cell passaging on cell spreading, migration, and cell-surface ultrastructures of cultured vascular endothelial cells.* Cytotechnology, 2014. **66**(2): p. 229-238.
291. Tomko, N., et al., *4-Hydroxy-7-oxo-5-heptenoic acid lactone is a potent inducer of brain cancer cell invasiveness that may contribute to the failure of anti-angiogenic therapies.* Free radical biology & medicine, 2020. **146**: p. 234-256.
292. Qiu, B., et al., *Human brain glioma stem cells are more invasive than their differentiated*

progeny cells in vitro. Journal of Clinical Neuroscience, 2012. **19**(1): p. 130-134.

293. Joseph, J.V., et al., *Hypoxia enhances migration and invasion in glioblastoma by promoting a mesenchymal shift mediated by the HIF1α-ZEB1 axis.* Cancer letters, 2015. **359**(1): p. 107-116.
294. Qiu, W., et al., *Hypoxia-induced EPHB2 promotes invasive potential of glioblastoma.* International journal of clinical and experimental pathology, 2019. **12**(2): p. 539-548.
295. Huang, W., et al., *Hypoxia enhances the migration and invasion of human glioblastoma U87 cells through PI3K/Akt/mTOR/HIF-1α pathway.* Neuroreport, 2018. **29**(18): p. 1578-1585.
296. Tong, J.J., et al., *RhoA regulates invasion of glioma cells via the c-Jun NH2-terminal kinase pathway under hypoxia.* Oncology letters, 2012. **4**(3): p. 495-500.
297. Liu, Z.-J., et al., *TIPE2 Inhibits Hypoxia-Induced Wnt/β-Catenin Pathway Activation and EMT in Glioma Cells.* Oncology research, 2016. **24**(4): p. 255-261.
298. Liu, J., et al., *Hypoxia induced ferritin light chain (FTL) promoted epithelia mesenchymal transition and chemoresistance of glioma.* Journal of experimental & clinical cancer research : CR, 2020. **39**(1): p. 137.
299. Maciaczyk, D., et al., *CBF1 is clinically prognostic and serves as a target to block cellular invasion and chemoresistance of EMT-like glioblastoma cells.* British journal of cancer, 2017. **117**(1): p. 102-112.
300. Iwadate, Y., et al., *Transforming growth factor-β and stem cell markers are highly expressed around necrotic areas in glioblastoma.* Journal of neuro-oncology, 2016. **129**(1): p. 101-107.
301. Yang, M.-H., et al., *Direct regulation of TWIST by HIF-1alpha promotes metastasis.* Nature cell biology, 2008. **10**(3): p. 295-305.
302. Mikheeva, S.A., et al., *TWIST1 promotes invasion through mesenchymal change in human glioblastoma.* Molecular cancer, 2010. **9**: p. 194.
303. Kim, J.-Y., J.-H. Park, and S. Lee, *GLTSCR2 contributes to the death resistance and invasiveness of hypoxia-selected cancer cells.* FEBS letters, 2012. **586**(19): p. 3435-3440.
304. Tang, Z., L.M. Araysi, and H.M. Fathallah-Shaykh, *c-Src and neural Wiskott-Aldrich syndrome protein (N-WASP) promote low oxygen-induced accelerated brain invasion by gliomas.* PloS one, 2013. **8**(9): p. e75436.

305. Liu, Z., et al., *EGFRvIII/integrin β3 interaction in hypoxic and vitronectinenriching microenvironment promote GBM progression and metastasis.* Oncotarget, 2016. **7**(4): p. 4680-4694.

306. Kelly, N.J., et al., *Hypoxia activates cadherin-22 synthesis via eIF4E2 to drive cancer cell migration, invasion and adhesion.* Oncogene, 2018. **37**(5): p. 651-662.

307. Xu, Y., et al., *Procollagen-lysine 2-oxoglutarate 5-dioxygenase 2 promotes hypoxia-induced glioma migration and invasion.* Oncotarget, 2017. **8**(14): p. 23401-23413.

308. Fujimura, A., et al., *Cyclin G2 promotes hypoxia-driven local invasion of glioblastoma by orchestrating cytoskeletal dynamics.* Neoplasia (New York, N.Y.), 2013. **15**(11): p. 1272-1281.

309. Gopal, U., et al., *A novel extracellular Hsp90 mediated co-receptor function for LRP1 regulates EphA2 dependent glioblastoma cell invasion.* PloS one, 2011. **6**(3): p. e17649.

310. Chigurupati, S., et al., *Receptor channel TRPC6 is a key mediator of Notch-driven glioblastoma growth and invasiveness.* Cancer research, 2010. **70**(1): p. 418-427.

311. Torres, Á., et al., *Extracellular adenosine promotes cell migration/invasion of Glioblastoma Stem-like Cells through A Adenosine Receptor activation under hypoxia.* Cancer letters, 2019. **446**: p. 112-122.

312. Cheng, P., et al., *High Mobility Group Box 1 (HMGB1) Predicts Invasion and Poor Prognosis of Glioblastoma Multiforme via Activating AKT Signaling in an Autocrine Pathway.* Medical science monitor : international medical journal of experimental and clinical research, 2018. **24**: p. 8916-8924.

313. Gessler, F., et al., *Inhibition of tissue factor/protease-activated receptor-2 signaling limits proliferation, migration and invasion of malignant glioma cells.* Neuroscience, 2010. **165**(4): p. 1312-1322.

314. Wang, Y., et al., *Hypoxia and macrophages promote glioblastoma invasion by the CCL4-CCR5 axis.* Oncology reports, 2016. **36**(6): p. 3522-3528.

315. Mao, P., et al., *Mesenchymal glioma stem cells are maintained by activated glycolytic metabolism involving aldehyde dehydrogenase 1A3.* Proceedings of the National Academy of Sciences of the United States of America, 2013. **110**(21): p. 8644-8649.

316. Cheng, L., et al., *Elevated invasive potential of glioblastoma stem cells.* Biochemical and

biophysical research communications, 2011. **406**(4): p. 643-648.

317. Binda, E., et al., *Wnt5a Drives an Invasive Phenotype in Human Glioblastoma Stem-like Cells.* Cancer research, 2017. **77**(4).
318. Saito, N., et al., *Genetic and Lineage Classification of Glioma-Initiating Cells Identifies a Clinically Relevant Glioblastoma Model.* Cancers, 2019. **11**(10).
319. De Bacco, F., et al., *The MET oncogene is a functional marker of a glioblastoma stem cell subtype.* Cancer research, 2012. **72**(17): p. 4537-4550.
320. Beckner, M.E., et al., *Glycolysis as primary energy source in tumor cell chemotaxis.* Journal of the National Cancer Institute, 1990. **82**(23): p. 1836-1840.
321. Beckner, M.E., et al., *Proteomic characterization of harvested pseudopodia with differential gel electrophoresis and specific antibodies.* Laboratory investigation; a journal of technical methods and pathology, 2005. **85**(3): p. 316-327.
322. Beckner, M.E., et al., *Glycolytic glioma cells with active glycogen synthase are sensitive to PTEN and inhibitors of PI3K and gluconeogenesis.* Laboratory investigation; a journal of technical methods and pathology, 2005. **85**(12): p. 1457-1470.
323. Kathagen-Buhmann, A., et al., *Glycolysis and the pentose phosphate pathway are differentially associated with the dichotomous regulation of glioblastoma cell migration versus proliferation.* Neuro-oncology, 2016. **18**(9): p. 1219-1229.
324. Keunen, O., et al., *Anti-VEGF treatment reduces blood supply and increases tumor cell invasion in glioblastoma.* Proceedings of the National Academy of Sciences of the United States of America, 2011. **108**(9): p. 3749-3754.
325. Basanta, D., et al., *Evolutionary game theory elucidates the role of glycolysis in glioma progression and invasion.* Cell proliferation, 2008. **41**(6): p. 980-987.
326. Zhu, X., et al., *Lactate induced up-regulation of KLHDC8A (Kelch domain-containing 8A) contributes to the proliferation, migration and apoptosis of human glioma cells.* Journal of cellular and molecular medicine, 2020. **24**(20): p. 11691-11702.
327. Baumann, F., et al., *Lactate promotes glioma migration by TGF-beta2-dependent regulation of matrix metalloproteinase-2.* Neuro-oncology, 2009. **11**(4): p. 368-380.
328. Parkkila, S., et al., *Carbonic anhydrase inhibitor suppresses invasion of renal cancer cells in vitro.* Proceedings of the National Academy of Sciences of the United States of America, 2000. **97**(5): p. 2220-2224.

329. Lou, Y., et al., *Targeting tumor hypoxia: suppression of breast tumor growth and metastasis by novel carbonic anhydrase IX inhibitors.* Cancer research, 2011. **71**(9): p. 3364-3376.

330. Li, Y., et al., *Roles of Carbonic Anhydrase IX in Development of Pancreatic Cancer.* Pathology oncology research : POR, 2016. **22**(2): p. 277-286.

331. Sang, Y., et al., *Oncogenic roles of carbonic anhydrase IX in human nasopharyngeal carcinoma.* International journal of clinical and experimental pathology, 2014. **7**(6): p. 2942-2949.

332. Robertson, N., C. Potter, and A.L. Harris, *Role of carbonic anhydrase IX in human tumor cell growth, survival, and invasion.* Cancer research, 2004. **64**(17): p. 6160-6165.

333. Debreova, M., et al., *CAIX Regulates Invadopodia Formation through Both a pH-Dependent Mechanism and Interplay with Actin Regulatory Proteins.* International journal of molecular sciences, 2019. **20**(11).

334. Csaderova, L., et al., *The effect of carbonic anhydrase IX on focal contacts during cell spreading and migration.* Frontiers in physiology, 2013. **4**: p. 271.

335. Svastova, E., et al., *Carbonic anhydrase IX interacts with bicarbonate transporters in lamellipodia and increases cell migration via its catalytic domain.* The Journal of biological chemistry, 2012. **287**(5): p. 3392-3402.

336. Radvak, P., et al., *Suppression of carbonic anhydrase IX leads to aberrant focal adhesion and decreased invasion of tumor cells.* Oncology reports, 2013. **29**(3): p. 1147-1153.

337. Sansone, P., et al., *Cyclooxygenase-2/carbonic anhydrase-IX up-regulation promotes invasive potential and hypoxia survival in colorectal cancer cells.* Journal of cellular and molecular medicine, 2009. **13**(9B): p. 3876-3887.

338. Swayampakula, M., et al., *The interactome of metabolic enzyme carbonic anhydrase IX reveals novel roles in tumor cell migration and invadopodia/MMP14-mediated invasion.* Oncogene, 2017. **36**(45): p. 6244-6261.

339. Yang, J.-S., et al., *Overexpression of carbonic anhydrase IX induces cell motility by activating matrix metalloproteinase-9 in human oral squamous cell carcinoma cells.* Oncotarget, 2017. **8**(47): p. 83088-83099.

340. Ciccone, V., et al., *Pharmacological Inhibition of CA-IX Impairs Tumor Cell Proliferation, Migration and Invasiveness.* International journal of molecular sciences, 2020. **21**(8).

341. Chu, C.-Y., et al., *CA IX is upregulated in CoCl2-induced hypoxia and associated with cell invasive potential and a poor prognosis of breast cancer.* International journal of oncology, 2016. **48**(1): p. 271-280.

342. Zandberga, E., et al., *Depletion of carbonic anhydrase IX abrogates hypoxia-induced overexpression of stanniocalcin-1 in triple negative breast cancer cells.* Cancer biology & therapy, 2017. **18**(8): p. 596-605.

343. Kim, B.-R., et al., *Dickkopf-1 (DKK-1) interrupts FAK/PI3K/mTOR pathway by interaction of carbonic anhydrase IX (CA9) in tumorigenesis.* Cellular signalling, 2012. **24**(7): p. 1406-1413.

344. Schönichen, A., et al., *Considering protonation as a posttranslational modification regulating protein structure and function.* Annual review of biophysics, 2013. **42**: p. 289-314.

345. Frantz, C., et al., *Positive feedback between Cdc42 activity and H+ efflux by the Na-H exchanger NHE1 for polarity of migrating cells.* The Journal of cell biology, 2007. **179**(3): p. 403-410.

346. Frantz, C., et al., *Cofilin is a pH sensor for actin free barbed end formation: role of phosphoinositide binding.* The Journal of cell biology, 2008. **183**(5): p. 865-879.

347. Magalhaes, M.A.O., et al., *Cortactin phosphorylation regulates cell invasion through a pH-dependent pathway.* The Journal of cell biology, 2011. **195**(5): p. 903-920.

348. Srivastava, J., et al., *Structural model and functional significance of pH-dependent talin-actin binding for focal adhesion remodeling.* Proceedings of the National Academy of Sciences of the United States of America, 2008. **105**(38): p. 14436-14441.

349. Choi, C.-H., et al., *pH sensing by FAK-His58 regulates focal adhesion remodeling.* The Journal of cell biology, 2013. **202**(6): p. 849-859.

350. Paradise, R.K., D.A. Lauffenburger, and K.J. Van Vliet, *Acidic extracellular pH promotes activation of integrin α(v)β(3).* PloS one, 2011. **6**(1): p. e15746.

351. Busco, G., et al., *NHE1 promotes invadopodial ECM proteolysis through acidification of the peri-invadopodial space.* FASEB journal : official publication of the Federation of American Societies for Experimental Biology, 2010. **24**(10): p. 3903-3915.

352. Rozhin, J., et al., *Pericellular pH affects distribution and secretion of cathepsin B in malignant cells.* Cancer Research, 1994. **54**(24): p. 6517-6525.

353. Bourguignon, L.Y.W., et al., *CD44 interaction with Na+-H+ exchanger (NHE1) creates acidic microenvironments leading to hyaluronidase-2 and cathepsin B activation and breast tumor cell invasion.* The Journal of biological chemistry, 2004. **279**(26): p. 26991-27007.

354. Giusti, I., et al., *Cathepsin B mediates the pH-dependent proinvasive activity of tumor-shed microvesicles.* Neoplasia (New York, N.Y.), 2008. **10**(5): p. 481-488.

355. Kato, Y., et al., *Induction of 103-kDa gelatinase/type IV collagenase by acidic culture conditions in mouse metastatic melanoma cell lines.* The Journal of biological chemistry, 1992. **267**(16): p. 11424-11430.

356. Kato, Y., et al., *Acidic extracellular pH induces matrix metalloproteinase-9 expression in mouse metastatic melanoma cells through the phospholipase D-mitogen-activated protein kinase signaling.* The Journal of biological chemistry, 2005. **280**(12): p. 10938-10944.

357. Kapoor, N., et al., *Interaction of ASIC1 and ENaC subunits in human glioma cells and rat astrocytes.* American journal of physiology. Cell physiology, 2011. **300**(6): p. C1246-C1259.

358. Xu, J., et al., *Silencing Promotes Mitochondrial Biogenesis, Increases Putrescine Toxicity and Decreases Cell Motility to Suppress ccRCC Progression.* International journal of molecular sciences, 2020. **21**(16).

359. Choi, J., W.-H. Jung, and J.S. Koo, *Metabolism-related proteins are differentially expressed according to the molecular subtype of invasive breast cancer defined by surrogate immunohistochemistry.* Pathobiology : journal of immunopathology, molecular and cellular biology, 2013. **80**(1): p. 41-52.

360. Gibadulinova, A., et al., *CAIX-Mediated Control of LIN28/ Axis Contributes to Metabolic Adaptation of Breast Cancer Cells to Hypoxia.* International journal of molecular sciences, 2020. **21**(12).

361. Jamali, S., et al., *Hypoxia-induced carbonic anhydrase IX facilitates lactate flux in human breast cancer cells by non-catalytic function.* Scientific reports, 2015. **5**: p. 13605.

362. Starinsky-Elbaz, S., et al., *The pre-GAP-related domain of neurofibromin regulates cell migration through the LIM kinase/cofilin pathway.* Molecular and cellular neurosciences, 2009. **42**(4): p. 278-287.

363. Fadhlullah, S.F.B., et al., *Pathogenic mutations in neurofibromin identifies a leucine-rich*

domain regulating glioma cell invasiveness. Oncogene, 2019. **38**(27): p. 5367-5380.

364. Furukawa, K., et al., *PTEN gene transfer suppresses the invasive potential of human malignant gliomas by regulating cell invasion-related molecules.* International journal of oncology, 2006. **29**(1): p. 73-81.
365. Daniel, P.M., et al., *PI3K activation in neural stem cells drives tumorigenesis which can be ameliorated by targeting the cAMP response element binding protein.* Neuro-oncology, 2018. **20**(10): p. 1344-1355.
366. Baldwin, R.M., D.A.E. Parolin, and I.A.J. Lorimer, *Regulation of glioblastoma cell invasion by PKC iota and RhoB.* Oncogene, 2008. **27**(25): p. 3587-3595.
367. Baldwin, R.M., et al., *Coordination of glioblastoma cell motility by PKCι.* Molecular cancer, 2010. **9**: p. 233.
368. Raftopoulou, M., et al., *Regulation of cell migration by the C2 domain of the tumor suppressor PTEN.* Science (New York, N.Y.), 2004. **303**(5661): p. 1179-1181.
369. Dey, N., et al., *The protein phosphatase activity of PTEN regulates SRC family kinases and controls glioma migration.* Cancer research, 2008. **68**(6): p. 1862-1871.
370. Alam, R., et al., *PTEN suppresses SPARC-induced pMAPKAPK2 and inhibits SPARC-induced Ser78 HSP27 phosphorylation in glioma.* Neuro-oncology, 2013. **15**(4): p. 451-461.
371. Chen, Q., et al., *ARL4C stabilized by AKT/mTOR pathway promotes the invasion of PTEN-deficient primary human glioblastoma.* The Journal of pathology, 2019. **247**(2): p. 266-278.
372. Liu, L., et al., *Knockdown of PREX2a inhibits the malignant phenotype of glioma cells.* Molecular medicine reports, 2016. **13**(3): p. 2301-2307.
373. Yin, X.-F., et al., *NLRP3 in human glioma is correlated with increased WHO grade, and regulates cellular proliferation, apoptosis and metastasis via epithelial-mesenchymal transition and the PTEN/AKT signaling pathway.* International journal of oncology, 2018. **53**(3): p. 973-986.
374. Wu, W., et al., *Hypoxia induces H19 expression through direct and indirect Hif-1α activity, promoting oncogenic effects in glioblastoma.* Scientific reports, 2017. **7**: p. 45029.
375. Li, S.-J., et al., *The effect of miR-21 on SWOZ2 glioma cells and its biological mechanism.* Journal of B.U.ON. : official journal of the Balkan Union of Oncology, 2017. **22**(2): p.

468-473.

376. Zhao, Y., et al., *MicroRNA-29a activates a multi-component growth and invasion program in glioblastoma.* Journal of experimental & clinical cancer research : CR, 2019. **38**(1): p. 36.
377. Song, H., et al., *miR-92b regulates glioma cells proliferation, migration, invasion, and apoptosis via PTEN/Akt signaling pathway.* Journal of physiology and biochemistry, 2016. **72**(2): p. 201-211.
378. Li, X.-T., et al., *miR-494-3p Regulates Cellular Proliferation, Invasion, Migration, and Apoptosis by PTEN/AKT Signaling in Human Glioblastoma Cells.* Cellular and molecular neurobiology, 2015. **35**(5): p. 679-687.
379. Lan, F., et al., *Serum exosomal miR-301a as a potential diagnostic and prognostic biomarker for human glioma.* Cellular oncology (Dordrecht), 2018. **41**(1): p. 25-33.
380. Gu, J.-J., et al., *Suppression of microRNA-130b inhibits glioma cell proliferation and invasion, and induces apoptosis by PTEN/AKT signaling.* International journal of molecular medicine, 2018. **41**(1): p. 284-292.
381. Sun, B., et al., *Stepwise detection and evaluation reveal miR-10b and miR-222 as a remarkable prognostic pair for glioblastoma.* Oncogene, 2019. **38**(33): p. 6142-6157.
382. Jin, L., et al., *MicroRNA-193a-5p exerts a tumor suppressor role in glioblastoma via modulating NOVA1.* Journal of cellular biochemistry, 2019. **120**(4): p. 6188-6197.
383. Chen, Z., et al., *MicroRNA-216b inhibits cell proliferation and invasion in glioma by directly targeting metadherin.* Molecular Medicine Reports, 2017. **16**(6): p. 9749-9757.
384. Li, L. and H. Zhang, *MicroRNA-379 inhibits cell proliferation and invasion in glioma via targeting metadherin and regulating PTEN/AKT pathway.* Molecular medicine reports, 2018. **17**(3): p. 4049-4056.
385. Zhu, X.-P., et al., *LncRNA GAS5 regulates epithelial-mesenchymal transition and viability of glioma cells by targeting microRNA-106b and regulating PTEN expression.* Neuroscience research, 2020.
386. Ding, Y., et al., *Long noncoding RNA-GAS5 attenuates progression of glioma by eliminating microRNA-10b and Sirtuin 1 in U251 and A172 cells.* BioFactors (Oxford, England), 2020. **46**(3): p. 487-496.
387. Chu, L., et al., *Long intergenic non-coding LINC00657 regulates tumorigenesis of*

glioblastoma by acting as a molecular sponge of miR-190a-3p. Aging, 2019. **11**(5): p. 1456-1470.

388. Qin, N., et al., *Long Noncoding RNA MEG3 Suppresses Glioma Cell Proliferation, Migration, and Invasion by Acting as a Competing Endogenous RNA of miR-19a.* Oncology research, 2017. **25**(9): p. 1471-1478.
389. Wang, D., C.-W. Fu, and D.-Q. Fan, *Participation of tumor suppressors long non-coding RNA MEG3, microRNA-377 and PTEN in glioma cell invasion and migration.* Pathology, research and practice, 2019. **215**(10): p. 152558.
390. Zhang, Y., et al., *Long noncoding RNA MT1JP inhibits proliferation, invasion, and migration while promoting apoptosis of glioma cells through the activation of PTEN/Akt signaling pathway.* Journal of cellular physiology, 2019. **234**(11): p. 19553-19564.
391. Gao, Z.-G., et al., *CircFBXW7 alleviates glioma progression through regulating miR-23a-3p/PTEN axis.* Anatomical record (Hoboken, N.J. : 2007), 2020.
392. Kim, Y., et al., *Platelet-derived growth factor receptors differentially inform intertumoral and intratumoral heterogeneity.* Genes & development, 2012. **26**(11): p. 1247-1262.
393. Ohkawa, Y., et al., *Ganglioside GD3 Enhances Invasiveness of Gliomas by Forming a Complex with Platelet-derived Growth Factor Receptor α and Yes Kinase.* The Journal of biological chemistry, 2015. **290**(26): p. 16043-16058.
394. Feng, H., et al., *Activation of Rac1 by Src-dependent phosphorylation of Dock180(Y1811) mediates PDGFRα-stimulated glioma tumorigenesis in mice and humans.* The Journal of clinical investigation, 2011. **121**(12): p. 4670-4684.
395. Zhang, Y., et al., *The p53 Pathway in Glioblastoma.* Cancers, 2018. **10**(9).
396. Giese, A., *Glioma invasion--pattern of dissemination by mechanisms of invasion and surgical intervention, pattern of gene expression and its regulatory control by tumorsuppressor p53 and proto-oncogene ETS-1.* Acta neurochirurgica. Supplement, 2003. **88**: p. 153-162.
397. Huang, X., et al., *A novel PTEN/mutant p53/c-Myc/Bcl-XL axis mediates context-dependent oncogenic effects of PTEN with implications for cancer prognosis and therapy.* Neoplasia (New York, N.Y.), 2013. **15**(8): p. 952-965.
398. Yi, L., et al., *Stabilization of LSD1 by deubiquitinating enzyme USP7 promotes glioblastoma cell tumorigenesis and metastasis through suppression of the p53 signaling*

pathway. Oncology reports, 2016. **36**(5): p. 2935-2945.

399. Kim, C.K., et al., *Negative regulation of p53 by the long isoform of ErbB3 binding protein Ebp1 in brain tumors.* Cancer research, 2010. **70**(23): p. 9730-9741.
400. Li, Y., et al., *MicroRNA-34a inhibits glioblastoma growth by targeting multiple oncogenes.* Cancer research, 2009. **69**(19): p. 7569-7576.
401. Sun, G., et al., *MiR-15b/HOTAIR/p53 form a regulatory loop that affects the growth of glioma cells.* Journal of cellular biochemistry, 2018. **119**(6): p. 4540-4547.
402. Zhan, X.-H., et al., *MicroRNA16 regulates glioma cell proliferation, apoptosis and invasion by targeting Wip1-ATM-p53 feedback loop.* Oncotarget, 2017. **8**(33): p. 54788-54798.
403. Zhang, Y., et al., *Long Noncoding RNA LINC00467 Promotes Glioma Progression through Inhibiting P53 Expression via Binding to DNMT1.* Journal of Cancer, 2020. **11**(10): p. 2935-2944.
404. Cao, W., B. Liu, and H. Ma, *Long non-coding RNA GHET1 promotes viability, migration and invasion of glioma cell line U251 by down-regulation of miR-216a.* European review for medical and pharmacological sciences, 2019. **23**(4): p. 1591-1599.
405. Xiao, S., et al., *The Long Noncoding RNA TP73-AS1 Interacted with miR-124 to Modulate Glioma Growth by Targeting Inhibitor of Apoptosis-Stimulating Protein of p53.* DNA and cell biology, 2018. **37**(2): p. 117-125.
406. Mboge, M.Y., et al., *A non-catalytic function of carbonic anhydrase IX contributes to the glycolytic phenotype and pH regulation in human breast cancer cells.* The Biochemical journal, 2019. **476**(10): p. 1497-1513.

8 Aberravations

Abbreviation	Full name or comment
11C-MET	[11C-methyl]-methionine
18F-FDG	18F-2-fluoro-2-deoxy-D-glucose
18F-FDOPA	3,4-dihydroxy-6-[18F]-fluoro-L-phenylalanine
18F-FET	O-(2-[18F]-fluoroethyl)-L-tyrosine
2-HG	2-hydroxyglutarate
3D	3 dimension
3'-UTR	3′ untranslated region
A3AR	A3 adenosine receptor
ABC	ATP-binding cassette
ACNU	nimustine
ADAM	a disintegrin and metalloproteinase
ADAMTS	ADAMs with a thrombospondin motif
AEBSF	4-(2-aminoethyl)benzenesulfonyl fluoride hydrochloride
AEDs	antiepileptic drugs
AEs	anion exchangers
AG	anchoring group
Akt(PKB)	AKT serine/threonine kinase, also named protein kinase B
ALT	alternative lengthening of telomeres
ANOVA	analysis of variance
AP	activator protein
APS	ammonium per sulfate
ARD-1	arrest defective-1
ARF	ADP ribosylation factor
ARL4C	ADP-ribosylation factor like-4C
ARNT	aryl hydrocarbon receptor nuclear translocator
ARP2/3 complex	actin related protein 2/3 complex
ASCL1	achaete-scute homolog 1
ASICs	acid-sensing ion channels

ATF	activating transcription factor
ATP	adenosine triphosphate
ATRX	alpha-thalassemia/mental retardation, X-linked
BAX	Bcl-2-associated X
BBB	blood brain barrier
Bcl-XL	B cell lymphoma extra large
BCNU	carmustine
bFGF	basic fibroblast growth factor
bHLH	basic helix-loop-helix
BMI1	BMI1 proto-oncogene, also named polycomb ring finger
BMPs	Bone morphogenetic proteins
BMs	basement membranes
bp	base pairs
BSA	bovine serum albumin
BTCG	Brain Tumor Cooperative Group
BTICs	brain tumor-initiating cells
BTs	bicarbonate transporters
BTSG	Brain Tumor Study Group
C	chemotherapy
CA	catalytic domain
CAIs	carbonic anhydrase inhibitors
CAIX	carbonic anhydrase IX
cAMP	cyclic adenosine monophosphate
CAMs	cell adherein molecules
CA-RPs	CA-related proteins
CAs	carbonic anhydrases
CBF1	also known as recombination signal binding protein for immunoglobulin kappa J, RBPJ
CBP	CREB-binding protein
CBTRUS	the Central Brain Tumor Registry of the United States

CCDC26	coiled-coil domain containing 26
CCK8	cell counting kit-8
CCL4	chemokine C-C motif ligands 4
CCNU	lomustine
CCR5	C-C chemokine receptor type 5
CD	cluster of differentiation
CD133	cluster of differentiation 133, prominin-1
CDK	cyclin dependent kinase
CDKN2A	cyclin-dependent kinase inhibitor 2A, coding $p16^{INK4a}$ and $p14^{ARF}$
CDKN2B	cyclin-dependent kinase 4 inhibitor B, coding $p15^{INK4b}$
cDNA	complementary DNA
CH1	cysteine-histidine rich domain
CHI3L1	chitinase-3-like protein 1
circRNAs	circular RNAs
CITED2	CBP/p300 interacting transactivator with ED-rich tail 2
cm	centimeters
c-Myc	MYC proto-oncogene
CNS	central nervous system
COOH	carboxyl
COX-2	cyclooxygenase-2
CREB	cAMP response element binding protein
CrkII	a central signal adapter protein
CS	chondroitin sulfate
CSCs	cancer stem cells
CSF	cerebrospinal fluid
CS-GAG	chondroitin sulfate glycosaminoglycan
CSPGs	chondroitin sulfate proteoglycans
CT	computed tomography
CTA	CT angiography
DABCO	1,4-diazobicyclo(2,2,2)-octane

Dbl	diffuse B-cell lymphoma
Dbs	Dbl's big sister
DCX	doublecortin
DEPC	diethyl pyrocarbonate
Dk	donkey
DKK-1	dickkopf-1, a negative regulator Wnt pathway
DLL3	delta-like 3
DMEM	Dulbecco's Modified Eagle's Medium
DMSO	dimethylsulfoxid
DNA	deoxyribonucleic acid
DNMT1	DNA methyltransferase 1
dNTP	deoxy-ribonucleoside triphosphate
Dock	dedicator of cytokinesis
DS	dermatan sulfate
DTI	diffusion tensor imaging
DTPA	diethylenetriaminepentaacetic acid
DTT	dithiothreitol
DVT	deep venous thromboembolism
DWI	diffusion-weighted imaging
EANO	European Association of Neuro-Oncology
Ebp1	a human homologue of the mouse protein p38-2AG4
ECM	extracellular matrix
EDTA	ethylenediamine tetraacetic acid
EGF/EGFR	epidermal growth factor/epidermal growth factor receptor
EGFR vIII	epidermal growth factor receptor variant III
EGTA	ethylene glycol tetraacetic acid
eIF4E2	eukaryotic initiation factor 4
EMEA	European Medicines Agency
EMSA	electrophoretic mobility shift assay
EMT	epithelial mesenchymal transition

ENaC	epithelial sodium channel
EORTC	the European Organisation for Research and Treatment of Cancer
EphB2	Ephrin type-B receptor 2
EPO	erythropoietin
ErbB3	receptor tyrosine-protein kinase erbB-3, also known as HER3 (human epidermal growth factor receptor 3)
etc.	Et cetera
Ets-I	erythroblast transformation specific-I
Exp.	experiment
f	female
FAK	focal adhesion kinase
FBS	fetal bovine serum
FIH-1	factor inhibiting HIF-1
FITC	fluorescein isothiocyanate
FLAIR	fluid-attenuated inversion recovery
FTL	ferritin light chain
FVIIa	factor VIIa
GABRA1	gamma-aminobutyric acid receptor subunit alpha-1
GAG	glycosaminoglycan
GAPDH	glyceraldehyde-3-phosphate dehydrogenase
GAS1	growth arrest specific 1
GBM	glioblastoma multiforme
G-CIMP	glioma-CpG island methylator phenotype
GEFs	guanine nucleotide exchange factors
GF	growth factor
GFAP	glial fibrillary acidic protein
GHET1	gastric carcinoma highly expressed transcript 1
GLI2	GLI family zinc finger 2
GLTSCR2	glioma tumor suppressor candidate region gene 2 protein
GRD	GAP-related domain

GSCs	glioma stem cells
GSK3β	glycogen synthase kinase 3β
GTP	guanosine triphosphate
GWASs	genome-wide association studies
Gy	Gray
H	hypoxia
HA	hyaluronic acid
HAPLNs	hyaluronan and proteoglycan link proteins
HBS	HIF-binding site
HCl	hydrogen chloride
HDM2	a p53 E3 ligase of human homologue of MDM2
HEPES	4-(2-hydroxyethyl)-1-piperazineethanesulfonic acid
HGF/HGFR(MET)	hepatocyte growth factor/hepatocyte growth factor receptor
HGG	high-grade glioma
HIF	hypoxia-inducible factor
HMGB1	high mobility group box 1
HOTAIR	HOX transcript antisense RNA
HREs	hypoxia response elements
HRP	horseradish peroxidase conjugates
HS	heparan sulfate
Hsp	heat shock protein
HSPGs	heparin sulfate proteoglycans
hTERT	human telomerase reverse transcriptase
IARC	the International Agency for Research on Cancer
IC	intracytoplasmic domain
ICD-O-3	3rd edition international classification of diseases for oncology
ID	inhibitory domain
IDH1/2	isocitrate dehydrogenase 1/2
IFRT	involved field RT
IGFBP-2	insulin-like growth factor binding protein-2

IgG	Immunoglobulin G
JAG1	jagged canonical Notch ligand 1
JAK	Janus kinases
JNK	Jun NH2-terminal kinase
kb	kilo base pairs
kDa	kilodaltons
K_i value	inhibition constant
KLHDC8A	kelch domaincontaining 8A
KPS	Karnofsky Performance Status
KS	keratan sulfate
L1CAM (CD171)	L1 cell adhesion molecule
let-7	lethal-7
LFNG	LFNG O-fucosylpeptide 3-beta-N-acetylglucosaminyltransferase
LGG	low-grade glioma
Lgl	lethal (2) giant larvae
LIMK1	LIM domain kinase 1
LIN28	Lin-28 homolog A
lncRNAs	long non-coding RNA
LOH	loss of heterozygosity
LRD	leucine-rich domain
LRP1	low-density lipoprotein receptor-related protein 1
LSD1	lysine-specific demethylase 1
m	male
mA	milliampere
mAbs	monoclonal antibodies
MAPK(ERK)	mitogen-activated protein kinase, also named extracellular signal-regulated kinase
MAPKAPK2	MAPK activated protein kinase 2
MCTs	monocarboxylate transporters
MDM2/4	mouse double minute 2/4 homolog

MDT	multidisciplinary discussion
MEK	also named MAPKK (mitogen-activated protein kinase kinase)
MERTK	c-mer proto-oncogene tyrosine kinase
Mes.	mesenchymal
meth.	methylated
MGMT	O^6-methylguanine DNA methyltransferase
miRNA/miR	microRNA
ml	milliliters
MLC	myosin light chain
MLH1	mutL homolog 1
mm	millimeters
mmHg	millimetre of mercury
MMPs	metalloproteases
MORC2	microrchidia 2
MRI	magnetic resonance imaging
mRNA	messenger RNA
MRS	magnetic resonance spectroscopy
MRV	magnetic resonance venography
MSH2/6	mutS homolog 2/6
MT1-MMP	membrane-type MMP
mTOR	mammalian target of rapamycin
MTT	3-(4,5-Dimethylthiazol-2-yl)-2,5-diphenyltetrazolium bromide
mut	mutant
N	normoxia
N/C-TAD	N/C-terminal transactivation domain
NADPH	nicotinamide adenine dinucleotide phosphate
NBCs	Na^+/HCO_3^- co-transporters
NCCN	National Comprehensive Cancer Network
NCIC	the National Cancer Institute of Canada
NDCBEs	Na^+-driven Cl^-/HCO_3^- exchangers

NEFL	neurofilament light polypeptide
NES	nestin
NF1/2	neurofibromatosis 1/2
NFAT	nuclear factor of activated T-cell
NFYA	nuclear transcription factor Y subunit alpha
NF-κB	nuclear factor kappa B
NHEs	Na^+/H^+ exchangers
NHGRI	the National Human Genome Research Institute
NIH	the National Cancer Institute's Center for Cancer Genomics
NKX2-2	NK2 homeobox 2
NLRP3	nucleotide-binding domain leucine-rich family pyrin-containing 3
NLS	nuclear localization signal domain
nm	nanometers
NMR	nuclear magnetic resonance
No.	number
NOD-SCID	non-obese diabetic, severe combined immunodeficient
NOVA1	neuro-oncological ventral antigen 1
ns	not significant
NSAIDS	non-steroidal anti-inflammatory drugs
NSCs	neural stem cells
NTC	no template control
NWASP	neural Wiskott-Aldrich syndrome protein
Oct-4	octamer-binding transcription factor 4
ODDD	oxygen-dependent degradation domain
OH	hydroxyl
OLIG2	oligodendrocyte transcription factor 2
OS	overall survival
OXPHOS	oxidative phosphorylation
p	p value
Pak1	p21 (Rac1) activated kinase 1

PAP	prostatic acid phosphatase
PAR-2	protease-activated receptor 2
PAS	PER(Period)-ARNT-SIM
PBS	phosphate buffered saline
PBS-T	phosphate buffered saline with Tween
PCR	polymerase chain reaction
PDB ID	Protein Data Bank identification code
PDGF/PDGFR	platelet-derived growth factor/platelet-derived growth factor receptor
PDGFRA	platelet derived growth factor alpha
PDH	pyruvate dehydrogenase
PDK1	pyruvate dehydrogenase kinase 1
PE	pulmonary emboli
PET	positron emission tomography
PFA	paraformaldehyde
PFS	progression-free survival
PG	proteoglycan-like domain
PGE2	prostaglandins E2
PHD2	prolyl hydroxylase domain protein 2
PHLDB1	pleckstrin homology-like domain family B member 1
p*I*	Isoelectric point
PI3K	phosphoinositide 3-kinases
PIK3CA	the phosphatidylinositol-4,5-bisphosphate 3-kinase, catalytic subunit alpha
PIK3R1	phosphatidylinositol 3-kinase regulatory subunit alpha
PIP2	phosphatidylinositol 4,5-bisphosphate
PIP3	phosphatidylinositol-3,4,5-triphosphate
PIPs	phosphoinosites
PKA	protein kinase A
pKa values	acid dissociation constants
PKC	protein kinase C

PLD	phospholipase D
PLOD2	procollagenlysine 2-oxoglutarate 5-dioxygenase 2
PMS2	postmeiotic segregation increased 2
PMSF	phenylmethanesulfonylfluoride
PMT	proneural to mesenchymal transition
PNN	perineural nets structure
pos.	positive
PRC	People's Republic of China
pre-Exp.	pre-experiment
PREX2a	phosphatidylinositol-3,4,5-trisphosphate-dependent Rac exchange factor 2a
prim.	primary
Pro.	proneural
PRs	protected regions
PTEN	phosphatase and tensin homolog
PTK	protein tyrosine kinase
PVA	polyvinyl alcohol
pVHL	von Hippel-Lindau protein
PWI	perfusion-weighted imaging
qPCR	quantitative real-time PCR
R	radiotherapy
Rac1	Rac family small GTPase 1
RANO	the Response Assessment in Neuro-Oncology working group
RAS	rat sarcoma
Rb	retinoblastoma
rbt	rabbit
rCBV	relative cerebral blood volume
RCT	randomized controlled trail
RDD	RNase-free DNA digest
RELB	v-rel reticuloendotheliosis viral oncogene homolog B

RHAMM	receptor for hyaluronan mediated motility
RIPA	radioimmunoprecipitation assay
RLC	regulatory light chain
RNA	ribonucleic acid
RNAi	RNA interference
ROCK1	RhoA-associated protein kinase 1
ROS	reactive oxygen species
RPL13A	ribosomal protein L13
rpm	revolutions per minute
RSB	reducing sample buffer
RT	radiotherapy
RT	reverse transcription
RTEL1	regulator of telomere elongation helicase 1
RTK	receptor tyrosine kinases
S6K	ribosomal protein S6 kinase beta-1
SD	standard deviation
SDS-PAGE	sodium dodecyl sulfate-polyacrylamide gel electrophoresis
sec.	secondary
SEMA3C	semaphorin 3C
SFKs	src family kinases
SG	sticky group
SH2	Src homology 2
shRNA	short hairpin RNA
siRNA	small interfering RNA
SLC12A5	solute carrier family 12 member 5
SMO	smoothened gene
SNPs	single nucleotide polymorphisms
SOCS3	suppressor of cytokine signaling 3
SOX	SRY-related HMG-box
SP	specificity protein

SP	signal peptide domain
SPARC	secreted protein acidic and rich in cysteine
SRC-1	steroid-receptor co-activator-1
SSEA1 (CD15)	stage-specific embryonic antigen-1
STAT	signal transducer and activator of transcription protein
SUMO	Small ubiquitin-related modifier
suPAR	soluble urokinase-type plasminogen activator receptor
SWI	susceptibility-weighted imaging
SYT1	synaptotagmin 1
T1P	dynamic contrast-enhanced T1-weighted imaging
TBE	Tris/Borate/EDTA
TBS	Tris-buffered saline
TBS-T	Tris-buffered saline with Tween
TCA	tricarboxylic acid
TCF4	transcription factor 4
TCGA	the Cancer Genome Atlas
TEMED	N,N,N',N'-Tetra-methyl ethylene-diamine
TET	ten-eleven translocation
TF	tissue factor
TGF	transforming growth factor
TIF2	transcription intermediary factor 2
TIMPs	tissue inhibitor of metalloproteinases
TIPE2	tumor necrosis factor-a-induced protein 8-like 2
TM	transmembrane domain
TME	tumour microenvironment
TMZ	Temozolomide
TNF	tumor necrosis factor
TNFRSF1A	TNF receptor superfamily member 1A
TP53	tumor protein P53
TRADD	tumor necrosis factor receptor type 1-associated death domain protein

TRPC6	transient receptor potential 6
TSC1/2	tuberous sclerosis 1/2
TTFields	tumor-treating fields
TWIST	twist family bHLH transcription factor
UK	United Kingdom
unmeth.	unmethylated
uPA/tPA	urokinase-type/tissue-type plasminogen activator
uPAR	urokinase plasminogen activator surface receptor
USA	United States of America
USP7	ubiquitin specific peptidase 7
V-ATPases	vacuolar ATPases
VEGF/VEGFR	vascular endothelial growth factor/vascular endothelial growth factor receptor
Vent.	ventilate
VTE	venous thromboembolism
w/	with
w/o	without
WASP	Wiscott-Aldrich syndrome protein
WB	western blot
WBRT	whole-brain RT
WHO	World Health Organization
Wo	Wortmannin
wt	wild type
y	years
Yes	Src kinase
ZBG	zinc-binding group
ZEB1	zinc finger E-box binding homeobox 1
α-KG	alpha-ketoglutarate
µl	microliter
µm	micrometer

μM	micromole per liter

9 Acknowledgments

Foremost, I would like to express my deep and sincere gratitude and acknowledgment to all the people who gave me a lot of help for my study, research, life in the past two and a half years. Friendship forever!

My sincere thanks to Prof. Dr. med. Alexander Brawanski who offered me the opportunity to do exciting research in laboratory of Neurosurgery and write a thesis. Meanwhile, thanks to the recommendation and various support by Dr. He Hongjun from DCTA.

My special thanks to Prof. Dr. med. Martin Proescholdt for the guidance of experiments, knowledge transfer, correction of the manuscript and various dedicated support. His patience, motivation, enthusiasm, immense knowledge and experience, as well as constructive advice inspired and guided me to the success of this work significantly. He gave me a second academic life and scientific thinking.

My special thanks to Annette Lohmeier who taught me laboratory technology with great patience and rigorousness, as well as plan making. She is one of the best teachers and friends in my life.

Thank to Eva-Maria Störr for organization and support in the laboratory.

Thank to Petra Eberl for her help in any situation.

Thank to Dr. Arabel Vollmann-Zwerenz, Birgit Jachnik and other colleagues from Department of Neurooncology for their help and advice in difficult situations.

Furthermore, I would also like to thank all the members of Dr. Urs Nissen's team from Westküstenklinikum Heide. They showed me a perfect medical and education system 4 years ago, which prompted me the strong motivation to study in Germany again.

Last but not the least, thanks to the support and encouragement from my family throughout my whole life spiritually and materially.